# Geological Survey of Finland

## Bulletin 367

# Petrology of the Pechenga ferropicrites and cogenetic, Ni-bearing gabbro-wehrlite intrusions, Kola Peninsula, Russia

by Eero J. Hanski

Geologian tutkimuskeskus
Espoo 1992

**Geological Survey of Finland, Bulletin 367**

# PETROLOGY OF THE PECHENGA FERROPICRITES AND COGENETIC, Ni-BEARING GABBRO-WEHRLITE INTRUSIONS, KOLA PENINSULA, RUSSIA

by

EERO J. HANSKI

with 103 figures and 26 tables in the text and 2 appendices

ACADEMIC DISSERTATION

GEOLOGIAN TUTKIMUSKESKUS
ESPOO 1992

Vammalan Kirjapaino Oy 1992

**Hanski, Eero J., 1992.** Petrology of the Pechenga ferropicrites and cogenetic, Ni-bearing gabbro-wehrlite intrusions, Kola Peninsula, Russia. *Geological Survey of Finland, Bulletin* 367, 192 pages, 103 figures, 26 tables, and 2 appendices.

This study reviews the geology of the early Proterozoic Pechenga Series, which comprises four sedimentary-volcanic cycles attaining a total thickness of 10 km, and presents new petrographical, mineralogical, geochemical, and Sm-Nd, Pb-Pb, Re-Os and Rb-Sr isotopic data, with particular emphasis on ferropicritic rocks. The ferropicritic magmatism led to the formation of gabbro-wehrlite intrusions and related Ni-Cu deposits in the so-called productive pile, the sedimentary part of the uppermost cycle (Pilgujärvi Suite). An extrusive facies is represented by ferropicritic tuffs, massive and pillowed lavas, and thick, differentiated lava flows, which occur mainly in the upper part of the productive pile and at three levels in the overlying volcanic unit.

Layered ferropicritic flows display various types of spinifex textures including randomly oriented olivine spinifex, parallel olivine spinifex, and pyroxene spinifex. The presence of spinifex texture in the Pechenga ferropicrites demonstrates that this texture is not restricted to rocks of komatiitic affinity.

The $TiO_2$-rich nature of the parental magma is reflected in the composition of primary minerals such as Ti-rich chrome spinel, titanaugite, kaersutite-ferrokaersutite, and titanian phlogopite. It is deduced that the parental magma contained about 15 wt. % MgO and more than 14 wt. % $FeO_{tot}$ and was relatively low in $Al_2O_3$. Many incompatible element ratios in ferropicrites correspond closely to those found in modern ocean island basalts. A literature survey of primitive magmas has revealed that, with respect to major elements, close analogues of the Pechenga ferropicrites are found in some Archean and early Proterozoic greenstone belts in Canada and the Ukraine, respectively.

The mode of occurrence of kaersutite as overgrowths on spinifex pyroxenes or as interstitial skeletal needles strongly argues for crystallization *in situ* from a hydrous magma after the emplacement of the flows. This observation is in obvious disagreement with the experimentally determined stability conditions of hydrous kaersutite requiring a minimum water pressure of at least 0.5 kbar, which is equivalent to a water depth deeper than 5 km.

Sulfur isotope and geochemical data obtained for ore deposits from the western ore field are consistent with an interpretation that the bulk of sulfur is of juvenile origin. This is difficult to reconcile with the radiogenic initial Os isotopic compositions of sulfide-bearing samples from the Kammikivi sill. High $^{187}Os/^{186}Os$ may have resulted from assimilation of country rock phyllites, postmagmatic leaching of Re or gain of radiogenic Os from country rock, although each of these processes should have involved a very extensive metal migration. More research is required to solve this problem.

On the basis of published moderate to high-pressure experimental data on basic to ultrabasic systems, an $Al_2O_3$ vs. $MgO+K_D \times FeO$ diagram has been constructed and is used to show that the ferropicrites left behind a garnet-free residual mineral assemblage. This inference seems to be in conflict with the high La/Yb observed in the ferropicrites, suggesting that garnet fractionation took place, but an alternative explanation invokes a mantle source enriched in LREE and presumably in other incompatible trace elements including HFSE. It is also shown that the only feasible explanation for the iron-enrichment in ferropicrites is the high $FeO_{tot}$ content of the mantle source, with an estimated value falling between 13-15 wt. %.

Nd, Sr, and Os isotopic and geochemical data for the ferropicrites are inconsistent with substantial degrees of contamination with older crustal material and favor an intraplate

geotectonic setting. An initial $\varepsilon_{Nd}$ value of +1.4±0.4 indicates a time-integrated mantle source depleted in LREE relative to MREE but the depletion was not so extensive as in the contemporaneous mid-ocean-ridge basalt reservoir or the source of the accompaning tholeiites. The viability of a metasomatically enriched subcontinental lithosphere or an upwelling mantle plume as potential source regions for the ferropicritic magmatism are also discussed.

Key words (Georef Thesaurus, AGI): Metavolcanic rocks, picrite, gabbros, wehrlite, Ni ores, spinifex texture, kaersutite, electron probe data, geochemistry, isotopes, genesis, Proterozoic, Pechenga, Kola Peninsula, Russia

*Eero J. Hanski, Geological Survey of Finland, P.O. Box 77, SF-96101 Rovaniemi, Finland*

ISBN 951-690-489-0
ISSN 0367-522-X

*To Anneli,*
*Mikko, Henriikka and Lauri*

## FOREWORD

The impetus for the author's study of the Pechenga rocks came in 1982 while the author was involved in research into the Archean Kuhmo greenstone belt, carried out at the Department of Geology, University of Oulu, under the leadership of Professor Tauno Piirainen. At that time, the author examined old thin sections of Pechenga rocks prepared by Heikki Väyrynen and other Finnish geologists in the 1920's and 1930's. The textures and mineralogy of several of these samples were similar to those observed by the author in mica and amphibole-bearing peridotites that had been found in Proterozoic layered sills in the Kuhmo and Koli areas in eastern Finland. These observations and subsequently obtained geochemical data led to the proposal that the Pechenga, Kuhmo, and Koli intrusions could all be assigned to a common rock family called the gabbro-wehrlite association (Hanski, 1986).

After moving to the Regional Office of the Geological Survey of Finland (GSF) in Rovaniemi in 1984, the author commenced a more detailed geochemical and mineralogical study of the Pechenga rocks in collaboration with Dr. Valery Smolkin from the Geological Institute at the Kola Science Center in Apatity, Kola Peninsula (Russia). Later, joint endeavours in the field of isotope geology were begun with Drs. Hannu Huhma and Matti Vaasjoki at the GSF in Espoo and Prof. Richard Walker at the Department of Geology of the University of Maryland (USA). Other coworkers include Dr. Gerhard Brügmann from the Department of Geology of the University of Toronto (Canada) who performed trace element and PGE analyses on Pechenga rocks.

Collaboration with Valery Smolkin was initiated at the same time as the former leader of the then Soviet Union Mikhael Gorbachev embarked on his programs of glasnost and perestroika. One of the immediate benefits of these reforms was that the Pechenga region was opened to outsiders after a period of 40 years, during which the region was almost completely isolated from foreign visitors. It thus became possible for the author to make two short field excursions in the area. The first visit was held under the guidance of Valery Smolkin and Peter Skufin on August 6-11, 1990. The second excursion was organized by Valery Smolkin, Anatoly Borisov, and Marat Abzalov and took place on June 20-24, 1991. Gerhard Brügmann also participated in the 1990 excursion and Richard Walker in 1991.

It should be stressed that the amount of field work undertaken in the present investigation is minimal (altogether only 5 days were spent examining ferropicritic rocks and related ores during the two excursions) and therefore the field description of ferropicritic rocks in this paper is of necessity limited. Instead, the investigations have been based mainly on mineralogical, geochemical, and isotopic studies of hand specimens and drill core samples. In addition to samples donated by Russian colleagues and those collected by the author during the excursion, the author has had access to the comprehensive collection of hand specimens obtained by Finnish workers in the 1920's and 1930's, which is now stored at the Regional Office of the GSF in Rovaniemi, as well as old drill cores kept in the GSF core store at Loppi in southern Finland.

## CONTENTS

# INTRODUCTION

The Pechenga area in the Kola Peninsula, also known by the Finnish name Petsamo, has been the subject of intensive geological research since the first magmatic Ni-Cu sulfide deposits were discovered in the 1920's. These deposits are associated with the lower parts of sill-like gabbro-wehrlite intrusions intruded into a sequence of sedimentary rocks. Even after more than half a century of exploitation, several mines are still in operation.

Recent geochemical investigations have revealed that the parental magma of the ore-bearing intrusions at Pechenga is characterized by high MgO and FeO contents and is identical in composition with that of primitive volcanic rocks, known as ferropicrites, which also occur in the area (Hanski and Smolkin, 1990). In addition to their peculiar chemical composition, the Pechenga ferropicrites are of interest because of the presence of spinifex textures reminiscent of those found in komatiitic volcanic rocks (Hanski and Smolkin, 1991).

The Pechenga region is also of significance in that it was chosen by Soviet researchers as the site for the Kola superdeep drill hole in the 1960's. One of the aims of this program was to reach the Conrad discontinuity, i.e., the boundary between the supposed granitic and basaltic layers of the earth's crust. On the basis of geophysical measurements, this boundary had been interpreted to lie at a depth of about 7 km in the Pechenga area (Kozlovsky, 1987). At present, the well has been drilled to a depth of more than 12 km with the interval below 6842 m being composed of Archean basement gneisses on which the early Proterozoic Pechenga supracrustal rocks were deposited. The superdeep drill hole together with other drilling activities and field investigations have resulted in a detailed understanding of the stratigraphy of the Pechenga volcanic-sedimentary sequence, which totals more than 8 km in thickness. This makes the Pechenga area an ideal place for studying the volcanic and sedimentary evolution of an early Proterozoic greenstone belt.

Despite the long history of investigation, there still exist diverse opinions on many aspects of the geology of the Pechenga area. Furthermore, the Pechenga rocks have not received much attention internationally because the results of most studies undertaken in the area have been published in Russian. In this paper, the geology of the Pechenga Complex is reviewed, with an emphasis on ferropicritic extrusive and intrusive rocks and related Ni-Cu deposits. Previous results are integrated with the textural, mineralogical, geochemical, and Pb-Pb, Sm-Nd, Re-Os, Rb-Sr, and sulfur isotopic data obtained in this study for ferropicritic rocks, Ni-Cu ores, and other rock types. The Pechenga ferropicrites are compared with other primary magma types, particularly other high-iron varieties described in the literature. The significance of the presence of primary magmatic amphibole in ferropicritic lavas is discussed as a paleodepth indicator. The new isotopic data are used to assess the genesis of the Ni-Cu deposits. Finally, special consideration is given to the mineralogical and geochemical characteristics of the mantle source of ferropicritic magmas. This relies heavily on the interpretation of published high-pressure experimental data on basic to ultrabasic systems.

## HISTORY OF THE PECHENGA ORE FIELD

The first observations of nickeliferous ultramafic rocks in the Pechenga area are recorded in a report from 1913 by the Russian geologist Konradi, as cited by Gorbunov (1968). After the Pechenga region was incorporated into the Finnish territory, in accord with the peace treaty of Tartu concluded between Finland and the Soviet Union in 1920, the Geological Commission of Finland sent an expedition to prospect for possible southerly continuations of the Archean iron ores of the Sydvaranger region in northern Norway. In 1921, the previously unknown volcanic formations of the Pechenga Mountains and the first copper-nickel sulfide occurrences were discovered. Sulfide minerals were observed to be closely associated with the lower parts of ultramafic rocks occurring within a zone of phyllites.

The remote location and arctic conditions of the Pechenga area rendered field investigations slow and laborious. After a period of ten short summer seasons, the Commission completed its exploration in the area in 1934. Although more than ten deposits had been discovered, only the Kaula deposit was regarded as economically promising. The estimated reserves at that time were 1.8 million tons of sulfide ore with 1.6% Ni and 1.3% Cu.

Because of a general distrust of the mining industry and the economic depression in Finland in the 1930's, the Finnish government negotiated a concession agreement with the English Mond Nickel Company, a subsidiary of the International Nickel Company Ltd. (INCO). On the basis of this agreement, the company was permitted to prospect in a 3 km wide and 45 km long zone and to freely exploit metals for the following 40 years. After the concession agreement with the Mond Nickel Co. had been signed in June 1934, a message arrived stating that Finnish explorers had penetrated a rich ore body in the Kaula deposit at a depth of 300 m. This finding upgraded the resources of the deposit considerably. After INCO had undertaken its own test drillings, the amount of ore in the Kaula deposit was shown to be 6 million tons and the grade had improved to 3.9% Ni and 1.7% Cu. The company had planned to start mining operations at Kaula in September 1940; ore was to have been concentrated at Pechenga and then transported to Canada for further refinement, but the beginning of World War II altered these plans.

After Germany's nickel supplies from Canada were discontinued as a result of the war between Britain and Germany, the Pechenga mine, the biggest nickel deposit in Europe, was drawn into an international controversy. In a highly complicated political situation where the keen interest of three big military powers, Germany, Britain, and the Soviet Union, was focussed on Pechenga, Finland signed a contract with Germany in July 1940, according to which the major part of the ore production was to be sold to Germany.

One of the conditions of the peace treaty negotiated between Finland and the Soviet Union in 1944 was that the Pechenga mine and the surrounding territory were to be surrendered to the Soviet Union. Since then, Soviet geological and industrial organizations have continued prospecting and exploiting the metals of the Pechenga ore field.

Exploitation of the ore deposits at Pechenga has continued virtually uninterrupted for half a century. Exact figures for the ore production during the Soviet regime have not been published, but it is obvious that the Pechenga ore zone proved to be much richer than was anticipated before World War II. Apparently, all deposits found by Finnish geologists in the 1920's and 1930's have subsequently been brought into production. According to Zak et al. (1982), of a total of 226 intrusions found in the ore field, 25 contain Ni-Cu deposits of economic interest and 68 are classi-

fied as "potential" with the remaining 133 as "barren". In the Kola superdeep drill hole, which penetrated the Pechenga supracrustal sequence to a depth of more than 6 km, the mineralized zone continues to a depth of at least 1680 m (Genkin et al., 1987).

## BRIEF REVIEW OF PREVIOUS INVESTIGATIONS

The first comprehensive account of the geology of the Pechenga area, the Ni-Cu ore deposits, and their host rocks was published by Väyrynen (1938). He put forward a magmatic model for sulfide ore formation according to which separation of an immiscible sulfide melt had occurred at some depth and its injection had taken place after that of the silicate magma. The first document on the stratigraphy and structure of the whole Pechenga synclinorium was published by Zagorodnyi et al. (1964). Detailed descriptions of various units have since been published by many investigators (e.g., Predovskii et al., 1974) but the general features established by Zagorodnyi et al. (1964) have remained unchanged, including the four sedimentary-volcanic cycles.

A summary of the results obtained in studies of the Ni-Cu deposits during the post-war period was published by Eliseev et al. (1961). G.I. Gorbunov, who has studied the Pechenga area from 1945 to the present, published his classical monograph on the ore deposits in 1968 (Gorbunov, 1968). He gave a thorough review of the genetic models presented for the deposits up until that time, varying from primary magmatic to hydrothermal-metasomatic models. He also provided a detailed description of the various ore deposits and their mineralogical and geochemical characteristics. Gorbunov could not substantiate the earlier concepts invoking independent injections of earlier silicate and later sulfide magmas, but considered that the immiscible sulfide phase, which had separated in a deep-seated magma chamber, was transported by the basic and ultrabasic magma to the surface. The separation of sulfides continued during magma ascent and was completed when syngenetic disseminated ore bodies formed in the lower parts of intrusions. The sulfide masses that separated from the magma at the magmatic stage subsequently remained in a liquid state for a long time after the parent rocks enclosing them had already become crystalline. At the late magmatic stage, a portion of the sulfides broke off from the parent rocks and was injected into fractures by mechanical failure near the lower contacts of ore-bearing intrusions and thereafter separated to form massive and breccia ores and also impregnations of vein-type mineralization in the country rock. Gorbunov (1968) emphasized the presence of intrastratal dislocations which are particularly well developed in the structurally heterogeneous tuffaceous-sedimentary pile and which, according to him, controlled the localization of the nickeliferous intrusions and the copper-nickel sulfide deposits. His model therefore implies that the emplacement of the ore-bearing intrusions occurred simultaneously with the folding.

In their review on the Pechenga ore field, Zak et al. (1982) presented the opinion that only mineralogical changes and negligible migration of ore material had occurred during the autometamorphic (late magmatic) stage and the massive, breccia and vein ores were essentially produced during regional metamorphism. They pointed out the significance of the primary magmatic disseminations, which were prerequisites for the development of rich epigenetic ore bodies during metamorphism, and the intrastratal dislocations which served as structures for magma injection during deformation of the Pechenga synclinorium and as channels for later mobilization of primary sulfides.

A compressional tectonic regime was favoured by Gorbunov et al. (1985a) who stated that the intrusion of ore-bearing magma was asso-

ciated with the initial stages of the progressive crustal shortening. They also regarded the big NE-SW trending Luotna fault (see Fig. 2 and 3) as a major feeding channel for the ore-producing magma.

Recent geochemical and isotopic investigations have yielded new insights on the timing and tectonic setting of the Pechenga nickeliferous intrusions. While the geochemical similarity between the ore-bearing gabbro-wehrlite intrusions and the associated and overlying picritic volcanic rocks had been noted in some earlier works (Predovskii et al., 1974; Zhangurov and Predovskii, 1974), Smolkin (1985) was the first to stress this point. He suggested that the intrusions and the picritic metavolcanites form a genetically related volcano-plutonic association. Later Hanski and Smolkin (1989) demonstrated that the chemical similarity between the picritic metavolcanites and the parental magma of the intrusions extends to both the major and trace elements. They emphasized the exceptionally high iron content of the magma and called it ferropicrite. Recent isotopic results have confirmed the contemporaneous crystallization of the gabbro-wehrlite intrusions and the ferropicritic volcanic rocks (Hanski et al., 1990). Consequently, the emplacement of the Ni-bearing intrusions was closely related in space and time with the volcanism and hence implies an extensional tectonic setting.

## GEOLOGY OF THE PECHENGA COMPLEX

The Pechenga Complex lies at the northwestern end of the early Proterozoic Imandra Varzuga-Pechenga belt, which traverses the Kola Peninsula in a NW-SE direction. Originally, the belt probably formed a continuous sedimentary-volcanic basin developed on the late-Archean granite-gneiss complex, although it is now represented by two separate greenstone belts (Fig. 1). For the stratigraphic correlation between the Imandra-Varzuga and Pechenga belts, the reader is referred to Predovskii et al. (1987) and Sharkov and Smolkin (in press).

The Pechenga Complex has traditionally been divided into two structurally different parts, the Pechenga Series* in the north and the South Pechenga Series in the south. They are separated by the major Poritash fault zone (Fig. 2). Because of the poor exposure and highly deformed nature of the South Pechenga Series, this unit is not well understood at present. As a result, various opinions have been presented with regard to its stratigraphic relation to the Pechenga Series. This paper will concentrate on the Pechenga Series which is well-preserved, well-exposed and, because of its Ni-Cu deposits, of considerable interest.

* As the regional geological data are based upon Russian literature which does not adhere to standard IUGS stratigraphic nomenclature, the Russian stratigraphic classification, including terms such as "series" and "suite", is retained in this paper.

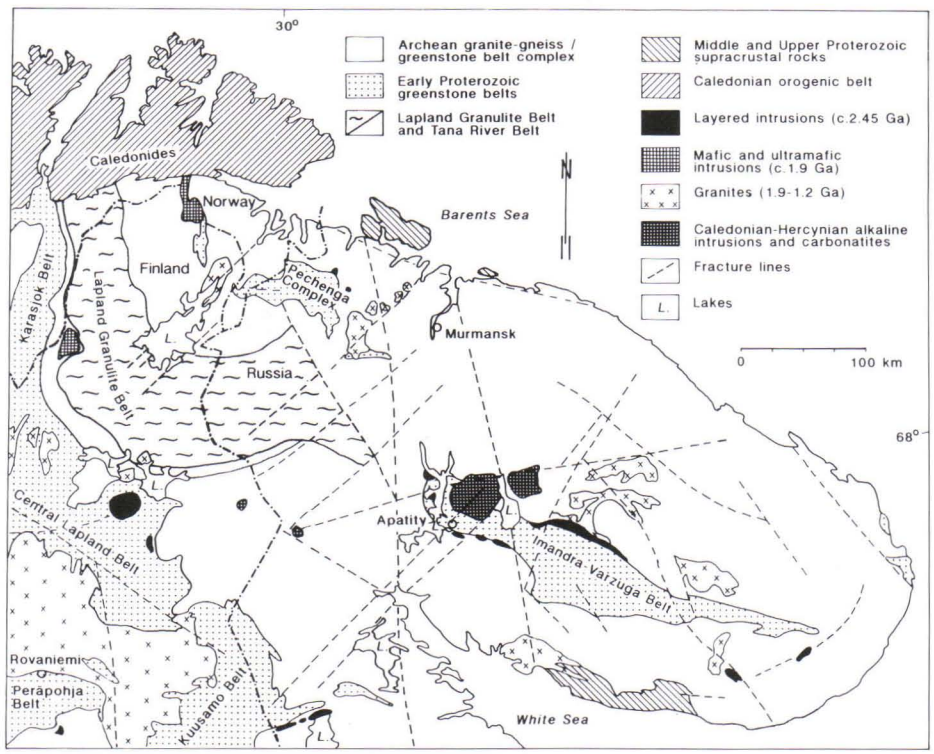


Fig. 1. Geology of the northern part of the Fennoscandian Shield (simplified after the map accompanying Papunen and Gorbunov, 1985).

## Pechenga Series

The Pechenga Series forms a SE-SW dipping (30-60°), asymmetric synclinorium with a length of 70 km and a maximum width of 30 km. The sequence is notable for its great thickness (>8 km), the predominance of volcanic rocks in the strata, and the cyclical repetition of volcanic and sedimentary rocks. The Pechenga Series is divided into four formations with the following names (Zagorodnyi et al., 1964): the Ahmalahti Suite, the Kuetsjärvi Suite, the Kolosjoki** Suite, and the Pilgujärvi Suite. Each of these commences with sedimentary rocks and ends with a much thicker succession of volcanic rocks (Fig. 2). The stratigraphic interpretation based on field observations has been confirmed by the Kola superdeep drill hole which penetrates the entire sequence from the lower part of the Pilgujärvi volcanic formation to the basement complex (Kozlovsky, 1987). Detailed descriptions of each stratigraphic unit are found in Zagorodnyi et al. (1964) and Predovskii et al. (1974). In the following discussion, only salient features are presented, augmented with recent isotopic data, to constrain the age relationships.

** The original Finnish name of the river from which this formation has gained its name is Kolosjoki. In the Russian literature, the name is spelled Колосйоки which has usually been transliterated into English as Kolasjoki with the result that the original Finnish name has been changed. In this paper, the original name Kolosjoki is used.

## Ahmalahti Suite

The Pechenga Series begins with the basal polymictic conglomerates of the Ahmalahti Suite, which were deposited unconformably on the Archean granite-gneiss basement (Fig. 2). The conglomerate unit attains a thickness of 250 m and the clast compositions reflect that of the underlying basement. The conglomerates grade upwards through the section to cross-bedded gravellites and coarse sandstones. The uppermost metasediments are interlayered with tuff material resulting in a gradual transition to the overlying volcanic subunit of the Ahmalahti Suite.

Because of the laterally discontinuous nature of the underlying sedimentary unit, volcanic rocks of the Ahmalahti Suite commonly rest directly on the Archean basement. They consist predominantly of amygdaloidal basalts and andesites but according to Zagorodnyi (1980), small amounts of picritic metaporphyrites are also present in the lower part of the unit. The total thickness of the volcanic sequence is 1100-1300 m.

The rocks of the Ahmalahti Suite also lie on the partly eroded Mt. Generalskaya layered intrusion. A Sm-Nd isochron age of 2453±42 Ma obtained recently by Mitrofanov et al. (1991) for this intrusion can thus be taken as the maximum age limit for the Ahmalahti Suite. Mitrofanov et al. (1991) also reported a Rb-Sr age of 2330±38 Ma for metavolcanites of the Ahmalahti Suite.

## Kuetsjärvi Suite

The sedimentary subunit of the Kuetsjärvi Suite was deposited, without any apparent discordance, on a thin regolith developed on the Ahmalahti metavolcanites (Fig. 2). Like the metasediments of the Ahmalahti Suite, the metasediments of the Kuetsjärvi Suite form discontinuous lenses with a maximum thickness of 250 m. Rock types vary upwards from silty and pelitic schists through hematite-bearing quartzites to dolomites with relict stromatolitic structures. The sequence is capped by tuffitic shales and tuffs, partly picritic in composition. The metasediments of the Kuetsjärvi Suite are characteristically red in color. Stromatolitic carbonates of this formation exhibit positive carbon isotope anomalies ($\delta^{13}C$ 4.6-8.0) which are typical of Jatulian carbonate rocks (Karhu and Melezhik, 1992).

The metavolcanites of the Kuetsjärvi Suite are massive and amygdaloidal lavas having a sodic alkaline affinity. A characteristic feature is the diversity of rock types, which include trachybasalts, trachyandesites, mugearites, albitophyres, and ignimbrites. The middle part of the volcanic sequence contains a thick sequence of tuffs. The total thickness of the volcanic part of the Kuetsjärvi Suite is 800-1100 m. Skufin et al. (1986) have published an imprecise Rb-Sr age of 2150±125 Ma for these metavolcanites.

## Kolosjoki Suite

The sedimentary rocks of the Kolosjoki Suite are separated from the underlying Kuetsjärvi metavolcanites by a small angular unconformity. The metasediments are represented by polymictic rudites and arenites, lenses of polymictic conglomerates with material from the underlying metavolcanites, hematite-rich sandstones, dolomites with stromatolitic structures, and tuffs of mafic and picritic composition. Unlike the carbonate rocks of the underlying Kuetsjärvi Suite, the carbonate metasediments of the Kolosjoki Suite show normal marine carbon isotope signatures (Karhu and Melezhik, 1992).

The upper section of the Kolosjoki Suite forms a thick (up to 1500-1800 m) accumulation of metavolcanites which are rather homogeneous, being composed mostly of tholeiitic pillow lavas and, in the upper part of the unit, tuffs. Some ferropicritic lavas are also present in the lower part of the unit. In addition, a predominantly sedimentary intercalation up to 100 m thick occurs in the middle part of the section, consisting of sulfide-bearing and carbonaceous silts, tuffs, and cherts.

## Pilgujärvi Suite

The thickest formation of the Pechenga Series, the Pilgujärvi Suite, rests conformably on the Kolosjoki Suite (Fig. 2). The geological map of the

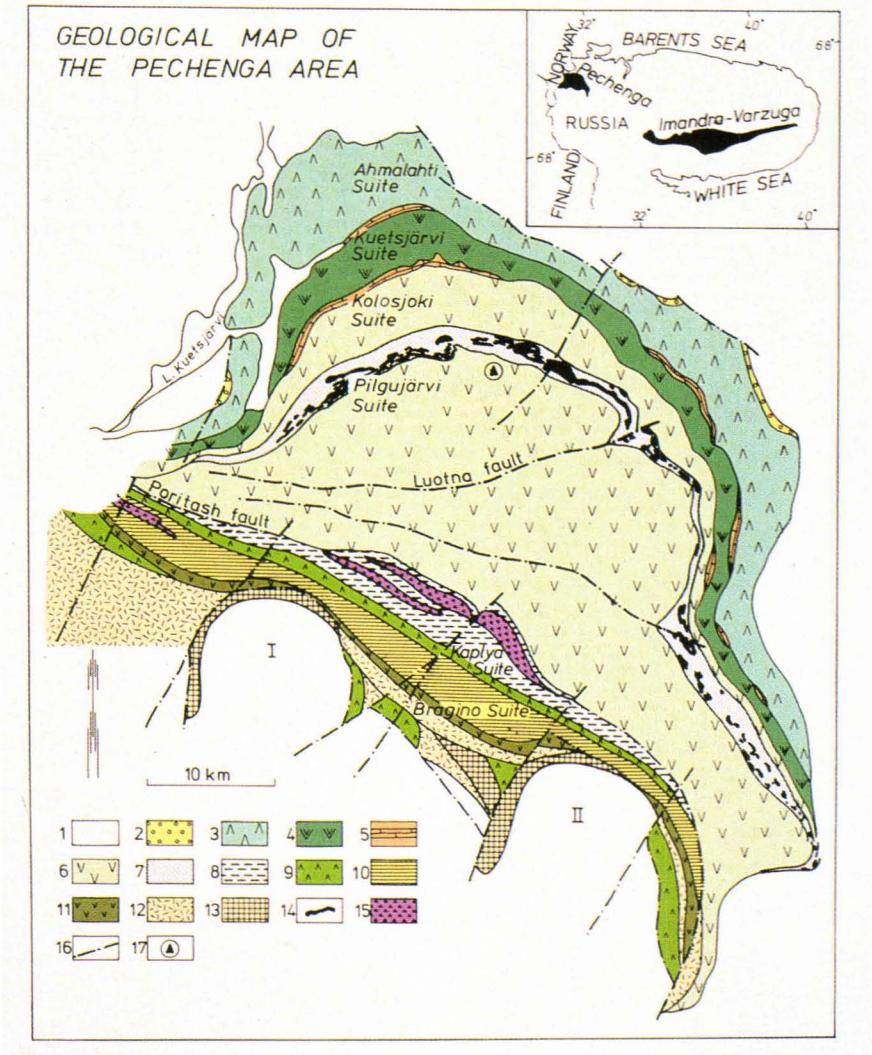


Fig. 2. Geological map of the Pechenga Complex, based upon information from Predovskii et al. (1974), Rusanov (1981), Radchenko (1984), and Kravtsov (1984). Legend: 1, Archean gneisses and schists, Archean and Proterozoic granitoids; 2, conglomerates; 3, andesites and basalts; 4, trachybasalts, trachyandesites, picrites; 5, quartzites, dolomites; 6, basalts, picrites; 7, productive pile (phyllites, sandstones, siltstones, tuffs, tuffites) and gabbro intrusions; 8, graphite-bearing phyllites, dolomites; 9, basalts; 10, psammites, siltstones, sericite schists; 11, picritic tuffs and tuffites, basalts; 12, andesites, dacites; 13, basalts, andesites, dacites; 14, gabbro-wehrlite intrusions; 15, subvolcanic andesites, dacites; 16, faults; 17, superdeep drilling site; I, Suonnu dome; II, Kaskeljärvi dome.

Pilgujärvi Suite is presented in Fig. 3 as reproduced from Rusanov (1981). It begins with a sedimentary unit, which outcrops as a predominantly northwesterly trending arcuate zone, more than 60 km in length. It reaches its maximum thickness of about 1.2 km in the central part of the Pechenga structure while thinning to a few tens of meters in the marginal parts of the synclinorium. The unit consists principally of sandstones, siltstones, phyllites, basaltic and picritic tuffs, and tuffites with sedimentary rocks prevailing in the lower part and tuffs and tuffites in the upper part of the section. The fine-grained metasediments are commonly rich in carbonaceous matter and sulfides. For a more comprehensive description of the sedimentary rocks of the Pilgujärvi Suite, the reader is referred to Predovskii et al. (1974) and Zak et al. (1982).

The sedimentary part of the Pilgujärvi Suite is called 'the productive pile', since the Ni-bearing intrusions are confined to this tuffaceous-sedimentary succession. In addition to nickeliferous gabbro-wehrlite intrusions, sill-like gabbro-diabase intrusions are present, which have been regarded as older than the gabbro-wehrlites (Gorbunov, 1968).

According to Gorbunov (1968), all the major ore-bearing differentiated intrusions and the commercial Ni-Cu deposits associated with them are concentrated in the central part of the ore field. In the western part of this central depression, in the vicinity of the Kaula, Kammikivi, and Ortoaivi deposits, the ore-bearing intrusions occur as a zone at the top of the productive pile close to the overlying volcanic subunit of the Pilgujärvi Suite. In the eastern part of the depression, in the sector containing ore bodies between Kierdzhipori and Onki, the ore-bearing rock masses are located in the lower part of the tuffaceous-sedimentary strata (Zak et al., 1982) (Fig. 3).

The uppermost volcanic unit of the Pechenga Series, which comprises the upper section of the Pilgujärvi Suite, is also the most voluminous stratigraphical unit with a maximum thickness of the order of 2000-2500 m. The boundary against the underlying productive pile is not sharp due to concomitant sedimentation and volcanic activity during the transition period. The volcanic unit is composed predominantly (>90%) of monotonous tholeiitic basalts which occur as massive and pillowed lavas and hyaloclastites. According to Rusanov (1981), picritic metavolcanites, which are marked in black in Fig. 3, make up about 5% of the sequence.

The lithologic variation within the volcanic formation has been described by Rusanov (1981). He divides the section into six members whose boundaries are delineated in Fig. 3. Furthermore, he distinguishes three major fault zones (Luotna, Lammas, and Poritash) which separate the volcanic region into four blocks. All six members are represented in the Kuorpukas (I) and Matert (II) blocks whereas the sections in the Valasjoki (III) and Kuchintundra (IV) blocks are incomplete, extending as far as the fifth and fourth members, respectively (Fig. 3). The metavolcanites of blocks I and II were metamorphosed under prehnite-pumpellyite facies, while both prehnite-pumpellyite and greenschist facies are present in block III and epidote-amphibolite facies prevails in block IV. The proportions of different volcanic rocks in each member are summarized in Table 1.

In the third member, at about 500-600 m above the base of the Pilgujärvi volcanic forma-

Table 1. Volume percentages of various volcanic rocks in different members of the volcanic part of the Pilgujärvi Suite (according to Rusanov, 1981).

| Member | 1 | 2 | 3 | 4 | 5 | 6 |
|---|---|---|---|---|---|---|
| Massive and layered ferropicritic lavas | 7 | - | 2 | - | 3 | - |
| Ferropicritic pillow lavas | 3 | - | 1 | - | 2 | - |
| Ferropicritic tuffs | 1 | - | 1 | - | 1 | - |
| Massive tholeiitic lavas | 60 | 47 | 50 | 57 | 45 | 28 |
| Tholeiitic pillow lavas | 5 | 50 | 30 | 40 | 40 | 70 |
| Basic tuffs with small fragment size | 20 | 3 | 3 | 3 | 2 | 2 |
| Tuffs of basic and hybrid compositions with medium to coarse fragment size | 5 | - | 5 | - | 8 | - |
| Dacite and dacite-liparite porphyries | - | - | 5 | - | - | - |
| Felsic tuffs | - | - | 3 | - | - | - |

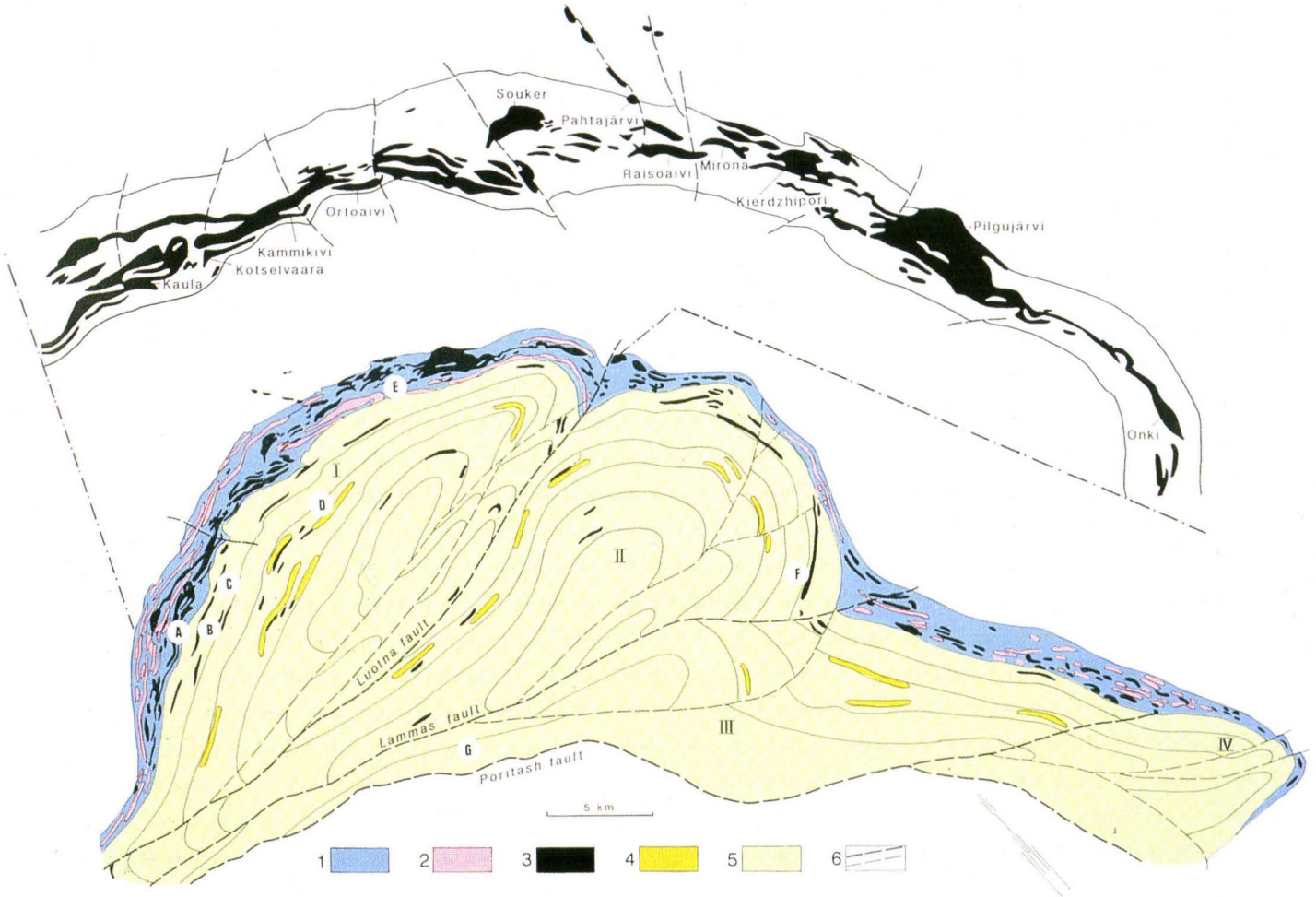


Fig. 3. Geological map of the Pilgujärvi Suite, based upon Rusanov (1981) and Smolkin (1991). Legend: 1; metasediments of the productive pile; 2, gabbro-diabase sills; 3, gabbro-wehrlite intrusions and ferropicritic metavolcanites; 4, ultrafelsic tuffs; 5, tholeiitic metavolcanites; 6, faults; 7, sampling sites. A, drill core S-3R, Kaula; B, outcrop 1684, Kaula; C, outcrop 1685, Kotselvaara; D, Lake Ilya Souker; E, drill core S-2986, Kierdzhipori; F, outcrop 1748, Lammas; G, drill cores S-VI, S-3077, Shuljärvi. Blocks: I, Kuorpukas; II, Matert; III, Valasjoki; IV, Kuchintundra.

tion, ferropicritic metavolcanites and tholeiitic pillow lavas are closely associated with volumetrically negligible but tectonically significant rocks called tufosilitsites by Russian geologists because of their high silica content (Borisov and Smolkin, 1992). They have also been called felsic and ultrafelsic tuffs (Zagorodny et al., 1989) or dacitic and dacitic-liparitic porphyries (Rusanov, 1981), and rhyolites or kagusites (Skufin, 1990). The felsic unit does not exceed 50 m in thickness but it has been traced over many tens of kilometers along strike. Due to its distinctive appearance and composition compared with the surrounding rock types and its restriction to the third member of the volcanic unit, it serves as an ideal marker horizon within the thick volcanic sequence. The felsic supracrustal rock in question is commonly distinctly stratified - including graded bedding - (Borisov and Smolkin, 1992) and varies from an extremely fine-grained, massive or thinly laminated variety resembling obsidian or chert to a coarse fragmental rock with lapilli-size fragments. The fragments consist mainly of euhedral, serisitized plagioclase and feldspar grains, euhedral quartz grains (in places with skeletal forms), and highly vesicular volcanic shards and, most importantly, of granite and granite gneiss fragments.

Utilizing the Sm-Nd method, Hanski et al. (1990) obtained a whole rock-mineral isochron age of 1990±66 Ma for the ferropicritic metavolcanites and gabbro-wehrlite intrusions, while a zircon fraction from the ultrafelsic tuff yielded a minimum U-Pb age of 1970±5 Ma. Mitrofanov et al. (1991) also reported a Rb-Sr isochron age of 1980±44 Ma for tholeiitic metavolcanites of the Pilgujärvi Suite. Younger Rb-Sr isochron ages between 1760±62 - 1790±42 Ma recently obtained for various rock types from the Pechenga Series most likely reflect resetting of this system during regional metamorphism at that time (Balashov et al., 1991).

The sedimentary and volcanic record of the Pechenga Series obviously represents the progressive evolution from shallow-water to deeper-water conditions (Zagorodnyi, 1980). The oldest metasediments of the Ahmalahti Suite on the Archean basement represent alluvial and colluvial fans and talus breccias associated with generally fluviatile deposits while the amygdaloidal nature of the initial volcanism indicates eruption under subaerial conditions. The deposition of the sediments of the next cycle took place in a shallow, presumably intracontinental basin under relatively tranquil conditions. The predominance of amygdaloidal and massive structures over pillows in the overlying metavolcanites of the Kuetsjärvi Suite suggests that the volcanism was still mainly subaerial at this stage. The transition to a deeper-water regime took place during the deposition of the next, transgressive quartzitic and calcareous sediments comprising the sedimentary part of the Kolosjoki Suite, followed by a thick sequence of pillow lavas of the same suite. There are differing opinions on the ultimate amount of basin subsidence. Namely, some authors argue that the deposition of the tuffaceous-sedimentary rocks of the productive pile took place in a relatively shallow, quiescent basin which was followed by a regressive stage related to the subsequent volcanism (Zagorodnyi, 1980). According to some others, eruption of the volcanites of the Pilgujärvi Suite took place in a marine basin at a substantial water depth (Smolkin, 1991).

With respect to the regional stratigraphic scheme of Lower Proterozoic deposits in the Fennoscandian (Baltic) Shield, the Ahmalahti, Kuetsjärvi, Kolosjoki, and Pilgujärvi Suites have been correlated respectively with the Sariolian, Lower Jatulian, Upper Jatulian, and Ludicovian formations (Predovskii et al., 1987). The geological position and lithological character as well as the age of the Ahmalahti Suite metavolcanites are reminiscent of the lowermost units in the Peräpohja schist belt in northern Finland, where conglomerates were deposited on 2.44-Ga-old layered intrusions and are overlain by metavolcanites with a Sm-Nd age of 2330±180 Ma (Huhma et al., 1990). As noted earlier, the carbon isotope results on the carbonate rocks of the Kuetsjärvi Suite are compatible with the results of Jatulian carbonates elsewhere in the Fennoscandian Shield, but the normal marine values for carbonates from the Kolosjoki Suite makes the correlation of this unit

with Jatulian formations more problematic (Karhu and Melezhik, 1992). As was pointed out by Hanski et al. (1990), the age of the uppermost metavolcanites of the Pechenga Series approximates, within the error limits, that of ophiolitic rocks close to the southwestern margin of the Archean craton in the Jormua and Outokumpu areas (Kontinen, 1987; Huhma, 1986).

## South Pechenga Series

As noted earlier, a high degree of tectonic and metamorphic reworking combined with inadequate exposure have made it difficult to firmly establish the stratigraphy of the South Pechenga Series. However, several different rock units can be discerned. Proceeding to the south from the Poritash fault zone, Kravtsov (1984) distinguished the following units: The section begins with graphite-bearing phyllites containing chert, dolomite, and relatively rare conglomerate lenses. These rocks are succeeded by basalts occurring as porphyrites, pillow lavas, and tuff breccias. Kravtsov (1984) assigned the above mentioned rock series to the Kaplya Suite. This suite is overlain by the Bragino Suite which begins with rhythmically alternating psammites and siltstones containing rare andesitic and basaltic intercalations. They are followed by a sequence of picritic tuffs and tuff breccias with varying amounts of basic metavolcanites. These in turn are succeeded by tuffs and lavas of intermediate and acid composition including the Porojärvi volcanic dome structure (Skufin et al., 1988). The southernmost unit comprises pillowed or amygdaloidal basic metavolcanites.

Kravtsov (1984) regarded the above mentioned succession as stratigraphically coherent with the oldest rocks occurring in the north and the youngest in the south. The correlation of the South Pechenga Series with the Pechenga Series is nevertheless still an open question. Golubev et al. (1984) considered the northernmost phyllites to be analogs of the productive pile. Balashov et al. (1991) have obtained a Rb-Sr isochron age of 1970±82 Ma for basalts and andesites of the Porojärvi structure, which broadly corresponds to that of the Pilgujärvi Suite. On the other hand, there exist rock types in the South Pechenga region that are unknown or rare in the Pechenga Series including abundant andesites and dacites (Skufin et al., 1988) and high-silica picrites enriched in LIL-elements (Skufin and Hanski, unpublished data).

The youngest rocks of the South Pechenga region are subvolcanic andesite porphyries which intruded along the Poritash Fault Zone after the main phase of movement; for these rocks Balashov et al. (1991) reported a Rb-Sr age of 1770±42 Ma.

# FIELD CHARACTERISTICS AND PETROGRAPHY OF FERROPICRITIC METAVOLCANITES

Ferropicrites are ultramafic volcanic rocks with high abundances of MgO and total iron (Hanski and Smolkin, 1989).

By analogy with the proposals of Arndt and Nisbet (1982) for the komatiite terminology, rocks petrogenetically related to ferropicrite are identified with the prefix ferropicritic even though some evolved varieties, for example in layered lava flows, are rather felsic, plagioclase-rich rocks. The same prefix is also used for intru-

Fig. 4. Photomicrograph of texture in a massive lava, Shuljärvi area, sample S-3077/322.5. Olivine phenocrysts (now serpentine) set in a groundmass of serpentinized olivine microlites, devitrified glass and fine-grained pyroxene. Width of field 3.0 mm, plane-polarized light.

Fig. 5. Photomicrograph of texture in a pillow lava, Shuljärvi area, sample S-3077/E. Olivine phenocrysts (now serpentine) set in a groundmass of serpentinized olivine microlites, devitrified glass and fine-grained pyroxene. Width of field 3.5 mm, plane-polarized light.

sions generated from magmas compositionally similar to ferropicrite.

Ferropicritic volcanic rocks have been encountered in both the Kolosjoki and Pilgujärvi Suites with the majority occurring in the latter formation. A sequence of ferropicrites about 30 m thick was penetrated at the base of the Kolosjoki Suite during the superdeep drilling program but here they are metamorphosed to actinolite-chlorite schists.

Ferropicritic volcanic rocks are mostly concentrated at four stratigraphic levels in the Pilgujärvi Suite, i.e., in the upper part of the productive pile and in the lower, middle, and upper part of the volcanic unit. They occur as massive lava flows, pillow lavas, tuffs, and thick, layered lava flows. Tuffs prevail in the productive pile while the relative proportions of pillow lavas and layered lava flows progressively increase upwards through the volcanic part of the Pilgujärvi Suite.

## Massive and pillowed lavas

The extrusive nature of the massive ferropicritic lavas is indicated by their conformable relations with respect to the enclosing sedimentary or volcanic rocks and the absence of contact metamorphic effects on the overlying sedimentary rocks. Furthermore, the upper part of the lavas commonly contain amygdales and cooling cracks and are rich in chloritized glass. In some places, massive lavas grade laterally into pillow lavas (Smolkin, 1991).

Figure 4 shows an example of microscopic textures of massive ferropicritic lavas. These are composed of euhedral olivine phenocrysts set in a brownish groundmass, with phenocrysts ranging from 0.3 to 1.5 mm in size and varying in abundance from a few per cent up to about 30%. The groundmass consists of acicular or hollow, lantern-shaped olivine microlites, feathery to prismatic clinopyroxene and devitrified glass. Olivine is replaced by serpentine, and clinopyroxene, while in some cases almost fresh, has typically been replaced by amphibole of the tremolite-actinolite series. Needles of brown magmatic amphibole are also present, particularly in the varieties of lavas rich in amygdules. The size of the calcite-filled amygdules ranges from 0.5 to 4 mm and their abundance varies between 0-15 volume per cent. The absence of plagioclase or any other felsic mineral means that the rocks under discussion are totally ultramafic, and therefore the term picrite is appropriate in this connection.

Ferropicritic pillow lavas are found mainly in the central part of the Pilgujärvi volcanic formation, where they are exposed, for example, on Dvoinaya Mountain. They have also been encountered in some drill cores as described briefly by Skufin and Fedotov (1989). Pillows display slightly flattened forms and range in size from 0.3 to 1.5 m. The internal structure of the pillows is concentrically zoned due to the presence of amygdules filled with either a chlorite-quartz aggregate or carbonate in the marginal zone, and a textural change from the glass-rich chilled zone to the olivine-porphyritic inner part. Figure 5 illustrates a photomicrograph of the texture in the core zone of a pillow containing olivine phenocrysts in a groundmass of skeletal olivine microlites and plumose pyroxene.

## Layered lava flows with spinifex textures

The most interesting mode of occurrence of ferropicritic rocks is layered lava flows which locally display well developed spinifex textures. Detailed descriptions of spinifex textures in the Pechenga ferropicrites have not previously been published. A short depiction of the layered lava flows is reported by Smolkin et al. (1987) and Hanski and Smolkin (1989). Skufin (1980b) published a photomicrograph of a texture that appears to be a randomly oriented olivine spinifex, but they described it as crystallitic texture. In addition, a reference to spinifex texture can be found in Skufin (1980a), Skufin and Fedotov (1989), and Rusanov (1981). These authors have referred to groundmass textures with needle-like olivines similar to that presented in Fig. 5 as spinifex textures. In this paper however, the term spinifex texture is restricted to textures that are coarse enough to be mesoscopically recognizable according to the recommendations of Arndt et al. (1979).

The layered lava flows are rarely exposed in entirety but have been intersected in many drill cores. Individual flow units normally range in thickness from a few meters to 25 m, but may attain 50 m, and along strike they can be followed from 0.2 to 3.0 km. Figure 6 shows two examples of schematic cross sections of layered lava flows.

A 24-m-thick lava flow was recovered from drill core S-2986 in the Kierdzhipori area. It is enclosed between massive and pillowed tholeiites with a thin veneer of pelitic metasediment above the upper contact zone. The layered Kierdzhipori flow like most of the other layered lava flows has undergone strong post-emplacement differentiation processes. Between the lower and upper chilled margins, three major units can be distinguished, namely, the upper spinifex zone, the middle pyroxene cumulate, and the lower olivine cumulate. Globular rocks are also present in the upper, evolved part of the lava flow; these will be described later.

Another, 16-m-thick layered lava flow, depicted in Fig. 6, was penetrated by drill core S-VI at Shuljärvi in the southwestern part of the Pilgujärvi Suite volcanic formation and is representative of the ferropicrites occurring in the upper part of this unit. The extent of differentiation in this flow is not as high as in the Kierdzhipori flow (S-2986), since even the most evolved portions of the upper spinifex zone are still ultramafic olivine spinifex rocks. This lava flow is overlain by a thick pile of massive ferropicrites and immediately underlain by another layered lava flow, which in turn overlies tholeiitic massive metavolcanites.

Despite the greenschist facies metamorphism, original textures are commonly exquisitely preserved and therefore the emphasis is given to primary features in the following description. Titaniferous primary silicates, such as augite and brown amphibole, kaersutite, are in many cases fresh but olivine is almost without exception replaced by secondary minerals. The contrasting behavior of olivine and pyroxene during metamorphism is illustrated by some samples in which olivine has been replaced by quartz whereas pyroxene is completely fresh.

The lava flows are capped with chilled, fractured flow tops relatively rich in amygdules, although the author has only been able to examine the flow tops in Fig. 6. Figure 7 illustrates the microscopic texture of a sample from the top of the Kierdzhipori flow. In this case, the amygdules range from 0.6 to 2.4 mm in size, occupy 5-10% of the rocks volume, and are filled by calcite and pyrrhotite. The fine-grained groundmass also encloses pseudomorphs of olivine phenocrysts now composed of the same secondary minerals as the amygdules. The groundmass, which originally consisted predominantly of feathery clinopyroxene, is now composed of secondary amphibole and fine-grained sphene.

The development of true spinifex texture in the A zone is variable. In some lava flows, almost the entire A zone is characterized by spinifex texture while some other lava flows contain only scattered portions of spinifex rock with the remainder having a texture that is best described by Lofgren et al.'s (1975) term 'porphyritic-spherulitic'. This term is derived from the porhyritic appearance caused by coarse, commonly skeletal pyroxene grains which are set in a groundmass dominated by fan-like spherulites of plagioclase.

Several different spinifex types can be distinguished and are described below. The randomly oriented olivine spinifex texture is formed by skeletal plates of olivine up to 15 mm in length (Fig. 8). Olivine has totally altered to serpentine. The angular spaces between them are infilled with fine-grained sheaves of augite and devitrified glass. A minor component is brown amphibole which occurs as tiny needles and is difficult to distinguish from the brownish pyroxene and devitrified glass using a normal petrographic microscope but can be recognized more easily under reflected light using a stereomicroscope.

The parallel olivine spinifex texture is the coarsest spinifex type and most easiest to identify in both outcrop and hand specimen. The olivine "booklets" attain several cm in length and impinge obliquely upon each other (Fig. 10). They are formed by 0.1 mm thick, platy crystals which are spaced 0.2-1 mm apart and can be many tens in number. Olivine is not preserved but is everywhere replaced by secondary minerals including calcite, albite, and orthoclase. Pink clinopyroxene occurs as large, skeletal, randomly oriented, prismatic crystals. The interstitial areas between the olivine megacrysts and pyroxene grains are composed of devitrified glass, fan spherulites or skeletal laths of plagioclase, and skeletal crystals

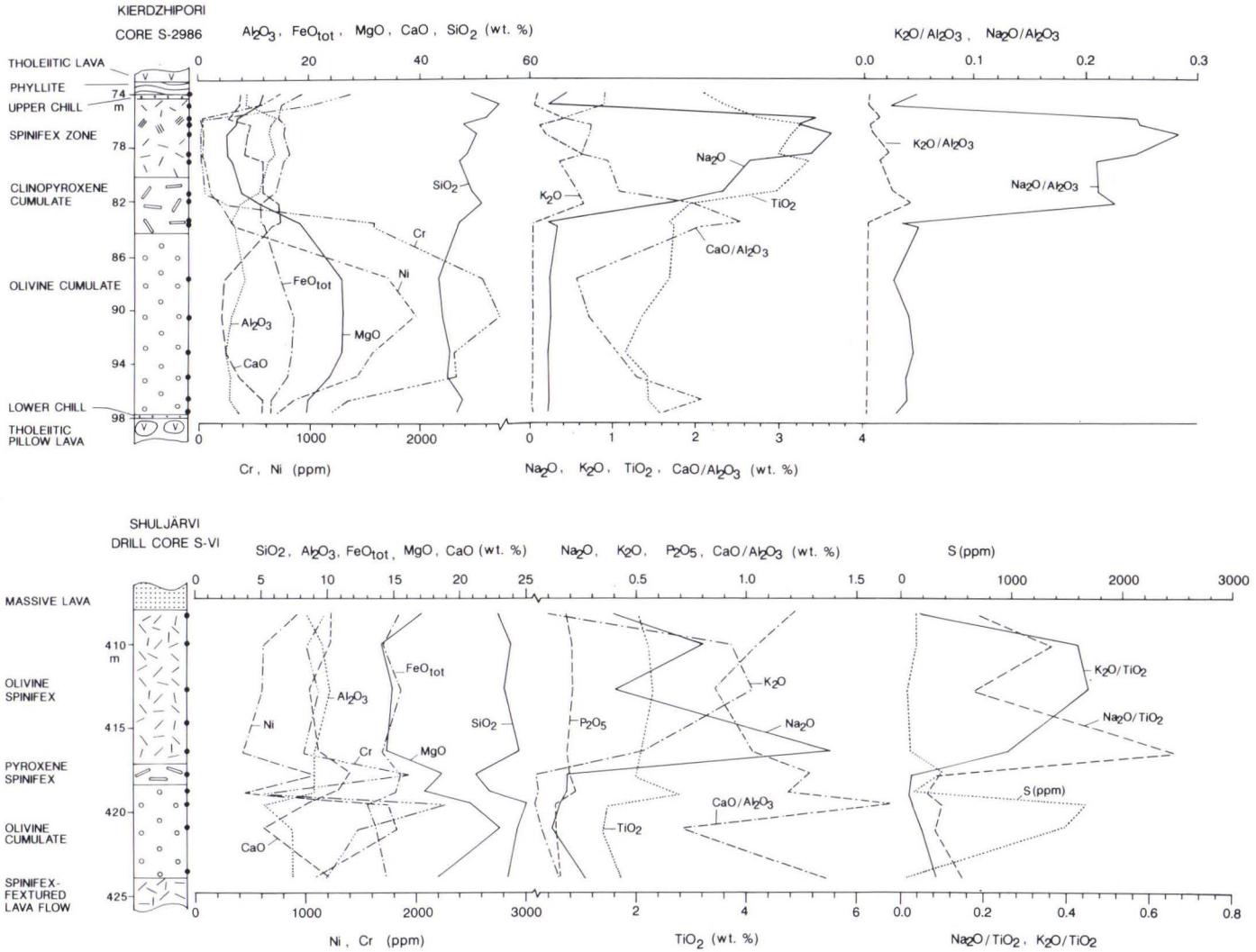


Fig. 6. Rock types and chemical profiles across differentiated ferropicritic lava flows in drill core S-2986 from Kierdzhipori and drill core S-VI from Shuljärvi.

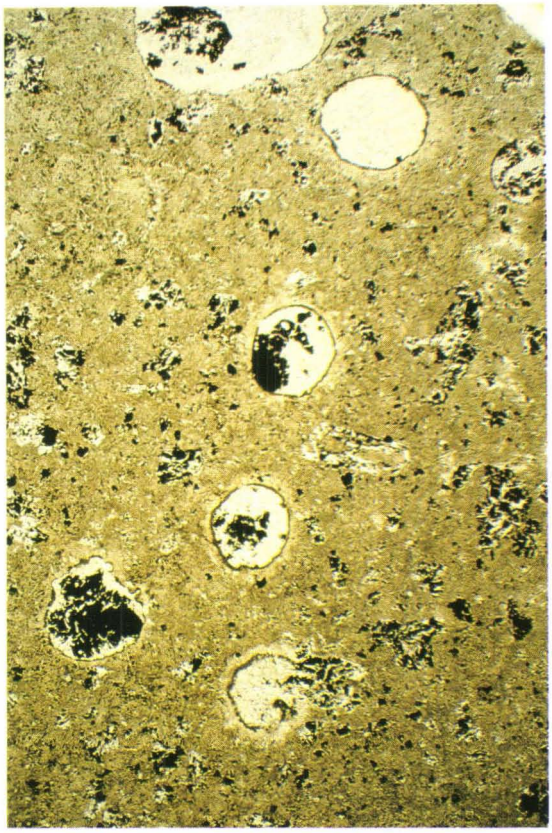

Fig. 7. Photomicrograph of flow top from the Kierdzhipori layered lava flow showing amygdules and olivine phenocrysts respectively filled with and replaced by calcite and pyrrhotite, sample S-2986/74.2. Width of field 7 mm, plane-polarized light.

Fig. 8. Photomicrograph of olivine spinifex texture in layered lava flow from drill core S-VI, Shuljärvi, sample S-VI/416.4. Serpentinized olivine wafers are randomly oriented in a matrix of fine, acicular clinopyroxene and kaersutite grains and devitrified glass. Width of field 1.6 cm, plane-polarized light.

of ferrokaersutite, magnetite, and ilmenite. Oxides nucleated on the olivine plates and now mark the locations of former olivine grains (Fig. 11B). In evolved samples, plagioclase is rather abundant and forms intergrowths with augite.

The ferropicritic rocks containing parallel olivine spinifex textures show some enigmatic features, one of which is their chemical composition, which will be discussed later. The other is related to the mutual spatial relationship between olivine and clinopyroxene and between olivine and plagioclase. Figure 11A shows how parallel olivine grains seem to "cut" across coarse pyroxene grains. The pyroxenes are optically continuous grains on both sides of the olivine plates. The same phenomenon is also observed between olivine and plagioclase in those samples where plagioclase forms relatively coarse crystals. In general, the interstitial spaces between olivine plates in komatiites have crystallized independently on each other as evidenced by differences in the crystal size and orientation of pyroxene grains between individual inter-olivine spaces. However, according to N.T. Arndt (pers. comm., 1991), skeletal chromite grains may extend across several olivine grains in some spini-

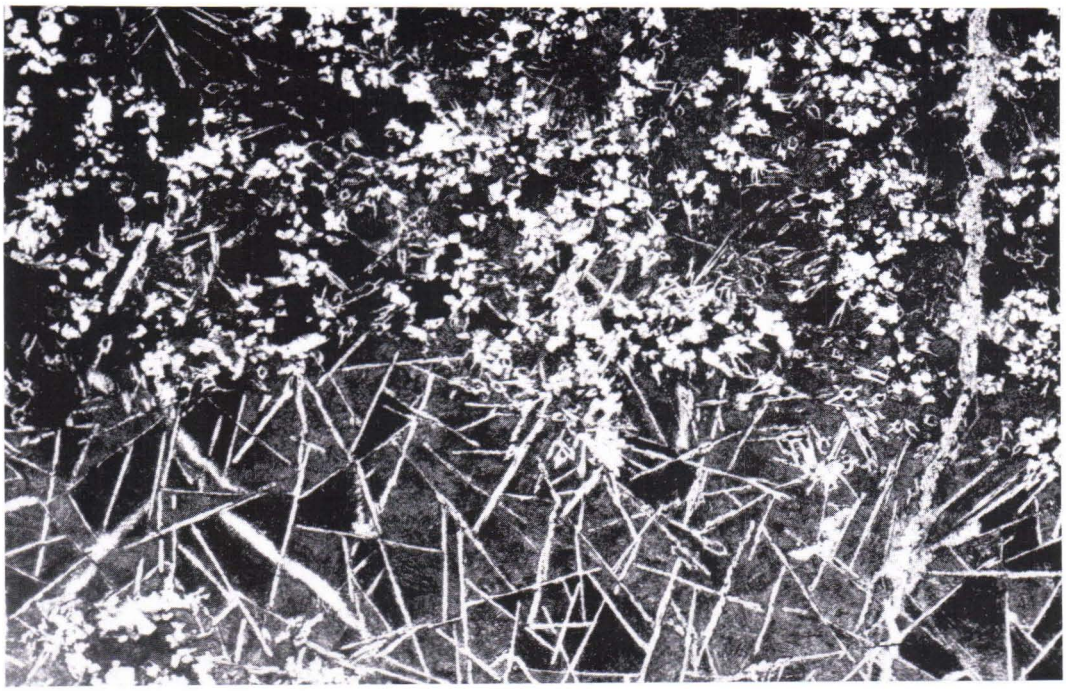

Fig. 9. Transition from olivine porphyritic texture to randomly oriented olivine spinifex texture, Shuljärvi, sample S-VI/410.0. Width of field 2.0 cm, plane-polarized light.

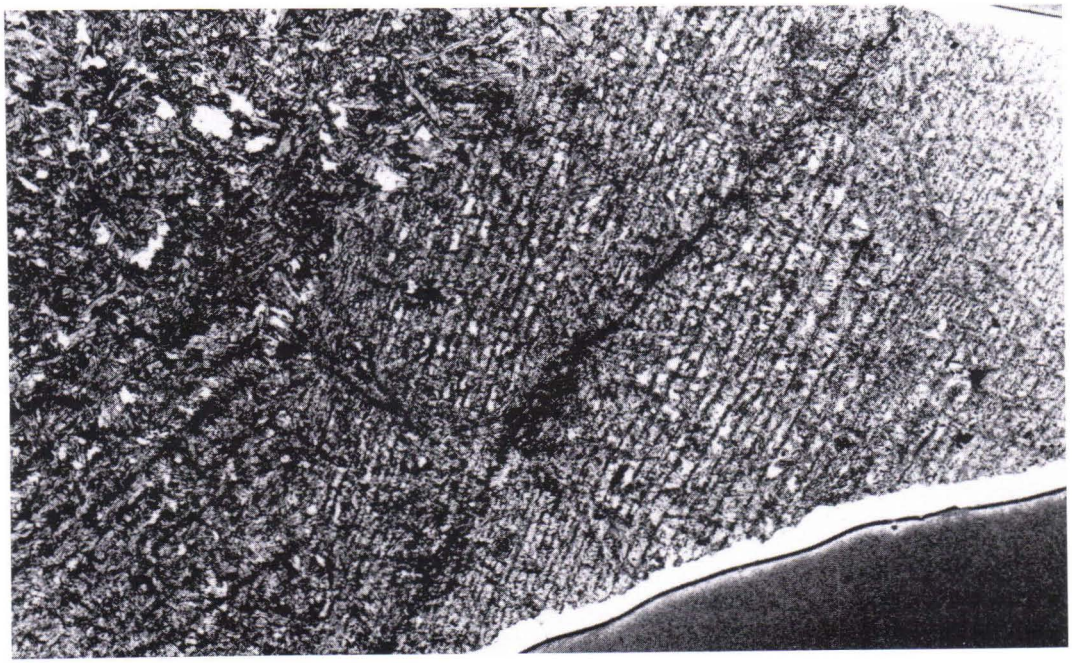

Fig. 10. Photomicrograph of parallel olivine spinifex texture in layered lava flow, Kaula area, sample PS4. Width of field 2.7 cm, plane-polarized light.

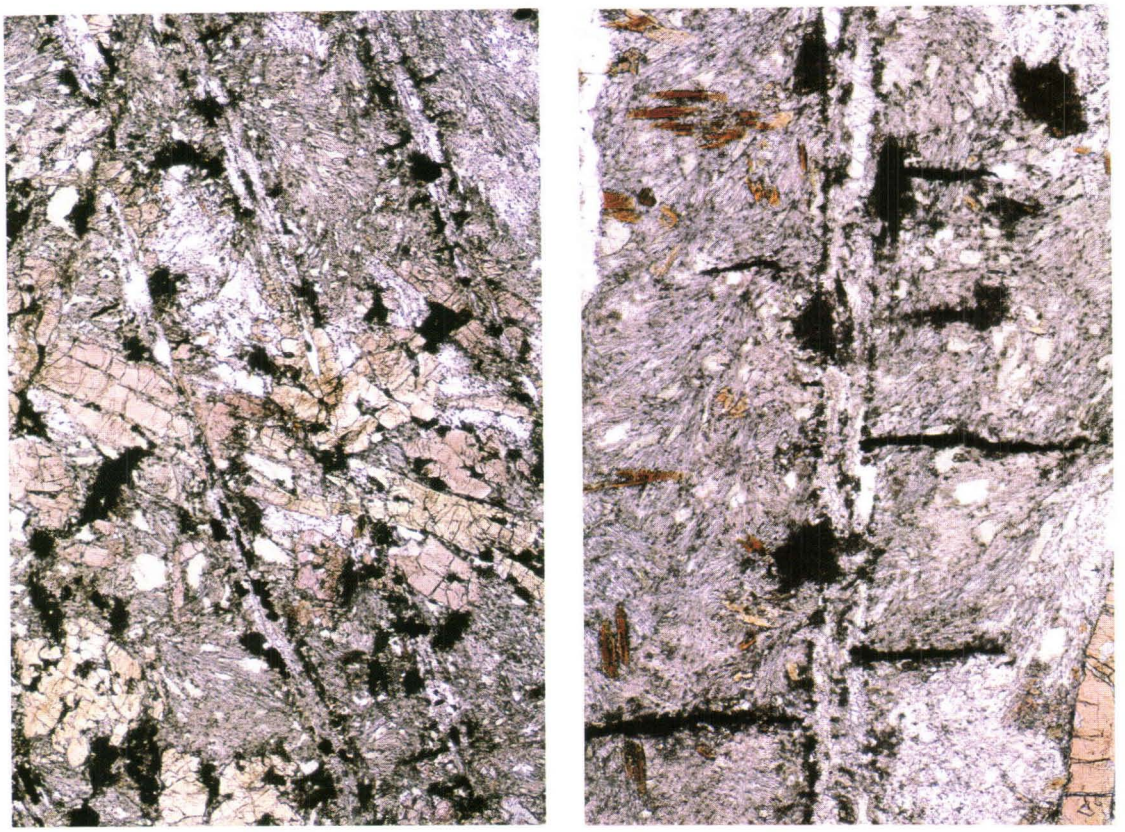

A B

Fig. 11. Photomicrographs of parallel olivine spinifex texture in the Kierdzhipori layered flow, sample S-2986/S. A. Olivine plates (now albite and calcite) "cutting" across a clinopyroxene grain. Width of field 4.4 mm, plane-polarized light. B. A close view of a pseudomorph after platy olivine. Note equant magnetite and needle-like ilmentite crystals nucleated on olivine. Width of field 3.4 mm, plane-polarized light.

fex-textured komatiites. This may indicate that olivine and chromite crystallized simultaneously as highly skeletal grains. The same process might have operated in the Pechenga samples but it would require cotectic crystallization of olivine, clinopyroxene, and plagioclase from an unusually low-MgO melt. As will be shown later in the context of the gabbro-wehrlite intrusions, olivine typically ceased to crystallize before plagioclase appeared as a liquidus phase. The cotectic crystallization of the three phases is also problematic in the light of results of dynamic crystallization experiments showing that the liquidus temperature of plagioclase is suppressed more than that of Mg-Fe-silicates as a function of cooling rate (Walker et al., 1976).

Another problem is to explain why olivine crystallized as oriented sets of tens of parallel crystals while at the same time, pyroxene and plagioclase grew without any preferred orientation. Nevertheless, the intersection of crystals has been duplicated in some high rate cooling experiments.

For example, Grove and Beaty (1980) crystallized an Apollo 11 basalt with a cooling rate of 200 °C/hr and obtained a microporphyritic texture in which skeletal, platy and subparallel ilmenite crystals cut across several pyroxene crystals.

The pyroxene spinifex texture is the most common spinifex type. Although small-grained compared with pyroxene spinifex textures in many komatiitic rocks, the pyroxene spinifex in ferropicrites is easily discernible with the naked eye and consists of parallel, randomly oriented or fan-like bundles of clinopyroxene (Figures 12 and 20). The width of individual pyroxene grains is between 0.05-0.15 mm and their length attains 1 cm. A characteristic feature is the abundance of kaersutite which occurs as epitaxial overgrowths on augite crystals or as discrete, frequently hollow needles in the groundmass. Magnetite occurs as equidimensional grains altered to sphene. Ilmenite is acicular in form and is encountered most abundantly in the vicinity of previous olivine grains analogous to the morphology described for the parallel olivine spinifex rocks. Olivine occurs as randomly oriented or parallel plates and its abundance varies from negligible to the extent that the rock might well be called a parallel olivine spinifex-textured rock. Being totally altered and occurring as sparse and thin plates, olivine is not always easy to distinguish and may be confused with fractures and veinlets. The groundmass in pyroxene spinifex rocks was presumably originally partly glassy and partly composed of pla-

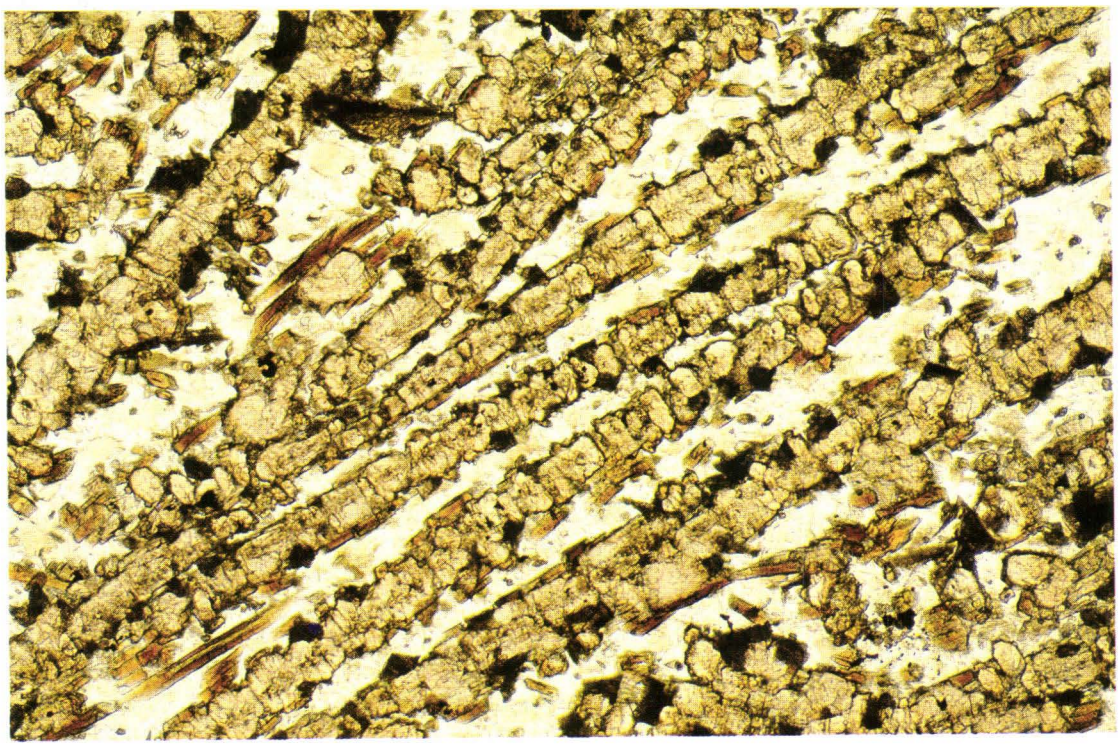

Fig. 12. Photomicrograph of pyroxene spinifex from layered lava flow, Kotselvaara area, sample 1685/2SP. Clinopyroxene needles rimmed by brown kaersutite and set in an albitic groundmass. Width of field 1.8 mm, plane-polarized light.

gioclase. However in most cases, it is now composed of fine-grained chloritic and felsic material generated during secondary processes, producing globular structures as will be discussed later.

As a general rule, the amount of groundmass plagioclase increases at the expense of devitrified glass when going from the flow top downwards in the layered flows. Grain size and morphology of plagioclase also change from small fan spherulites to bigger ones with a concomitant increase in width of individual plagioclase laths. Eventually in the most evolved parts of the lavas, the rock is composed mostly of plagioclase which occurs as tabular, hollow crystals up to 1.5 cm in length (Fig. 13). The order of the change of the plagioclase crystal morphology is compatible with the trends pruduced experimentally with a decreasing cooling rate (Lofgren, 1974; Grove and Walker, 1977). The overall textural variation of the flow units indicates strong heat loss upwards from the interior of the flows.

Pyroxene cumulates in the middle part of the lava flows are composed of stubby or prismatic clinopyroxene grains many of which have amoeboid or ribbon-like cavities and kaersutite rims. Interstitial spaces comprise plagioclase, sphene pseudomorphs of skeletal magnetite grains, and kaersutite needles (Figures 14 and 15). Magnetites rarely display cruciform crystal morphologies similar to those of chrome spinels in the upper part of komatiitic layered lava flows. Euhedral or elongate serpentine pseudomorphs of olivine are also found. The former olivines are easy to distinquish because, despite their total alteration, they frequently contain dark, rounded melt inclusions (Fig. 14).

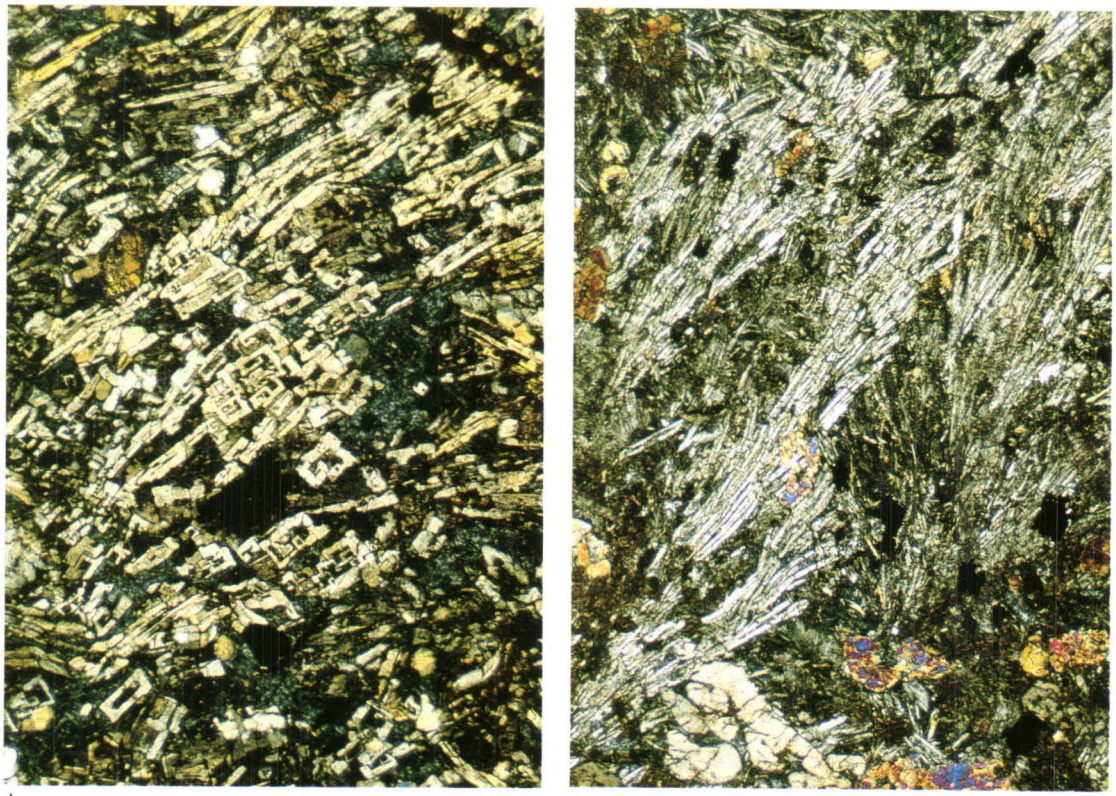

A B

Fig. 13. Photomicrographs of skeletal (A, sample S-2986/76.0) and spherulitic (B, sample S-2986/76.5) plagioclase crystals in evolved part of the Kierdzhipori layered lava flow. Width of fields 3.3 mm, cross-polarized light.

Fig. 14. Photomicrograph of pyroxene cumulate in the middle part of the Kierdzhipori layered lava flow, sample S-2986/82.4. Pyroxene crystals and rarer serpentine pseudomorphs of olivine crystals with rounded melt inclusions (on top) in a kaersutite-rich groundmass. Width of field 3.3 mm, plane-polarized light.

Fig. 15. Back scatted electron image of interstitial space in pyroxene cumulate showing skeletal kaersutites and magnetites, Kierdzhipori layered lava flow, sample S-2986/84.1. Width of field 0.5 mm.

The lower parts of the flow units are formed by cumulates of olivine and minor Ti-rich chrome spinel. The main intercumulus phases are clinopyroxene, kaersutite, and primary mica. The latter mineral is invariably altered but brownish chlorite pseudomorphs indicate the previous presence of titanian phlogopite, which has been encountered as fresh grains in the ultramafic cumulates of ferropicritic sills. From the base upwards, the modal olivine content increases and the morphology of interstitial pyroxene changes from acicular through stubby or prismatic, slightly elongated to poikilitic grains enclosing rounded olivines. As in the overlying pyroxene cumulate, a characteristic feature of olivine grains is the presence of rounded crystallized melt inclusions. The forms of the inclusions are generally well-preserved but they are typically mineralogically altered. Similar inclusions in olivines of the intrusive bodies are in places much better preserved, and therefore a more detailed description will be given in the next chapter.

## Globular rocks

A specific feature of the ferropicritic lavas and some sills and dykes is the presence of well-developed globular structures. These structures have been interpreted to have generated through silicate liquid immiscibility (Smolkin et al., 1987). A detailed account of the globular rocks at Pechenga has been given by Hanski (in press) and only the most salient features are documented in this context.

Globules occur in differentiated varieties of ferropicritic rocks and range from 1 mm to 10 cm in size (Fig. 16). In outcrop, they are clearly distinguishable from their matrix due to their light colors when weathered. Characteristic features include sharp outlines and spheroidal forms of discrete globules and frequent coalescence of globules with sharp cusps being generally retained at the contact of two coalescing globules. In some cases, the globules appear to have accumulated to form layers up to 1.5 m thick (Fig. 17). Figure 18 illustrates an example of a globular dike, less than 1 m in thickness, cutting an ultrafelsic tuff in the Lake Ilya Souker area. This dike is full of globules with an average size of about 1 cm. As is revealed by Fig. 18, these globules can occur close to the contact between the dike and the felsic tuff. Furthermore, Hanski (in press) describes how the globule-forming material fringes the cooling cracks and also forms a band right at the contact with the country rock. These observations provide good evidence of a nonmagmatic origin for the globular structures, as will be discussed later in this paper.

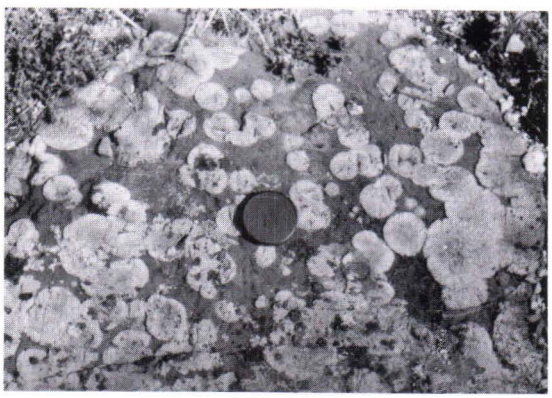

Fig. 16. Globular ferropicrite lava, Lake Ilya Souker area.

Microscopic examination shows that globules are not restricted to rocks of any particular texture or grain size, but they are found in rocks with textures varying from aphanitic to coarse spinifex textures. One common feature, however, appears to be that the mesostatic groundmass in all globular rocks was originally rather rich in glass. Glass is now replaced by chlorite in the matrix and a fine-grained assemblage of albite, orthoclase, and chlorite in the globules. In fact, this difference in the mesostasis is the most essential petrographical dissimilarity between the globules and matrix. As depicted by Figures 19 and 20, the phenocrystal and microcrystal phases are the same and occur in the same proportions in both the globules and the matrix. Furthermore, these minerals have similar crystal habits, sizes and orientations on both sides of the globule-matrix boundary. In other words, the overall textures are identical in the globules and in the matrix.

In globular rocks, the primary crystalline phases are composed of olivine (now replaced by secondary minerals), clinopyroxene, kaersutite, magnetite (replaced by sphene), and ilmenite. With respect to the genesis of the globules, it is important to stress that the more MgO and FeO-rich matrix does not have a higher olivine content than the less mafic globules and that the more alkali-rich globules do not have a higher kaersutite content than the alkali-poor matrix. Also it is noteworthy that plagioclase is not observed to be a liquidus phase in these rocks, but it is confined to the mesostasis of the globules as irregular or spherulitic albitic aggregates. It thus appears that the residual liquid quenched to abundant mesostatic glass before the appearance of liquidus pla-

Fig. 17. Light-colored material forming globules and layers in ferropicritic lava, Kotselvaara area.

Fig. 18. 1-m thick, globular dike in Lake Ilya Souker area.

gioclase.

The textural similarity between the globules and the matrix is most strikingly demonstrated by spinifex-textured rocks where clinopyroxene needles cross the boundary and even traverse the whole globule without any effect upon their abundance, morphology, or orientation (Fig. 20). This is firm evidence for the formation of the globules after the crystallization of the pyroxene needles.

In summary, the phenocryst and microcryst phases are the same in both the globules and the matrix, and the only mineralogical difference is in the fine-grained mesostasis which is chlorite-rich in the matrix and alkali feldspar-rich in the globules. The globular rocks display a great textural variation, but without exception, both the globules and matrix possess identical fabrics.

Fig. 19. Photomicrograph of globule-matrix boundary, Lake Ilya Souker area, sample Souker4/90. Clinopyroxene and magnetite grains set in an albitic mesostasis in the globule (above) and in a chloritic mesostasis in the matrix (below). Note the indistinguishable textures on both sides of the globule-matrix boundary. Width of field 3.3 mm, plane-polarized light.

Fig. 20. Photomicrograph of pyroxene spinifex rock with pyroxene needles extending from the chloritic mesostasis of the matrix (right) to the albitic mesostasis of the globule (left), Kotselvaara area, sample 1685/2SP. Width of field 0.7 cm, reflected light.

## Tuffs

The discovery of ferropicritic tuffs is significant, for they provide conclusive evidence for the existence of a high-MgO liquid from which these rocks were derived, thus excluding the possibility that ferropicrites were merely basaltic melts rich in phenocrystal olivine.

As mentioned earlier, tuffs are widespread in the productive pile but they are also found among the overlying metavolcanites. They occur as lenses and layers varying from a few decimeters to a few meters in thickness, but in some locations, such as the Lammas and Kierdzhipori areas, tuffs form voluminous accumulations up to 400-600 m in total thickness.

Bedding is developed due to alternation of coarse and fine-grained varieties with the grain size of the ferropicrite fragments ranging from a few mm to 1 cm. The fragments are angular in form and they comprise 60-75% of the total volume. The fragments are commonly highly altered but forms of tiny amygdules are still recognized under the microscope. The original minerals have been replaced by talc, chlorite, carbonate, and actinolite. In addition to lava fragments, blocks of country rock which may attain sizes of several decimeters are also present.

## FIELD CHARACTERISTICS AND PETROGRAPHY OF GABBRO-WEHRLITE INTRUSIONS

The gabbro-wehrlite intrusions form about 25% by volume of the productive pile and their areal extent at the present erosional surface is 19 $km^2$. The thickness of the intrusions generally ranges between 5 to 250 m and along strike they can be followed from 100 m to 6.5 km. The largest, Pilgujärvi intrusion, attains a thickness of 540 m (Smolkin, 1977). It is noteworthy that about half of the studied intrusions are less than 20 m thick (Zak et al., 1982). On the basis of their internal structure, the intrusions are divided into differentiated and nondifferentiated bodies, the dimensions of the latter commonly being smaller. In general, gabbro-wehrlite intrusions are concordant with respect to the primary bedding of the enclosing sedimentary rocks. However, according to Zak et al. (1982), the larger intrusions display discordant relationships with the country rocks.

The magmatic cumulates underwent metamorphic and metasomatic alteration to varying degrees, leading to the formation of serpentinites, soapstone, amphibole-chlorite rocks, etc. Nevertheless, the original textures are frequently beautifully preserved and in many places primary minerals are partly or almost wholly unchanged, so that the original cumulus and intercumulus minerals can be recognized or deduced.

The differentiated intrusions have an olivine cumulate at the base passing upwards through a generally thin clinopyroxenite to a gabbroic upper part. The crystallization sequence of the cumulus minerals is generally chrome spinel, olivine, clinopyroxene, titanomagnetite, ilmenite, and plagioclase. As a rule, olivine had ceased to crystallize when plagioclase started to precipitate as a liquidus phase. Orthopyroxene is characteristically absent from every rock type. Primary hydrous minerals, kaersutite, and titanian phlogopite-biotite occur as intercumulus phases throughout the intrusions.

Two examples of the ore-bearing intrusions are described in more detail. These are the intrusive bodies at Pilgujärvi and Kammikivi which represent a large layered intrusion and a thin sill-like intrusion, respectively.

## The Pilgujärvi layered intrusion

The largest Ni-bearing intrusions are located in the central part of the ore field, close to the bottom of the productive pile (Fig. 3). One of them is the Pilgujärvi intrusion investigated in detail by Smolkin (1977). A geological map of this intrusion and a vertical cross section from its northern part are shown in Figures 21 and 22, respectively. The intrusion constitutes two branches separated by a wedge of sedimentary rocks. The southern branch is dominated by gabbroic rocks while the northern branch contains a wider range of rock types. Several Ni-Cu sulfide ore deposits occur in the Pilgujärvi intrusion and in smaller, lense-like intrusions in its SE and NW continuations. In the northern branch of the Pilgujärvi intrusion, Gorbunov et al. (1985b, Fig. 13) distinguished five ore deposits called the Western, Central, Eastern, Southeastern, and Northern deposits (Fig. 21). Most of the ore consists of low-grade sulfide disseminations in the lowermost metaperidotites with smaller amounts of epigenetic sulfides. The Northern deposit is totally epigenetic and is located in a tectonic zone in the country rock metasediments beneath the central part of the intrusion.

The following description concerns the northern branch of the intrusion whose maximum thickness is 540 m. It can be followed for 2.2 km along strike and dips at about 50° to the SW. The country rocks are represented by sandstones, phyllites, and tuffs of the productive pile. As a whole, it is concordant with primary structures in the country rock metasediments, but closer inspection reveals distinct cross-cutting relations in some locations. In the central part of the intrusion in particular, a step-like flexure in the lower contact of the intrusion is present (Fig. 21). Here the contact makes a wide angle with respect to bedding in the metasediments. A chilled zone is observed at the lower contact in the flexure indicating that the contact at this place reflects the primary form of the magma chamber.

The ultramafic rocks occupy the lower third of the intrusion while the upper part is dominated by gabbroic rocks. Smolkin (1977) divided the intrusion into seven zones which are, from the base upwards: the lower marginal zone (I), the wehrlite-olivinite zone (II), the intermediate zone (III), the gabbro-pyroxenite zone (IV), the gabbro zone (V), the essexitic gabbro zone (VI), and the upper marginal zone (VII) (Fig. 23). Boundaries between these zones are mostly gradational and rarely sharp. Primary flow structures such as banding, cross-bedding, and preferred orientation of primary minerals are developed in mafic rocks and less widely in ultramafic rocks. Country rock xenoliths have been found in the gabbroic part of the intrusion, mostly at the contacts between different zones.

The lower marginal zone (I) is present in places that have not been disturbed by tectonic movements, and has a thickness of to 3-3.5 m, although in some places it attains 5 m. When proceeding upwards from the contact, rock types vary as follows: 1-1.5 cm, a zone of intensively altered rock originally composed of glass or fine-grained pyroxene-plagioclase aggregate; 1-50 cm, small to medium grained pyroxenite; 50-100 cm, medium-grained pyroxenite and olivine-bearing pyroxenite; 1.0-3.0 m, olivine pyroxenite transitional into mineralized wehrlite. The zoning in the lower marginal unit is caused by a gradual increase in grain size and the abundance of olivine with increasing distance from the contact.

The thickness of the wehrlite-olivinite zone (II) varies between 60-190 m (average 135 m) and it is not internally homogenous; the lower and upper parts are composed of pyroxenite-wehrlites with a 25-50 vol. % of olivine while the middle part is made up of intercalated pyroxene olivinites (75-90 vol. % olivine) and wehrlites (50-75 vol. % olivine). Zone II is important due to the existence of ore-bearing wehrlites containing interstitial sulfide dissemination in its lower part (Fig. 21). The thickness of mineralized ultramafites varies between 20-75 m. Low grade ore dissemi-

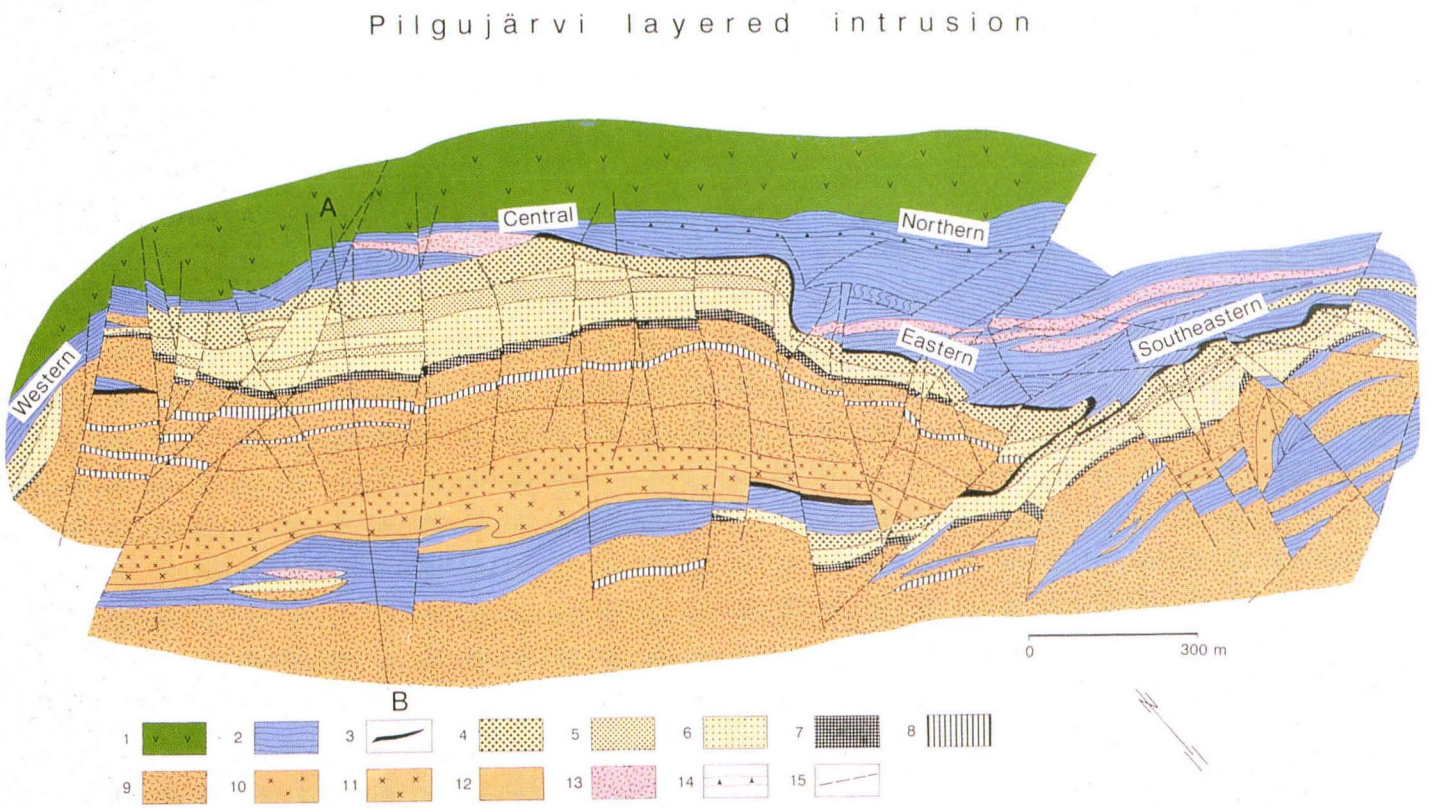


Fig. 21. Geological map of the Pilgujärvi intrusion, modified from Smolkin (1977, 1991). Legend: 1, tholeiitic metavolcanites of the Kolosjoki Suite; 2, metasediments of the productive pile; 3, marginal zones; 4, peridotite with disseminated Ni-Cu ore; 5, wehrlite; 6, olivinite; 7, intermediate zone (olivine pyroxenite, kazanskite, kosvite); 8, pyroxenite; 9, gabbro; 10, coarse-grained gabbro; 11, pegmatitic and essexitic gabbro; 12, diorite; 13, gabbro-diabase; 14, mineralized tectonic zone; 15, fault.

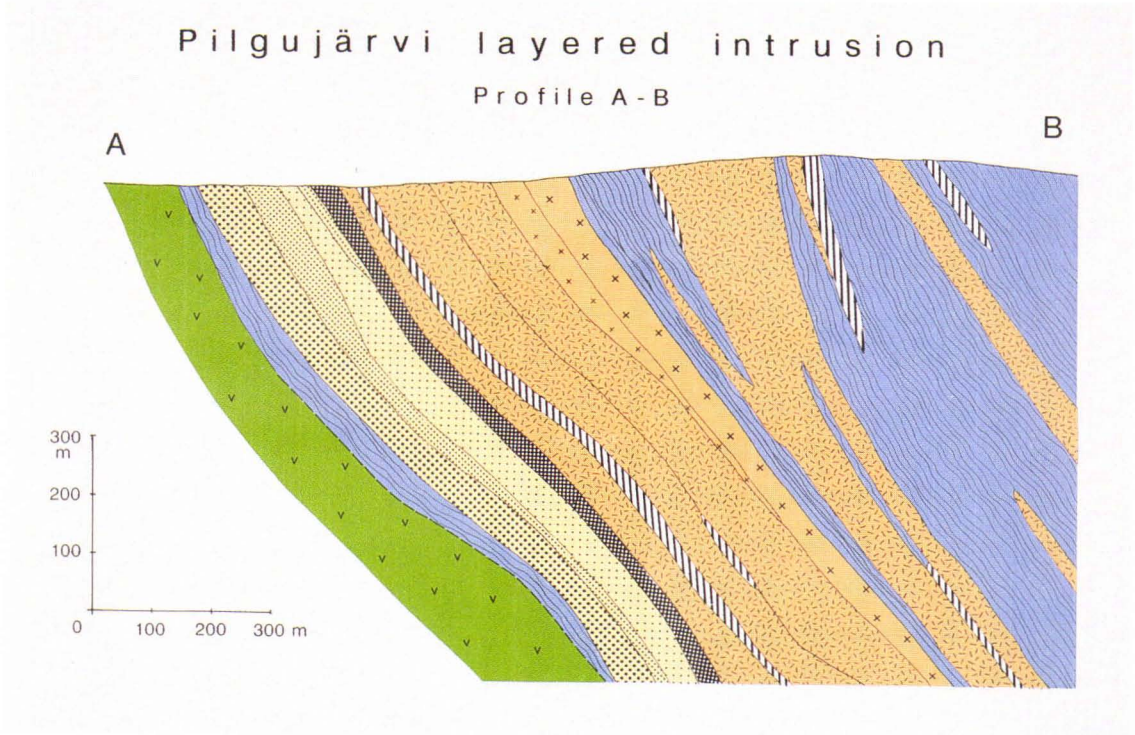


Fig. 22. Vertical profile across the Pilgujärvi intrusion along line A-B (Fig. 21). Ornamentation as in Fig. 21.

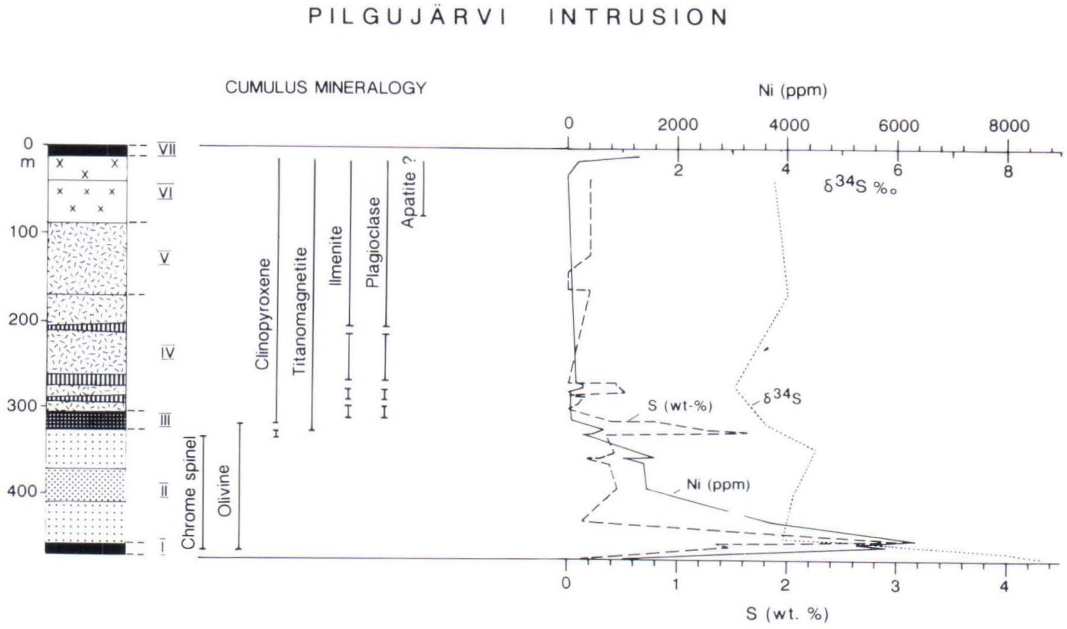


Fig. 23. Cumulus mineralogy and variation of Ni, S, and $\delta^{34}S$ across the Pilgujärvi layered intrusion. Ornamentation as in Fig. 21. Sulfur isotope data taken from Grinenko and Smolkin (1991).

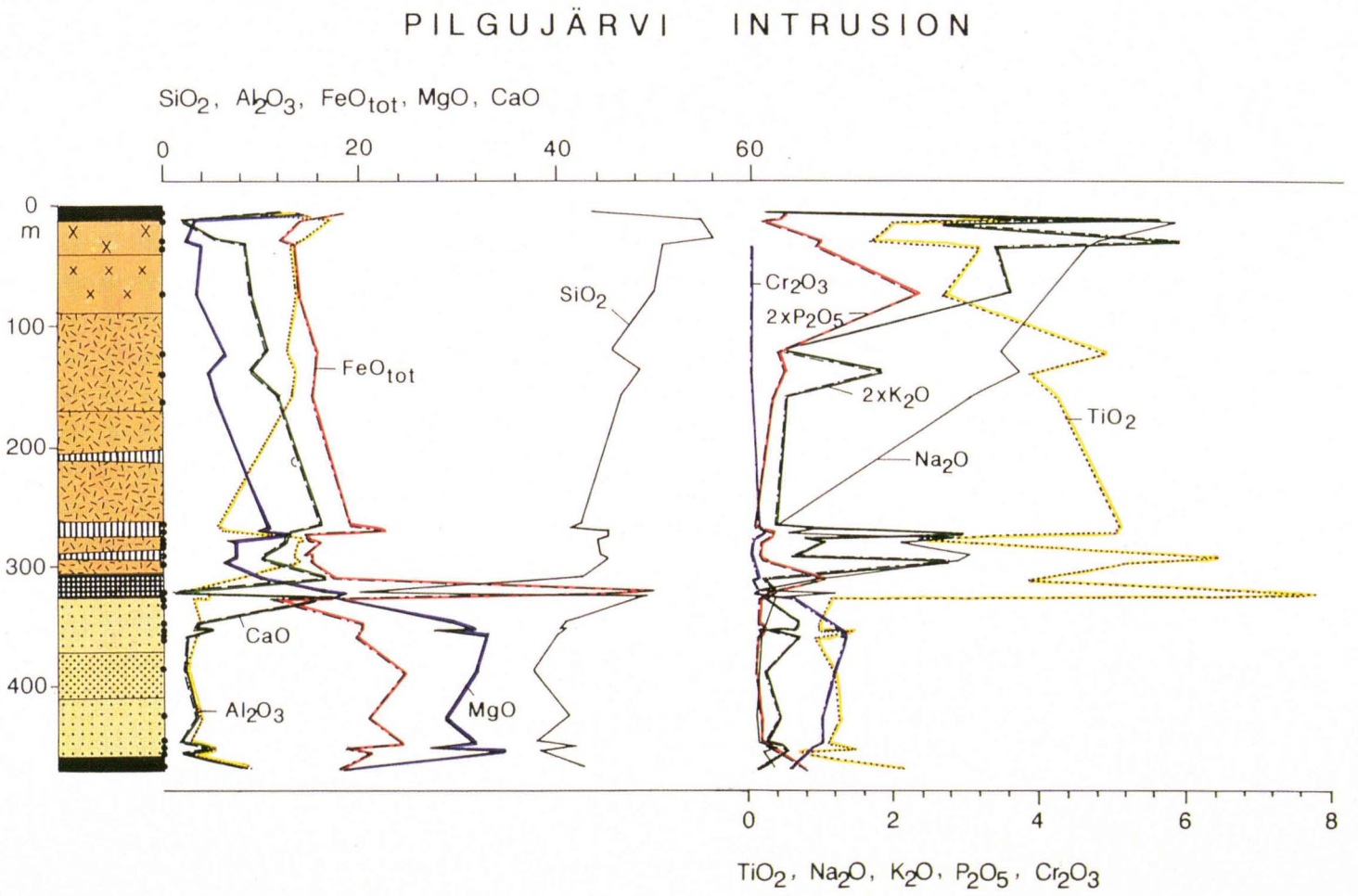


Fig. 24. Variation of chemical components across the Pilgujärvi intrusion.

nations are also found in the upper part of zone II.

Besides modal classifications, it is informative to classify the rocks of layered intrusions according to their cumulus phases (Fig. 23). The cumulus minerals in zone II are olivine and chrome spinel while intercumulus phases consist of clinopyroxene, kaersutitic amphibole, brown mica, plagioclase, and ilmenite. With the exception of ilmenite, they chiefly form poikilitic crystals enclosing olivine grains. Pyroxene oikocrysts in places attain more than 10 mm in diameter, and the enclosed olivine grains are typically rounded. A typical feature of the olivine grains is the presence of spherical or ovoid, crystallized melt inclusions composed mainly of the same minerals as those occupying interstitial spaces, including augite, kaersutite, and phlogopite (Fig. 25). The grain size of the daughter minerals within the inclusions is much smaller than that of the same minerals in the interstitial spaces. This affirms that these are really melt portions trapped inside olivine crystal and not embayments in olivine crystals exposing underlying intercumulus phases (cf. Roedder and Weiblen, 1971).

The intermediate zone (III) forms a transition layer between the ultramafic and mafic rocks. Its general thickness varies between 8 - 16 m, and infrequently up to 29 m. Three subzones can be distinguished which are, from the base upwards: 1) pyroxenites and olivine pyroxenites with rare lenses of wehrlites, plagiopyroxenites, and gabbro (average thickness 6.3 m); 2) kazanskites and

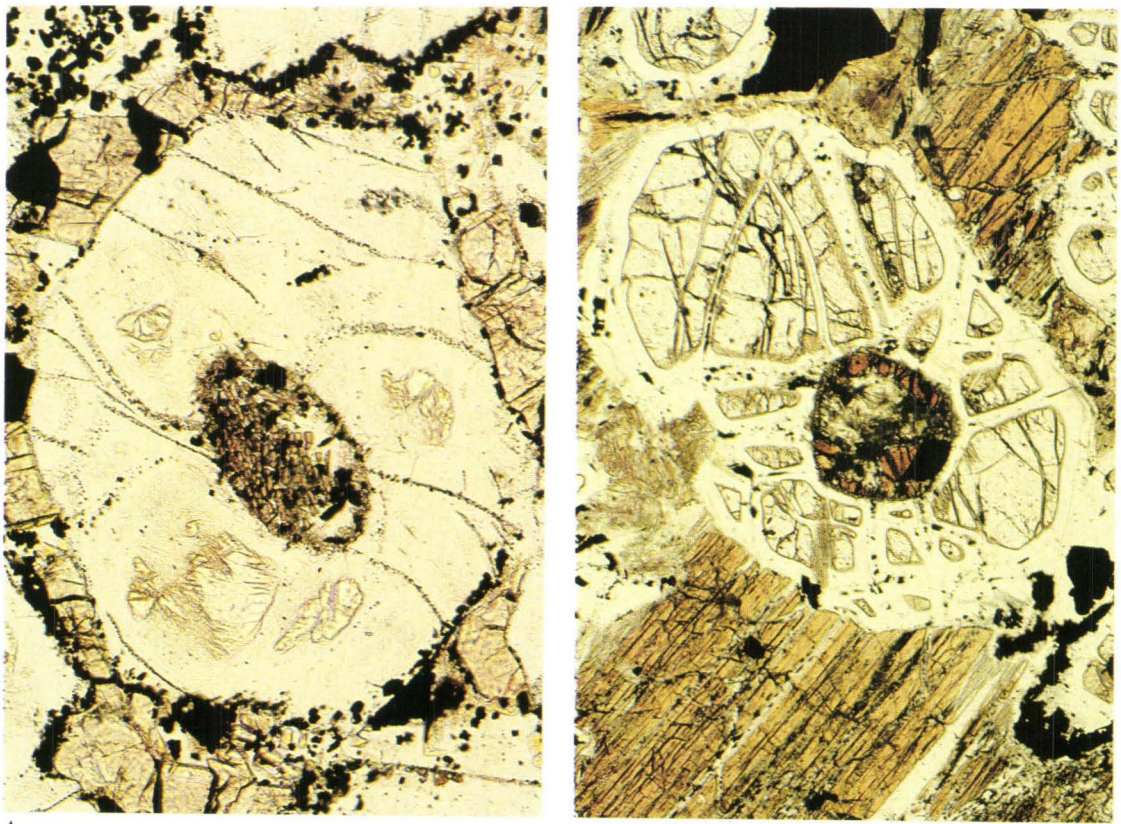

A B

Fig. 25. Photomicrographs of crystallized melt inclusions in olivines. A. Almost totally serpentinized olivine with a melt inclusion composed of augite microlites, Kammikivi sill, sample Pet1/33.00. Width of field 0.5 mm, plane-polarized light. B. Partly serpentinized olivine with a melt inclusion composed of kaersutite, Ortoaivi intrusion, sample 0-HV-1928. Intercumulus space filled with more coarse-grained kaersutite. Width of field 0.5 mm, plane-polarized light.

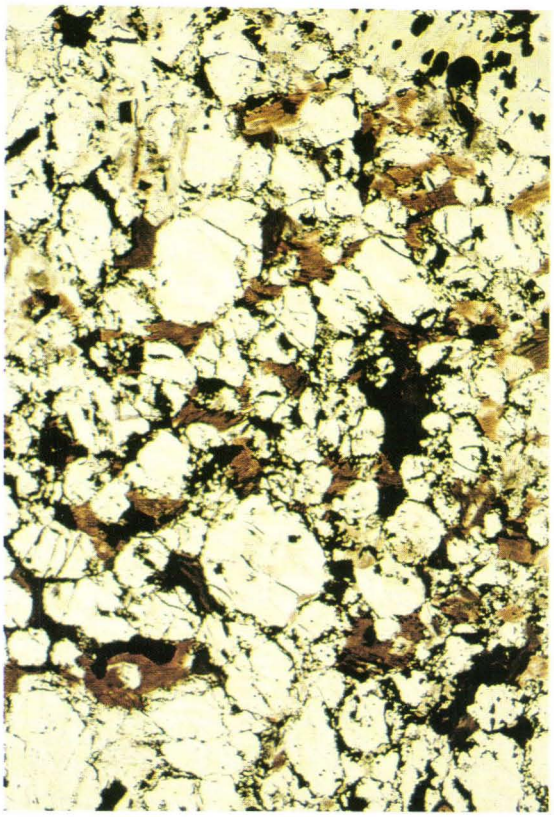

Fig. 26. Photomicrograph of serpentinized peridotite with intercumulus phlogopite, Ortoaivi intrusion, sample 3401-UJ-1935. Width of field 3.3 mm, plane-polarized light.

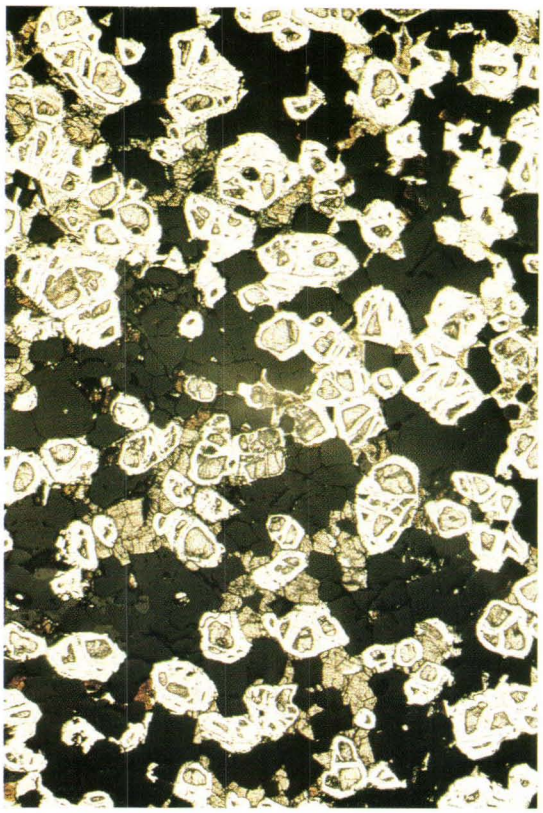

Fig. 27. Photomicrograph of partly serpentinized olivine-magnetite mesocumulate (kazanskite) from the intermediate zone of the Pilgujärvi intrusion, sample PJ9. Width of field 3.3 mm, plane-polarized light.

kosvites which form a magnetite ore layer (average thickness 4.7 m); 3) plagiopyroxenite and titanomagnetite-rich plagiopyroxenite with rare gabbro pegmatite dikes (average thickness 3.0 m). By kazanskite, Smolkin (1977) denoted a pyroxene olivinite or wehrlite exceptionally rich in titanomagnetite ($FeO_{tot}$ >30 wt. %) (Fig. 24). Kosvite in turn is an olivine pyroxenite with a high content of titanomagnetite ($FeO_{tot}$ >20 wt. %). Other intrusions in the Pechenga area are not known to contain exact equivalents of the kazanskites and kosvites of the Pilgujärvi intrusion.

The lower subzone of the intermediate zone is an olivine-pyroxene mesocumulate. The amount of olivine is subordinate compared to that of pyroxene. Intercumulus phases are brown amphibole and mica and ilmenite. Kazanskites of the middle subzone are olivine-titanomagnetite cumulates containing clinopyroxene, kaersutite, and phlogopite as intercumulus phases (Fig. 27). The least magnesian olivine (Fo 68.2%) so far analysed in the Pechenga intrusions occurs in this zone. The cumulus phases in kosvites are clinopyroxene and titanomagnetite, and the main intercumulus phases amphibole, mica, and plagioclase. The upper subzone (plagiopyroxenite) is mineralogically similar to kosvite except having a lesser amount of magnetite. Olivine may occur as

an accessory phase in both kosvites and plagiopyroxenites.

The thickness of the gabbro-pyroxenite zone (VI) varies between 110-175 m with an average value of 141 m, thus constituting about one third of the volume of the intrusion. A characteristic feature of this zone is the rhythmic interlayering of plagiopyroxenite and gabbro. The thickness of the alternations varies from 20 to 50 m. Plagiopyroxenites are pyroxene-titanomagnetite cumulates while gabbros are plagioclase-pyroxene-titanomagnetite-ilmenite cumulates. Intercumulus phases in these rocks are brown amphibole and mica augmented with plagioclase in pyroxenites. In gabbros, ilmenite and titanomagnetite form separate oxide phases. Preferred orientation of ilmenite plates together with plagioclase laths impart a foliated texture to the rock. Olivine gabbro has been found in the lower part of the gabbro-pyroxenite zone in rare instances. In general, olivine and plagioclase do not coexist as liquidus phases in the gabbro-wehrlite intrusions.

The thickness of the gabbro zone (V) is between 40 and 110 m (average 86 m). This zone exhibits a rhythmic alternation of banded and trachytoid gabbro with rare interlayers of pyroxenite or essexitic gabbro. Mineralogically, the zone is similar to the gabbros of the underlying IV zone.

The evolved part of the intrusion forming the essexitic gabbro zone (VI) varies from 25 to 125 m in thickness (average 93 m). Two subzones are distinguished: the lower one comprising coarse-grained, massive, mesocratic gabbro with a characteristic "stellate" structure and the upper one represented by heterogeneous, locally pegmatoidal, meso-leucocratic gabbro and essexitic gabbro. The stellate structure is caused by the growth of plagioclase laths in star- or cross-like forms. The cumulus phases in the zone are the same as in the gabbro zone except for the possible addition of apatite. Intercumulus phases comprise amphibole, mica, and quartz. Potassium feldspar occurs mostly as antiperthitic exsolution lamellae in the outer zones of plagioclase crystals but it may also form separate, anhedral grains, and comprises at its maximum about 15% of the rock.

The upper marginal zone (VII) against the hanging wall phyllite is a heterogeneous unit composed of quartz diorites, pyroxenites, plagiopyroxenites, and hornfelsed country rock fragments. This zone is commonly 1.0-1.5 m thick but occasionally attains a thickness of 8.0 m. Pyroxenite, which represents the proper upper chilled zone, varies from small to medium-grained and is composed mainly of acicular to prismatic clinopyroxene. It can also contain a notable amount of kaersutite and a weak sulfide dissemination. Quartz diorite is composed mainly of plagioclase, clinopyroxene, and potassium feldspar with minor amphibole and quartz. It forms a discontinuous zone of complex-shaped injections in the quench zone pyroxenite and contact hornfels.

## The Kammikivi layered sill

The Kammikivi layered sill is located in the western part of the ore field (Fig. 3). Figure 28 presents a schematic cross section through the body. This section was constructed on the basis of a drill core obtained by Finnish geologists in the 1920's (see Väyrynen, 1938, Fig. 52). Unfortunately, the drill core studied did not penetrate the upper contact but it begins from the gabbroic part of the body. Nevertheless, the textural evidence suggests that the uppermost rock penetrated was not far from the upper contact of the magmatic body. On the other hand, the lowermost portion of the body, containing a Ni-Cu ore deposit, was well represented in the core.

Both the footwall and hanging wall rock of the Kammikivi layered body is S-poor phyllite in the section studied in this work. Here, the thickness of the intrusion is about 40 m. The densely disseminated ore at the base (Fig. 29) varies in thickness, being about 5 m at its maximum.

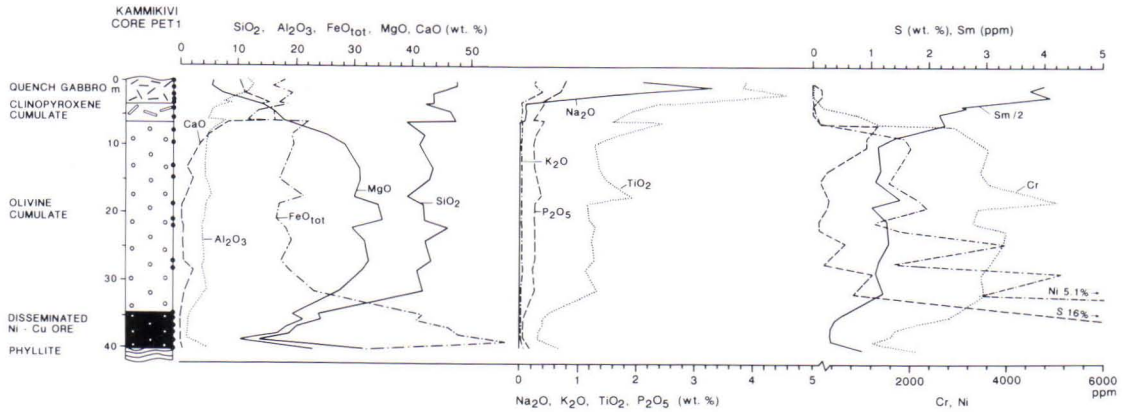


Fig. 28. Stratigraphic profile and chemical variation across the ore-bearing Kammikivi layered sill.

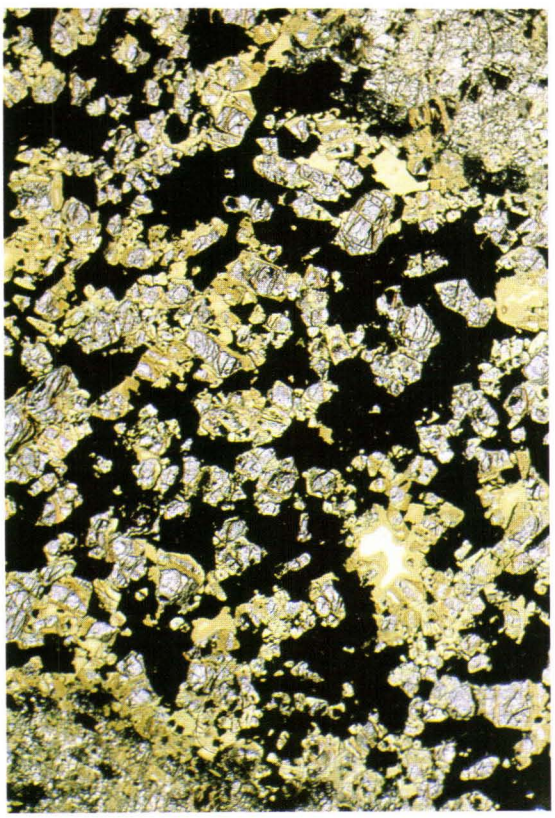

Fig. 29. Photomicrograph of the disseminated Ni-Cu ore containing serpentinized olivine and intercumulus sulfide from the Kammikivi sill, sample Pet1/40.60. Width of field 7.0 mm, plane-polarized light.

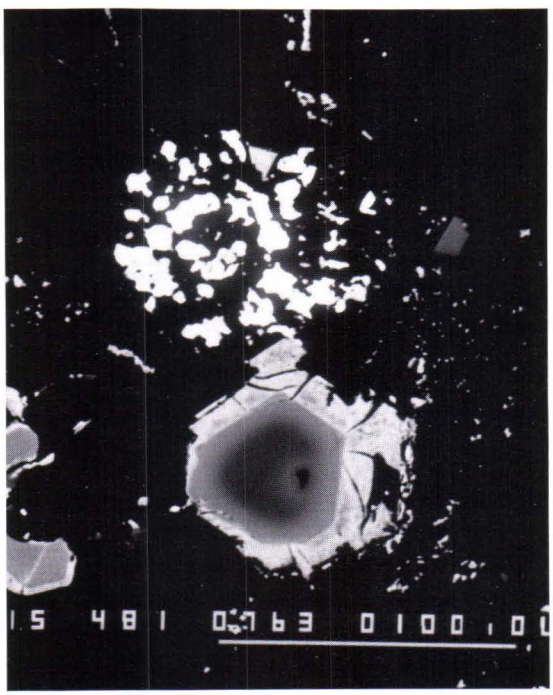

Fig. 30. Back scattered electron image of a zoned chrome spinel and disintegrated sulfide droplet from the middle part of the Kammikivi sill, sample Pet1/25.66. Width of field 0.2 mm.

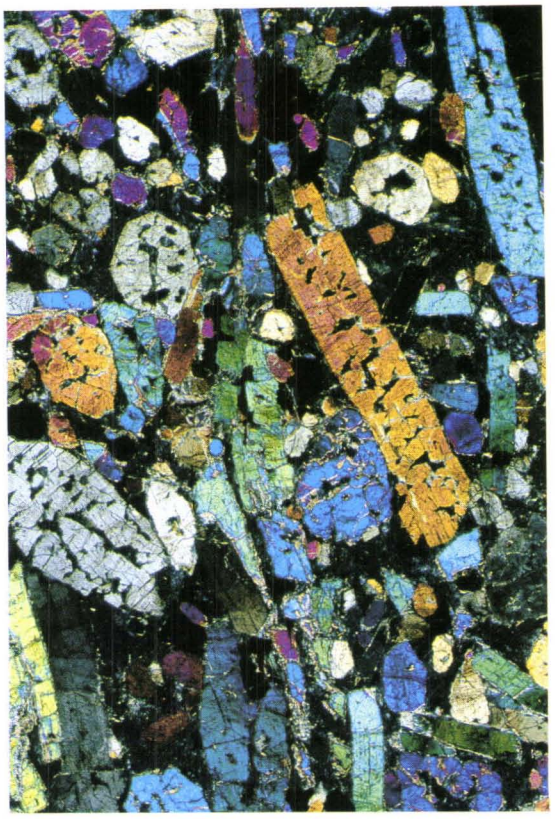

Fig. 31. Photomicrograph of pyroxene cumulate from upper part of the Kammikivi sill, sample Pet1/7.35. Note internal skeletal structure of pyroxene crystals. Width of field 3.1 mm, cross-polarized light.

Fig. 32. Photomicrograph of rapidly crystallized rock from the gabbroic part of the Kammikivi sill, sample Pet1/0.10. Clinopyroxene crystals rimmed by kaersutite are embedded in fine-grained groundmass composed of devitrified glass and kaersutite microlites. Width of field 1.3 mm, plane-polarized light.

The bulk of the section consists of metaperidotite (an olivine-chrome spinel cumulate) containing scattered, weak sulphide disseminations. Sulfides occur as irregular fillings of interstices between olivine grains or tiny spherical droplets (Figures 29 and 30). The most abundant silicate intercumulus phase is clinopyroxene which is accompanied by kaersutite and phlogopite. Pyroxene and amphibole may occur as poikilitic grains but mostly they are prismatic or needle-like. As in other ultramafic rocks in the Pechenga area, olivine frequently contains crystallized melt inclusions (Fig. 25).

Metaperidotite is overlain by a 2.5-m-thick pyroxenite (Fig. 31). The upper part of the pyroxenite is fine-grained with grain size varying between 0.05 - 0.6 mm. The grain size increases downwards to a typical range of 0.5-1.5 mm. With respect to its mineralogy and texture, this unit is identical to the pyroxene cumulate observed in the middle part of the layered lava flows, although it has been more affected by alteration processes. It is composed of clinopyroxene grains locally with skeletal interiors and brown amphibole fringes and less abundant euhedral olivines altered to serpentine. These are in a chloritic groundmass which in many places still contains kaersutite needles (or their actinolite

pseudomorphs) and skeletal sphene pseudomorphs after magnetite. In some thin sections, chlorite pseudomorphs after olivines up to 1 cm long and 0.2 mm wide are present.

The uppermost portion of the Kammikivi section is composed of evolved rocks crystallized from the residual liquid. At the top, the rock is pyroxene-phyric and contains abundant cryptocrystalline groundmass material, probably after original glass (Fig. 32). For this reason, it is called vitrophyre. When going downwards, the glass is gradually partially displaced by skeletal plagioclase, and the rock is termed quench gabbro. Other minerals in the upper part of the body, include an equant but skeletal magnetite and a rather abundant needle-like kaersutite (Fig. 32).

The presence of devitrified glass and other textural features indicative of rapid cooling in the upper part of a sulfide-bearing layered body in the Kammikivi area suggest that some of the ore-bearing bodies in the productive pile, which have been regarded as intrusive, may in fact be extrusive or at least were emplaced very close to the earth's surface (Hanski and Smolkin, 1990).

## Ni-Cu SULFIDE DEPOSITS

Practically all of the productive intrusions occur in the sedimentary part of the Pilgujärvi Suite, and Gorbunov et al. (1985b) observed that the number of intrusions increases as the thickness of the metasediments increases. All the major ore-bearing differentiated intrusions and the commercial Ni-Cu deposits associated with them are concentrated laterally in the central, thickest part of the productive pile, north of the Luotna fault (Fig. 3). In the western part of this central zone, in the region containing the Kaula, Promezhutochnoye, Kotselvaara, Kammikivi, and Ortoaivi deposits, the ore-bearing intrusions occur in the upper part of the productive pile close to the overlying volcanic subunit of the Pilgujärvi Suite. In the eastern part of the zone, in the sector from Kierdzhipori through Pilgujärvi to Onki, the ore-bearing rock masses are located in the lower part of the tuffaceous-sedimentary strata (Fig. 3).

The bulk of the sulfide ore bodies are associated with the lower parts of differentiated intrusions. In most of the deposits, sulfides are not solely confined to the intrusive parent rocks, but also extend for some distance into the enclosing tuffaceous-sedimentary rocks as lit-par-lit injections, small veinlets, and impregnations (Gorbunov, 1968). This, however, accounts for only a minor portion of the total mass of sulfide ores. Within the sedimentary formation, the ore deposits appear to be located in synclinal folds and along fault zones near the base of the intrusions (Gorbunov et al., 1985b). Sulfide ores are also found outside the intrusions where the faults extend into the country rocks.

On the basis of their structural characteristics, Gorbunov (1968) classified the Ni-Cu ores into the following four major types:

1) Disseminated ores in altered peridotites
2) Massive sulfide ores
3) Breccia ores
4) Vein-impregnations in footwall schists

Pyrrhotite, pentlandite, and chalcopyrite are the main ore minerals in all the ore types. The most common minor ore minerals are pyrite, magnetite, violarite, sphalerite, bornite, cubanite, mackinawite, and valleriite. Distler et al. (1990) also described platinum-group minerals of the cobaltite-gersdorffite series in several sulfide deposits. For mesoscopic and microscopic descriptions of the different ore types, the reader

is referred to Gorbunov et al. (1973).

The volumetrically most prevalent ore type at Pechenga, namely the peridotite-hosted disseminations, have been further divided into four subtypes (Gorbunov, 1968): 1) low-grade impregnation ores, 2) low-grade pyrrhotite-free ores, 3) high-grade impregnation and vein-impregnation ores, and 4) spotted impregnation ores. The pyrrhotite-free type, in which pyrrhotite is replaced by secondary magnetite, occurs widely in the Kierdzhipori deposit. The third type is found in direct contact with breccia or massive ore and the fourth type occurs in the contact zones of those ore-bearing intrusions that have not undergone strong tectonic movements. Typically, the sulfide content of the ultramafic cumulates increases gradually from the low-grade disseminated ore downwards to the lower contact of the intrusions. The transition from disseminated ores to overlying barren peridotites is also gradual. In weakly altered peridotites, the sulfides occupy interstitial spaces between olivine and pyroxene grains, forming net-textured and disseminated ore. In more altered rocks, a negative texture is widely developed where sulfides replace olivine, while the interstices are now infilled with serpentine. The average sulfide mineral content of the disseminated ore type is pyrrhotite 80%, pentlandite 10%, and chalcopyrite 10%. The Pilgujärvi intrusion contains the largest Ni deposit at Pechenga with about 95% of the ore occurring as disseminated sulfides.

The economically most important breccia and massive ores are located in tectonic zones along the lower contacts of the ore-bearing intrusions. They form 0.5-11 m thick ore bodies which in places extend along tectonic dislocations into the enclosing tuffaceous-sedimentary rocks over a distance of up to 400 m along strike. Breccia ores contain elongated or flattened phyllite, tuffite and serpentinite fragments cemented by sulfides. With the decreasing content of silicate rock fragments, breccia ores gradually become replaced by massive ores, with which they are spatially closely related. Among massive ores three varieties are distinguished: massive fine-grained ores, massive ores with pentlandite porphyroblasts and banded ores.

Vein-impregnation ores in country rocks were injected into crumbled and crushed footwall rocks around mineralized tectonic zones. This ore type occurs abundantly only in the Kaula deposit where it reaches a thickness of up to 10 m, while in other ore bodies mineralization extends generally from a few decimeters to 1-2 m to the metasediments. Mineralogically this ore type differs from the others, being rich in chalcopyrite.

In summary, the Ni-Cu sulfide ores at Pechenga display the following asymmetric pattern. The lowermost part of an ore body typically consists of vein-impregnation ores in sedimentary country rocks. This is overlain by a zone of breccia and massive ores of variable thickness at the tectonic contact between country rock and the layered intrusion. Finally, a zone of disseminated ores, a few meters to 100 m thick, occurs in the ultramafic rocks forming the base of the intrusions. The contacts between disseminated and massive ore as well as those between barren and mineralized serpentinites are commonly gradual.

## MINERAL CHEMISTRY OF FERROPICRITIC ROCKS

In this chapter, emphasis is placed on the primary igneous silicate and oxide minerals in ferropicritic rocks; sulfide ore mineralogy remains outside the scope of this study. Analyses of sulfide minerals have been published, for example, by Yakovleva et al. (1983). Secondary metamorphic minerals are not considered in detail except where closely related to the alteration of some primary minerals.

## Analytical techniques

Electron microprobe analyses of minerals were performed by the wavelength dispersive technique using a Jeol JCXA 733 microprobe at the Institute of Electron Optics at the University of Oulu and a Jeol JXA-733 Superprobe instrument at the Geological Survey of Finland (GSF) in Espoo. All analyses done in Oulu were determined using an accelerating voltage of 15 keV, a sample current of approx. 33 nA, and a beam diameter of 10m. Details of the analytical method and a table of simple mineral and metal standards have been published by Alapieti and Sivonen (1983). At the GSF (Espoo), the analytical conditions for silicate minerals were an accelerating potential of 15 keV, a sample current of 25 nA, and a beam diameter of 10 μm. For spinels and ilmenites, a current of 30 nA and a beam of 1 μm were used. Natural and synthetic minerals (Kakanui hornblende, ELY-garnet, anorthoclase, biotite, F-phlogopite, tugtupite, diopside, rutile, almandine, rhodonite, albite, sanidine, magnetite, willemite, chromite, olivine) were employed as standards. Results were corrected using the ZAF on-line correction programme both in Oulu and in Espoo. The analytical results of the two laboratories are generally comparable. The most important exception is chromium which appeared to be about 1.5-3.0% lower in the Oulu analyses probably due to the nonstoichiometry of the $Cr_2O_3$ standard used in Oulu.

## Olivine

Relict igneous olivine is well preserved in some portions of thick intrusions such as the Pilgujärvi intrusion, but in thin sill-like intrusions, olivine is commonly replaced by secondary minerals, and in lava flows it is invariably altered. Alteration products vary depending upon the rock type. In ultramafic rocks, olivine is typically replaced by serpentine, talc, or chlorite augmented by sulfides in ore-bearing metaperidotites. In volcanic, evolved ferropicritic rocks, olivine pseudomorphs are composed of carbonate, alkali feldspar, and rarely quartz.

Because olivine ceased to crystallize at a relatively early stage, it exhibits a limited range of Fo contents. In olivine cumulates, the previously published Fo contents range between 74.1-83.4% (Smolkin and Pakhomovskiy, 1985). During this study, this range has been somewhat expanded, while some olivines in the Kammikivi layered body contain up to 84.2% Fo component. Analyses of olivines from the olivine-titanomagnetite cumulates in the intermediate zone of the Pilgujärvi intrusion have not so far been published but a few analyses undertaken in this study display Fo values between 68.2-70.0% (Table 2).

Figure 33 illustrates the variation of Ni as a function of the forsterite content in Pechenga olivines. As would be expected, Ni increases with the Fo content. With the exception of low-Fo olivines from olivine-magnetite cumulates, the Pechenga olivines plot within the field of olivines from layered intrusions as constructed by Simkin and Smith (1970). Closer inspection reveals that separate intrusions display slightly different trends. The Ni contents of olivines from the barren Souker intrusion do not differ substantially from those analysed from the other, mineralized intrusions, as shown in Fig. 33. A similar observation led Smolkin and Pakhomovskiy (1985) to conclude that the nickel content of olivine is of no use as a criterion for distinguishing potential ore-bearing intrusions.

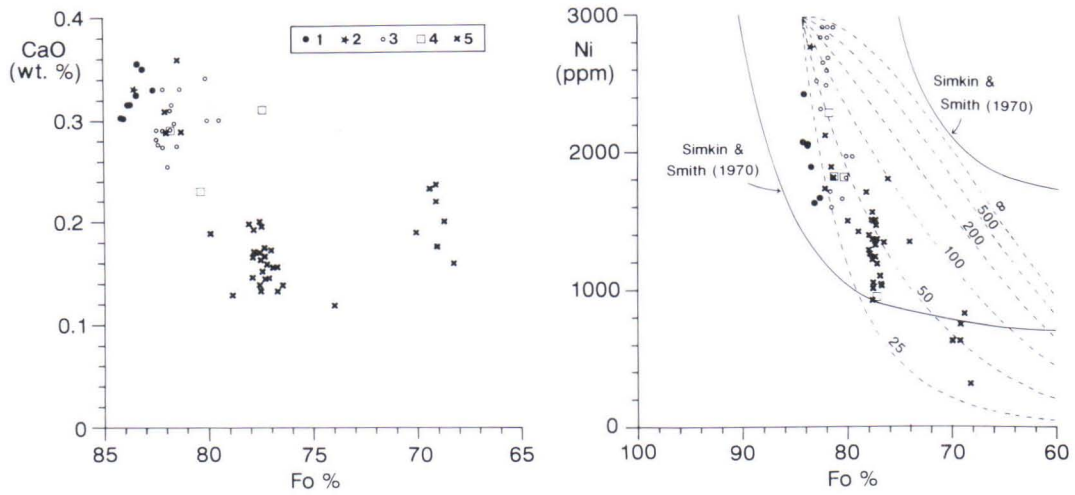


Fig. 33. CaO (wt. %) and Ni (ppm) contents as a function of Fo in olivines from gabbro-wehrlite intrusions. Data from this study and Smolkin and Pakhomovskiy (1985). Symbols: 1, Kammikivi; 2, Kierdzhipori; 3, Ortoaivi; 4, Souker; 5, Pilgujärvi. The upper and lower boundaries of the field of olivines from layered intrusions (Simkin and Smith, 1970) are marked in the Ni vs. Fo plot. Also shown are model fractionation curves computed with various weight ratios of olivine and sulfide. Calculations were based on experimental data of Arndt (1977b) for the distribution of nickel between olivine and komatiitic liquid and Naldrett's (1989a) estimation on the distribution of nickel between sulfide and silicate liquids.

Separation of an immiscible sulfide liquid will lead to a depletion of chalcophile elements, including Ni, in both the equilibrium silicate liquid and silicate minerals crystallized from it. Accordingly, the strong depletion of Ni in olivine in some basic intrusions and komatiite lava flows has been attributed to the crystallization of these olivines from a liquid impoverished in Ni due to sulfide segregation. In these cases, olivine compositions are shown to plot clearly below the Simkin-Smith field (Thompson and Naldrett, 1984) or fall below the normal range of olivines in komatiites (Steven Barnes et al., 1988). As noted above, the Pechenga olivines are not particularly low in Ni. Nevertheless, they exhibit extremely deep trends which, according to the model calculations presented in Fig. 33, deviate considerably from trends expected for olivines crystallizing from a sulfur-undersaturated ferropicritic magma. The rapid decrease in Ni content of olivine with decreasing atomic Mg/(Mg+Fe) of olivine suggests that the silicate magma equilibrated with a considerable amount of sulfide liquid during the crystallization of olivine.

Manganese shows an overall increase with falling Fo content and ranges from 0.16-0.40 wt. % MnO. In this respect, the Pechenga olivines are typical magmatic olivines (Simkin and Smith, 1970). As illustrated in Fig. 33, the CaO content of the Pechenga olivines is relatively high, being almost without exception greater than 0.14 wt. % which is diagnostic of low-pressure olivines from volcanic and hypabyssal environments (Simkin and Smith, 1970). In addition to pressure, other factors contribute to the elevated CaO content of olivine. These include the high concentration of CaO and the low activity of silica in the melt from which olivine precipitated (Stormer, 1973). Jurewicz and Watson (1988) showed that high iron activity increases the solubility of CaO in olivine. Experiments on simple synthetic systems also suggest that the solubility is inversely proportional to the $Al_2O_3$ content and directly proportional to the alkali content of the liquid

Table 2. Representative analyses of olivines from gabbro-wehrlite intrusions.

| Intrusion$ | 1 Ka | 2 Ka | 3 Ka | 4 Or | 5 Or | 6 Or | 7 Or | 8 Pi | 9 Pi | 10 Pi | 11 Pi | 12 Pi | 13 Pi | 14 Pi | 15** So |
|---|---|---|---|---|---|---|---|---|---|---|---|---|---|---|---|
| $SiO_2$ | 39.78 | 39.51 | 39.67 | 39.69 | 39.51 | 39.14 | 39.21 | 39.22 | 39.30 | 38.76 | 39.23 | 38.64 | 37.45 | 36.82 | 38.86 |
| $TiO_2$ | 0.03 | 0.00 | 0.00 | 0.01 | 0.01 | 0.02 | 0.03 | 0.03 | 0.05 | 0.06 | 0.04 | 0.00 | 0.00 | 0.03 | 0.00 |
| $Al_2O_3$ | 0.05 | 0.07 | 0.05 | 0.04 | 0.04 | 0.03 | 0.03 | 0.02 | 0.04 | 0.03 | 0.01 | 0.01 | 0.02 | 0.04 | 0.00 |
| FeO | 14.82 | 15.19 | 15.60 | 16.32 | 16.49 | 17.21 | 17.19 | 19.58 | 19.67 | 20.59 | 20.25 | 20.39 | 27.71 | 28.14 | 21.09 |
| MnO | 0.22 | 0.18 | 0.16 | 0.22 | 0.22 | 0.19 | 0.21 | 0.26 | 0.26 | 0.30 | 0.23 | 0.23 | 0.37 | 0.36 | 0.24 |
| MgO | 44.19 | 43.90 | 44.09 | 44.00 | 43.50 | 42.79 | 42.37 | 41.27 | 41.22 | 40.73 | 40.15 | 39.50 | 34.19 | 33.92 | 40.31 |
| CaO | 0.30 | 0.31 | 0.32 | 0.21 | 0.28 | 0.30 | 0.27 | 0.19 | 0.22 | 0.11 | 0.15 | 0.17 | 0.20 | 0.16 | n.a. |
| $Na_2O$ | 0.00 | 0.01 | 0.01 | 0.02 | 0.00 | 0.01 | 0.02 | 0.01 | 0.01 | 0.00 | 0.00 | 0.03 | n.a. | 0.00 | n.a. |
| $K_2O$ | 0.00 | 0.00 | 0.01 | 0.02 | 0.00 | 0.01 | 0.01 | n.a. | n.a. | n.a. | n.a. | 0.00 | n.a. | 0.01 | n.a. |
| $Cr_2O_3$ | 0.07 | 0.08 | 0.08 | 0.02 | 0.01 | 0.04 | 0.00 | 0.02 | 0.00 | 0.00 | 0.00 | 0.01 | 0.00 | 0.00 | 0.00 |
| NiO | 0.26 | 0.26 | 0.24 | 0.32 | 0.29 | 0.22 | 0.20 | 0.07 | 0.16 | 0.11 | 0.16 | 0.13 | 0.10 | 0.04 | 0.12 |
| Total | 99.73 | 99.52 | 100.23 | 100.86 | 100.36 | 99.96 | 99.55 | 100.65 | 100.93 | 100.69 | 100.23 | 99.10 | 100.07 | 99.50 | 100.62 |
| Structural formula based on 4 oxygens | | | | | | | | | | | | | | | |
| Si | 1.002 | 0.999 | 0.998 | 0.996 | 0.997 | 0.995 | 1.001 | 1.000 | 1.000 | 0.994 | 1.007 | 1.005 | 1.001 | 0.993 | 0.998 |
| Ti | 0.001 | 0.000 | 0.000 | 0.000 | 0.000 | 0.000 | 0.001 | 0.001 | 0.001 | 0.001 | 0.001 | 0.000 | 0.000 | 0.001 | 0.000 |
| Al | 0.001 | 0.002 | 0.001 | 0.001 | 0.001 | 0.001 | 0.001 | 0.001 | 0.001 | 0.001 | 0.000 | 0.000 | 0.001 | 0.001 | 0.000 |
| Fe | 0.312 | 0.321 | 0.328 | 0.343 | 0.348 | 0.366 | 0.367 | 0.418 | 0.418 | 0.441 | 0.435 | 0.444 | 0.619 | 0.634 | 0.453 |
| Mn | 0.005 | 0.004 | 0.004 | 0.005 | 0.005 | 0.004 | 0.005 | 0.006 | 0.006 | 0.007 | 0.005 | 0.005 | 0.008 | 0.008 | 0.005 |
| Mg | 1.660 | 1.655 | 1.653 | 1.646 | 1.636 | 1.622 | 1.611 | 1.568 | 1.563 | 1.556 | 1.536 | 1.532 | 1.362 | 1.363 | 1.543 |
| Ca | 0.008 | 0.009 | 0.009 | 0.006 | 0.008 | 0.008 | 0.008 | 0.005 | 0.006 | 0.003 | 0.004 | 0.005 | 0.006 | 0.005 | - |
| Na | 0.000 | 0.001 | 0.000 | 0.001 | 0.000 | 0.001 | 0.001 | 0.001 | 0.000 | 0.000 | 0.000 | 0.001 | - | 0.000 | - |
| K | 0.000 | 0.000 | 0.000 | 0.001 | 0.000 | 0.001 | 0.000 | - | - | - | - | 0.000 | - | 0.000 | - |
| Cr | 0.001 | 0.002 | 0.002 | 0.000 | 0.000 | 0.001 | 0.000 | 0.000 | 0.000 | 0.000 | 0.000 | 0.000 | 0.000 | 0.000 | 0.000 |
| Ni | 0.005 | 0.005 | 0.005 | 0.006 | 0.006 | 0.004 | 0.004 | 0.001 | 0.003 | 0.002 | 0.003 | 0.003 | 0.002 | 0.001 | 0.003 |
| Fo | 84.2 | 83.7 | 83.4 | 82.8 | 82.5 | 81.6 | 81.5 | 79.0 | 78.9 | 77.9 | 77.9 | 77.5 | 68.7 | 68.2 | 77.3 |
| Anal.* | O | O | O | O | O | O | O | E | E | E | E | O | E | E | A |

n.a. = not analysed.
* Analysis laboratory: O, University of Oulu; E, Geological Survey of Finland, Espoo; A, Kola Science Center, Apatity.
$ Intrusion: Ka = Kammikivi, Or = Ortoaivi, Pi = Pilgujärvi, So = Souker.
** taken from Smolkin and Pakhomosvkiy (1985).
Rock types:
**1-12** and **15** olivine cumulates, **13-14** olivine-magnetite cumulates.
Samples:
**1-3**, Pet1/33.00; **4**, HV-57.2-1928; **5**, HV-57.1-1928; **6-7**, Ortoaivi; **8-10**, PJ 8; **11-12**, SA-14; **13-14**, PJ 9; **15**, S-1834/403.5.

(Libourel, 1989). It is apparent that many of the chemical characteristics of ferropicritic rocks and their conditions of crystallization favor a high CaO content of olivine.

Significant differences exist in CaO between olivines with different Fo content. Figure 33 demonstrates that the CaO content decreases by half when Fo decreases from 82-84% to 77-78% and increases slightly in the least magnesian olivines in the olivine magnetite cumulates of the Pilgujärvi intrusion. Provided that the compositions measured represent magmatic values, such a variation is enigmatic, for the CaO content of olivine is expected to increase with decreasing Fo content. This prediction is based on the increasing CaO content of the residual liquid during olivine fractionation and the growing capacity of olivine to dissolve CaO when its FeO content increases (Jurewicz and Watson, 1988). Also the partition coefficient for Ca between olivine and liquid tends to increase with decreasing temperature and increasing oxygen fugacity (Miyamoto et al., 1992). Indeed, in volcanic rocks, it is generally observed that the CaO content of olivine progressively increases with decreasing Fo content (e.g., Ewart, 1989). It is hard to imagine that the conditions of crystallization were so different between different intrusions that the partition coeffi-

cient of CaO between olivine and liquid could have varied by more than two, even though most of the high-Fo olivines come from small-size, high-level sills and the low-Fo olivines from the large Pilgujärvi intrusion which was presumably emplaced at a deeper level in the crust. Neither do the general geochemical data support the alternative that the difference in CaO could be a result of differences in parental magma compositions.

## Clinopyroxene

Clinopyroxene is the silicate mineral that is least affected by secondary alteration in ferropicrites. It may be completely fresh in rocks where olivine is totally replaced, for example, by quartz or carbonates. It occurs as a major constituent in almost all rock types and varies in morphology from large poikilitic oikocrysts and spinifex needles to tiny microlites and fine-grained, plumose aggregates. In ultramafic cumulates, clinopyroxene is typically colorless but in more evolved rocks, it becomes pinkish or purplish in color, which is related to its increasing $TiO_2$ content. Particularly in volcanic ferropicrites, clinopyroxene grains display concentric zoning and, less commonly, sector zoning which is typical of Ti-rich augites. No detailed microprobe investigation of the zoning patterns in clinopyroxene has been performed during this study.

Microprobe analyses of Pechenga pyroxenes have only been published previously by Smolkin (1978) and Hanski and Smolkin (1989). Representative pyroxene analyses obtained in this study are listed in Table 3. Pyroxenes from gabbro-wehrlite intrusions show a range of atomic Mg/(Mg+Fe) (Mg number) between 0.88-0.63. Layered lava flows display a larger spread between 0.85-0.48. As demonstrated by their position on the conventional pyroxene quadrilateral in Fig. 34, pyroxenes from lava flows fall within the fields of diopside, salite, and augite and the pyroxenes richest in iron plot close the joining point of the fields of augite, ferroaugite, salite, and ferrosalite. Compared with pyroxenes from the Munro Township komatiites, the Pechenga pyroxenes have in most cases a higher wollastonite component even though there is a considerable overlap in compositions. On average, the pyroxenes from ferropicritic metavolcanites show a slight increase in the wollastonite component with decreasing Mg/(Mg+Fe). The relationship between the relative positions of the clinopyroxene trends in the Mg-Ca-Fe diagram and the undersaturation of the host rocks has been established by several authors. A flat or a slight Ca-enrichment trend has been observed in pyroxenes from mildly alkaline to alkaline intrusions and a Ca-depletion trend in pyroxenes from intrusions of tholeiitic affinity (e.g., Bedard et al., 1988; Nwe, 1976).

$TiO_2$ and $Al_2O_3$ show a wide variation between 0.5-4.2 wt. % and 1.0-9.1 wt. %, respectively. These components increase systematically with decreasing Mg number and show a good positive mutual correlation. The high Al and Ti contents of the pyroxenes from ferropicritic layered flows are probably functions of many factors including a rapid rate of crystallization, retarded nucleation of plagioclase, and enrichment of the residual liquid in these components. Irrespective of the rock type or position in a flow unit or an intrusion, the Al-Ti ratio remains approximately constant. As depicted in Fig. 35, this ratio is in most cases close to 3:1. In terms of end member molecules, the Al-Ti ratio observed in Pechenga pyroxenes is accounted for by the simultaneous substitution of $CaTi(Al_2)O_6$ and $CaAl(AlSi)O_6$ molecules coupled in an approximate 2:1 ratio. The low-Al pyroxenes from intrusions and lower parts of layered flows display a slightly higher Al/Ti which can be at least partly explained by the incorporation of Cr as a $CaCr(AlSi)O_6$ component. The earliest, most

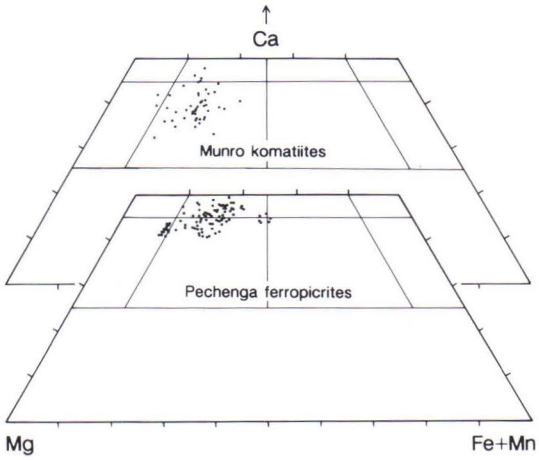


Fig. 34. Compositions of clinopyroxenes from ferropicritic and komatiitic metavolcanites on a ternary Mg-Ca-Fe+Mn diagram. Komatiite data taken from Fleet and MacRae (1975).

magnesian pyroxenes show elevated chromium contents, up to 1.0 wt. % $Cr_2O_3$, but the crystallization of chrome spinel and later clinopyroxene apparently rapidly depleted the magma in Cr. Consequently, pyroxenes with Mg/(Mg+Fe) smaller than 0.7 contain less than 0.2 wt. % $Cr_2O_3$.

$Fe^{3+}/(Fe^{3+}+Fe^{2+})$ in pyroxenes reaches a maximum of 0.3 in the least magnesian pyroxenes from layered flows, calculated according to the method of Papike et al. (1974). $Na_2O$ contents vary between 0.2 wt. % and 0.6 wt. % with the lowest values measured in interstitial pyroxenes from olivine cumulates of intrusions and the highest values in pyroxenes from fractionated parts of layered lava flows.

On the basis of pyroxene analyses from recent

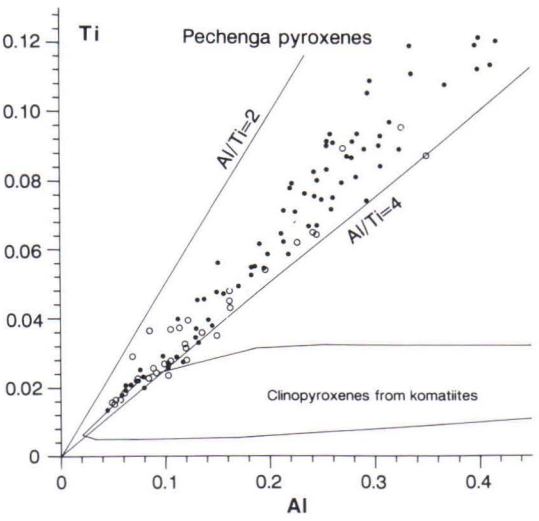


Fig. 35. Variation of Ti and Al (cations per formula unit based on 6 O) in clinopyroxenes from ferropicritic metavolcanites (dots) and gabbro-wehrlite intrusions (circles). Field for clinopyroxenes from komatiitic volcanic rocks taken from Hanski and Smolkin (1989).

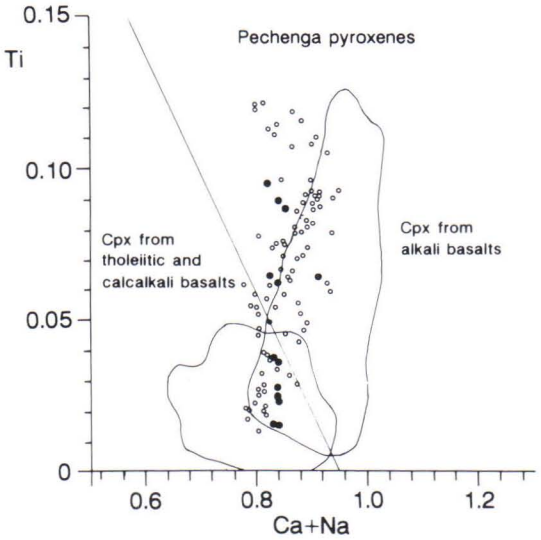


Fig. 36. Clinopyroxene compositions from layered ferropicritic flows (circles) and the Kammikivi sill (dots) plotted on the discrimination diagram of Leterrier et al. (1982).

Table 3. Representative analyses of clinopyroxenes from gabbro-wehrlite intrusions and ferropicritic metavolcanites.

| Location[$] | 1 Or | 2 Or | 3 NK | 4 NK | 5 Pi | 6 Ka | 7 Ki | 8 Ki | 9 Ki | 10 Ko | 11 Ko | 12 Ko |
|---|---|---|---|---|---|---|---|---|---|---|---|---|
| $SiO_2$ | 50.25 | 50.86 | 50.71 | 51.75 | 49.51 | 51.81 | 53.28 | 48.73 | 46.94 | 49.79 | 50.64 | 48.89 |
| $TiO_2$ | 1.02 | 1.42 | 0.59 | 1.16 | 1.93 | 0.99 | 0.80 | 2.19 | 2.59 | 1.39 | 1.61 | 2.08 |
| $Al_2O_3$ | 1.54 | 2.80 | 1.22 | 2.73 | 4.45 | 2.73 | 1.66 | 4.76 | 6.49 | 3.15 | 2.94 | 4.45 |
| FeO | 4.67 | 5.82 | 5.24 | 7.33 | 10.02 | 7.79 | 5.95 | 10.64 | 11.51 | 9.93 | 9.91 | 10.30 |
| MnO | 0.09 | 0.10 | 0.10 | 0.14 | 0.18 | 0.11 | 0.16 | 0.16 | 0.19 | 0.19 | 0.21 | 0.18 |
| MgO | 16.17 | 16.24 | 17.61 | 13.71 | 12.78 | 14.74 | 16.54 | 13.58 | 11.45 | 14.68 | 14.46 | 14.29 |
| CaO | 23.58 | 22.40 | 23.86 | 22.98 | 21.32 | 20.44 | 20.19 | 18.53 | 19.54 | 19.65 | 19.39 | 19.28 |
| $Na_2O$ | 0.40 | 0.34 | 0.30 | 0.36 | 0.41 | 0.30 | 0.31 | 0.39 | 0.45 | 0.35 | 0.38 | 0.33 |
| $K_2O$ | 0.01 | 0.03 | 0.01 | 0.02 | 0.02 | 0.00 | 0.01 | 0.00 | 0.00 | n.a. | n.a. | n.a. |
| $Cr_2O_3$ | 0.60 | 0.64 | 0.55 | 0.02 | 0.01 | 0.00 | 0.45 | 0.03 | 0.02 | 0.15 | 0.14 | 0.13 |
| NiO | 0.07 | 0.05 | 0.00 | n.a. | n.a. | 0.00 | 0.06 | 0.00 | 0.00 | 0.00 | 0.08 | 0.01 |
| $V_2O_3$ | n.a. | n.a. | 0.05 | n.a. | n.a. | 0.08 | 0.06 | 0.13 | 0.15 | n.a. | n.a. | n.a. |
| ZnO | n.a. | n.a. | 0.00 | n.a. | n.a. | n.a. | n.a. | n.a. | n.a. | n.a. | n.a. | n.a. |
| Total | 98.40 | 100.70 | 100.22 | 100.20 | 100.63 | 99.00 | 99.47 | 99.14 | 99.34 | 99.28 | 99.75 | 99.94 |
| Structural formula based on 6 oxygens | | | | | | | | | | | | |
| Si | 1.893 | 1.871 | 1.881 | 1.920 | 1.849 | 1.933 | 1.961 | 1.840 | 1.786 | 1.877 | 1.896 | 1.834 |
| Ti | 0.029 | 0.039 | 0.016 | 0.032 | 0.054 | 0.028 | 0.022 | 0.062 | 0.074 | 0.040 | 0.045 | 0.059 |
| Al | 0.068 | 0.121 | 0.053 | 0.119 | 0.196 | 0.120 | 0.072 | 0.212 | 0.291 | 0.140 | 0.130 | 0.197 |
| Fe | 0.147 | 0.179 | 0.163 | 0.227 | 0.313 | 0.243 | 0.183 | 0.336 | 0.366 | 0.313 | 0.310 | 0.323 |
| Mn | 0.003 | 0.003 | 0.003 | 0.004 | 0.006 | 0.004 | 0.005 | 0.005 | 0.006 | 0.006 | 0.007 | 0.006 |
| Mg | 0.908 | 0.890 | 0.974 | 0.758 | 0.712 | 0.820 | 0.907 | 0.764 | 0.649 | 0.825 | 0.807 | 0.799 |
| Ca | 0.952 | 0.883 | 0.948 | 0.913 | 0.853 | 0.817 | 0.796 | 0.750 | 0.797 | 0.794 | 0.778 | 0.775 |
| Na | 0.029 | 0.024 | 0.021 | 0.026 | 0.030 | 0.022 | 0.022 | 0.028 | 0.034 | 0.026 | 0.028 | 0.024 |
| K | 0.001 | 0.001 | 0.000 | 0.001 | 0.001 | 0.000 | 0.000 | 0.000 | 0.000 | - | - | - |
| Cr | 0.018 | 0.019 | 0.016 | 0.001 | 0.000 | 0.000 | 0.013 | 0.001 | 0.001 | 0.004 | 0.004 | 0.004 |
| Ni | 0.002 | 0.002 | 0.000 | - | - | 0.000 | 0.002 | 0.000 | 0.000 | 0.000 | 0.002 | 0.001 |
| V | - | - | 0.001 | - | - | 0.002 | 0.002 | 0.004 | 0.005 | - | - | - |
| Zn | - | - | 0.000 | - | - | - | - | - | - | - | - | - |
| Anal.* | O | O | O | O | O | O | O | O | O | E | E | E |

volcanic rocks, Leterrier et al. (1982) constructed discrimination diagrams distinguishing three major basaltic groups from each other: alkali basalts and related rocks, tholeiites from spreading centres, and orogenic basalts. Their diagram, in which Ca+Na is plotted against Ti, is applied to pyroxenes from ferropicritic metavolcanites and the Kammikivi layered sill in Fig. 36. Most of the pyroxenes located on the tholeiitic and calc-alkaline side of the dividing line are low-Ti pyroxenes from the lower part of the layered flows and the Kammikivi sill while the pyroxenes located on the alkali basalt side come from evolved parts of the layered bodies. Taken as a whole, the Pechenga pyroxenes define a trend which straddle the left-hand boundary of the alkali basalt pyroxene field.

In globular rocks, pyroxene grains from the globules and matrix are virtually indistinguishable with respect to all chemical components (Hanski, in press). This applies to early crystallized phenocrysts and small late-stage microlites as well as to large spinifex crystals. If pyroxene crystallized from drastically different liquid compositions in the globule and matrix portions of these rocks, this should be reflected at least in the composition of rapidly crystallized late-stage microlites or margins of zoned crystals; pyroxene

Table 3. (*Continued*)

| Location$ | 13 Ko | 14 Ka | 15 Ka | 16 IS | 17 IS | 18 IS | 19 IS | 20 IS | 21 IS | 22 IS | 23 U | 24 U |
|---|---|---|---|---|---|---|---|---|---|---|---|---|
| $SiO_2$ | 50.46 | 49.56 | 48.51 | 46.40 | 46.33 | 45.80 | 46.01 | 47.72 | 44.80 | 46.48 | 43.78 | 43.63 |
| $TiO_2$ | 1.30 | 1.87 | 2.54 | 3.20 | 2.79 | 3.16 | 3.25 | 2.34 | 3.65 | 3.03 | 4.23 | 4.15 |
| $Al_2O_3$ | 2.87 | 4.12 | 4.80 | 6.20 | 5.98 | 5.72 | 5.68 | 5.28 | 6.43 | 6.16 | 8.85 | 9.11 |
| FeO | 9.66 | 8.83 | 8.92 | 10.62 | 10.67 | 11.56 | 11.50 | 9.50 | 10.75 | 10.87 | 14.83 | 15.15 |
| MnO | 0.21 | 0.13 | 0.12 | 0.18 | 0.18 | 0.20 | 0.21 | 0.18 | 0.13 | 0.20 | 0.31 | 0.32 |
| MgO | 13.96 | 13.67 | 13.27 | 11.25 | 11.69 | 11.12 | 11.23 | 13.13 | 11.23 | 11.72 | 8.89 | 7.83 |
| CaO | 19.73 | 21.25 | 21.30 | 21.63 | 22.34 | 21.60 | 21.18 | 20.41 | 21.73 | 20.57 | 18.92 | 18.46 |
| $Na_2O$ | 0.33 | 0.41 | 0.43 | 0.49 | 0.43 | 0.47 | 0.44 | 0.50 | 0.47 | 0.52 | 0.49 | 0.42 |
| $K_2O$ | n.a. | 0.01 | 0.00 | n.a. | n.a. | n.a. | n.a. | n.a. | n.a. | n.a. | 0.00 | 0.01 |
| $Cr_2O_3$ | 0.08 | 0.15 | 0.21 | 0.01 | 0.00 | 0.09 | 0.03 | 0.08 | 0.01 | 0.00 | 0.00 | 0.00 |
| NiO | 0.00 | 0.04 | 0.00 | 0.02 | 0.06 | 0.04 | 0.00 | 0.04 | 0.00 | 0.00 | 0.00 | 0.03 |
| $V_2O_3$ | n.a. | 0.14 | 0.14 | n.a. | n.a. | n.a. | n.a. | n.a. | n.a. | n.a. | n.a. | n.a. |
| ZnO | n.a. | n.a. | n.a. | n.a. | n.a. | n.a. | n.a. | n.a. | n.a. | n.a. | 0.02 | 0.05 |
| Total | 98.60 | 100.17 | 100.24 | 100.00 | 100.47 | 99.77 | 99.53 | 99.18 | 99.22 | 99.55 | 100.32 | 99.16 |
| Structural formula based on 6 oxygens | | | | | | | | | | | | |
| Si | 1.909 | 1.851 | 1.815 | 1.762 | 1.756 | 1.755 | 1.763 | 1.807 | 1.722 | 1.769 | 1.681 | 1.695 |
| Ti | 0.037 | 0.053 | 0.072 | 0.091 | 0.079 | 0.091 | 0.094 | 0.067 | 0.106 | 0.087 | 0.122 | 0.121 |
| Al | 0.128 | 0.181 | 0.212 | 0.277 | 0.267 | 0.259 | 0.257 | 0.236 | 0.292 | 0.276 | 0.401 | 0.417 |
| Fe | 0.306 | 0.276 | 0.279 | 0.337 | 0.338 | 0.370 | 0.368 | 0.301 | 0.346 | 0.346 | 0.476 | 0.492 |
| Mn | 0.007 | 0.004 | 0.004 | 0.006 | 0.006 | 0.007 | 0.007 | 0.006 | 0.004 | 0.007 | 0.010 | 0.011 |
| Mg | 0.787 | 0.761 | 0.740 | 0.637 | 0.660 | 0.635 | 0.641 | 0.741 | 0.644 | 0.665 | 0.509 | 0.453 |
| Ca | 0.800 | 0.851 | 0.854 | 0.880 | 0.907 | 0.887 | 0.869 | 0.828 | 0.895 | 0.839 | 0.778 | 0.768 |
| Na | 0.024 | 0.029 | 0.031 | 0.036 | 0.032 | 0.035 | 0.033 | 0.036 | 0.035 | 0.038 | 0.037 | 0.032 |
| K | - | 0.000 | 0.000 | - | - | - | - | - | - | - | 0.000 | 0.001 |
| Cr | 0.002 | 0.005 | 0.006 | 0.000 | 0.000 | 0.003 | 0.001 | 0.003 | 0.001 | 0.000 | 0.000 | 0.000 |
| Ni | 0.000 | 0.001 | 0.000 | 0.001 | 0.002 | 0.001 | 0.000 | 0.001 | 0.000 | 0.000 | 0.000 | 0.001 |
| V | - | 0.004 | 0.004 | - | - | - | - | - | - | - | - | - |
| Zn | - | - | - | - | - | - | - | - | - | - | 0.001 | 0.001 |
| Anal.* | E | O | O | E | E | E | E | E | E | E | E | E |

n.a. = not analysed.
* Analysis laboratory: O, University of Oulu; E, Geological Survey of Finland, Espoo.
$ Location: Or = Ortoaivi intrusion, NK = Northern Kotselvaara intrusion, Pi = Pilgujärvi intrusion, Ka = Kammikivi sill, Ki = Kierdzhipori layered flow, Ko = layered flow, Kotselvaara area, Ka = layered flow, Kaula area, IS = globular rock, Lake Ilya Souker area, U = exact location unknown.
Rock types and samples:
**1-2**, olivine cumulate, 3395-UJ-1935, 3401-UJ-1935; **3-4**, pyroxene-magnetite cumulate, -60/140S; **5**, pyroxene-plagioclase-magnetite cumulate, Pilgu 14; **6**, pyroxene cumulate, Pet1/4.00; **7**, olivine cumulate, S-2986/93.5; **8-9**, rock with porphyritic-spherulitic texture, spinifex zone, S-2986/76.0, S-2986/76.5; **10-13**, pyroxene spinifex rock, 1685/2SP; **14-15**, pyroxene spinifex rock, S-3R/731.4; **16-17**, matrix, Soukerjärvi 4; **18**, matrix, Soukerjärvi 1; **19**, globule, Suokerjärvi 1; **20**, globule, 1833-6; **21-22**, globule, Soukerjärvi 4; **23-24**, evolved ferropicritic rock, 35E No. 13.

compositions do not provide any evidence for this.

From the data presented above, it can be concluded that clinopyroxenes in ferropicritic rocks are reminiscent of those in mildly alkaline rocks and differ markedly from clinopyroxenes observed in komatiitic intrusive and extrusive bodies (see Fig. 35). Apart from the $TiO_2$-rich nature of the Pechenga pyroxenes, differences include the absence of pigeonite cores which are typical of clinopyroxenes from komatiitic lavas (Arndt and Fleet, 1979).

## Amphibole

Brown igneous amphibole is ubiquitous in extrusive and intrusive ferropicritic rocks, being present in small amounts in almost all differentiates. It occurs as an euhedral intercumulus phase, as fringes around clinopyroxene grains, or as discrete skeletal needles. It also commonly forms patchy subsolidus replacements in pyroxene cumulus grains in intrusive bodies.

Primary igneous amphiboles are best preserved in the central and upper parts of layered flows and ultramafic cumulates of intrusions. For this reason, microprobe analyses were mainly restricted to these rocks. Selected analyses are reported in Table 4. In the gabbroic cumulates of intrusions, alteration renders the analyses generally useless. An exception is the upper part of the Kammikivi layered sill where brown amphibole is commonly well preserved.

The igneous amphiboles from ferropicritic rocks are rich in $TiO_2$, with a maximum value of 6.9 wt. %. This feature, together with other parameters, such as Ca+Na+K > 2.5 and Si < 6.25 classifies the amphibole as kaersutite (Ti>0.5) or pargasite (Ti<0.5) (Leake, 1978). Amphiboles show large variations in their Mg/(Mg+Fe) values. Intercumulus amphiboles in olivine cumulates have the lowest Mg/(Mg+Fe) value (0.82-0.70) while amphiboles crystallized in the upper parts of layered flows are rich in iron oxide (up to 22 wt. % $FeO_{tot}$) and therefore deserve to be termed ferrokaersutites or ferropargasites. The averages of the stoichiometrically-acceptable lower and upper limits of the ferric iron content, as calculated by using the method of Spear and Kimball (1984), commonly result in $Fe^{3+}/Fe^{2+}$ of less than 0.3 (Table 4). The $Al_2O_3$ content of amphiboles is relatively low, varying between 10-14 wt. %. The maximum value is attained by the ferrokaersutites (Table 4).

The $Na_2O$ content of the Pechenga amphiboles is generally between 2.5-3.5 wt. % while the $K_2O$ content varies in the range 0.3-0.8 wt. %. $K_2O$ is relatively low compared with its abundance in most high-pressure kaersutite megacrysts found in alkaline volcanic rocks (Fig. 37). The latter amphiboles mostly possess a $K_2O$ content between 1.0-2.5 wt. % (e.g., Irving, 1974). The low potassium content of the Pechenga amphiboles compared with megacrystic amphiboles is compatible with the experimental studies of Ulmer et al. (1990) which suggest that the potassium content of amphibole is directly proportional to the crystallization pressure. Its usefulness as a geobarometer in our case is, however, negligible because amphiboles with potassium abundances equivalent to those of the Pechenga kaersutites have been experimentally synthesized from tholeiitic and alkali basalts at pressures as high as 2-8 kbar (Helz, 1973; Nesbitt and Hamilton, 1970; Holloway and Burnham, 1972). These amphiboles are higher in $Al_2O_3$ due to bulk compositional and pressure effects. It is interesting to note that among the few low-K kaersutites that compositionally approach the Pechenga amphiboles are those analysed by Morawski et al. (1976) from an alkali basalt lava crystallized at low pressure on the sea floor.

Some anomalous features in the alkali content of the Pechenga amphiboles warrant special comment. The first is the relatively low potassium content of kaersutites coexisting with K-rich titanian phlogopites as intercumulus phases in ultramafic rocks. Crystallization of phlogopite from a silicate melt implies a considerable potassium content in this melt. At low pressures, the minimum $K_2O$ content required for stabilizing phlogopite is even higher than at elevated pressures. For example, Esperanca and Holloway (1987) measured a minimum $K_2O$ content of 3.3 wt. % in liquids saturated in phlogopite at 10 kbar, but at 1 kbar pressure, Barton and Hamilton (1978) obtained phlogopite as one of the liquidus phases in a wyomingite containing 10.2 wt. % $K_2O$. It follows that when phlogopite started to precipitate in ultramafic cumulates, the interstitial liquid was highly fractionated and enriched in potassium.

The kaersutite crystals accompanying phlogopite do not have higher $K_2O$ contents than 0.8 wt. %, which appears to be anomalously low, since the partition coefficient for $K_2O$ between amphibole and silicate liquid is known to vary between 0.17-0.68 (Gilbert et al., 1982). Taking the minimum D value of 0.17 and the $K_2O$ content of 0.8 wt. % in amphibole, a value of 4.7 wt. % $K_2O$ is obtained for the liquid. The interpretation of the alkali contents of the Pechenga kaersutites is hampered by the scarcity of experimental data on the exchange of alkalies between coexisting mica and amphibole at magmatic temperatures.

Another problem is related to the observation that the $K_2O$ contents of the Pechenga amphiboles form two major populations with values at about 0.4 wt. % and 0.8 wt. % (Fig. 37). The lower values belong to ferrokaersutites from evolved parts of layered flows while the higher values were obtained for low-Fe kaersutites from ultramafic cumulates in intrusions. Amphiboles from olivine-magnetite cumulates show intermediate $K_2O$ abundances. The inverse relation between the FeO and $K_2O$ contents, as depicted in Fig. 38, is strange because, as an incompatible element, potassium should be enriched in the residual liquid and hence also in high-Fe crystals crystallized from it. The alkali content of amphibole is dependent on the $K_2O/Na_2O$ value of the liquid, since both of these elements compete for the same structural site in the amphibole lattice. A diminution of $K_2O/Na_2O$ in the residual liquid from which ferrokaersutites have crystallized is not likely because the only feasible K-rich mineral that might cause such an effect is titanian phlogopite. The occurrence of this mineral is restricted to interstitial and poikilitic grains in the lower parts of the layered flows and intrusions and thus it does not impose a fractionation effect on the residual liquid. The explanation for the low $K_2O$ abundances in ferrokaersutites may be related to the exchange coefficient $(K/Na)^{amph}/(K/Na)^{liq}$ which increases with increasing temperature approaching unity at temperatures of about 1050 °C (Helz, 1979; Foden and Green, 1992). A temperature decrease of 220 °C is sufficient for the reduction of the coefficient

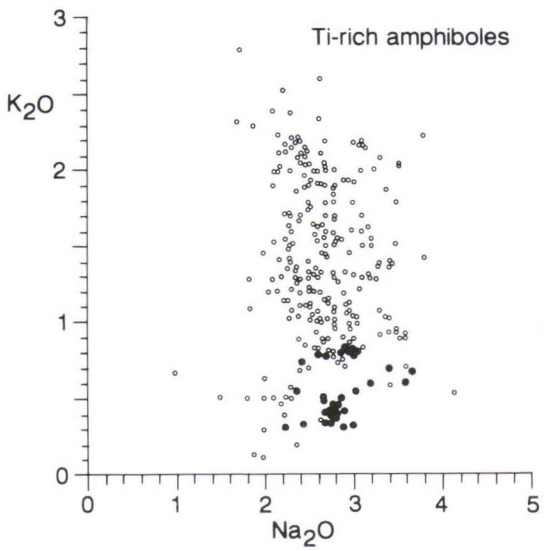


Fig. 37. Alkali contents (wt. %) of primary igneous amphiboles from ferropicritic rocks (dots) compared with alkali contents of Ti-rich ($TiO_2$ > 3 wt. %) amphiboles (circles) from the literature.

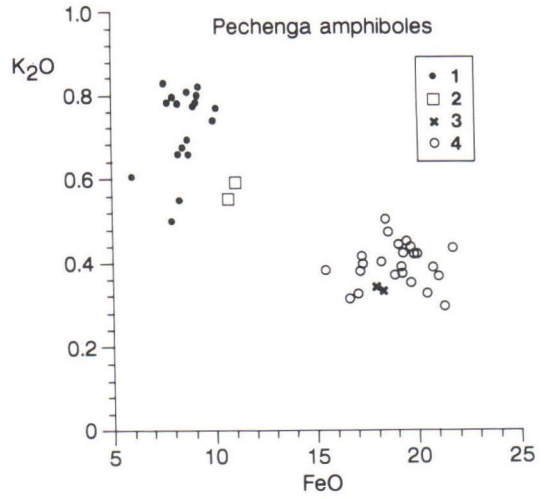


Fig. 38. $K_2O$ against $FeO_{tot}$ (wt. %) for Pechenga igneous amphiboles. Symbols: 1, interstitial amphibole in ultramafic cumulates of intrusions; 2, interstitial amphibole from olivine-magnetite cumulate (Pilgujärvi intrusion); 3, interstitial amphibole needles in pyroxene cumulates from layered flows; 4, amphibole rims on pyroxenes and discrete amphibole needles from evolved parts of layered flows.

Table 4. Representative microprobe analyses of brown amphiboles from gabbro-wehrlite intrusions and ferropicritic metavolcanites.

| Location$ | 1<br>Ka | 2<br>K | 3<br>Ka | 4<br>Or | 5<br>Or | 6<br>Or | 7<br>Or | 8<br>Or | 9<br>Or |
|---|---|---|---|---|---|---|---|---|---|
| $SiO_2$ | 39.74 | 38.78 | 37.45 | 41.68 | 42.77 | 45.73 | 43.71 | 39.72 | 39.73 |
| $TiO_2$ | 6.27 | 6.40 | 5.91 | 4.78 | 4.78 | 4.57 | 4.09 | 5.74 | 5.99 |
| $Al_2O_3$ | 10.73 | 11.94 | 13.06 | 10.77 | 10.02 | 7.85 | 10.53 | 13.20 | 12.93 |
| FeO | 16.58 | 17.15 | 19.17 | 8.42 | 8.70 | 8.74 | 8.30 | 8.26 | 7.86 |
| MnO | 0.20 | 0.15 | 0.25 | 0.11 | 0.09 | 0.07 | 0.11 | 0.08 | 0.06 |
| MgO | 9.41 | 9.06 | 6.89 | 15.29 | 15.21 | 15.30 | 15.27 | 14.24 | 14.20 |
| CaO | 10.23 | 10.83 | 10.51 | 11.27 | 11.01 | 10.28 | 11.24 | 11.47 | 11.69 |
| $Na_2O$ | 2.87 | 2.75 | 2.87 | 3.65 | 3.40 | 4.10 | 3.68 | 2.36 | 2.84 |
| $K_2O$ | 0.31 | 0.42 | 0.43 | 0.67 | 0.69 | 0.66 | 0.66 | 0.55 | 0.50 |
| $Cr_2O_3$ | 0.00 | 0.00 | 0.02 | 0.05 | 0.06 | 0.05 | 0.11 | 0.16 | 0.11 |
| NiO | 0.00 | 0.01 | 0.01 | 0.07 | 0.06 | 0.09 | 0.08 | 0.06 | 0.12 |
| $V_2O_3$ | 0.07 | 0.06 | 0.20 | n.a. | 0.22 | n.a. | n.a. | 0.21 | 0.29 |
| ZnO | n.a. | n.a. | n.a. | n.a. | 0.06 | n.a. | n.a. | n.a. | 0.00 |
| F | n.a. | n.a. | n.a. | 0.28 | n.a. | 0.22 | 0.08 | n.a. | n.a. |
| CL | n.a. | n.a. | n.a. | 0.02 | n.a. | 0.03 | 0.05 | n.a. | n.a. |
| -O=F | - | - | - | 0.12 | - | 0.09 | 0.03 | - | - |
| -O=Cl | - | - | - | 0.00 | - | 0.01 | 0.01 | - | - |
| Total | 96.42 | 97.55 | 96.77 | 96.95 | 97.06 | 97.58 | 97.87 | 96.04 | 96.32 |
| Structural formula based on 23 oxygens | | | | | | | | | |
| Si | 6.095 | 5.911 | 5.820 | 6.158 | 6.289 | 6.661 | 6.354 | 5.893 | 5.884 |
| Ti | 0.723 | 0.734 | 0.691 | 0.532 | 0.528 | 0.501 | 0.447 | 0.641 | 0.667 |
| Al | 1.939 | 2.146 | 2.392 | 1.875 | 1.736 | 1.347 | 1.805 | 2.308 | 2.258 |
| $Fe^{3+}$# | 0.260 | 0.236 | 0.186 | 0.000 | 0.008 | 0.000 | 0.000 | 0.299 | 0.000 |
| $Fe^{2+}$ | 1.867 | 1.951 | 2.305 | 1.041 | 1.062 | 1.064 | 1.009 | 0.726 | 0.973 |
| Mn | 0.026 | 0.019 | 0.033 | 0.014 | 0.011 | 0.009 | 0.014 | 0.010 | 0.008 |
| Mg | 2.151 | 2.058 | 1.597 | 3.366 | 3.335 | 3.321 | 3.308 | 3.148 | 3.135 |
| Ca | 1.681 | 1.769 | 1.750 | 1.783 | 1.739 | 1.604 | 1.751 | 1.824 | 1.855 |
| Na | 0.854 | 0.812 | 0.866 | 1.047 | 0.970 | 1.158 | 1.039 | 0.679 | 0.816 |
| K | 0.062 | 0.081 | 0.085 | 0.127 | 0.130 | 0.122 | 0.122 | 0.104 | 0.095 |
| Cr | 0.000 | 0.000 | 0.002 | 0.005 | 0.006 | 0.005 | 0.013 | 0.018 | 0.013 |
| Ni | 0.000 | 0.002 | 0.002 | 0.008 | 0.007 | 0.010 | 0.009 | 0.007 | 0.014 |
| V | 0.009 | 0.007 | 0.024 | - | 0.026 | - | - | 0.025 | 0.034 |
| Zn | - | - | - | - | 0.006 | - | - | - | 0.000 |
| Anal.* | O | O | O | E | O | O | E | O | O |

to such an extent that the late-crystallized ferrokaersutites will have a potassium level of about half that of early crystallized kaersutites.

It is interesting to note that brown amphiboles in the upper part of the Kammikivi ore-bearing layered body are compositionally identical to the low-K ferrokaersutites from pyroxene-spinifex textured rocks in layered flows (Table 4).

The fluorine content was analysed for a few amphibole grains and was found to vary between 0.3-0.6 wt. % in ferrokaersutites from the upper part of layered flows, but is less than 0.3 wt. % in interstitial kaersutite in an olivine cumulate from an intrusion.

Among the critical factors essential for the stability of amphibole with a silicate liquid are the sufficiently high alkali and water contents of the melt. According to Gilbert et al. (1982), the total

Table 4. (*Continued*)

| Location$ | 10 Pi | 11 Ki | 12 Ko | 13 Ko | 14 Ko | 15 Ko | 16 U | 17 U | 18 U |
|---|---|---|---|---|---|---|---|---|---|
| $SiO_2$ | 40.62 | 37.22 | 39.10 | 38.58 | 38.32 | 38.12 | 37.34 | 36.85 | 39.68 |
| $TiO_2$ | 4.59 | 5.79 | 3.87 | 5.63 | 4.12 | 3.67 | 6.95 | 7.02 | 6.04 |
| $Al_2O_3$ | 11.81 | 14.08 | 13.46 | 12.76 | 13.47 | 14.15 | 14.03 | 14.20 | 13.15 |
| FeO | 11.05 | 17.98 | 19.81 | 18.77 | 21.63 | 20.94 | 18.56 | 18.41 | 19.09 |
| MnO | 0.15 | 0.21 | 0.28 | 0.25 | 0.25 | 0.35 | 0.17 | 0.24 | 0.23 |
| MgO | 12.90 | 7.46 | 8.56 | 8.41 | 7.59 | 7.04 | 8.03 | 7.87 | 7.78 |
| CaO | 11.98 | 10.64 | 10.27 | 10.74 | 9.78 | 10.67 | 10.84 | 10.80 | 9.77 |
| $Na_2O$ | 3.18 | 2.68 | 2.75 | 2.78 | 2.75 | 2.65 | 2.69 | 2.67 | 2.82 |
| $K_2O$ | 0.59 | 0.34 | 0.43 | 0.37 | 0.44 | 0.37 | 0.48 | 0.51 | 0.45 |
| $Cr_2O_3$ | n.a. | 0.00 | n.a. | n.a. | n.a. | n.a. | n.a. | n.a. | n.a. |
| NiO | n.a. | 0.00 | n.a. | n.a. | n.a. | n.a. | n.a. | n.a. | n.a. |
| $V_2O_3$ | n.a. | 0.20 | n.a. | n.a. | n.a. | n.a. | n.a. | n.a. | n.a. |
| ZnO | n.a. | 0.05 | n.a. | n.a. | n.a. | n.a. | n.a. | n.a. | n.a. |
| F | n.a. | n.a. | 0.55 | 0.58 | 0.50 | 0.35 | 0.07 | 0.16 | 0.16 |
| Cl | n.a. | n.a. | n.a. | n.a. | n.a. | n.a. | 0.03 | 0.03 | 0.02 |
| -O=F | - | - | 0.23 | 0.24 | 0.21 | 0.15 | 0.03 | 0.07 | 0.07 |
| -O=Cl | - | - | - | - | - | - | 0.01 | 0.01 | 0.00 |
| Total | 96.88 | 96.65 | 98.84 | 98.65 | 98.63 | 98.17 | 99.15 | 98.67 | 99.12 |
| Structural formula based on 23 oxygens | | | | | | | | | |
| Si | 6.070 | 5.751 | 5.944 | 5.873 | 5.888 | 5.871 | 5.647 | 5.606 | 5.968 |
| Ti | 0.516 | 0.672 | 0.442 | 0.645 | 0.476 | 0.425 | 0.790 | 0.803 | 0.683 |
| Al | 2.080 | 2.564 | 2.411 | 2.290 | 2.439 | 2.570 | 2.500 | 2.546 | 2.331 |
| $Fe^{3+}$# | 0.000 | 0.321 | 1.721 | 0.615 | 2.271 | 1.130 | 0.498 | 0.485 | 0.714 |
| $Fe^{2+}$ | 1.381 | 2.002 | 0.797 | 1.775 | 0.509 | 1.568 | 1.849 | 1.858 | 1.687 |
| Mn | 0.019 | 0.028 | 0.036 | 0.032 | 0.032 | 0.046 | 0.022 | 0.031 | 0.029 |
| Mg | 2.873 | 1.718 | 1.939 | 1.909 | 1.739 | 1.615 | 1.810 | 1.785 | 1.744 |
| Ca | 1.917 | 1.761 | 1.673 | 1.753 | 1.611 | 1.761 | 1.756 | 1.761 | 1.574 |
| Na | 0.922 | 0.804 | 0.810 | 0.821 | 0.820 | 0.793 | 0.789 | 0.788 | 0.822 |
| K | 0.113 | 0.068 | 0.083 | 0.072 | 0.086 | 0.073 | 0.093 | 0.099 | 0.086 |
| Cr | - | 0.000 | - | - | - | - | - | - | - |
| Ni | - | 0.000 | - | - | - | - | - | - | - |
| V | - | 0.025 | - | - | - | - | - | - | - |
| Zn | - | 0.006 | - | - | - | - | - | - | - |
| Anal.* | E | O | E | E | E | E | E | E | E |

n.a. = not analysed.
* Analysis laboratory: O, University of Oulu; E, Geological Survey of Finland, Espoo.
# $Fe^{2+}$ and $Fe^{3+}$ calculated after the method of Spear and Kimball (1984).
$ Location: Ka = Kammikivi sill, Or = Ortoaivi intrusion, Pi = Pilgujärvi intrusion, Ki = Kierdzhipori layered flow, Ko = layered flow, Kotselvaara area, U = exact location unknown.
Rock types and samples:
**1-3**, gabbroic part of the sill, Pet1/0.02,; **4-7**, olivine cumulate, HV-70d-1928; **8-9**, olivine cumulate, HV-61a-1928; **10**, olivine-magnetite cumulate, PJ 9; **11**, pyroxene cumulate, S-2986/84.1; **12-15**, pyroxene spinifex-textured rock, 1685/2SP; **16-18**, evolved ferropicritic rock, 35E No. 13.

alkali content of melt in equilibrium with magmatic amphibole must exceed 3 wt. %. Because water and low valency cations such as the alkali elements preferentially partition into the more polymerized silica-rich liquid (Roedder, 1979), much less amphibole is expected to occur in the mafic counterpart of the crystallized products of immiscible melts. As noted previously, there are no obvious modal differences in the abundances of brown amphibole between the matrix and the globules. In addition, microprobe analyses of amphiboles show that they have virtually identical compositions both in the matrix and the globules. This applies to all components in the amphiboles including alkali elements and their ratios, halogen contents, and Mg/Fe. This is an important observation because amphibole crystallized relatively late in these rocks and thus should reflect the composition of the residual liquid. The present contrasting mineralogical compositions of the albite-rich mesostasis of the globules and the ferrochlorite-rich mesostasis of the matrix are in striking contrast with the homogeneous amphibole compositions.

Metamorphic recrystallization has to varying degrees changed the original color and chemical composition of magmatic amphibole. With an increasing degree of alteration, the color changes from dark reddish brown to shades with a pleochroism varying from pale brown to green, light green or almost colorless. This is accompanied by a concomitant loss of aluminum, titanium, and sodium and a gain of silica, with the result that amphibole changes its composition from kaersutite and pargasite through edenite to tremolite-actinolite.

## Mica

Brown phlogopite-biotite solid solution is another primary hydrous phase in ferropicritic rocks. It occurs as an intercumulus phase in the ultramafic portion of ferropicritic layered flows and from the lowermost olivine cumulates to the uppermost gabbros in gabbro-wehrlite intrusions. Unaltered grains in ultramafic rocks are strongly pleochroic with shades of dark brown or are almost opaque and form small, anhedral plates up to 1.5 mm in maximum dimension (Fig. 26). In highly altered rocks, the previous magmatic mica is still recognized by virtue of the pleochroism of its pseudomorphs, which vary from pale orange to green in color, and the common presence of fine ilmenite disseminations in the pseudomorphs.

Representative analyses of micas are presented in Table 5. In ultramafic rocks, mica has a sufficiently low $FeO_{tot}$ (8-14 wt. %) and high atomic Mg-Fe ratio to be called phlogopite. In olivine-magnetite cumulates from the intermediate zone in the Pilgujärvi intrusion, mica shows a Mg-Fe ratio close to 2, which is the boundary value between phlogopite and biotite. Its iron content presumably increases to the level of biotite in gabbroic rocks but because of extensive alteration effects, mica from gabbros was not analysed.

The most striking feature of the phlogopites is their high $TiO_2$ content, up to 7.5 wt. %, classifying this mineral as titanian phlogopite. The high $TiO_2$ accounts for the dark color and strong pleochroism of the mineral. Many factors can explain the elevated titanium contents of the Pechenga micas, including high $TiO_2$ in the silicate melt from which they crystallized and low pressures and high temperatures of crystallization (cf. Robert, 1976). The $Al_2O_3$ content is relatively low (11.2-13.5 wt. %) which is apparently a reflection of the low $Al_2O_3$ content of the liquid (cf. Barton, 1979). Structural formulae calculated on the basis of 22 oxygens show that the number of Si atoms range from 5.2-5.6. The calculations indicate that there is insufficient aluminum to fully occupy the expected 8 tetrahedrally coordinated cation sites per formula unit which means that $Al^{VI}$ is absent. The $Na_2O$ content attains a maxi-

**Table 5. Representative analyses of intercumulus titanian phlogopites (#1-8) from gabbro-wehrlite intrusions and chlorites (#9-10) from a globular ferropicritic rock.**

| Location[$] | 1 Or | 2 Or | 3 Pi | 4 Pi | 5 Pi | 6 Pi | 7 Pi | 8 Pi | 9 Ko | 10 Ko |
|---|---|---|---|---|---|---|---|---|---|---|
| $SiO_2$ | 36.22 | 35.85 | 37.06 | 35.85 | 37.55 | 38.13 | 34.17 | 35.08 | 25.92 | 26.85 |
| $TiO_2$ | 7.49 | 7.20 | 6.94 | 6.59 | 6.66 | 7.04 | 6.08 | 6.09 | 0.04 | 0.01 |
| $Al_2O_3$ | 11.70 | 12.46 | 13.04 | 12.31 | 12.87 | 13.19 | 13.65 | 12.05 | 18.00 | 17.65 |
| FeO | 11.56 | 12.83 | 11.25 | 14.18 | 9.49 | 9.26 | 14.62 | 12.39 | 35.63 | 34.99 |
| MnO | 0.40 | 0.42 | 0.13 | 0.16 | 0.07 | 0.06 | 0.10 | 0.36 | 0.33 | 0.41 |
| MgO | 20.98 | 19.23 | 18.13 | 18.29 | 18.68 | 19.54 | 17.04 | 20.88 | 7.61 | 7.77 |
| CaO | 0.06 | 0.15 | 0.02 | 0.04 | 0.01 | 0.03 | 0.14 | 0.06 | 0.17 | 0.28 |
| $Na_2O$ | n.a. | 0.07 | 0.47 | 0.22 | 0.65 | 0.74 | 0.00 | 0.00 | 0.00 | 0.05 |
| $K_2O$ | 7.41 | 7.29 | 8.77 | 7.89 | 7.48 | 8.65 | 7.15 | 8.28 | n.a. | n.a. |
| $Cr_2O_3$ | 0.76 | 0.62 | n.a. | n.a. | n.a. | n.a. | n.a. | n.a. | 0.00 | 0.01 |
| NiO | 0.16 | n.a. | n.a. | n.a. | n.a. | n.a. | n.a. | n.a. | 0.11 | 0.05 |
| Total | 96.74 | 96.12 | 95.81 | 95.51 | 93.46 | 96.64 | 92.95 | 95.19 | 87.82 | 88.08 |
| Structural formula based on 22 oxygens | | | | | | | | | | |
| Si | 5.260 | 5.261 | 5.428 | 5.332 | 5.540 | 5.470 | 5.219 | 5.223 | 4.548 | 4.670 |
| Ti | 0.818 | 0.795 | 0.764 | 0.737 | 0.739 | 0.760 | 0.699 | 0.682 | 0.006 | 0.002 |
| Al | 2.003 | 2.155 | 2.251 | 2.158 | 2.237 | 2.158 | 2.457 | 2.115 | 3.721 | 3.617 |
| Fe | 1.404 | 1.575 | 1.378 | 1.764 | 1.171 | 1.111 | 1.867 | 1.542 | 5.226 | 5.089 |
| Mn | 0.049 | 0.052 | 0.017 | 0.020 | 0.009 | 0.007 | 0.013 | 0.045 | 0.050 | 0.060 |
| Mg | 4.541 | 4.206 | 3.957 | 4.055 | 4.109 | 4.178 | 3.879 | 4.635 | 1.988 | 2.014 |
| Ca | 0.009 | 0.024 | 0.004 | 0.006 | 0.001 | 0.005 | 0.022 | 0.010 | 0.032 | 0.052 |
| Na | - | 0.020 | 0.132 | 0.064 | 0.185 | 0.204 | 0.000 | 0.000 | 0.000 | 0.017 |
| K | 1.373 | 1.365 | 1.638 | 1.496 | 1.407 | 1.584 | 1.393 | 1.573 | - | - |
| Cr | 0.087 | 0.072 | - | - | - | - | - | - | 0.000 | 0.002 |
| Ni | 0.019 | - | - | - | - | - | - | - | 0.016 | 0.007 |
| Anal.* | O | O | E | E | E | E | E | E | E | E |

n.a. = not analysed.
* Analysis laboratory: O, University of Oulu; E, Geological Survey of Finland, Espoo.
$ Location: Or = Ortoaivi intrusion, Pi = Pilgujärvi intrusion, Ko = layered flow, Kotselvaara area.
Rock types and samples:
**1-2**, olivine cumulate, 3401-UJ-1935; **3-6**, olivine cumulate, SA-14; **7**, olivine cumulate, PJ 8;
**8**, olivine-magnetite cumulate, PJ 9; **9-10** = matrix of globular, pyroxene spinifex-textured rock, 1685/2SP.

mum value of about 0.9 wt. % while a maximum value of 8.8 wt. % has been measured for $K_2O$. The $Cr_2O_3$ content varies between 0.1-0.8 wt. %, being higher than 0.4 wt. % in most samples.

With respect to the high $TiO_2$ content, phlogopites similar to those found in ferropicritic rocks occur in lamproites, minettes, and sills and intrusions generated from alkali basaltic magmas (e.g., Mitchell and Bergman, 1991; Bachinski and Simson, 1984; Lipman, 1984). There are, however, some differences. Phlogopites from lamproites are typically lower in FeO while micas from minettes and alkali basaltic intrusions commonly have higher $Al_2O_3$ at equivalent Mg numbers.

The $H_2O$, F, or Cl contents of titanian phlogopites were not determined. However, judging from the anhydrous totals of the analyses, which

are close to the theoretical value of approximately 96 wt. % for hydrous phlogopites, the substitution involving $O^{2-}$ is likely not significant.

The alteration of titanian phlogopite causes impoverishment in its potassium and titanium content. Aluminum remains low and the alteration products approach sheridanitic chlorite in composition (cf. Deer et al., 1962). Sodium seems to be sensitive to alteration, being frequently impoverished while potassium still retains its high abundance (Fig. 39).

Microprobe analyses of chlorite from the chloritic mesostasis of the matrix in a globular rock revealed it to be a very iron-rich and silica-poor mica containing 34.4-35.6 wt. % $FeO_{tot}$ and 25.5-27.2 wt. % $SiO_2$ and hence corresponding to pseudothurite in composition (cf. Deer et al., 1962). As is illustrated in Fig. 39, this mica is extremely low in $TiO_2$ compared with the primary igneous mica and its alteration products. The high field strength elements such as Ti are observed to be enriched in the less polymerized conjugate liquid in liquid immiscibility processes (e.g., Philpotts, 1982). The composition of ferromica in the matrix does not show any trace of Ti-enrichment in the matrix glass whose alteration product it represents.

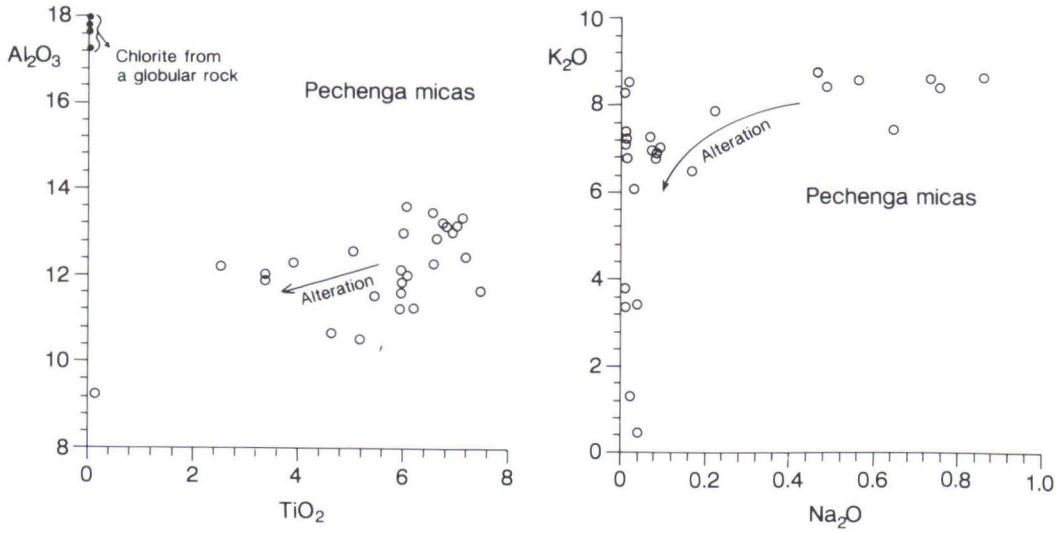


Fig. 39. $Al_2O_3$, $TiO_2$, $K_2O$ and $Na_2O$ contents (wt. %) in micas from Pechenga rocks. Circles - titanian phlogopite and its pseudomorphs in ultramafic cumulates from intrusions, dots - interstitial chlorite in matrix of globular ferropicritic lava.

## Spinel

Considerable attention has been previously devoted to spinel in the gabbro-wehrlite intrusions at Pechenga (Papadakis, 1972; Smolkin, 1981; Neradovskii, 1985; Neradovskii and Smolkin, 1977; Smolkin and Pakhomovskiy, 1985; Plaksenko and Smolkin, 1990; Abzalov et al., 1991a). Chrome spinel occurs as an accessory phase in olivine cumulates in the lower parts of layered flows and intrusions, including cumulates containing primary sulfide ore. Chrome spinel was obviously the first liquidus phase to crystallize from the ferropicritic magma as deduced from its existence as small, euhedral crystals embedded in olivine grains. It also occurs interstitially between olivine grains and is enclosed in postcumulus phases such as clinopyroxene and kaersutite.

Chromium-poor titanomagnetite is an essential liquidus phase in gabbroic rocks of the intrusions. In the special case of the Pilgujärvi intrusion, it began to precipitate early with olivine and forms magnetite-rich cumulates in the intermediate zone of this intrusion.

Characteristic features of chrome-bearing spinel in ultramafic rocks are the concentric zoning patterns of individual grains (Fig. 30) and a large compositional range within individual grains as well as in the whole data set. Typically the core is composed of chrome spinel surrounded by titanian chrome magnetite with secondary, pure magnetite forming the outer rim. In serpentinized rocks, both homogeneous chrome spinel grains as well as grains containing ilmenite exsolution lamellae can occur. The latter type is found particularly in the southeastern part of the Pechenga structure, metamorphosed to amphibolite facies grade (Abzalov et al., 1991a).

Smolkin and Pakhomovskiy (1985) distinguished four spinel types of which the first three occur in olivine cumulates in layered flows and intrusions and the fourth in the intermediate zone and overlying gabbroic cumulates of the intrusions. Type I is found as euhedral inclusions in olivine and corresponds to titanian chromite in composition. Type II occurs typically as idiomorphic crystals with complex zoning enclosed in clinopyroxene. The cores of zoned crystals are similar to Type I in composition while the next zone is composed of Ti-Cr magnetite followed by a two-phase zone composed of ilmenite-chromiferous magnetite. Besides zoned crystals, homogeneous crystals having compositions corresponding to Ti-Cr magnetite also are present. These spinels Smolkin and Pakhomovskiy (1985) designated Type III. Type IV is represented by ilmenomagnetite crystals in kazanskites, kosvites, and gabbroic rocks.

Figure 40 displays the compositional variation of spinels and the boundaries of the spinel generations of Smolkin and Pakhomovskiy (1985). There appears to be a continuous gradation in composition from Type I to III with a decrease in MgO, $Al_2O_3$, and $Cr_2O_3$, coupled with an increase in total FeO and $TiO_2$.

Although Smolkin and Pakhomovskiy (1985) admitted the possibility of postcrystallization processes masking the original regularity of certain components, they regard the chemical variation between types I to III essentially as a result of magmatic processes. According to these authors, the first generation of spinel may have been in equilibrium with olivine and the second and third generations with clinopyroxene. One of their arguments was the distribution of magnesium and iron between the spinels and olivines in Pechenga rocks. They plotted $Fe^{2+}/(Fe^{2+}+Mg)$ values of coexisting olivines and spinels against each other and noticed that the analyses of the Pechenga olivine-spinel pairs lie on the continuation of the trend of various magmatic rocks from other regions. The reference data used by Smolkin and Pakhomovskiy (1985) were mainly gathered from slowly cooled igneous complexes including large layered intrusions and Alpine-type ultramafic complexes, and mantle xenoliths. It is well known that in such environments, chrome spinel is prone

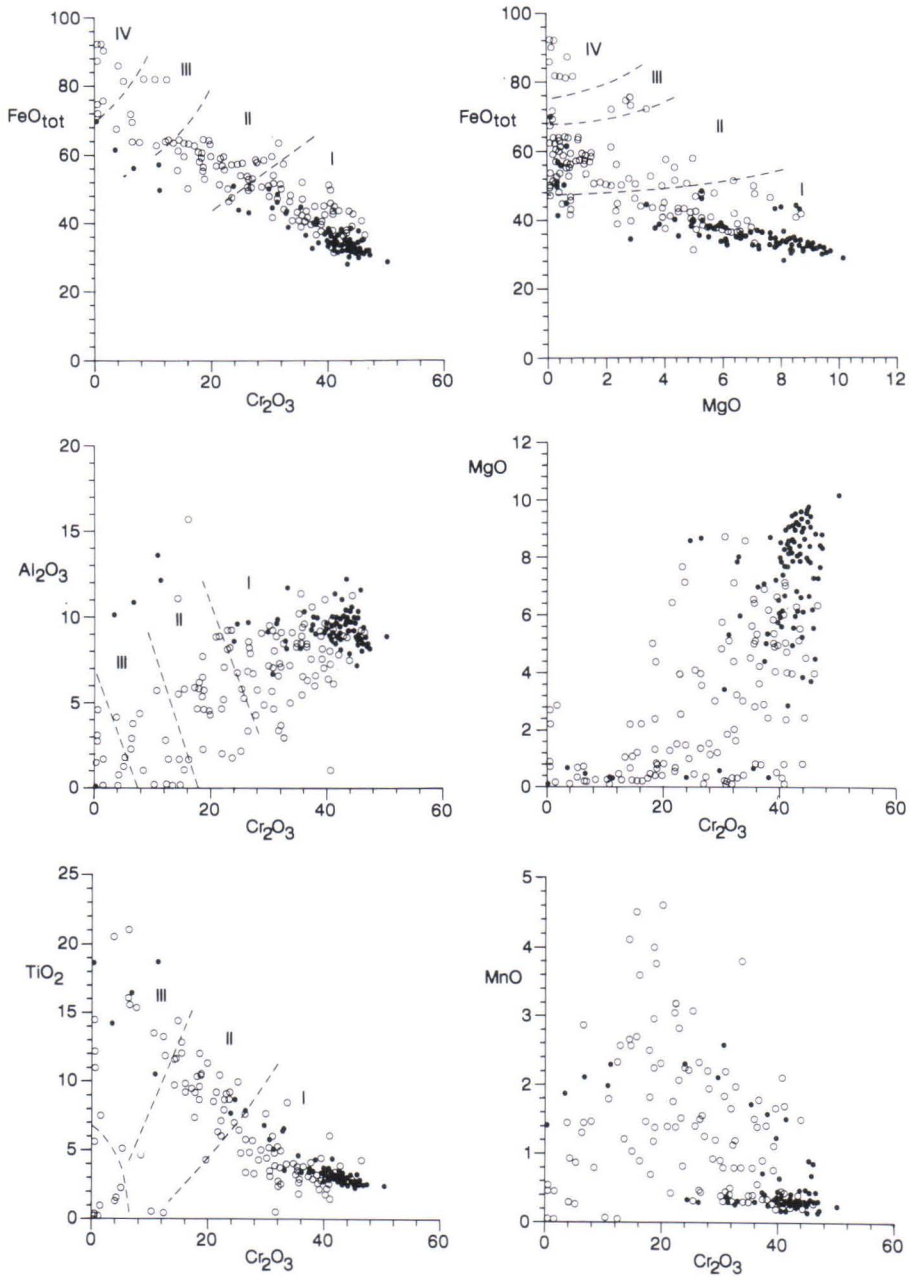


Fig. 40. Compositional variation (wt. %) of spinels from ferropicritic intrusive and extrusive rocks. Dots: this study, circles: data from the literature (Neradovskii and Smolkin, 1977; Smolkin, 1979, 1981; Yakovleva et al. 1983; Smolkin and Pakhomovskiy, 1985; Plaksenko and Smolkin, 1990; Abzalov et al., 1991a). Also shown are boundaries of different spinel generations as defined by Smolkin and Pakhomovskiy, 1985).

to various postcrystallization modifications promoted by subsolidus reactions with enclosing minerals and later alteration processes (e.g., Roeder and Campbell, 1985). Therefore, the comparison made by Smolkin and Pakhomovskiy (1985) does not provide conclusive evidence that the present-day compositions represent a magmatic olivine-spinel equilibrium in the Pechenga rocks.

Different approach was adopted in this study. Over the last decade, many experimental studies have been published on spinel-silicate liquid equilibria including those carried out by Fisk and Bence (1980), Barnes (1986), Murck and Campbell (1986), Roeder and Reynolds (1991), and Thy et al. (1991). These authors have conducted atmospheric experiments under widely varying $fO_2$ conditions on chrome spinel-saturated liquids with compositions such as komatiite, MORB, alkali basalt, tholeiitic basalt, boninite etc.. Compositions of olivines and spinels from these studies are compared with compositions of Pechenga olivine-spinel pairs in Fig. 41. When olivine had not been analysed or synthesized in these experimental runs, the equilibrium olivine composition was calculated using the exchange coefficient $K_D$* of 0.30 and the MgO and FeO contents of the corresponding experimental liquids. FeO was estimated from the total FeO of liquid by employing the method of Sack et al. (1980). From Fig. 41, it is evident that all the olivine-spinel pairs from Pechenga, including the MgO-rich ones discovered in this study, plot above the experimental array.

It is difficult to envisage that the chemical variation between spinel types I to III is a result of magmatic processes for the following reasons. In olivine cumulates in intrusions, chrome spinel is normally strongly zoned but associated primary silicates such as olivine and clinopyroxene are relatively homogeneous. As the first liquidus mineral, chrome spinel could equilibrate with a large reservoir of liquid and it is not likely that crystallization of a few per cent of chrome spinel could change the liquid composition so drastically as to bring about the observed zoning patterns. The second spinel generation, with evolved compositions in terms of low $Mg/(Mg+Fe^{2+})$ (0.01-0.4), is inferred to have begun to crystallize partly before olivine ceased to crystallize and continued during pyroxene crystallization (Smolkin and Pakhomovskiy, 1985). However, because it is enclosed within intercumulus pyroxene, it is presumably earlier than pyroxene. Intercumulus pyroxene as well as later intercumulus kaersutite in olivine cumulates possess high Mg/(Mg+Fe) values of between 0.81-0.88 and 0.70-0.82, respectively. These figures are hard to reconcile with very low Mg/(Mg+Fe) values in the chrome spinel of the second generation if its composition

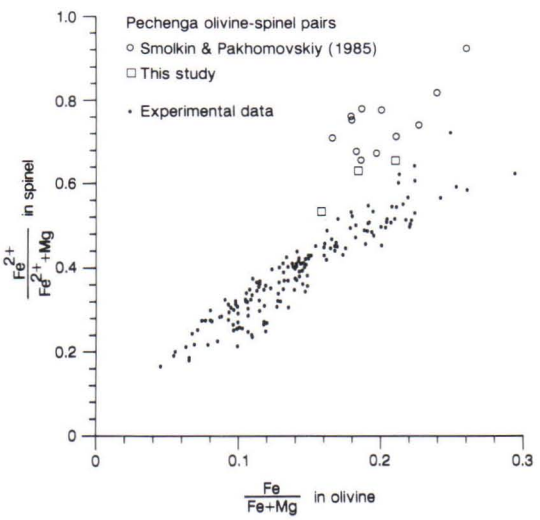


Fig. 41. Compositions of coexisting olivine-chrome spinel pairs from the Pechenga intrusions and experimental melting studies. Experimental data taken from Barnes (1986), Murck and Campbell (1986), Thy et al. (1991), Fisk and Bence (1980), and Roeder and Reynolds (1991).

* For the exchange coefficient of iron and magnesium between olivine and liquid, the symbol $K_D$ is used in this work, while the single element distribution coefficients of iron and magnesium are designated as $K_d$.

is magmatic and it crystallized earlier than or even coevally with pyroxene. Furthermore, the high $Cr_2O_3$ content in intercumulus pyroxenes (0.4-1.0 wt. %) and also in some amphiboles (up to 0.75 wt. %) indicates that much chromium was available during the crystallization of the spinel enclosed in these silicate minerals. Given the high affinity of chromium for spinel (e.g., Barnes, 1986; Murck and Campbell, 1986), it is improbable that the spinel of the second generation with only 15-30 wt. % $Cr_2O_3$ could crystallize before the high-Cr pyroxene.

From the above consideration, it can be concluded that the Pechenga spinels have undergone pervasive postcrystallization alteration processes. In fact, most of the so far published chrome spinel analyses are relatively low-MgO varieties which have lost a varying amount of their original MgO (Fig. 40). It is certainly true that magmatic fractionation of $Mg/(Mg+Fe^{2+})$ has taken place but this fractionation is likely to be revealed in a progressive change of the chrome spinel composition with height in a magmatic body and not as a strong zonation in individual spinel grains, at least not to the extent indicated in previous studies.

In this study, several chrome spinel grains have been analysed which contain relatively high MgO contents, up to 10 wt. %, and which represent the most pristine and primitive spinel compositions so far discovered. Table 6 gives the compositions of selected high-MgO chrome spinel grains. The MgO-rich spinels (MgO 8-10 wt. %, Mg number 0.38-0.48) have the following chemical characteristics. The $Cr_2O_3$ content is relatively low (mostly less than 50 wt. %) which is compensated for by the high abundance of iron (FeO 19-23 wt. %, $Fe_2O_3$ 10-15 wt. %). The $Fe^{3+}/(Fe^{3+}+Fe^{2+})$ value is commonly between 0.30-0.38 which is typical of spinels crystallized under $fO_2$ conditions varying from the FMQ buffer curve to about one log unit above this curve (e.g., Murck and Campbell, 1986). The $Al_2O_3$ contents are also low, falling below 10 wt. %, which is primarily a consequence of the low $Al_2O_3$ content of the ferropicritic liquid (cf. Maurel and Maurel, 1983). A notable feature of the

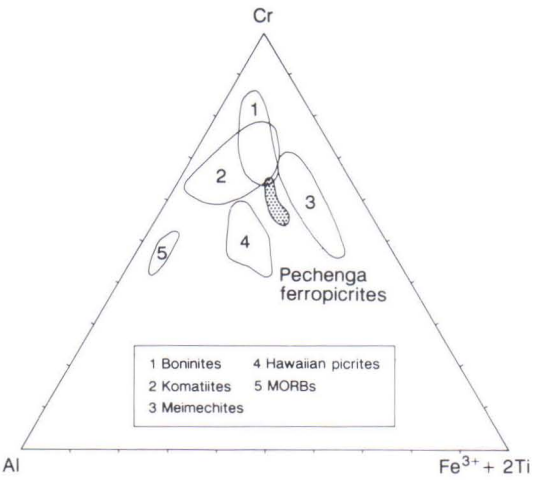


Fig. 42. Ternary Al-Cr-($Fe^{3+}$+2Ti) plot comparing most magnesian (8-10 wt. % MgO) Pechenga spinels with spinels from komatiites (1), boninites (2), meimechites (3), Hawaiian picrites (4) and MORBs (5). Fields 1-3 have been taken from Plaksenko and Smolkin (1990), field 4 is based on data from Nicholls and Stout (1988) and Hawkins and Melchior (1983), and field 5 on data from Sigurdsson and Schilling (1976).

ferropicritic spinels is their high abundance of $TiO_2$, averaging about 3.0 wt. %. This feature is an obvious reflection of the $TiO_2$-rich nature of the magma. The above listed chemical properties justify the classification of the most primitive spinels at Pechenga as titanian aluminous magnesiochromites. Comparable $TiO_2$ values have been observed in alkali basalts (Evans, 1987) and $TiO_2$-rich Hawaiian picrites (Hawkins and Melchior, 1983). The chrome spinel compositions of ferropicrites are compatible with other mineralogical and whole rock geochemical data which show many of the characteristics of intraplate magmas (cf. Arai, 1992).

In Fig. 42, which shows the cation proportions of Cr-Al-($Fe^{3+}$+2Ti), the Pechenga spinels with MgO 8-10 wt. % are compared with spinels from other primitive magmas including komatiites, boninites, meimechites, Hawaiian picrites, and MORBs. The high $FeO_{tot}$ and $TiO_2$ contents of the ferropicritic magma accounts for the location of the Pechenga spinels towards the $Fe^{3+}$+2Ti cor-

ner from the komatiite and boninite fields. On the other hand, the location of the Pechenga spinels between the fields of spinels from Hawaiian picrites and meimechites is compatible with the decreasing $Al_2O_3$ content of the liquid from Hawaiian picrites through Pechenga ferropicrites to meimechites (see below).

A few spinels with high $Al_2O_3$ and low $Cr_2O_3$ contents in Fig. 40 represent altered spinels in sulfide ore samples from the Kammikivi deposit. They have lost most of their chromium but retained their original abundances of aluminum presumably because of the absence of suitable enclosing minerals which could have captured the $Al_2O_3$ from these spinels. Alteration also accounts for the high MnO content of low-MgO spinels, increasing to several per cent MnO (Fig. 40) which, as also recognized by Smolkin and Pakhomovskiy (1985), is anomalous when compared with the manganese contents of spinels from other magmatic complexes.

It should be added that some compositionally anomalous spinels have also been discovered in the Ortoaivi and Pilgujärvi intrusions. These spinels look fresh under the microscope and the primary silicate mineralogy is also well preserved in the samples. The MgO content in these grains is relatively high (7.8-8.7 wt. %) which, together with petrographic evidence, suggest a low degree of metamorphic alteration. They differ from other

Table 6. Representative microprobe analyses of chrome spinels (#1-15) from the Kammikivi sill, Pilgujärvi intrusion and Lammas layered flow and chemical analysis of titanomagnetite (#16) from the Pilgujärvi intrusion.

| Location$ | 1 Ka | 2 Ka | 3 Ka | 4 Ka | 5 Ka | 6 Ka | 7 Ka | 8 Ka | 9 Ka | 10 Pi | 11 La | 12 La | 13 La | 14 La | 15 La | 16** Pi |
|---|---|---|---|---|---|---|---|---|---|---|---|---|---|---|---|---|
| $SiO_2$ | 0.09 | 0.09 | 0.07 | 0.06 | 0.00 | 0.06 | 0.00 | 0.07 | 0.00 | 0.00 | 0.07 | 0.06 | 0.00 | 0.00 | 0.06 | 2.18 |
| $TiO_2$ | 2.84 | 2.83 | 2.97 | 3.45 | 3.20 | 3.64 | 3.30 | 3.29 | 3.19 | 5.11 | 2.45 | 2.85 | 2.62 | 2.47 | 2.75 | 10.97 |
| $Al_2O_3$ | 9.95 | 9.96 | 9.90 | 9.20 | 9.02 | 9.43 | 8.44 | 9.24 | 8.86 | 9.68 | 8.84 | 9.40 | 8.13 | 8.29 | 8.87 | 2.83 |
| $Fe_2O_3$ | 11.82 | 11.93 | 12.06 | 12.95 | 13.12 | 13.33 | 13.52 | 11.69 | 14.17 | 18.81 | 10.06 | 10.69 | 9.68 | 9.88 | 11.13 | 46.43 |
| FeO | 20.57 | 21.73 | 21.50 | 21.56 | 22.23 | 21.99 | 22.55 | 22.07 | 23.67 | 29.28 | 19.64 | 21.51 | 21.71 | 22.33 | 22.09 | 32.88 |
| MnO | 0.29 | 0.30 | 0.29 | 0.28 | 0.16 | 0.30 | 0.16 | 0.33 | 0.17 | 0.36 | 0.24 | 0.30 | 0.01 | 0.17 | 0.46 | 0.44 |
| MgO | 9.52 | 9.06 | 9.01 | 9.15 | 8.58 | 8.51 | 8.47 | 8.39 | 8.14 | 5.30 | 10.16 | 8.82 | 8.80 | 8.33 | 7.88 | 2.71 |
| CaO | 0.02 | 0.03 | 0.00 | 0.00 | n.a. | 0.03 | n.a. | 0.02 | n.a. | n.a. | 0.02 | 0.02 | n.a. | n.a. | 0.02 | 0.07 |
| $Na_2O$ | 0.01 | 0.00 | 0.00 | 0.00 | n.a. | 0.03 | n.a. | 0.00 | n.a. | n.a. | 0.00 | 0.00 | n.a. | n.a. | 0.00 | n.a. |
| $K_2O$ | 0.00 | 0.00 | 0.00 | 0.00 | n.a. | 0.00 | n.a. | 0.01 | n.a. | n.a. | 0.00 | 0.00 | n.a. | n.a. | 0.00 | n.a. |
| $Cr_2O_3$ | 42.41 | 43.05 | 41.85 | 41.05 | 41.63 | 38.16 | 41.41 | 41.10 | 41.67 | 31.30 | 47.75 | 43.93 | 47.31 | 47.38 | 42.69 | 0.05 |
| NiO | 0.16 | 0.20 | 0.16 | 0.17 | 0.07 | 0.17 | 0.33 | 0.13 | 0.08 | n.a. | 0.25 | 0.22 | 0.16 | 0.15 | 0.23 | 0.05 |
| ZnO | n.a. | n.a. | n.a. | 0.08 | n.d. | 0.07 | n.a. | 0.07 | n.a. | 0.20 | n.a. | 0.08 | n.a. | n.a. | 0.03 | n.a. |
| Total | 97.67 | 99.17 | 97.83 | 97.97 | 98.02 | 95.71 | 98.18 | 96.39 | 99.95 | 100.02 | 99.49 | 97.89 | 98.42 | 99.00 | 96.22 | 98.61 |
| Structural formula based on 32 oxygens | | | | | | | | | | | | | | | | |
| Si | 0.024 | 0.024 | 0.019 | 0.017 | 0.000 | 0.018 | 0.000 | 0.019 | 0.000 | 0.000 | 0.020 | 0.017 | 0.000 | 0.000 | 0.016 | 0.626 |
| Ti | 0.579 | 0.571 | 0.608 | 0.707 | 0.661 | 0.764 | 0.678 | 0.687 | 0.646 | 1.060 | 0.493 | 0.586 | 0.538 | 0.505 | 0.579 | 2.367 |
| Al | 3.184 | 3.154 | 3.174 | 2.955 | 2.921 | 3.106 | 2.722 | 3.025 | 2.815 | 3.147 | 2.782 | 3.025 | 2.613 | 2.659 | 2.928 | 0.957 |
| $Fe^{3+}$# | 2.415 | 2.412 | 2.471 | 2.655 | 2.711 | 2.802 | 2.785 | 2.443 | 2.873 | 3.905 | 2.023 | 2.196 | 1.985 | 2.022 | 2.344 | 10.024 |
| $Fe^{2+}$ | 4.670 | 4.882 | 4.895 | 4.913 | 5.106 | 5.135 | 5.164 | 5.126 | 5.334 | 6.758 | 4.390 | 4.911 | 4.950 | 5.080 | 5.171 | 7.889 |
| Mn | 0.067 | 0.068 | 0.068 | 0.065 | 0.038 | 0.072 | 0.038 | 0.077 | 0.038 | 0.083 | 0.054 | 0.069 | 0.003 | 0.040 | 0.109 | 0.107 |
| Mg | 3.852 | 3.627 | 3.656 | 3.718 | 3.513 | 3.541 | 3.458 | 3.473 | 3.268 | 2.178 | 4.048 | 3.588 | 3.576 | 3.376 | 3.288 | 1.159 |
| Ca | 0.005 | 0.008 | 0.000 | 0.000 | - | 0.008 | - | 0.006 | - | - | 0.007 | 0.006 | - | - | 0.005 | 0.022 |
| Na | 0.005 | 0.000 | 0.001 | 0.000 | - | 0.017 | - | 0.000 | - | - | 0.000 | 0.000 | - | - | 0.000 | - |
| K | 0.000 | 0.000 | 0.000 | 0.000 | - | 0.000 | - | 0.002 | - | - | 0.001 | 0.000 | - | - | 0.000 | - |
| Cr | 9.105 | 9.145 | 9.005 | 8.842 | 9.040 | 8.426 | 8.964 | 9.028 | 8.877 | 6.828 | 10.09 | 9.481 | 10.20 | 10.19 | 9.450 | 0.011 |
| Ni | 0.034 | 0.043 | 0.035 | 0.037 | 0.015 | 0.037 | 0.073 | 0.028 | 0.017 | - | 0.054 | 0.049 | 0.034 | 0.032 | 0.052 | 0.011 |
| Zn | - | - | - | 0.017 | - | 0.015 | - | 0.015 | - | 0.040 | - | 0.016 | - | n.a. | 0.007 | - |
| Anal.* | O | O | O | O | E | O | E | O | E | E | O | O | E | E | O | A |

n.a. = not analysed.
* Analysis place: O, University of Oulu; E, Geological Survey of Finland, Espoo; A, Geological Institute, Apatity (chemical analysis).
# The ferric iron contents of chromites were calculated by assuming perfect spinel stoichiometry, after removing an ulvospinel component based on $TiO_2$ content.
** Taken from Neradovskii and Smolkin (1977).
$ Location: Ka = Kammikivi sill, Pi = Pilgujärvi intrusion; La = Lammas layered flow.
Rock types: 1-15, olivine cumulate; 16, olivine-magnetite cumulate.
Samples: **1-3**, Pet1/25.60; **4-9**, Pet1/33.00; **10**, PJ 8; **11-14**, 1748/3; **15**, 1748/2; **16**, 4208.

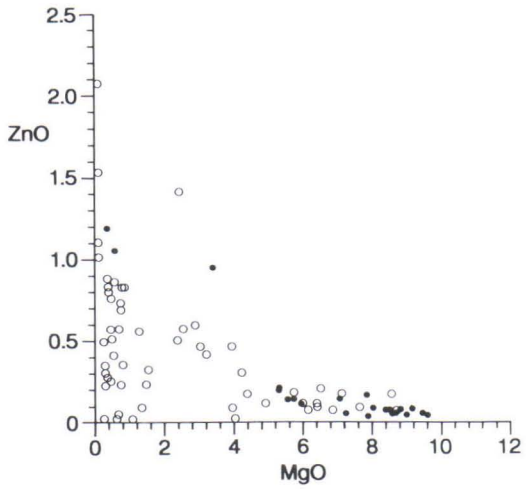


Fig. 43. Zinc content (wt. %) of Pechenga spinels as a function of their MgO content (wt. %). Dots: this study, circles: data from the literature (Smolkin and Pakhomovskiy, 1985; Plaksenko and Smolkin, 1990; Abzalov et al., 1991a).

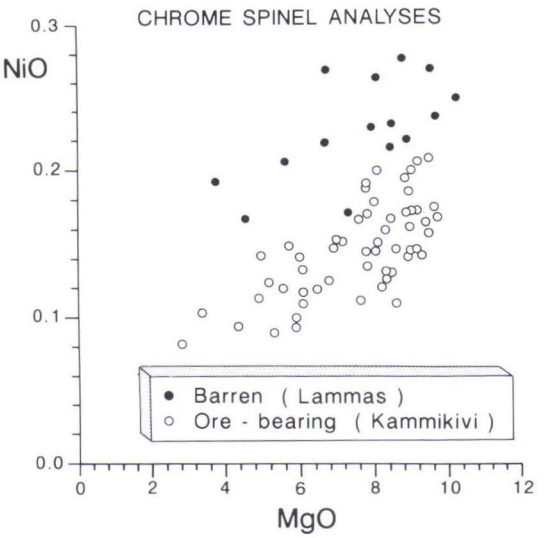


Fig. 44. NiO versus MgO (wt. %) for spinels from the mineralized Kammikivi layered sill and the barren Lammas layered flow.

high-MgO spinels in having high $FeO_{tot}$ (43-44 wt. %) and low $Cr_2O_3$ (24.6-33.0 wt. %) contents (see Fig. 40) which coupled with anomalously high $TiO_2$ abundances (6.4-8.7 wt. %), indicate high contents of the ulvospinel component. Also the $V_2O_3$ content, between 0.65-0.70 wt. %, is about double the normal level. Whole rock analyses of corresponding peridotites show $Al_2O_3/TiO_2$ and $V/Al_2O_3$ values typical of other ferropicritic rocks. This rules out the existence of compositionally distinct magma batch from which these samples crystallized.

The elevated zinc content (>0.6 atomic % Zn; Groves et al., 1977) of chrome spinels occurring in mineralized komatiite units in the Kambalda area in Western Australia has been attributed to assimilation of zinc by komatiitic magma from Zn-bearing, sulfide-rich sedimentary rocks. The high zinc content has been used as an indicator of a mineralized ultramafic sequence. Against this background, it is interesting to consider the behavior of zinc in the Pechenga chrome spinels, particularly, because the ore-bearing intrusions at Pechenga are spatially associated with phyllitic metasediments rich in sulfur and in some cases also in Zn (up to 700 ppm). According to data published earlier, the zinc content of spinels from Pechenga rocks varies within wide limits (0.02-3.21) (Smolkin and Pakhomovskiy, 1985; Plaksenko and Smolkin, 1990) but its significance has not been clearly stated. In Fig. 43, the MgO and ZnO contents of the analysed Pechenga spinels are plotted against each other. It is obvious that the most primitive, MgO-rich spinels possess low ZnO contents, falling below 0.2 wt. %. This is true for chrome spinels from both ore-bearing and barren bodies. The ZnO content varies widely and in some cases may exceed 1 wt. % in low-Mg spinels which are interpreted not to have retained their primary igneous composition. Thus, the ZnO content of spinel does not appear to be a useful tool in distinguishing potential exploration targets at Pechenga.

Smolkin and Pakhomovskiy (1985) compared

chrome spinels from the Ni-bearing Pilgujärvi intrusion and the barren Souker intrusion. They did not discover any notable differences in the nickel content of spinels from these two areas and concluded that the nickel content of chrome spinels does not have any practical prospecting significance. However, there are significant differences between separate magmatic bodies when the nickel content is compared at the same MgO level of spinel. An example is illustrated in Fig. 44 where spinel compositions from the mineralized Kammikivi layered sill and unmineralized Lammas layered flow are plotted. More data are needed to test whether this kind of plot has more general applicability as an indicator of the chalcophile element depletion of the magma. In any case, because of the ubiquitous alteration of olivine in layered flows, MgO-rich chrome spinels appear to provide a possibility for comparing the behavior of nickel in different intrusions and lava flows.

Neradovskii and Smolkin (1977) have published chemical analyses of the fourth spinel type, titanomagnetite, from pyroxene-magnetite and olivine-magnetite cumulates of the intermediate layer in the Pilgujärvi intrusion (Table 6). When the possible sulfide and silicate impurities are taken into account, the analyses show that titanomagnetite is very low in $Cr_2O_3$ and NiO. Broad beam microprobe analyses performed on a few titanomagnetite grains with trellis exsolution patterns give the following results (wt. %): $TiO_2$ 15.0-16.6%, $Al_2O_3$ 4.0-4.7%, $FeO_{tot}$ 72.0-75.7%, MnO 0.43-0.49%, and MgO 1.0-1.3%.

Table 7. Representative analyses of ilmenites from ferropicritic rocks (analysed at the Geological Survey of Finland, Espoo).

| | 1 | 2 | 3 | 4 | 5 | 6 |
|---|---|---|---|---|---|---|
| $SiO_2$ | 0.00 | 0.01 | 0.00 | 0.04 | n.a. | n.a. |
| $TiO_2$ | 47.62 | 49.66 | 47.35 | 48.73 | 47.83 | 46.50 |
| $Al_2O_3$ | 0.04 | 0.03 | 0.13 | 0.17 | 0.22 | 0.06 |
| $Fe_2O_3$ | 6.29 | 3.45 | 7.73 | 5.45 | 5.02 | 6.07 |
| FeO | 41.06 | 41.50 | 42.99 | 43.83 | 42.82 | 41.64 |
| MnO | 2.15 | 2.01 | 1.38 | 1.22 | 3.19 | 3.58 |
| MgO | 1.66 | 1.83 | 0.97 | 0.78 | 0.02 | 0.00 |
| CaO | 0.02 | 0.00 | 0.01 | 0.01 | n.a. | n.a. |
| $Cr_2O_3$ | 1.18 | 1.22 | 0.06 | 0.05 | 0.02 | 0.01 |
| ZnO | 0.03 | 0.03 | 0.03 | 0.00 | n.a. | n.a. |
| Total | 100.07 | 99.74 | 100.66 | 100.28 | 99.12 | 97.86 |
| Structural formula based on 32 oxygens | | | | | | |
| Si | 0.001 | 0.004 | 0.001 | 0.012 | - | - |
| Ti | 9.640 | 10.020 | 9.587 | 9.874 | 9.739 | 9.609 |
| Al | 0.013 | 0.009 | 0.040 | 0.054 | 0.070 | 0.019 |
| $Fe^{3+}$ | 1.275 | 0.696 | 1.566 | 1.105 | 1.022 | 1.256 |
| $Fe^{2+}$ | 9.241 | 9.311 | 9.680 | 9.876 | 9.695 | 9.570 |
| Mn | 0.491 | 0.457 | 0.315 | 0.279 | 0.731 | 0.832 |
| Mg | 0.665 | 0.732 | 0.391 | 0.315 | 0.009 | 0.000 |
| Ca | 0.006 | 0.000 | 0.004 | 0.002 | - | - |
| Cr | 0.252 | 0.259 | 0.013 | 0.011 | 0.004 | 0.002 |
| Zn | 0.007 | 0.006 | 0.007 | 0.000 | - | - |

n.a. = not analysed.
Rock types and samples: **1-2**, olivine cumulate, Pilgujärvi intrusion, PJ 8; **3-4**, olivine-titanomagnetite cumulate, Pilgujärvi intrusion, PJ 9; **5-6**, evolved ferropicritic lava, Lake Ilya Souker, Souker1/90.

## Ilmenite

Ilmenite is an accessory phase in almost all rock types. It occurs as subhedral intercumulus phases in ultramafic cumulates, euhedral cumulus grains in gabbroic rocks and as skeletal needles in evolved ferropicritic metavolcanites. Ilmenites analysed in this work occur in olivine and olivine-magnetite cumulates from the Pilgujärvi intrusion and in a globular rock from the Lake Ilya Souker area. Examples of ilmenite analyses are reported in Table 7. Recalculated compositions show that they are low in $Fe_2O_3$ with the hematite component typically falling below 8 mol. %.

Ilmenites have significant MgO contents in olivine and olivine-magnetite cumulates (1.7-1.8

wt. % and 0.8-1.1 wt. %, respectively), but in evolved ferropicritic lavas these minerals are virtually devoid of MgO. Instead, the latter are most enriched in manganese containing 3.1-3.7 wt. % MnO while the analysed ilmenites in olivine and olivine-magnetite cumulates possess 2.0-2.2 wt. % and 1.2-1.4 wt. % MnO, respectively.

## Other minerals

Plagioclase is typically absent from primitive ferropicritic metavolcanites but occurs as skeletal laths in the differentiated parts of layered flows. In layered intrusions, it occurs as a poikilitic intercumulus phase in ultramafic cumulates but its recognition is generally possible only in the best-preserved samples. The abundance of plagioclase increases upwards with a change in its mode of occurrence from an intercumulus phase in pyroxenites to a cumulus phase in gabbros. Plagioclase has not retained its magmatic composition but is everywhere more or less albitized. Analyses of plagioclases from the Pilgujärvi intrusion show An values between 10-24% while $An_{43}$ has been measured in a plagioclase relict in the Western Ortoaivi intrusion (Smolkin, 1977).

Microprobe analyses were made on apatites in one olivine cumulate from the Ortoaivi intrusion in which this mineral occurs as an intercumulus phase. Its F and Cl contents range between 1.0-1.6 wt. % and 0.7-1.1 wt. %, respectively. Apatite with a higher F content (3.05 wt. %) has been reported from a gabbro-pegmatite in the middle part of the Pilgujärvi intrusion (Hanski et al., 1990).

# MAJOR AND TRACE ELEMENT GEOCHEMISTRY

## Analytical techniques and samples

Major elements and the trace elements Cu, S, V, Zr, and Sr were determined by applying conventional X-ray fluoresence analysis (XRF) and by using Philips PW1400 spectrometers at the research laboratory of the Rautaruukki Co. in Raahe, Finland and at the Geological Survey of Finland (GSF) in Espoo. All the other trace elements including rare earth elements (REE) were analysed by instrumental neutron activation analysis (INAA), mostly at the Reactor Laboratory of the State Technical Research Center (STRC) in Espoo. For details of the method used at the STRC, the reader is referred to Rosenberg et al. (1982). INAA analyses were also carried out by G. Brügmann at the Department of Geology of the University of Toronto. In addition, some XRF major element and INAA trace element analyses were performed at two commercial laboratories, X-ray Assay Laboratories Ltd. and Activation Laboratories Ltd. in Canada. Trace element analyses of a few key samples were also carried out by J. Bitmead employing spark source mass spectro-

metry at the Australian National University in Canberra.

Volatiles and the oxidation state of iron were determined for selected samples at the GSF in Espoo. Because ultramafic rocks in the Pechenga area were hydrated and carbonated to varying degrees during regional metamorphism and may contain large amounts of volatiles, the compositions were recalculated to 100% on a volatile free basis.

The chemical laboratory of the GSF in Rovaniemi provided Se and Te analyses produced by graphite furnace atomic absorption spectromery (GFAAS) and As analyses performed by inductively coupled plasma-atomic emission spectrometry (ICP-AES). Platinum-group elements (PGE) were determined by G. Brügmann using fire-assay preconcentration at the Department of Geology of the University of Toronto and radiochemical neutron activation analysis (RNAA) at the McMaster University (Hamilton, Ontario) (Brügmann et al., 1990).

INAA data from more than one laboratory permitted a comparison to be made on the analytical results. The most significant observation was that the Sc values from the STRC are systematically higher than those from the other laboratories. STRC reports values which are on average 1.4 times higher than those reported by the other laboratories. This is surprising, because Sc is generally regarded as an ideal element for analysis by INAA. This conclusion concerning exceedingly high Sc contents in analyses produced by the STRC was not merely an artefact of the interlaboratory comparison of the Pechenga samples since the same features were apparent from an examination of a large data file gathered during the Lapland Volcanite Project on various metavolcanites from northern Finland. Literature data on corresponding rock types generally show distinctly lower values for Sc. Despite the erroneous absolute Sc abundances in some of the analyses, some petrological information can nevertheless be obtained from these results because the relative abundances of Sc between various samples seem to be pertinent. For example, in olivine cumulates, the ratio of Sc to some other incompatible elements such as Ti appears to remain constant as is predicted.

Samples from various sources were utilized in this study. The geochemical investigation of ferropicrites, gabbro-wehrlite intrusions, and ultrafelsic tuffs greatly benefitted from the provision of representative samples by V. Smolkin. Some ferropicrite specimens were also donated by P. Skufin. Also numerous hand specimens and a few drill cores, including those penetrating the Kammikivi Ni-Cu deposit, dating back to Finnish control of the region in the 1920's and 1930's, served as valuable background material for geochemical and mineralogical study (see Väyrynen, Figures 52, 53, and 55). Additional samples of basic metavolcanites, globular ferropicritic rocks, layered lava flows, sulfide ores and associated host and country rocks were collected by the author during his two excursions to the Pechenga area.

A large amount of analytical data collected from the literature has been used as reference material in many diagrams. These include analyses of komatiites and other primitive magmas, analyses of other recent volcanic rocks from various tectonic settings, compositions of upper mantle materials, and chemical data published earlier on the Pechenga area. Results from moderate to high pressure melting experiments have also been compiled. While most of the figure captions in this study do not include references to these literature data, such references are available from the author upon request. The analytical data were manipulated by employing a VAX 4000-300 computer and the HST data processing system (Kaivosoja and Koivumaa, 1984).

## Geochemistry of the different volcanic suites of the Pechenga Series

Each volcanic unit of the Pechenga Series has its own chemical characteristics (Kremenetskii and Ovchinnikov, 1986; Sharkov and Smolkin, 199O). Nonferropicritic rock compositions are plotted on a TAS diagram in Fig. 45 and typical analyses of volcanic rocks from each unit are listed in Table 8. Figure 45 shows that intermediate volcanics predominate in the Ahmalahti Suite while there is a wide, continuous compositional spread in the Kuetsjärvi metavolcanites. In contrast, the overlying Kolosjoki Suite exhibits only a restricted range of compositions in the basaltic part of the diagram. The Pilgujärvi Suite is characterized by a bimodal distribution of chemical compositions and comprises basalts and high-silica rhyolites.

The metavolcanites of the Ahmalahti Suite range from basalts to dacites in their silica content and straddle the boundary between the tholeiitic and calc-alkaline magma series. They are enriched in light REE with $(La/Yb)_N$ >10 in which $(La/Yb)_N$ denotes the chondrite-normalized ratio of La to Yb. The Ahmalahti metavolcanites also have relatively low concentrations of high field strength elements (HFSE). This results in low Ti-Zr ratios (about 50) and negative Ta anomalies (Fig. 46). These trace element characteristics are general features of granitoids in Archean granite-gneiss terrains (e.g., Taylor and McLennan, 1985). Similar properties are also recognizable in the basement complex at Pechenga, as exemplified by two granite samples taken from the basement below the first volcanic formation (Fig. 46). The striking similarity of many elemental ratios in the spidergrams of the metavolcanite and granite samples implies a marked crustal signature in the composition of the metavolcanites of the Ahmalahti Suite. An analogous situation appears to prevail with regard to volcanic rocks that represent initial stages of the early Proterozoic volcanism in the Baltic Shield (Räsänen et al., 1989; Huhma et al., 1990; Manninen, 1991) and also in the Circum-Superior Belt in Canada (Arndt et al., 1987; Jolly, 1987). The compositional properties of these metavolcanites have commonly been attributed to crustal contamination, which, in the Pechenga area, is also supported by the existence of eruptive centers in which volcanic rocks contain large granitic fragments.

Apart from minor amounts of picrites, the volcanic rocks of the Kuetsjärvi Suite include mildly alkaline lavas ranging in composition from alkali basalts to trachytes (Skufin et al., 1986). These clearly show higher total alkali contents at equivalent $SiO_2$ levels compared with metavolcanites from the other stratigraphic units (Fig. 45). They are LREE-enriched but have variable $(La/Yb)_N$ values (Fig. 47). The Kuetsjärvi metavolcanites have relatively high $TiO_2$ contents. They also possess high contents of other HFSE as opposed to the underlying HFSE-depleted metavolcanites

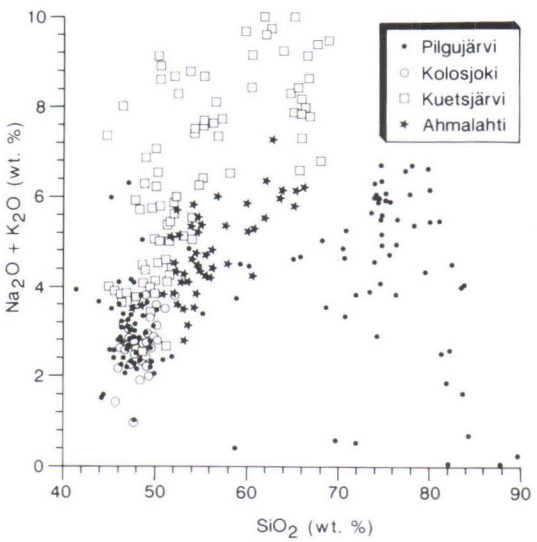


Fig. 45. Total alkali versus $SiO_2$ diagram (TAS) for volcanic rocks (excluding ferropicritic metavolcanites) from the four volcanic units of the Pechenga Series (data from this study and the literature).

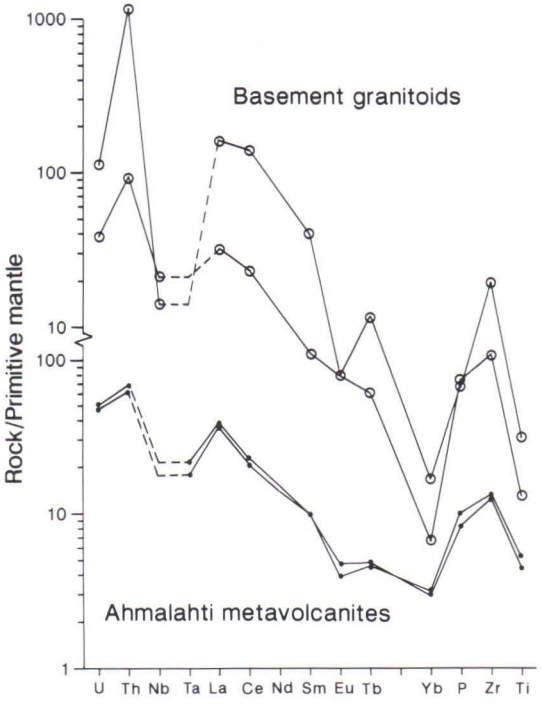


Fig. 46. Incompatible elements normalized to primitive mantle values for basaltic andesites from the Ahmalahti Suite and two granites from the basement complex.

of the Ahmalahti Suite and plot into the field of intra-plate volcanites on various discrimination diagrams.

The mafic metavolcanites of the Kolosjoki and Pilgujärvi Suites are relatively homogeneous iron-rich tholeiitic basalts. In terms of major element geochemistry, tholeiites from both units are very similar. They commonly have 48-52% $SiO_2$, 5.5-8% MgO, and 13-15% $FeO_{tot}$. They have a slight but significant difference in their chondrite-normalized REE patterns; the Kolosjoki metavolcanites display flat or slightly LREE-enriched patterns while the Pilgujärvi metavolcanites are slightly LREE-depleted (Kremenetskii and Ovchinnikov, 1986) (Fig. 47).

Sharkov and Smolkin (1990) emphasized the similarity of the REE patterns between the Kolosjoki and Pilgujärvi tholeiites and those of MORBs. The major element composition of these metavolcanites, however, have features that distinguish them from modern MORBs and also from contemporaneous MORB-like basalts represented by tholeiites from the 1.97-Ga-old Jormua ophiolite in Central Finland (Kontinen, 1987). On the $MgO-Al_2O_3-FeO_{tot}$ discrimination diagram by Pearce et al. (1977), the tholeiites of the Kolosjoki and Pilgujärvi Suites plot into the fields of continental and ocean island basalts (Fig. 48) reflecting the relatively high total iron content of the Pechenga metavolcanites. In contrast, the Jormua metavolcanites are located in the field of ocean ridge and floor basalts. Crystal fractionation could drive the residual liquid composition from the MORB field to the field of continental tholeiites on this diagram, but as is illustrated in Fig. 49, the Pechenga tholeiites differ from MORBs with respect to their $FeO_{tot}$ and $TiO_2$ relationships, two components which show similar behavior during crystallization processes. Modern MORBs and related differentiates form a field distinctly to the right of the fields of the Kolosjoki and Pilgujärvi tholeiites. This difference is also observed when the Kolosjoki and Pilgujärvi tholeiites are compared with Phanerozoic volcanites from various tectonic settings, including flood basalts and other volcanites related to continental rifting (Fig. 50). Data obtained in the Lapland Volcanite Project and literature data from Russian Karelia indicate that high $FeO_{tot}$ coupled with relatively low $TiO_2$ values appears to be a general feature of Jatulian and younger Karelian basic metavolcanites in the eastern and northern part of the Fennoscandian Shield.

The ferropicritic metavolcanites of the Kolosjoki and Pilgujärvi Suites cannot be distinguished from each other on the basis of their major element compositions. It is significant that the products of similar ferropicritic volcanism were erupted intermittently during the deposition of kilometers of supracrustal rocks from the base of the Kolosjoki Suite to the upper part of the Pilgujärvi Suite. The geochemistry of ferropicrites of the Pilgujärvi Suite is considered in detail in the succeeding chapter.

The silica content of the so-called tufosilitsites

Table 8. Analyses of volcanic rocks from different units of the Pechenga Series.

| Unit[$] | 1<br>Ah | 2<br>Ah | 3<br>Ah | 4<br>Ku | 5<br>Ku | 6<br>Ku | 7<br>Ku | 8<br>Ku | 9<br>Ko |
|---|---|---|---|---|---|---|---|---|---|
| $SiO_2$ | 51.00 | 51.70 | 54.17 | 50.35 | 47.86 | 50.11 | 44.95 | 46.85 | 48.43 |
| $TiO_2$ | 0.97 | 1.12 | 0.73 | 2.39 | 2.27 | 2.36 | 2.22 | 1.48 | 1.64 |
| $Al_2O_3$ | 12.60 | 13.90 | 13.43 | 17.10 | 14.22 | 13.44 | 11.82 | 9.16 | 13.19 |
| $Fe_2O_3$ | 3.27 | 3.07 | n.a. | 11.92 | 3.48 | n.a. | n.a. | 8.28 | 3.24 |
| FeO | 8.23 | 7.63 | n.a. | 2.84 | 12.39 | n.a. | n.a. | 6.34 | 10.96 |
| $FeO_{tot}$ | 8.95 | 8.04 | 8.45 | 13.56 | 15.52 | 13.02 | 13.53 | 13.79 | 13.87 |
| MnO | 0.19 | 0.17 | 0.15 | 0.08 | 0.23 | 0.16 | 0.24 | 0.21 | 0.19 |
| MgO | 8.50 | 6.54 | 5.06 | 2.05 | 6.25 | 4.05 | 7.86 | 14.18 | 6.35 |
| CaO | 7.17 | 7.34 | 7.61 | 1.42 | 5.53 | 7.97 | 9.21 | 8.05 | 9.40 |
| $Na_2O$ | 3.47 | 4.04 | 3.96 | 5.97 | 3.10 | 4.71 | 1.97 | 3.02 | 2.36 |
| $K_2O$ | 0.33 | 1.06 | 1.81 | 3.15 | 0.55 | 1.51 | 2.02 | 0.79 | 0.27 |
| $P_2O_5$ | 0.18 | 0.22 | 0.13 | 0.34 | 0.20 | 0.65 | 0.56 | n.a. | 0.13 |
| L.O.I. | n.a. | n.a. | n.a. | 2.13 | 2.78 | n.a. | n.a. | n.a. | 3.50 |
| Cr | 695 | 319 | 111 | 200 | n.a. | 99 | 180 | n.a. | 78.2 |
| Ni | 150 | 34.8 | 55 | 55 | n.a. | 92 | 100 | n.a. | 51.5 |
| Co | 58.2 | 49.0 | n.a. | n.a. | n.a. | n.a. | 49 | n.a. | 49.2 |
| Sc | 38.5 | 43.5 | n.a. | n.a. | n.a. | n.a. | 11 | n.a. | 17.4 |
| V | 230 | 240 | 238 | n.a. | n.a. | 440 | 411 | n.a. | 330 |
| Zr | 140 | 150 | 100 | n.a. | n.a. | 187 | 163 | n.a. | 57.1 |
| Ta | 0.713 | 0.869 | n.a. | n.a. | n.a. | n.a. | 3 | n.a. | n.a. |
| Nb | n.a. | n.a. | 6 | n.a. | n.a. | 54 | 50 | n.a. | 3.0 |
| Th | 5.30 | 5.89 | n.a. | n.a. | n.a. | n.a. | 4.4 | n.a. | n.a. |
| U | 0.988 | 1.05 | n.a. | n.a. | n.a. | n.a. | 1.4 | n.a. | n.a. |
| La | 24.6 | 26.8 | 23 | n.a. | 21 | 58 | 36.6 | n.a. | n.a. |
| Ce | 36.7 | 39.9 | n.a. | n.a. | 51 | n.a. | 80 | n.a. | n.a. |
| Nd | 18.7 | 20.3 | n.a. | n.a. | n.a. | n.a. | 32 | n.a. | n.a. |
| Sm | 4.34 | 4.40 | n.a. | n.a. | 7 | n.a. | 4.3 | n.a. | n.a. |
| Eu | 0.788 | 0.648 | n.a. | n.a. | 1.7 | n.a. | 1.2 | n.a. | n.a. |
| Tb | 0.523 | 0.493 | n.a. | n.a. | 1.5 | n.a. | n.a. | n.a. | n.a. |
| Yb | 1.45 | 1.54 | n.a. | n.a. | 4.1 | n.a. | 1.03 | n.a. | n.a. |
| Lu | 0.229 | 0.259 | n.a. | n.a. | 0.58 | n.a. | 0.15 | n.a. | n.a. |
| Y | n.a. | n.a. | 14 | n.a. | n.a. | 13 | 14 | n.a. | n.a. |
| Sr | 230 | 300 | 431 | n.a. | n.a. | 902 | 982 | n.a. | 45.2 |
| Ba | 153 | 434 | 352 | n.a. | n.a. | 436 | 684 | n.a. | 74.7 |
| Rb | n.a. | n.a. | 42 | n.a. | n.a. | 34 | 46 | n.a. | 6.0 |

Table 8. (*Continued*)

| Unit[$] | 10 Ko | 11 Ko | 12 Pi | 13 Pi | 14 Pi | 15 Pi | 16 Pi | 17 Pi | 18 Pi |
|---|---|---|---|---|---|---|---|---|---|
| $SiO_2$ | 47.73 | 44.00 | 74.01 | 74.51 | 83.90 | 81.10 | 49.33 | 45.10 | 46.30 |
| $TiO_2$ | 1.55 | 2.34 | 0.40 | 0.38 | 0.23 | 0.15 | 1.20 | 1.45 | 1.78 |
| $Al_2O_3$ | 13.08 | 6.52 | 10.80 | 10.62 | 7.75 | 7.68 | 13.99 | 13.30 | 13.07 |
| $Fe_2O_3$ | 3.48 | 3.10 | 0.65 | 0.49 | n.a. | n.a. | 1.32 | n.a. | 2.62 |
| FeO | 10.87 | 11.95 | 3.94 | 4.14 | n.a. | n.a. | 11.16 | n.a. | 12.62 |
| $FeO_{tot}$ | 14.00 | 14.74 | 4.48 | 4.58 | 2.26 | 1.43 | 12.46 | 13.63 | 14.98 |
| MnO | 0.20 | 0.20 | 0.09 | 0.09 | 0.02 | 0.01 | 0.20 | 0.23 | 0.23 |
| MgO | 6.68 | 12.83 | 1.03 | 0.76 | 0.40 | 0.12 | 6.68 | 5.72 | 6.18 |
| CaO | 10.62 | 11.06 | 0.83 | 1.10 | 0.54 | 0.34 | 5.83 | 10.70 | 10.01 |
| $Na_2O$ | 2.33 | 0.24 | 3.56 | 2.70 | 2.87 | 1.48 | 4.36 | 2.49 | 2.30 |
| $K_2O$ | 0.22 | 0.20 | 3.58 | 4.39 | 1.16 | 3.98 | 0.90 | 0.09 | 0.34 |
| $P_2O_5$ | 0.16 | 0.29 | 0.02 | 0.02 | 0.01 | 0.04 | 0.10 | 0.12 | 0.24 |
| L.O.I. | 2.86 | 9.09 | 1.38 | 1.05 | n.a. | n.a. | 4.89 | n.a. | 3.83 |
| Cr | 100 | 1100 | 59 | 28 | 52 | 26.8 | 233 | 77.3 | 90.6 |
| Ni | 80 | 590 | 43 | 18 | 17.6 | 17.6 | 135 | 36 | 88.1 |
| Co | n.a. | n.a. | n.a. | n.a. | 1.03 | 1.08 | n.a. | 56.8 | 46.4 |
| Sc | n.a. | n.a. | n.a. | n.a. | 0.74 | 1.01 | 46.4 | 56 | 7.5 |
| V | 340 | 270 | 32 | 23 | 10 | 1 | 333 | 420 | 134 |
| Zr | n.a. | n.a. | 802 | 673 | 590 | 350 | 76.4 | 90 | 45.7 |
| Ta | n.a. | n.a. | n.a. | n.a. | 5.56 | 4.07 | n.a. | .298 | n.a. |
| Nb | n.a. | n.a. | 88 | 79 | n.a. | n.a. | 4.3 | n.a. | 2.9 |
| Th | n.a. | n.a. | 14 | 10 | 13.9 | 11.9 | 0.6 | .362 | n.a. |
| U | n.a. | n.a. | 4 | 2 | 2.98 | 2.14 | 0.6 | 0.09 | n.a. |
| La | n.a. | n.a. | 66 | 91 | 85 | 71 | 3.2 | 5.1 | n.a. |
| Ce | n.a. | n.a. | n.a. | n.a. | 145 | 134 | n.a. | 10.6 | n.a. |
| Nd | n.a. | n.a. | n.a. | n.a. | 78 | 65 | n.a. | 9.9 | n.a. |
| Sm | n.a. | n.a. | n.a. | n.a. | 14.2 | 12.9 | n.a. | 3.2 | n.a. |
| Eu | n.a. | n.a. | n.a. | n.a. | 3.2 | 1.59 | n.a. | 1.17 | n.a. |
| Tb | n.a. | n.a. | n.a. | n.a. | 1.54 | 1.03 | n.a. | 0.66 | n.a. |
| Yb | n.a. | n.a. | n.a. | n.a. | 2.5 | 1.63 | n.a. | 2.3 | n.a. |
| Lu | n.a. | n.a. | n.a. | n.a. | 0.26 | 0.17 | n.a. | 0.27 | n.a. |
| Y | n.a. | n.a. | 52 | 51 | n.a. | n.a. | 24.3 | n.a. | n.a. |
| Sr | n.a. | n.a. | 101 | 78 | 30 | 50 | 241.2 | 50 | 86.4 |
| Ba | n.a. | n.a. | 263 | 304 | 173 | 565 | 596.2 | 38.5 | 27.1 |
| Rb | n.a. | n.a. | 67 | 78 | 22 | 96.4 | 32.3 | 6.44 | 11.3 |

n.a. = not analysed.
Unit: Ah = Ahmalahti Suite, Ku = Kuetsjärvi Suite, Ko = Kolosjoki Suite,
Pi = Pilgujärvi Suite.
Rock types and samples:
**1-3**, basaltic andesite, 13734, 13733, A1/91; **4**, mugearite, S-6 (Skufin et al., 1986); **5**, average of two basalts, superdeep drill core (Kremenetskii and Ovchinnikov, 1986); **6**, mugearite, PII/1; **7**, basalt, PII/2 ; **8**, picrito-basalt, 2-0 (Predovskii et al., 1987); **9**, average of 177 tholeiitic basalts, superdeep drill core (Kremenetskii and Ovchinnikov, 1986); **10**, average of 150 tholeiitic basalts (Predovskii et al., 1987); **11**, picrito-basalt, 2-2 (Predovskii et al., 1987); **12-15**, felsic tuff, 1833/5, Souker3/90, 1750/1, 87/68; **16-17**, tholeiitic basalt, S-VI/450.3, 87/26; **18**, average of 28 tholeiitic basalts, superdeep drill core (Kremenetskii and Ovchinnikov, 1986).

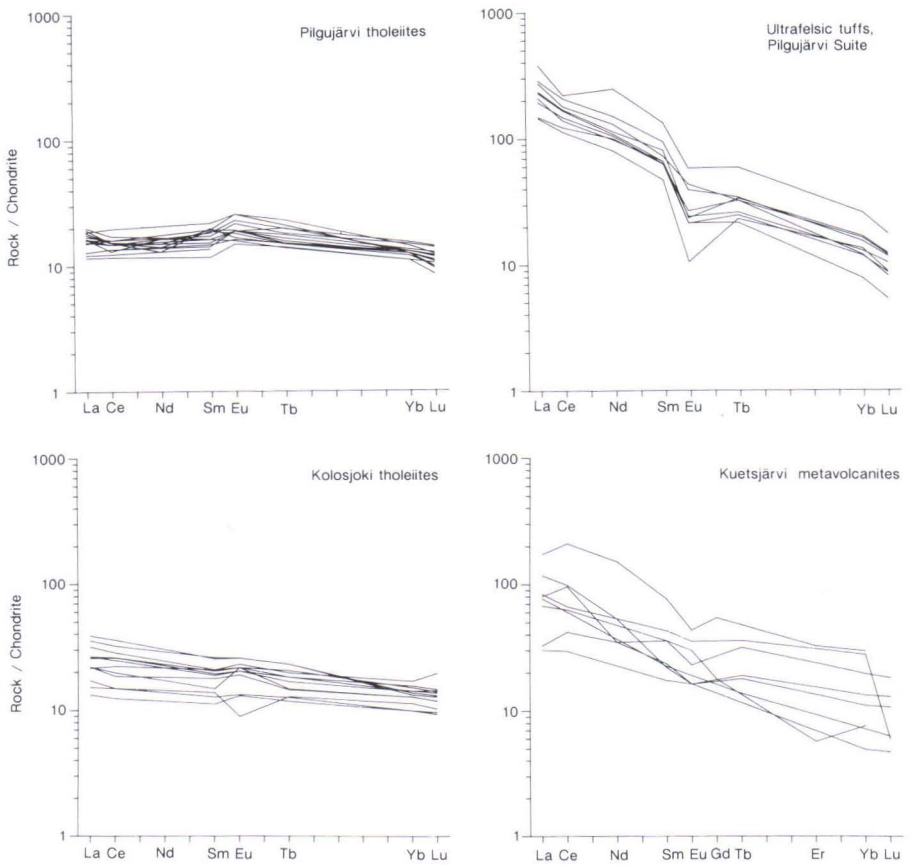


Fig. 47. Chondrite-normalized REE profiles for mildly alkaline metavolcanites from the Kuetsjärvi Suite, tholeiitic basalts from the Kolosjoki and Pilgujärvi Suites and ultrafelsic tuffs from the Pilgujärvi Suite. Data from Kremenetskü and Ovchinnikov (1986), Romanko et al., (1992) and this study.

or ultrafelsic tuffs from the Pilgujärvi Suite ranges from 60% to 90%. They are relatively rich in iron ($FeO_{tot}$ 2-8%) and low in aluminium (2-12%) (Table 8). $Na_2O/K_2O$ is extremely variable. The correlation matrix in Table 9 shows that silica and alkalies do not have significant positive correlations with each other or most of the trace elements. In fact, $K_2O$ and $Na_2O$ behave antipathetically with each other. Many immobile incompatible elements like Zr, REE, Nb, Ta, Th, and U show a good positive correlation with each other. In contrast, $P_2O_5$ and $TiO_2$ typically decrease with increases in the above listed trace elements. Chondrite-normalized REE profiles are steeply sloping and straight with the exception of a notable negative Eu anomaly (Fig. 47). A typical feature of the felsic rocks is the high abundance of highly charged trace elements such as Zr (up to 810 ppm), Nb (up to 84 ppm), and La (up to 114 ppm) (see Table 8).

The genesis of the tufosilitsites has been controversial. They have been regarded as felsic lavas and tuffs (Zagorodny et al., 1989; Rusanov, 1981) and Skufin (1990) called them paleoignimbrites. He proposed a hypothesis for the genesis of high-silica liquid by silicate liquid immisci-

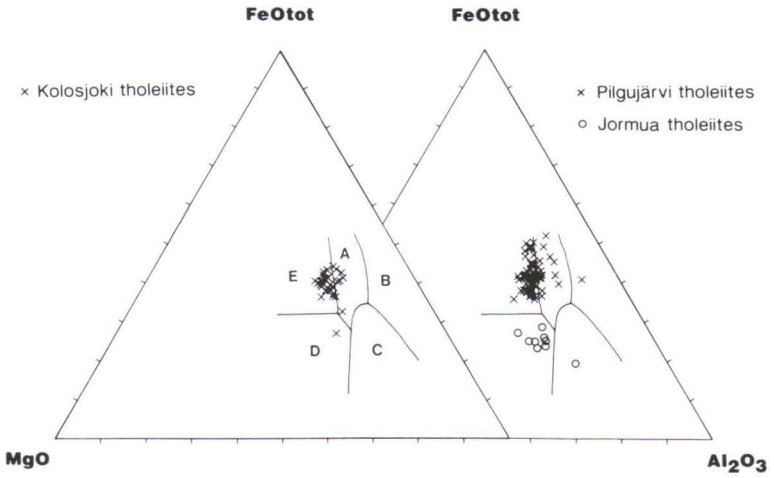


Fig. 48. Position of tholeiites from the Kolosjoki and Pilgujärvi Suites and from the early Proterozoic Jormua ophiolite (Kontinen, 1987) on the discrimination diagram of Pearce et al. (1977). Fields: A = continental, B = spreading center island, C = orogenic, D = ocean ridge and floor, E = ocean island.

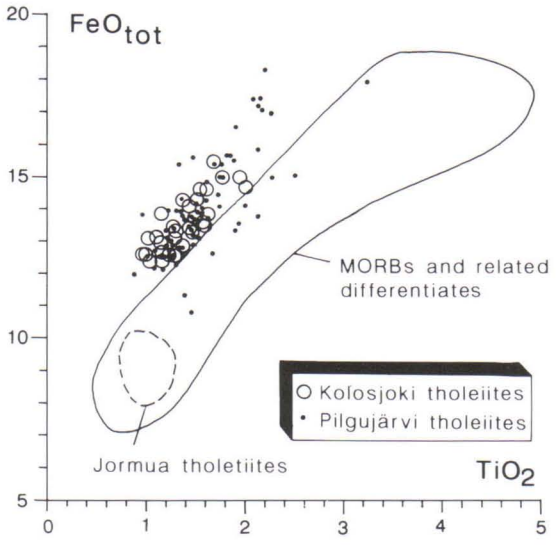


Fig. 49. Total FeO and $TiO_2$ contents (wt. %) of tholeiitic metavolcanites from the Kolosjoki and Pilgujärvi Suites compared with those of basalts from the Jormua ophiolite (Kontinen, 1987) and mid-ocean ridge basalts and related differentiates from the literature.

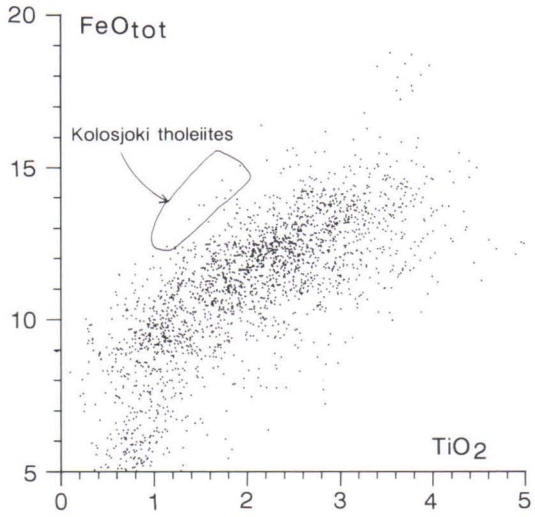


Fig. 50. Total FeO and $TiO_2$ contents (wt. %) for the Kolosjoki tholeiites and various Phanerozoic volcanic rocks from the literature (small dots).

**Table 9. Correlation matrix of selected element abundances in ultrafelsic tuffs.**

| | $SiO_2$ | $Na_2O$ | $K_2O$ | $P_2O_5$ | $TiO_2$ | Zr | La | Sm | Yb | Th | Ta |
|---|---|---|---|---|---|---|---|---|---|---|---|
| $Na_2O$ | 0.01 | | | | | | | | | | |
| $K_2O$ | -0.30 | -0.53 | | | | | | | | | |
| $P_2O_5$ | -0.14 | 0.18 | 0.18 | | | | | | | | |
| $TiO_2$ | -0.60 | -0.00 | 0.03 | 0.31 | | | | | | | |
| Zr | -0.44 | 0.58 | -0.16 | -0.34 | -0.22 | | | | | | |
| La | 0.22 | 0.05 | -0.36 | 0.13 | -0.08 | 0.54 | | | | | |
| Sm | 0.11 | -0.04 | -0.34 | 0.18 | 0.00 | 0.60 | 0.93 | | | | |
| Yb | 0.00 | 0.10 | -0.50 | 0.30 | 0.16 | 0.58 | 0.68 | 0.87 | | | |
| Th | -0.05 | 0.30 | -0.42 | -0.47 | -0.03 | 0.89 | 0.74 | 0.76 | 0.52 | | |
| Ta | 0.12 | 0.30 | -0.42 | -0.31 | 0.06 | 0.75 | 0.87 | 0.88 | 0.74 | 0.91 | |
| U | -0.11 | 0.27 | -0.30 | -0.31 | 0.15 | 0.84 | 0.75 | 0.88 | 0.85 | 0.89 | 0.94 |

bility from a basaltic or picrite-basaltic magma. The high concentration of high field strength elements in felsic tuffs and their possible peralkaline nature do not favor the immiscibility model. Borisov and Smolkin (1992) reached the conclusion that these rocks are hybrid chemogenic-tuffogenic-terrigenic formations transported by mud flows or turbidite flows. According to these authors, the high silica content is a product of subaqueous weathering and leaching of lavas and tuffs, and fragmental material represents erosion products of Archean rapakivi-like granites and underlying tholeiitic and ferropicritic metavolcanites. The decoupling of the chemistry of mobile major elements and immobile trace elements in these rocks indicate that the major elements probably are not representative of the original composition of the rocks and are of little use in unravelling the origin of these rocks. Instead, the coherent behavior of many trace elements provides an indication of the petrogenetic processes responsible for the geochemical variability. A hybrid origin with mixing of material from at least three chemically different sources through sedimentary processes is not likely to result in such coherent behavior of many incompatible trace elements. The approximately constant ratios of these elements rather suggest that the variation in their abundance is a result of a magmatic differentiation process. The low abundances of $TiO_2$ and $P_2O_5$ is also compatible with this interpretation because these elements tend to decrease with the degree of differentiation in rhyolites. Thus both geochemical and petrographical evidence suggests that the bulk of the material of the felsic supracrustal rocks are volcanic in origin. This implies the unexpected appearance of a short period of felsic volcanism in the evolutionary history of the Pilgujärvi Suite, which is overwhelmingly dominated by mafic and ultramafic volcanic rocks.

Although the peralkaline index, molecular $(Na_2O+K_2O)/Al_2O_3$, in ultrafelsic rocks is generally less than one, the high concentration of many incompatible elements suggests that the rocks originally had a peralkaline composition which enabled them to dissolve large amounts of highly charged elements (cf. Watson, 1979). The Zr-Nb ratio falls below 10 which is typical of peralkaline rhyolites from oceanic islands or continental rifts (Leat et al., 1986). This is compatible with their coexistence with ferropicrites with trace element characteristics of within-plate basalts (Hanski and Smolkin, 1989).

In summary, Pechenga Series volcanism commenced with eruptions of vesicular, contaminated basalts and andesites and continued with basalts to dacites having a mildly alkaline affinity. These were followed by monotonous, submarine tholeiitic basalts accompanied by lesser amounts of

ferropicritic lavas and minor ultrafelsic tuffs. Tholeiites exhibit MORB-like immobile trace element characteristics but differ in their major element composition, especially with respect to their FeO-$TiO_2$ relationhips, from modern and ancient MORB's and also from most Phanerozoic volcanic rocks. Arc type magmatism seems to be absent from the Pechenga Series. Only the metavolcanites of the Ahmalahti Suite possess an arc-like chemical signature, but their general geological position rules out any island arc or continental arc geotectonic setting. Instead, their chemical composition can be explained either by an ancient subducted arc component in their mantle source or by contamination with partial melts from the Archean granite gneiss complex at the base of the Pechenga Complex.

## Ferropicritic volcanic rocks

The geochemical pecularities of ferropicritic rocks have been briefly documented earlier by Hanski and Smolkin (1989). The ferropicritic volcanic suite is made up of rocks with an MgO content varying from 32% to less than 4% anhydrous. The most magnesian rocks occur in the lower parts of layered flows enriched in accumulated olivine and do not represent liquid compositions. In massive and pillowed lavas, MgO contents reach about 17% (Table 10). Silica contents most commonly fall between 46-48%. In this regard, ferropicrites do not differ from komatiites and in spite of having trace element characteristics similar to those of alkali basalts, they are far from undersaturated with respect to silica. As the name reveals, an outstanding feature of ferropicrites is their high iron content, accompanied inevitably by high $TiO_2$ and V contents. Total iron calculated as ferrous ($FeO_{tot}$) commonly exceeds 14% in anhydrous analyses. Because of the high FeO content, the Mg number [molecular MgO/(MgO+FeO) calculated after adjusting $Fe^{2+}$ as 0.9×total Fe as FeO] does not exceed 0.70 in rocks that are not enriched in intratelluric or cumulus olivine. $TiO_2$ is higher than 1% even in rocks most diluted by olivine crystals. In rocks with MgO of about 15%, $TiO_2$ rises to 2-2.5% (Table 10). This is one of the most fundamental differences in the major element geochemistry between ferropicrites and ordinary komatiites, for the latter possess a $TiO_2$ content of 0.5-0.7% at the corresponding MgO level.

Ferropicritic tuffs could be a good candidate for determining the magma composition but the high degree of alteration obscures their original chemistry. Examples of tuff analyses are shown in Table 11. MgO ranges between 11.3 and 17.0 wt. %. The sulfur content is high, ranging commonly between 0.3-1.0 wt. %.

Chemical profiles of two layered lava flows are illustrated in Fig. 6 and representative analyses of the principal units are listed in Table 12. The olivine spinifex-textured flow unit in flow S-VI is only moderately differentiated while the Kierdzhipori flow displays more extreme chemical variation. In the former, the MgO content varies between 12% and 20% while in the latter, it ranges from 4% in the most evolved part of the flow up to 22.5% in the lower part, which is most enriched in accumulated olivines. Chromium, nickel, and magnesium behave coherently reflecting the simultaneous crystallization of olivine and chrome spinel. This contrasts with the behavior of chromium in layered flows generated from a high-Mg komatiite. In these flows, chromium remains in the residual liquid and concentrates in the spinifex zone (Arndt et al., 1977). In lava flows with a less magnesian komatiite as a parental magma, chromite also starts to crystallize after olivine but the temperature gap is shorter, and chromium is concentrated in the upper part of the cumulate zone (Hanski, 1980).

As is to be expected, the upper part of the flows, containing spinifex-textured rocks, is much

Table 10. Analyses of ferropicritic massive and pillow lavas (major elements recalculated to 100% on an anhydrous basis).

| Location$ | 1 Or | 2* Ki | 3* Ki | 4* Ki | 5* Sh | 6* Sh | 7 Sh | 8* Sh | 9* Sh | 10 Sh | 11* Sh | 12 Sh | 13 Sh |
|---|---|---|---|---|---|---|---|---|---|---|---|---|---|
| $SiO_2$ | 46.00 | 47.64 | 47.13 | 44.47 | 49.31 | 49.27 | 50.58 | 48.75 | 48.10 | 48.20 | 46.00 | 45.62 | 46.83 |
| $TiO_2$ | 2.48 | 2.00 | 2.05 | 2.59 | 2.31 | 2.26 | 2.26 | 2.08 | 2.16 | 2.42 | 2.36 | 2.46 | 2.48 |
| $Al_2O_3$ | 8.10 | 6.66 | 6.81 | 6.52 | 8.59 | 7.16 | 7.62 | 5.61 | 5.57 | 7.64 | 8.55 | 9.65 | 9.27 |
| $FeO_{tot}$ | 16.92 | 15.03 | 16.99 | 16.70 | 15.22 | 14.29 | 14.77 | 15.14 | 15.11 | 15.27 | 15.12 | 15.09 | 14.96 |
| MnO | 0.30 | 0.24 | 0.23 | 0.21 | 0.19 | 0.19 | 0.18 | 0.21 | 0.18 | 0.19 | 0.19 | 0.22 | 0.23 |
| MgO | 12.60 | 13.33 | 16.33 | 14.13 | 12.50 | 13.53 | 16.09 | 16.05 | 17.56 | 17.02 | 14.37 | 14.45 | 13.88 |
| CaO | 12.23 | 14.43 | 9.54 | 14.43 | 10.94 | 12.59 | 7.39 | 11.11 | 10.59 | 8.18 | 12.69 | 11.75 | 11.62 |
| $Na_2O$ | 0.73 | 0.14 | 0.17 | 0.14 | 0.13 | 0.09 | 0.24 | 0.29 | 0.16 | 0.24 | 0.15 | 0.12 | 0.16 |
| $K_2O$ | 0.13 | 0.09 | 0.25 | 0.15 | 0.28 | 0.04 | 0.26 | 0.21 | 0.08 | 0.25 | 0.05 | 0.18 | 0.13 |
| $P_2O_5$ | 0.26 | 0.20 | 0.23 | 0.30 | 0.22 | 0.20 | 0.26 | 0.22 | 0.22 | 0.25 | 0.22 | 0.21 | 0.22 |
| $Cr_2O_3$ | 0.18 | 0.15 | 0.16 | 0.24 | 0.20 | 0.24 | 0.20 | 0.17 | 0.17 | 0.19 | 0.20 | 0.14 | 0.12 |
| NiO | 0.07 | 0.08 | 0.12 | 0.12 | 0.11 | 0.15 | 0.16 | 0.15 | 0.09 | 0.14 | 0.10 | 0.09 | 0.09 |
| L.O.I. | 3.77 | 10.65 | 5.79 | 9.96 | 9.28 | 9.92 | n.a. | 5.27 | 6.21 | n.a. | 10.83 | 11.51 | 10.76 |
| Cr | 1140 | 933 | 1000 | 1432 | 1220 | 1456 | 1260 | 1100 | 1100 | 1210 | 1186 | 825 | 737 |
| Ni | 552 | 567 | 910 | 855 | 782 | 1024 | 1160 | 1100 | 680 | 1060 | 728 | 653 | 605 |
| Co | 96 | 73 | 88 | 101 | 87 | 99.9 | n.a. | 89 | 76 | n.a. | 83 | n.a. | n.a. |
| Sc | 29.6 | 24.3 | n.a. | 32.4 | 32.3 | 31.6 | 32.1 | n.a. | n.a. | n.a. | 30.4 | 29.1 | 36.9 |
| V | 310 | 270 | 300 | 340 | 290 | 260 | 300 | 260 | 300 | 280 | 320 | 301 | 308 |
| Zr | 141 | 97 | 96 | 124 | 117 | 115 | 159 | 114 | 120 | 170 | 121 | 166 | 182 |
| Ta | n.a. | 0.8 | n.a. | 1.03 | 0.8 | 0.79 | 1.09 | n.a. | n.a. | n.a. | 0.83 | n.a. | n.a. |
| Nb | 18.4 | 18 | n.a. | 22 | 17 | n.a. | 17.4 | n.a. | n.a. | n.a. | n.a. | 18.9 | 19.6 |
| Th | 2.57 | 2.13 | n.a. | 2.41 | 2.01 | 1.80 | 1.95 | n.a. | n.a. | n.a. | 2.11 | n.a. | 2.00 |
| U | 0.56 | 0.55 | n.a. | 0.58 | 0.40 | 0.33 | 0.39 | n.a. | n.a. | n.a. | 0.37 | n.a. | 0.48 |
| La | 21.91 | 16.23 | n.a. | 10.44 | 14.73 | 29.23 | 21.61 | n.a. | n.a. | 12.2 | 21.55 | n.a. | 17.83 |
| Ce | 54.27 | 38.85 | n.a. | 26.85 | 36.91 | 58.06 | 46.31 | n.a. | n.a. | 28 | 46.60 | n.a. | 43.71 |
| Nd | 29.66 | 20.32 | n.a. | 18.68 | 22.30 | 24.90 | 29.71 | n.a. | n.a. | 21 | 24.00 | n.a. | 26.22 |
| Sm | 6.56 | 4.70 | n.a. | 5.66 | 5.68 | 5.51 | 6.84 | n.a. | n.a. | 6.2 | 5.55 | n.a. | 5.87 |
| Eu | 2.29 | 1.47 | n.a. | 1.72 | 1.81 | 1.57 | 2.18 | n.a. | n.a. | 1.80 | 1.52 | n.a. | 1.97 |
| Tb | 0.89 | 0.59 | n.a. | 0.71 | 0.74 | 0.65 | 0.93 | n.a. | n.a. | 0.77 | 0.78 | n.a. | 0.81 |
| Yb | 1.59 | 1.05 | n.a. | 1.36 | 1.59 | 1.41 | 1.62 | n.a. | n.a. | 1.56 | 1.64 | n.a. | 1.79 |
| Lu | 0.19 | 0.18 | n.a. | 0.23 | 0.23 | 0.23 | 0.17 | n.a. | n.a. | 0.18 | 0.25 | n.a. | n.a. |
| Ba | 31.8 | 35 | 50 | 20 | 106 | 20 | 40 | 20 | 70 | 20 | 21 | 54.9 | 51.3 |
| Sr | 60 | 270 | 90 | 250 | 180 | 130 | 50 | 50 | 30 | 60 | 210 | 272 | 256 |
| Rb | 6.3 | 6 | n.a. | 11 | 3 | n.a. | 11.1 | n.a. | n.a. | n.a. | 1 | 19.1 | 11.9 |
| S | 2940 | 1400 | 2400 | 6700 | 800 | 1200 | 600 | 300 | 200 | 650 | 400 | 85 | 20 |
| Cu | 172 | 110 | 210 | 200 | 120 | 130 | 190 | 140 | 210 | 290 | 160 | 161 | 118 |

n.a. = not analysed.
$ Location: Or = Ortoaivi, Ki = Kierdzhipori, Sh = Shuljärvi.
* Major element analyses taken from Skufin and Fedotov (1989).
Rock types: 1, 3-4, 6, 10-13 massive lavas; 2, 5, 7-9 pillow lavas.
Samples: **1**, Ortoaivi-42c; **2**, S-2728/749.2; **3**, S-2728/757.8; **4**, S-2728/773.2; **5**, S-3077/310.0; **6**, S-3077/313.0; **7**, S-3077/314.3; **8** = S-3077/318.4; **9**, S-3077/318.5; **10**, S-3077/322.5; **11**, S-3077/350.0; **12**, S-VI/375.6; **13** = S-VI/376.8.

richer in $Al_2O_3$, CaO, and $TiO_2$ and poorer in MgO than the olivine cumulate in the lower part of the flows. The iron content remains approximately constant through the whole section. The highest CaO and lowest $FeO_{tot}$ contents are measured in clinopyroxene-rich zones in the middle part of the flows. This zone is exceptional among rocks crystallized from a ferropicritic magma in that its $FeO_{tot}$ may descend to 11 wt. %.

Because olivine, chrome spinel, and clinopyroxene are the main fractionating minerals in layered ferropicritic flows, alkalis should be enriched in the residual liquid. Hence, the concentrations of $Na_2O$ and $K_2O$ are anticipated to be largest in the upper part of the flows, with their mutual ratios as well as their ratios with other incompatible elements like $TiO_2$, $Al_2O_3$, Zr, and Sm to be approximately constant through the lava flows. Figure 6 shows the fluctuations of the ra-

tios of alkalies to $Al_2O_3$ and $TiO_2$. Because $Al_2O_3$ and $TiO_2$ are generally regarded as relatively immobile elements during secondary alteration processes, the deviations of the ratios from a constant value can be deduced to be the results of alkali mobility. There appears to be a systematic pattern in the change of alkali to immobile element ratios from extremely low values in the lower part to high values in the upper part of the flows. This can be interpreted as a consequence of an enrichment of alkalies in the upper part of the flows or a depletion in the lower part or most likely both of these processes. The behavior of $K_2O$ and $Na_2O$ is somewhat different in the two cases of layered flows in Fig. 6, with the abundance of sodium more faithfully following the modal plagioclase content of the rocks. The analogous behavior of alkalies, i.e., a secondary depletion in ultramafic rocks and enrichment in mafic rocks, seems to be a general phenomenon in metamorphosed komatiitic layered lava flows (Hanski, 1988; Arndt et al., 1988). Probably the sensitivity of ultramafic volcanites and ultramafic parts of layered lava flows to alkali loss stems from the original incorporation of alkalies into groundmass glass and the absence of primary aluminosilicates which could capture alkalies during later alteration processes.

The $Al_2O_3$-$TiO_2$ ratio displays approximately constant values throughout the layered flows. In contrast, $CaO/Al_2O_3$ is highly variable (Fig. 6). This is partly caused by clinopyroxene accumulation in the middle part of the flows but also by the postmagmatic mobility of CaO, since the expected constant $CaO/Al_2O_3$ or $CaO/TiO_2$ values in the olivine cumulates of the flows are not observed.

In randomly oriented olivine spinifex rocks, the MgO content ranges between 12-15%, while in pyroxene spinifex rocks, it falls below 10%. As was intimated earlier, an enigmatic feature is the evolved composition of rocks possessing a parallel olivine spinifex texture like that depicted in Fig. 10. The MgO content in these rocks can be as low as 5% (Table 12, anal. 1 and 11) contrasting with MgO contents of 15-32% generally observed in olivine spinifex-textured komatiites (e.g., Nesbitt, 1971; Echeverria, 1980). The low MgO in these rocks is not a result of alteration but a true magmatic feature as shown by textural evidence, i.e., the abundant interstitial fan spherulitic plagioclase or coarser plagioclase laths intergrown with clinopyroxene. The interpretation of a primary origin for the low MgO content is also supported by the immobile trace element geochemistry, i.e., the high concentrations of incompatible elements (La 28-44 ppm, Zr 200-250 ppm) and low concentrations of compatible elements (Cr 10-20 ppm, Ni 30-45 ppm).

One example has been found where a ferropicritic rock with a parallel olivine spinifex texture is not so low in MgO, but this rock also has other puzzling features. This spinifex rock occurs in the upper part of a layered flow in the Lammas area and has an MgO content of 15-18% but is low in Ni (30-60 ppm) and Cr (40 ppm) (Table 12, anal. 2). It is also strongly enriched in incompatible elements (La 33-43 ppm) and obviously does not represent a liquid composition. The thin olivine plates were originally rimmed by abundant magnetite which accounts for the low silica (34-39%) and high total iron content ($FeO_{tot}$ 20-22%) of this

Table 11. Analyses of ferropicritic tuffs (major elements recalculated to 100% on an anhydrous basis).

| | 1 | 2 | 3 | 4 | 5 | 6 |
|---|---|---|---|---|---|---|
| $SiO_2$ | 45.73 | 44.17 | 46.81 | 48.06 | 45.72 | 45.03 |
| $TiO_2$ | 2.96 | 2.75 | 2.80 | 2.27 | 2.85 | 2.72 |
| $Al_2O_3$ | 9.10 | 8.32 | 7.87 | 7.71 | 8.93 | 8.15 |
| $FeO_{tot}$ | 18.60 | 17.95 | 19.71 | 15.78 | 17.61 | 17.53 |
| MnO | 0.11 | 0.18 | 0.15 | 0.20 | 0.16 | 0.24 |
| MgO | 18.33 | 17.69 | 18.32 | 15.43 | 14.98 | 15.94 |
| CaO | 4.22 | 7.40 | 4.18 | 9.33 | 8.29 | 9.69 |
| $Na_2O$ | 0.27 | 0.15 | 0.23 | 0.67 | 0.40 | 0.07 |
| $K_2O$ | 0.41 | 0.47 | 0.38 | 0.04 | 0.46 | 0.08 |
| $P_2O_5$ | 0.27 | 0.26 | 0.28 | 0.21 | 0.34 | 0.25 |
| $Cr_2O_3$ | n.a. | 0.53 | 0.20 | 0.17 | 0.16 | 0.19 |
| NiO | n.a. | 0.12 | 0.08 | 0.11 | 0.09 | 0.10 |
| L.O.I. | 7.70 | 10.06 | n.a. | 5.37 | 10.44 | 5.75 |
| Cr | n.a. | 3200 | 1250 | 1100 | 1000 | 1200 |
| Ni | n.a. | 850 | 558 | 820 | 600 | 750 |
| Co | n.a. | 120 | 92 | 84 | 60 | 70 |
| V | n.a. | n.a. | 370 | 310 | 200 | 210 |
| S | 6000 | n.a. | 5870 | 5300 | 6300 | 1500 |
| Cu | n.a. | 240 | 180 | 170 | n.a. | n.a. |

n.a. = not analysed.
**1**, Kotselvaara quarry, sample 2798 (Golubev et al., 1984); **2**, Kotselvaara quarry, P-I (Smolkin, 1991); **3**, Kotselvaara quarry, K-1; **4**, Kierdzhipori area, S-2792/773.0; **5**, upper part of the productive pile, PB-49 (Predovskii et al., 1974); **6**, Autiotupa Mountain, P1600 (Predovskii et al., 1974).

Table 12. Chemical analyses of various rock types from layered lava flows.

| Location[$] | 1 Ko | 2 La | 3 La | 4 La | 5 La | 6 La | 7 La | 8 La | 9 La | 10 Ki | 11 Ki | 12 Ki | 13 Ki | 14 Ki | 15 Ki |
|---|---|---|---|---|---|---|---|---|---|---|---|---|---|---|---|
| $SiO_2$ | 46.83 | 31.25 | 42.04 | 44.99 | 40.55 | 42.60 | 39.60 | 43.51 | 39.94 | 46.00 | 46.20 | 49.10 | 46.51 | 47.57 | 44.70 |
| $TiO_2$ | 3.03 | 4.53 | 2.62 | 1.81 | 2.05 | 1.25 | 1.12 | 1.40 | 2.13 | 2.11 | 3.11 | 2.60 | 3.04 | 3.00 | 1.58 |
| $Al_2O_3$ | 12.95 | 12.45 | 6.95 | 5.17 | 5.65 | 4.38 | 3.91 | 4.34 | 8.36 | 8.15 | 11.30 | 13.20 | 12.58 | 9.83 | 5.57 |
| $Fe_2O_3$ | 1.41 | 5.82 | 1.42 | 0.98 | 2.57 | 3.80 | 5.26 | 3.07 | 4.48 | 3.43 | n.a. | n.a. | 1.31 | 1.35 | 2.97 |
| FeO | 13.60 | 14.70 | 13.00 | 9.57 | 13.25 | 9.70 | 8.90 | 11.00 | 10.80 | 14.90 | n.a. | n.a. | 14.00 | 11.90 | 7.99 |
| $FeO_{tot}$ | - | - | - | - | - | - | - | - | - | - | 14.84 | 13.63 | - | - | - |
| MnO | 0.14 | 0.37 | 0.25 | 0.17 | 0.20 | 0.17 | 0.19 | 0.17 | 0.19 | 0.20 | 0.18 | 0.15 | 0.21 | 0.21 | 0.19 |
| MgO | 4.60 | 13.59 | 14.67 | 17.26 | 18.94 | 24.20 | 29.40 | 20.63 | 18.49 | 10.20 | 5.46 | 6.44 | 5.04 | 7.39 | 17.16 |
| CaO | 6.74 | 7.16 | 11.16 | 13.18 | 8.67 | 5.99 | 3.03 | 7.66 | 7.39 | 7.28 | 8.67 | 5.23 | 8.14 | 11.44 | 14.09 |
| $Na_2O$ | 3.44 | 0.05 | 0.12 | 0.11 | 0.05 | 0.19 | 0.24 | 0.03 | 0.02 | 0.39 | 2.46 | 3.24 | 3.13 | 2.22 | 0.19 |
| $K_2O$ | 0.09 | 0.04 | 0.06 | 0.02 | 0.02 | 0.03 | 0.02 | 0.02 | 0.02 | 0.11 | 0.12 | 0.19 | 0.32 | 0.30 | 0.02 |
| $P_2O_5$ | 0.38 | 0.45 | 0.26 | 0.14 | 0.19 | 0.14 | 0.13 | 0.15 | 0.22 | 0.20 | 0.24 | 0.38 | 0.34 | 0.22 | 0.16 |
| $Cr_2O_3$ | 0.00 | 0.01 | 0.12 | 0.24 | 0.54 | 0.22 | 0.37 | 0.23 | 0.18 | 0.21 | 0.00 | 0.00 | 0.00 | 0.01 | 0.22 |
| NiO | 0.00 | 0.01 | 0.04 | 0.03 | 0.18 | 0.20 | 0.23 | 0.17 | 0.08 | 0.09 | 0.01 | 0.00 | 0.00 | 0.01 | n.a. |
| $CO_2$ | 0.33 | 1.28 | 0.22 | 0.15 | 0.51 | 0.07 | 0.10 | 0.00 | 0.15 | n.a. | n.a. | n.a. | 1.06 | 0.73 | 0.09 |
| $H_2O$ | 4.11 | 8.76 | 5.72 | 4.73 | 6.10 | 7.29 | 9.04 | 5.96 | 6.46 | n.a. | n.a. | n.a. | 3.98 | 2.99 | 4.00 |
| L.O.I. | n.a. | n.a. | n.a. | n.a. | n.a. | n.a. | n.a. | n.a. | n.a. | 5.16 | n.a. | n.a. | n.a. | n.a. | n.a. |
| Total | 97.66 | 100.46 | 98.65 | 98.55 | 99.50 | 100.23 | 101.54 | 98.34 | 98.92 | 98.43 | - | - | 99.66 | 99.17 | 98.93 |
| Cr | 16 | 37.6 | 797 | 1624 | 3720 | 1500 | 2542 | 1600 | 1217 | 1440 | 11 | 14.9 | 21.3 | 46.9 | 1504 |
| Ni | 31 | 61.3 | 339 | 230 | 1450 | 1560 | 1770 | 1340 | 626 | 706 | 46 | 6.1 | 24.5 | 91.9 | n.a. |
| Co | n.a. | 74.9 | 73.2 | 52.3 | 133 | 115 | 128 | 114 | 89.0 | 93 | 85 | 56.7 | 54.2 | 73.5 | n.a. |
| Sc | n.a. | 40.3 | 33.7 | 68.4 | 40.1 | 24.5 | 19.7 | 24.6 | 28.4 | 27.5 | 22.9 | 17.2 | 25.7 | 36.0 | n.a. |
| V | 453 | 630 | 370 | 340 | 330 | 210 | 190 | 210 | 310 | 324 | 490 | 370 | 360 | 530 | n.a. |
| Zr | 246 | 280 | 140 | 80 | 110 | 80 | 70 | 80 | 130 | 132 | 200 | 220 | 220 | 150 | n.a. |
| Ta | n.a. | 3.17 | 1.3 | 0.67 | 1.44 | 0.90 | 0.63 | 0.91 | 0.97 | n.a. | n.a. | 1.78 | 2.09 | 1.23 | n.a. |
| Nb | 36 | n.a. | 19.6 | n.a. | n.a. | n.a. | n.a. | n.a. | n.a. | n.a. | 37 | n.a. | n.a. | n.a. | n.a. |
| Th | n.a. | 3.83 | 2.38 | 1.11 | 1.55 | 1.22 | 1.14 | 1.12 | 2.11 | n.a. | 2 | 3.99 | 3.34 | 2.56 | n.a. |
| U | n.a. | 0.68 | 0.56 | 0.19 | 0.12 | 0.22 | 0.16 | 0.28 | 0.34 | n.a. | 1.0 | 0.59 | 0.93 | 0.40 | n.a. |
| La | 44 | 42.8 | 21.6 | 11.4 | 35.4 | 11.8 | 11.9 | 12.8 | 19.0 | 17.3 | 28.6 | 30.2 | 49.5 | 19.6 | n.a. |
| Ce | n.a. | 51.7 | 51.1 | 29.7 | 39.8 | n.a. | 28.8 | n.a. | 47.4 | 39 | 62 | 71.7 | n.a. | 50.4 | n.a. |
| Nd | n.a. | 30.6 | 31.2 | 17.8 | 18.4 | n.a. | 12.4 | n.a. | 23.4 | 19 | 30 | 35.1 | n.a. | 28.9 | n.a. |
| Sm | n.a. | 9.60 | 7.28 | 4.55 | 4.70 | 3.85 | 3.39 | 3.60 | 6.06 | 4.0 | 6.4 | 8.31 | 9.96 | 6.98 | n.a. |
| Eu | n.a. | 2.78 | 2.11 | 1.33 | 0.63 | n.a. | 1.08 | n.a. | 3.22 | 1.4 | 2.4 | 2.41 | n.a. | 2.04 | n.a. |
| Tb | n.a. | 0.89 | 0.96 | 0.53 | 0.55 | n.a. | 0.24 | n.a. | 0.77 | 0.5 | 0.9 | 0.98 | n.a. | 0.71 | n.a. |
| Yb | n.a. | 1.61 | 1.62 | 1.02 | 0.67 | n.a. | 0.67 | n.a. | 1.27 | 1.3 | 1.7 | 1.85 | n.a. | 1.53 | n.a. |
| Lu | n.a. | 0.24 | 0.18 | 0.14 | 0.11 | n.a. | 0.13 | n.a. | 0.23 | 0.19 | 0.23 | 0.28 | n.a. | 0.28 | n.a. |
| Ba | 27 | 32.1 | 27.2 | 25.5 | 27.7 | 23.7 | 24.3 | 26.2 | 26.2 | 79 | 44 | 87.1 | 140 | 163 | n.a. |
| Sr | 53 | 80 | 100 | 40 | 40 | 20 | 20 | 10 | 10 | 18 | 62 | 100 | 100 | 100 | n.a. |
| Rb | 3 | 5.6 | 4.8 | 4.0 | 5.1 | 4.2 | 4.7 | 4.8 | 4.6 | 15 | n.a. | 5.4 | 6.2 | 5.3 | n.a. |

rock.

As was mentioned earlier, globular varieties of ferropicritic rocks have developed in differentiated parts of layered lava flows or in dikes and flows crystallized from an evolved derivative of a ferropicritic magma. This evolved nature is manifested by relatively low contents of MgO, Ni, and Cr and high abundances of incompatible elements in these rocks. Typical analyses of separated globule and matrix fractions are shown in Table 13. Harker diagrams for selected elements are presented in Fig. 51 with the conjugate globule-matrix pairs connected by tielines. The globules are systematically rich in $SiO_2$ and total alkalies but poor in MgO and $FeO_{tot}$. The exceptionally high FeO content in the interstitial chlorite (Table 5) is compatible with the high $FeO_{tot}$ content observed in matrix samples. CaO is equally distributed or slightly more abundant in the matrix while $Al_2O_3$ does not show any systematic pattern; it can be enriched in either the globules or the matrix with the difference being 0-2.7%.

With regard to trace elements, the ratios of immobile incompatible elements are approximately constant in the globules and matrix. This is clearly demonstrated in Fig. 52 which presents

Table 12. (*Continued*)

| Location$ | 16 Ki | 17 Ki | 18* K | 19* K | 20* K | 21* K | 22 Ka | 23 Ko | 24 Sh | 25 Sh | 26 Sh | 27 Sh | 28 Sh | 29 Sh | 30 Sh |
|---|---|---|---|---|---|---|---|---|---|---|---|---|---|---|---|
| $SiO_2$ | 41.20 | 46.06 | 45.70 | 43.40 | 42.60 | 44.83 | 47.22 | 48.13 | 41.97 | 44.25 | 43.05 | 46.01 | 45.51 | 44.47 | 44.13 |
| $TiO_2$ | 1.26 | 1.46 | 3.64 | 3.50 | 1.79 | 1.84 | 2.77 | 3.00 | 1.89 | 2.06 | 2.12 | 1.96 | 1.42 | 1.38 | 1.63 |
| $Al_2O_3$ | 5.45 | 4.88 | 11.29 | 11.30 | 5.84 | 4.77 | 9.36 | 11.34 | 7.78 | 8.94 | 9.39 | 8.48 | 4.67 | 6.56 | 6.85 |
| $Fe_2O_3$ | 5.21 | 1.01 | 3.35 | 2.72 | 5.67 | 1.77 | 2.35 | 2.07 | 2.17 | 1.51 | 1.58 | 1.46 | 1.39 | 1.49 | 6.42 |
| FeO | 10.10 | 10.50 | 13.37 | 14.18 | 9.45 | 12.22 | 12.19 | 11.90 | 12.20 | 11.80 | 12.90 | 11.90 | 10.60 | 11.30 | 7.62 |
| $FeO_{tot}$ | - | - | - | - | - | - | - | - | - | - | - | - | - | - | - |
| MnO | 0.18 | 0.16 | 0.18 | 0.23 | 0.16 | 0.13 | 0.18 | 0.17 | 0.20 | 0.17 | 0.18 | 0.19 | 0.15 | 0.13 | 0.21 |
| MgO | 24.30 | 18.49 | 6.00 | 7.60 | 17.35 | 20.86 | 8.74 | 6.88 | 15.76 | 13.04 | 13.72 | 13.51 | 19.36 | 21.89 | 17.07 |
| CaO | 3.84 | 11.13 | 8.81 | 10.20 | 9.53 | 5.74 | 11.02 | 8.95 | 9.51 | 9.50 | 7.99 | 8.72 | 7.99 | 4.87 | 9.25 |
| $Na_2O$ | 0.23 | 0.10 | 3.07 | 2.11 | 0.16 | 0.11 | 2.52 | 2.67 | 0.35 | 0.75 | 0.37 | 1.30 | 0.11 | 0.08 | 0.25 |
| $K_2O$ | 0.01 | 0.01 | 0.41 | 0.31 | 0.02 | 0.00 | 0.09 | 0.08 | 0.09 | 0.87 | 0.95 | 0.50 | 0.04 | 0.07 | 0.14 |
| $P_2O_5$ | 0.15 | 0.14 | 0.34 | 0.30 | 0.17 | 0.15 | 0.28 | 0.33 | 0.17 | 0.19 | 0.19 | 0.17 | 0.13 | 0.14 | 0.15 |
| $Cr_2O_3$ | 0.37 | 0.18 | 0.01 | 0.02 | 0.46 | 0.31 | 0.07 | 0.01 | 0.16 | 0.14 | 0.15 | 0.14 | 0.27 | 0.18 | 0.16 |
| NiO | 0.23 | 0.10 | 0.02 | 0.02 | 0.17 | 0.26 | 0.00 | 0.02 | 0.11 | 0.07 | 0.07 | 0.05 | 0.18 | 0.19 | 0.13 |
| $CO_2$ | 0.04 | 0.00 | n.a. | n.a. | 0.07 | 0.00 | n.a. | n.a. | 1.25 | 1.98 | 0.88 | 0.48 | 2.27 | 1.21 | 0.10 |
| $H_2O$ | 7.30 | 4.89 | 3.68 | 4.18 | 5.68 | 6.00 | n.a. | 3.91 | 6.10 | 5.31 | 5.90 | 4.56 | 5.66 | 6.82 | 5.43 |
| L.O.I. | n.a. | n.a. | n.a. | n.a. | n.a. | n.a. | 1.58 | n.a. | n.a. | n.a. | n.a. | n.a. | n.a. | n.a. | n.a. |
| Total | 99.86 | 99.12 | 99.87 | 100.07 | 99.11 | 98.99 | 98.37 | 99.46 | 99.70 | 100.58 | 99.46 | 99.43 | 99.74 | 100.77 | 99.53 |
| Cr | 2540 | 1260 | 100 | 130 | 3150 | 2120 | 468 | 48.5 | 1082 | 938 | 1032 | 926 | 1815 | 1216 | 1095 |
| Ni | 1830 | 803 | 130 | 130 | 1300 | 2070 | 35.5 | 190 | 853 | 573 | 558 | 402 | 1444 | 1528 | 1002 |
| Co | 136 | 81.2 | 80 | 110 | 150 | 150 | 63.1 | 54.8 | n.a. | n.a. | n.a. | n.a. | n.a. | n.a. | n.a. |
| Sc | 26.8 | 28.5 | n.a. | n.a. | n.a. | n.a. | 45.7 | 33.8 | 32.4 | 28.7 | 32.7 | 31.0 | 24.4 | 20.9 | 23.5 |
| V | 230 | 240 | 70 | 100 | 220 | 62 | 380 | 470 | 274 | 278 | 291 | 268 | 193 | 190 | 237 |
| Zr | 80 | 80 | n.a. | n.a. | n.a. | n.a. | 200 | 180 | 165 | 149 | 177 | 154 | 145 | 111 | 139 |
| Ta | 0.83 | 0.95 | n.a. | n.a. | n.a. | n.a. | 2.21 | 1.99 | n.a. | n.a. | 1.0 | n.a. | n.a. | n.a. | n.a. |
| Nb | n.a. | n.a. | n.a. | n.a. | n.a. | n.a. | n.a. | n.a. | 18.4 | 19.0 | 19.1 | 15.9 | 13.2 | 12.2 | 14.9 |
| Th | 1.27 | 1.59 | n.a. | n.a. | n.a. | n.a. | 2.56 | 2.72 | 2.10 | n.a. | 2.96 | n.a. | n.a. | n.a. | n.a. |
| U | 0.23 | 0.18 | n.a. | n.a. | n.a. | n.a. | 0.9 | 0.74 | 0.41 | n.a. | 0.62 | n.a. | n.a. | n.a. | n.a. |
| La | 10.2 | 14.3 | n.a. | n.a. | n.a. | n.a. | 27.4 | 21 | 12.1 | n.a. | 25.6 | n.a. | n.a. | n.a. | n.a. |
| Ce | n.a. | n.a. | n.a. | n.a. | n.a. | n.a. | n.a. | 45 | 35.3 | n.a. | 51.5 | n.a. | n.a. | n.a. | n.a. |
| Nd | n.a. | n.a. | n.a. | n.a. | n.a. | n.a. | n.a. | 33 | 24.5 | n.a. | 35.3 | n.a. | n.a. | n.a. | n.a. |
| Sm | 3.20 | 3.88 | n.a. | n.a. | n.a. | n.a. | 7.45 | 6.9 | 5.81 | n.a. | 7.34 | n.a. | n.a. | n.a. | n.a. |
| Eu | n.a. | n.a. | n.a. | n.a. | n.a. | n.a. | n.a. | 2.1 | 1.74 | n.a. | 2.29 | n.a. | n.a. | n.a. | n.a. |
| Tb | n.a. | n.a. | n.a. | n.a. | n.a. | n.a. | n.a. | 0.83 | 0.75 | n.a. | 0.89 | n.a. | n.a. | n.a. | n.a. |
| Yb | n.a. | n.a. | n.a. | n.a. | n.a. | n.a. | 1.7 | 1.54 | 1.57 | n.a. | 1.95 | n.a. | n.a. | n.a. | n.a. |
| Lu | n.a. | n.a. | n.a. | n.a. | n.a. | n.a. | n.a. | 0.16 | n.a. | n.a. | 0.19 | n.a. | n.a. | n.a. | n.a. |
| Ba | 29.3 | 25.7 | n.a. | n.a. | n.a. | n.a. | n.a. | 37.5 | 51.3 | 568 | 771 | 304 | 21.6 | 22.6 | 84.9 |
| Sr | 20 | 20 | n.a. | n.a. | n.a. | n.a. | 50 | 30 | 117 | 188 | 130 | 121 | 194 | 119 | 58.4 |
| Rb | 5.4 | 4.5 | n.a. | n.a. | n.a. | n.a. | n.a. | 6.6 | 5.8 | 17.5 | 17.8 | 13.3 | 6.0 | 9.0 | 9.3 |

n.a. = not analysed.

* = taken from Smolkin (1991).

$ Location: Ko = Kotselvaara; La = Lammas; Ki = Kierdzhipori, drill core S-2986; K = Kierdzhipori, drill core S-3056; Ka = Kaula, drill core S-3R; Sh = Shuljärvi, drill core S-VI.

Rock types and samples:

**1**, parallel olivine spinifex-textured rock, PS4; **2**, parallel olivine spinifex-textured rock with abundant primary magnetite, 1748/10; **3**, fine-grained rock composed of pyroxene needles, 1748/9; **4**, pyroxene cumulate, 1748/6; **5-9**, olivine cumulate, 1748/5, 1748/4, 1748/3, 1748/2, 1748/1; **10**, flowtop, S-2986-74.2; **11**, parallel olivine spinifex-textured rock, S-2986-A; **12-13**, evolved rock with porphyritic-spherulitic texture, S-2986-76.0, S-2986-78.7; **14-15**, pyroxene cumulate, S-2986-81.5, S-2986-83.8; **16-17**, olivine cumulate, S-2986-90.8, S-2986-97.0; **18-19**, spinifex zone, S-3056/476.0, S-3056/486.0; **20-21**, olivine cumulate, S-3056/498.0, S-3056/510.0; **22**, pyroxene spinifex-textured rock, S-3R/731.4; **23**, spinifex zone, 1684/9; **24-27**, randomly oriented olivine spinifex-textured rock, S-VI/408.2, S-VI/410.0, S-VI/412.7, S-VI/416.4; **28-30**, olivine cumulate, S-VI/419.5, S-VI/421.0, S-VI/423.9.

Table 13. Whole rock analyses of separated globule and matrix samples (major elements recalculated to 100% on an anhydrous basis).

| | 1 G | 2 M | 3 G | 4 M | 5 G | 6 M | 7 G | 8 M | 9 G | 10 M |
|---|---|---|---|---|---|---|---|---|---|---|
| $SiO_2$ | 48.72 | 45.76 | 50.97 | 42.41 | 50.19 | 39.08 | 55.55 | 44.65 | 53.50 | 44.08 |
| $TiO_2$ | 3.13 | 3.89 | 4.31 | 5.24 | 4.67 | 5.61 | 2.85 | 3.17 | 2.77 | 3.02 |
| $Al_2O_3$ | 9.60 | 10.95 | 12.68 | 12.44 | 13.22 | 10.86 | 10.70 | 10.73 | 10.64 | 10.39 |
| $FeO_{tot}$ | 14.31 | 19.36 | 11.31 | 18.68 | 12.90 | 22.21 | 9.95 | 19.05 | 10.43 | 18.66 |
| MnO | 0.19 | 0.21 | 0.17 | 0.23 | 0.17 | 0.26 | 0.18 | 0.24 | 0.18 | 0.25 |
| MgO | 8.79 | 7.54 | 4.38 | 6.45 | 4.55 | 8.27 | 5.87 | 8.03 | 6.89 | 9.54 |
| CaO | 12.21 | 9.97 | 10.24 | 11.47 | 8.39 | 12.45 | 10.70 | 12.02 | 11.67 | 12.35 |
| $Na_2O$ | 2.66 | 0.43 | 4.33 | 0.74 | 3.85 | 0.25 | 3.62 | 1.48 | 3.42 | 0.90 |
| $K_2O$ | 0.13 | 1.55 | 0.70 | 1.65 | 1.57 | 0.40 | 0.27 | 0.27 | 0.19 | 0.43 |
| $P_2O_5$ | 0.26 | 0.34 | 0.90 | 0.68 | 0.49 | 0.63 | 0.32 | 0.35 | 0.31 | 0.40 |
| L.O.I. | 2.95 | 3.45 | 2.05 | 4.26 | 2.47 | 5.22 | 1.71 | 3.58 | 1.40 | 4.05 |
| Cr | 471 | 218 | 66.3 | 117 | 61.7 | 49.8 | 140 | 157 | 274 | 299 |
| Ni | 190 | 120 | 28.5 | 65 | 27.2 | 26.3 | 22.8 | 77.9 | 90.7 | 91.3 |
| Co | 50.6 | 61.3 | 53.1 | 38.5 | 62.9 | 38.8 | 51.0 | 67.5 | 46.1 | 60.7 |
| Sc | n.a. | n.a. | 46 | 36.1 | 51.2 | 43.7 | 37.2 | 42.7 | 41.3 | 43.6 |
| V | 378 | 432 | 314 | 454 | 420 | 493 | 430 | 460 | 420 | 470 |
| Zr | 170 | 217 | n.a. | n.a. | 301 | 302 | 190 | 210 | 180 | 200 |
| Ta | n.a. | n.a. | 5.1 | 4.16 | 4.14 | 3.71 | 1.60 | 2.13 | 1.63 | 1.96 |
| Nb | n.a. | n.a. | n.a. | n.a. | n.a. | n.a. | n.a. | n.a. | n.a. | n.a. |
| Th | n.a. | n.a. | 5.09 | 4.69 | 5.12 | 4.07 | 3.22 | 3.73 | 2.87 | 3.74 |
| U | n.a. | n.a. | 1.48 | 1.08 | 1.17 | 0.94 | 0.63 | 0.87 | 0.66 | 0.57 |
| La | n.a. | n.a. | 40 | 55 | 35 | 51 | 24.4 | 30.6 | 22.3 | 31.8 |
| Ce | n.a. | n.a. | 82 | 105 | 65 | 101 | 38.6 | 43.7 | n.a. | n.a. |
| Nd | n.a. | n.a. | 54 | 66 | 44 | 67 | 22.5 | 25.0 | n.a. | n.a. |
| Sm | n.a. | n.a. | 11.3 | 13.6 | 10.6 | 14.9 | 6.51 | 7.43 | 7.01 | n.a. |
| Eu | n.a. | n.a. | 3.1 | 4.7 | 2.7 | 4.8 | 1.70 | 1.80 | n.a. | 7.22 |
| Tb | n.a. | n.a. | 1.25 | 1.51 | 1.08 | 1.67 | 0.682 | 0.736 | n.a. | n.a. |
| Yb | n.a. | n.a. | 2.3 | 2.7 | 2.1 | 2.9 | 1.17 | 1.25 | n.a. | n.a. |
| Lu | n.a. | n.a. | 0.23 | 0.31 | 0.23 | 0.29 | 0.182 | 0.214 | n.a. | n.a. |
| Y | n.a. | n.a. | n.a. | n.a. | n.a. | n.a. | n.a. | n.a. | n.a. | n.a. |
| S | 5500 | 200 | 900 | 800 | 1000 | 400 | 2820 | 740 | 3870 | 1870 |
| Cu | 130 | 120 | 150 | 140 | 160 | 150 | 150 | 150 | 140 | 170 |
| Sr | 79 | 87 | n.a. | n.a. | 199 | 238 | 180 | 140 | 140 | 80 |
| Ba | 98 | 1830 | 607 | 280 | 129 | 569 | 130 | 90.1 | 102 | 138 |
| Rb | 6.5 | 25.7 | 70.3 | 17.8 | 18 | 30 | 5 | 7.38 | 4.2 | 4.9 |

chondrite-normalized REE patterns for four globule-matrix pairs (matrix and globule portions marked by closed and open symbols, respectively). They show typical LREE-enriched trends with virtually identical slopes. In individual globule-matrix pairs, the level of REE is the same or slightly higher in the matrix samples. The roughly similar levels in the globule-matrix pairs also apply to the high field strength elements Ta and Nb. The HFSE have been shown to be enriched in the immiscible silicate liquid which is more depolymerized (e.g., Philpotts, 1982). In most globule-matrix pairs, this is qualitatively true for Ti and Zr, but the total Ti and Zr range of the matrix and the globules is similar (Fig. 51). It is significant that the variation of many trace components, including compatible and incompatible elements, is considerably larger in the whole data set than the variation within individual globule-matrix pairs. This is well illustrated, for example, in a plot of Ta against $SiO_2$ in Fig. 51. In contrast to the immobile trace elements, the lithophile ele-

Table 13. (*Continued*)

| | 11 G | 12 M | 13 G | 14 M | 15 G | 16 M | 17 G | 18 M |
|---|---|---|---|---|---|---|---|---|
| $SiO_2$ | 54.04 | 42.87 | 53.51 | 48.08 | 51.78 | 41.18 | 49.62 | 45.66 |
| $TiO_2$ | 3.40 | 4.03 | 3.80 | 3.89 | 3.81 | 4.05 | 3.59 | 4.42 |
| $Al_2O_3$ | 10.02 | 12.06 | 10.15 | 10.31 | 11.35 | 10.83 | 10.76 | 11.95 |
| $FeO_{tot}$ | 13.42 | 17.78 | 13.85 | 16.84 | 10.58 | 21.83 | 13.46 | 17.28 |
| MnO | 0.14 | 0.22 | 0.18 | 0.21 | 0.15 | 0.28 | 0.18 | 0.21 |
| MgO | 5.39 | 8.51 | 5.15 | 8.29 | 5.63 | 7.90 | 8.15 | 6.53 |
| CaO | 9.28 | 13.16 | 8.94 | 10.53 | 11.06 | 12.70 | 10.47 | 11.44 |
| $Na_2O$ | 2.79 | 0.32 | 2.76 | 0.40 | 2.14 | 0.42 | 3.03 | 0.41 |
| $K_2O$ | 1.13 | 0.63 | 1.32 | 1.03 | 3.18 | 0.44 | 0.31 | 1.62 |
| $P_2O_5$ | 0.39 | 0.43 | 0.34 | 0.42 | 0.33 | 0.37 | 0.44 | 0.47 |
| L.O.I. | 2.14 | 2.01 | 2.67 | 4.21 | n.a. | n.a. | 3.20 | 3.70 |
| Cr | 270 | 240 | 49 | 140 | 201 | 217 | 190 | 95 |
| Ni | 140 | 150 | 92 | 92 | 116 | 146 | 135 | 85 |
| Co | 49 | 56 | 51 | 52 | n.a. | n.a. | 55 | 60 |
| Sc | 27 | 32 | 24 | 30 | 39.7 | 45.9 | n.a. | n.a. |
| V | 320 | 320 | 310 | 270 | 415 | 470 | 190 | 270 |
| Zr | 288 | 320 | 296 | 326 | 227 | 249 | n.a. | n.a. |
| Ta | 2 | 3 | n.a. | 3 | n.a. | n.a. | n.a. | n.a. |
| Nb | 53 | 60 | 58 | 63 | 27.5 | 34.3 | n.a. | n.a. |
| U | 1.4 | 1.1 | n.a. | 1.3 | n.a. | n.a. | n.a. | n.a. |
| Th | 3.9 | 5.0 | 4.0 | 5.0 | n.a. | n.a. | n.a. | n.a. |
| La | 36.2 | 43.5 | 35.7 | 43.2 | n.a. | n.a. | n.a. | n.a. |
| Ce | 70 | 91 | 72 | 89 | n.a. | n.a. | n.a. | n.a. |
| Nd | 38 | 45 | 36 | 44 | n.a. | n.a. | n.a. | n.a. |
| Sm | 8.6 | 11 | 8.4 | 10 | n.a. | n.a. | n.a. | n.a. |
| Eu | 2.7 | 3.3 | 2.9 | 3.5 | n.a. | n.a. | n.a. | n.a. |
| Tb | 1.4 | 1.5 | 1.2 | 1.2 | n.a. | n.a. | n.a. | n.a. |
| Yb | 1.71 | 1.97 | 1.63 | 1.90 | n.a. | n.a. | n.a. | n.a. |
| Lu | 0.26 | 0.32 | 0.25 | 0.28 | n.a. | n.a. | n.a. | n.a. |
| Y | 26 | 28 | 27 | 30 | 28.7 | 30.4 | n.a. | n.a. |
| S | 9400 | 400 | 4500 | 300 | 2240 | 190 | 3600 | 800 |
| Cu | 190 | 230 | 200 | 170 | 187 | 172 | 170 | 115 |
| Sr | 116 | 116 | 113 | 142 | 249 | 95 | n.a. | n.a. |
| Ba | 460 | 470 | 340 | 740 | 851 | 160 | n.a. | n.a. |
| Rb | 23 | n.a. | 28 | 31 | 65.6 | 28.8 | n.a. | n.a. |

G = globule, M = matrix.
n.a. = not analysed.
Samples: **1-2**, 1003-G, 1003-M (Smolkin et al., 1987); **3-4**, 1685a-G, 1685a-M; **5-6**, 1685b-G, 1685b-M; **7-8**, 1824-3B, 1824-3A; **9-10**, 1824-3C, 1824-3D; **11-12**, S-87/74, S-87/73; **13-14**, S-87/76, S-87/75; **15-16**, Souker 2G/91, Souker 2M/91; **17**, Average of six globule samples (Sharkov and Smolkin, 1989); **18**, Average of five matrix samples (Sharkov and Smolkin, 1989).

ments that have generally been regarded as mobile including Sr and Ba show aberrant behavior (Fig. 51). As is revealed in Table 13, sulfur is generally higher in the globules relative to the matrix.

Figure 53 illustrates chondrite-normalized REE profiles for massive and pillowed lavas and samples from the spinifex zone of layered lava flows. As already shown in Fig. 52, ferropicritic rocks in general display a strong LREE enrichment over HREE and differ in this respect from the associated tholeiitic metavolcanites. In most cases, the REE patterns of ferropicrites are straight but anomalous samples exist with a rather flat distribution from La to Nd or Sm (Fig. 53). As a result, $(La/Yb)_N$ varies over a rather large

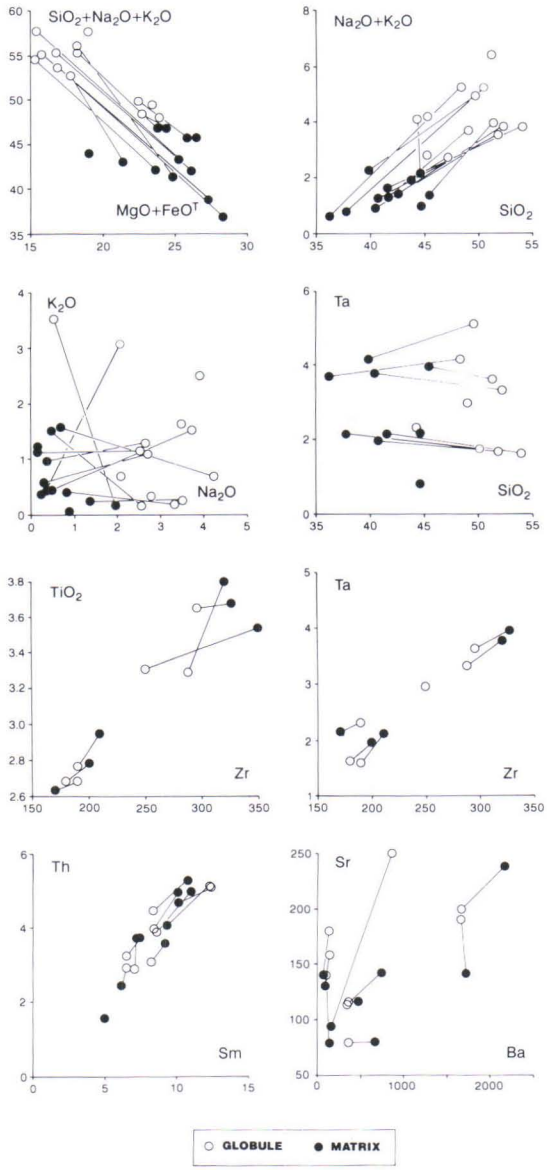


Fig. 51. Variation of chemical components (wt. %) in globule and matrix fractions. Coexisting globule-matrix pairs connected with tielines.

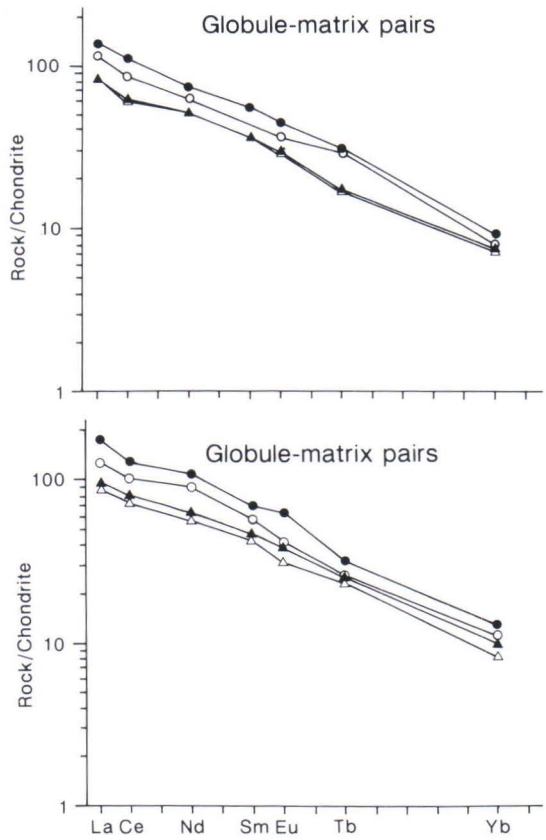


Fig. 52. Chondrite-normalized REE patterns for four coexisting globule-matrix pairs. Open symbols - globule, closed symbols - matrix.

range of 5-15 with the most common values being around 10. The $(Sm/Yb)_N$ value is more homogeneous falling most frequently between 4-5. The reason for abnormally low LREE abundances in some samples is not clear. It cannot be due to the accumulation of clinopyroxene crystals because these rocks do not contain clinopyroxene phenocrysts. Also, heterogeneity of the parental magma is not a likely explanation because the variation in La/Yb is observed in samples from single flow units.

In Fig. 54, abundances of olivine-incompatible elements of primitive ferropicritic metavolcanites are portrayed as a spidergram normalized to primitive mantle values. Three of the samples are massive lavas, two are olivine spinifex-textured rocks, and one represents a fine-

grained rock from the upper part of a layered flow. These ferropicrites are compared with average compositions of normal and enriched MORBs and oceanic alkali basalt as tabulated by Sun and McDonough (1989). The patterns of the ferropicrites follow most closely that of OIB but the

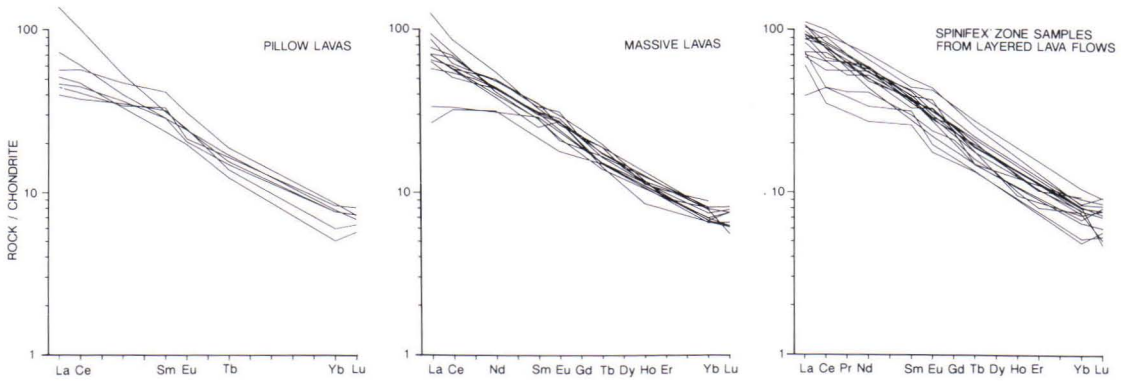


Fig. 53. Chondrite-normalized REE patterns for massive and pillowed ferropicrites and for samples from the spinifex zone of layered lava flows.

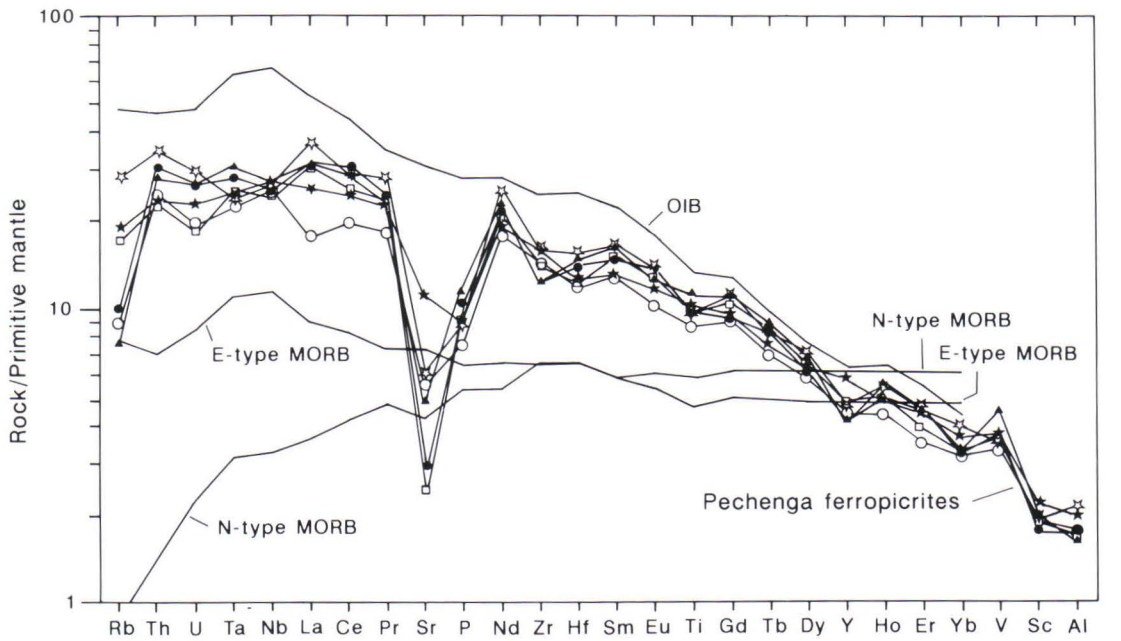


Fig. 54. Primitive mantle normalized abundance patterns for moderately and highly incompatible elements for ferropicrites, N-type and E-type MORBs and oceanic alkali basalt. MORB and OIB data from Sun and McDonough (1989) and normalizing values from Sun and McDonough (1989) and McDonough and Frey (1990).

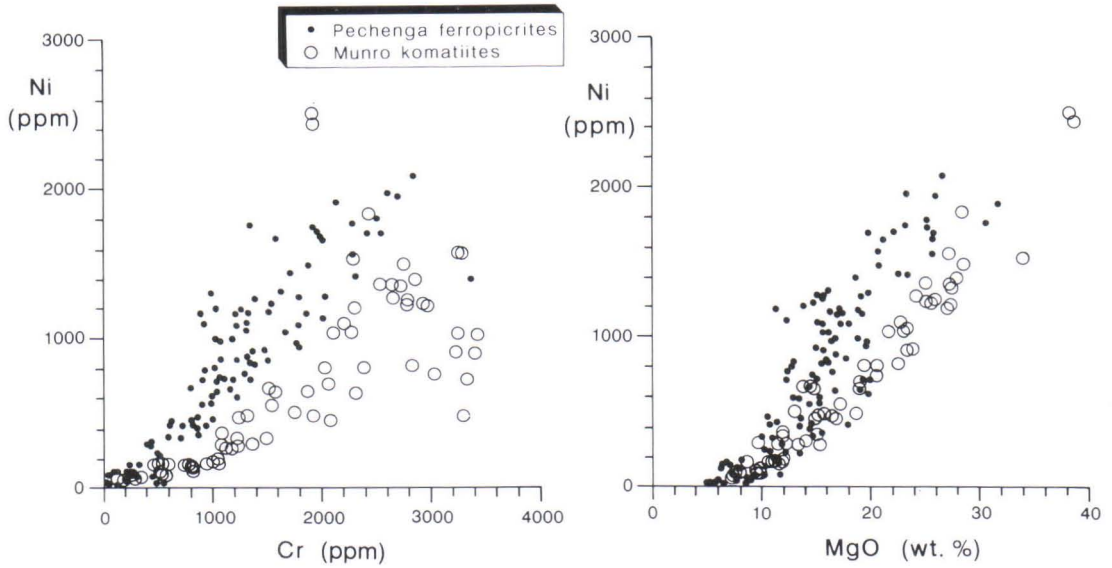


Fig. 55. Ni, Cr and MgO contents of ferropicritic metavolcanites compared with those of komatiitic metavolcanites from Munro Township, Canada (literature sources available from the author on request).

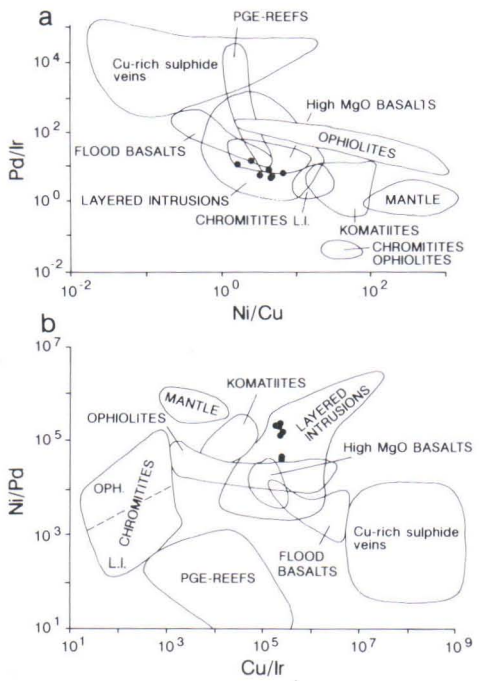


Fig. 56. Pechenga ferropicrites (dots) on Pd/Ir versus Ni/Cu and Ni/Pd versus Cu/Ir discrimination diagrams. Fields taken from Barnes and Often (1990).

level of the latter is somewhat higher. Ferropicrites clearly deviate from different MORBs in being enriched in most incompatible elements and depleted in heavy REE. The most striking anomalies in the ferropicritic patterns are the negative peaks at Rb and Sr which are probably consequences of the mobility of these elements. If K and Ba were added to the diagram, more positive and negative anomalies would be seen in the spidergram. Considering the immobile elements, HFSE-REE ratios seem to be slightly lower in ferropicrites compared with OIB. The most pronounced difference is, however, in the relative abundances of phosphorous. For example, the P-Nd ratio in ferropicrites is about half that in N-type and E-type MORBs or OIB. Also worth mentioning is a small positive anomaly at vanadium which is not a surprise when considering the high iron content of these rocks. Low Al and high V in ferropicrites produce exceptionally low Al/V, varying generally between 90-130. These values are clearly lower than those observed in komatiites. In Munro-type komatiites, Al/V is about 280, i.e., close to the estimated primitive

mantle value of 287 (McDonough and Frey, 1989) while in Al-depleted, Barberton-type komatiites, this ratio is commonly about 180 (Nesbitt et al., 1979).

The trace element patterns of ferropicrites in Fig. 54 clearly explain why ferropicrites plot in the field of alkalic or transitional within-plate basalts on many discrimination diagrams, such as Th/Yb versus Ta/Yb (Hanski and Smolkin, 1989). The comparatively low concentration of $P_2O_5$ in ferropicrites in turn accounts for their shift to the field of tholeiites on the $TiO_2$ versus $Zr/P_2O_5$ diagram (Hanski and Smolkin, 1989).

In Fig. 55, Ni and MgO contents of ferropicritic metavolcanites from Pechenga and komatiitic metavolcanites from Munro Township are compared. The ferropicritic analyses represent pillow lavas, massive lavas, and various rock types from layered lava flows screened by using an upper limit of 5000 ppm for sulfur. At an equivalent MgO content, ferropicrites appear to have a higher Ni concentration. The difference would be still larger if Mg number were used instead of MgO. The situation is reversed with respect to chromium; ferropicrites have a slightly lower Cr content at the same MgO level. A consequence is that ferropicrites and Munro-type komatiites separate well from each other when Ni is plotted against Cr (Fig. 55).

Platinum group elements (PGE) were analysed for several samples of ferropicritic volcanic rocks. In this context, only preliminary data are presented in the form of two plots designed by Sarah-Jane Barnes et al. (1988) employing ratios of chalcophile and noble metals (Fig. 56). A more detailed account will be published elsewhere (Brügmann et al., in prep.). Most primitive ferropicritic metavolcanites that are plotted on the Pd/Ir versus Ni/Cu diagram in Fig. 56 are shifted to the left of the komatiite field and plot on the field of layered intrusions and on the lower edge of the field of high-MgO basalts. In the Ni/Pd versus Cu/Ir diagram, ferropicrites are located again in the field of layered intrusions but plot above the field of high-MgO basalts. Figure 56 demonstrates that with regard to Ni-PGE relations, ferropicrites mimic komatiites. The low Pd/Ir values indicate little fractionation between platinum group elements, which is a typical feature of primitive magmas. The deviation from the komatiite field is primarily a consequence of a higher ratio of Cu to Ni and Cu to PGE in ferropicrites.

## Gabbro-wehrlite intrusions

Major element analyses of various rock types from the Pechenga gabbro-wehrlite intrusions have been published in several Russian publications. About 300 analyses are included in a collection of chemical analyses on basic to ultrabasic complexes in the Kola Peninsula (Gorbunov, 1982). Representative whole rock analyses of various rock types from gabbro-wehrlite intrusions are listed in Table 14 and average compositions of ultramafic rocks are shown in Table 15.

The maximum MgO content of metaperidotites reaches about 38% in volatile-free analyses, which is relatively low when compared, for example, with peridotitic rocks generated from komatiitic magmas. According to Zak et al. (1982), the average MgO in serpentinized peridotites is about 33% and in serpentinized olivinites 35%. In Fig. 57, $Al_2O_3$ and $TiO_2$ is plotted against MgO for S-poor ultramafic cumulates having MgO higher than 20%. Also shown are the compositional ranges of olivines with $Fo_{80\text{-}90}$. The trends displayed by metaperidotites imply that these rocks are mixtures of a ferropicritic liquid and olivine with a forsterite content within the range stated above. In fact, the X-axis intercepts of the trends suggest that the maximum Fo of 84.2% measured for Pechenga olivines is probably not far from the most magnesian olivine composition crystallized in the intrusions.

The $Al_2O_3$-$TiO_2$ ratio remains approximately

Table 14. Whole rock analyses of various rock types from gabbro-wehrlite intrusions.

| Intrusion$ | 1 U | 2 U | 3 U | 4 U | 5 U | 6 Ka | 7 Ka | 8 Ka | 9 Ka | 10 Ka | 11 Ka | 12 NK | 13 NK | 14 NK | 15 Or |
|---|---|---|---|---|---|---|---|---|---|---|---|---|---|---|---|
| $SiO_2$ | 38.35 | 43.46 | 41.81 | 43.16 | 53.60 | 37.58 | 38.45 | 34.69 | 42.89 | 44.94 | 43.10 | 37.27 | 49.04 | 37.84 | 39.85 |
| $TiO_2$ | 0.69 | 1.54 | 1.51 | 1.46 | 2.23 | 1.05 | 1.20 | 1.68 | 1.74 | 3.60 | 3.57 | 0.90 | 1.92 | 3.25 | 0.84 |
| $Al_2O_3$ | 2.25 | 5.08 | 4.72 | 5.02 | 14.68 | 3.43 | 3.68 | 4.68 | 5.09 | 11.85 | 12.70 | 3.11 | 8.16 | 9.52 | 2.89 |
| $Fe_2O_3$ | n.a. | n.a. | n.a. | n.a. | n.a. | 9.15 | 4.68 | 6.74 | 1.60 | 2.37 | n.a. | n.a. | n.a. | n.a. | n.a. |
| FeO | n.a. | n.a. | n.a. | n.a. | n.a. | 9.16 | 11.55 | 12.79 | 10.76 | 12.71 | n.a. | n.a. | n.a. | n.a. | n.a. |
| $FeO_{tot}$ | 11.94 | 16.38 | 16.91 | 14.88 | 11.47 | 17.39 | 15.76 | 18.85 | 12.19 | 14.84 | 17.09 | 14.15 | 11.54 | 16.95 | 15.37 |
| MnO | 0.19 | 0.23 | 0.22 | 0.17 | 0.20 | 0.17 | 0.18 | 0.25 | 0.18 | 0.20 | 0.25 | 0.17 | 0.18 | 0.23 | 0.19 |
| MgO | 33.76 | 27.01 | 25.18 | 23.29 | 2.27 | 28.87 | 27.27 | 26.50 | 15.00 | 5.07 | 4.99 | 29.69 | 9.73 | 8.69 | 33.48 |
| CaO | 0.84 | 2.87 | 4.27 | 5.05 | 6.14 | 2.17 | 1.03 | 0.89 | 14.85 | 10.08 | 8.16 | 2.86 | 14.52 | 16.01 | 2.83 |
| $Na_2O$ | 0.00 | 0.00 | 0.30 | 0.28 | 3.94 | 0.00 | 0.00 | 0.00 | 0.08 | 3.12 | 2.69 | 0.00 | 1.57 | 1.01 | 0.00 |
| $K_2O$ | 0.04 | 0.13 | 0.05 | 0.01 | 2.10 | 0.03 | 0.01 | 0.01 | 0.02 | 0.21 | 0.19 | 0.06 | 0.21 | 0.04 | 0.16 |
| $P_2O_5$ | 0.09 | 0.18 | 0.16 | 0.15 | 0.45 | 0.10 | 0.11 | 0.16 | 0.16 | 0.35 | 0.32 | 0.12 | 0.13 | 0.35 | 0.10 |
| $H_2O$ | n.a. | n.a. | n.a. | n.a. | n.a. | 9.38 | 10.04 | 10.34 | 3.23 | 2.84 | n.a. | n.a. | n.a. | n.a. | n.a. |
| $CO_2$ | n.a. | n.a. | n.a. | n.a. | n.a. | n.a. | 0.18 | 0.44 | n.a. | 0.18 | n.a. | n.a. | n.a. | n.a. | n.a. |
| L.O.I. | 3.06 | 2.99 | 3.13 | 3.34 | 4.17 | n.a. | n.a. | n.a. | n.a. | n.a. | 3.31 | 3.58 | 1.63 | 3.26 | 3.69 |
| Cr | 4550 | 1670 | 2970 | 2390 | 63.6 | 3487 | 3477 | 5061 | 922 | 27 | 13 | 4430 | 189 | 242 | 4660 |
| Ni | 2290 | 1120 | 1400 | 1180 | 49.3 | 5160 | 1717 | 2188 | 75 | 30 | 6 | 2380 | 213 | 149 | 2540 |
| Co | 167 | 119 | 133 | 112 | 26.3 | 179 | 130 | 197 | 63.3 | 37.8 | 67 | 153 | 57.8 | 68.9 | 151 |
| Sc | 14.8 | 22 | 32.1 | 20.4 | 17.1 | 20.7 | 23.9 | 29.5 | 91.8 | 32.7 | 20.1 | 18 | 77.4 | 45.1 | 17 |
| V | n.a. | n.a. | n.a. | n.a. | n.a. | 200 | 229 | 322 | 374 | 553 | 477 | n.a. | n.a. | n.a. | n.a. |
| Zr | n.a. | n.a. | n.a. | n.a. | n.a. | 68 | 72 | 115 | 109 | 250 | 248 | n.a. | n.a. | n.a. | n.a. |
| Ta | 0.41 | 1.56 | 0.80 | 0.85 | 3.08 | 0.59 | 0.78 | 0.78 | 1.03 | 1.87 | n.a. | 0.42 | 0.60 | 1.43 | 0.42 |
| Nb | n.a. | n.a. | n.a. | n.a. | n.a. | n.a. | n.a. | n.a. | n.a. | n.a. | 43 | n.a. | n.a. | n.a. | n.a. |
| Th | 0.81 | 2.44 | 1.18 | 1.47 | 6.14 | 0.84 | 0.91 | 1.22 | 1.26 | 2.97 | 3 | 0.69 | 0.99 | 2.24 | 0.78 |
| U | 0.23 | 0.75 | 0.74 | 0.54 | 2.25 | 0.18 | 0.20 | 0.43 | 0.43 | 1.03 | 1.1 | 0.27 | 0.48 | 0.92 | 0.28 |
| La | 4.4 | 20 | 10 | 10.1 | 45.5 | 7.61 | 7.32 | 10.4 | 11.4 | 25.5 | 34.3 | 6.69 | 10.4 | 21.4 | 6.45 |
| Ce | n.a. | 42 | n.a. | n.a. | n.a. | n.a. | n.a. | n.a. | n.a. | n.a. | 80 | n.a. | 25 | n.a. | n.a. |
| Nd | n.a. | 23 | n.a. | n.a. | n.a. | n.a. | n.a. | n.a. | n.a. | n.a. | 39 | n.a. | 19.6 | n.a. | n.a. |
| Sm | 1.44 | 6.7 | 3.2 | 3.02 | 10.9 | 2.19 | 2.38 | 3.04 | 4.39 | 7.51 | 8.6 | 1.87 | 6.4 | 6.57 | 1.75 |
| Eu | n.a. | 1.34 | n.a. | n.a. | n.a. | n.a. | n.a. | n.a. | n.a. | n.a. | 3.1 | n.a. | 2.2 | n.a. | n.a. |
| Tb | n.a. | 0.52 | n.a. | n.a. | n.a. | n.a. | n.a. | n.a. | n.a. | n.a. | 1.3 | n.a. | 0.75 | n.a. | n.a. |
| Yb | n.a. | 0.79 | n.a. | n.a. | n.a. | n.a. | n.a. | n.a. | n.a. | n.a. | 2.2 | n.a. | 1.28 | n.a. | n.a. |
| Lu | n.a. | 0.12 | n.a. | n.a. | n.a. | n.a. | n.a. | n.a. | n.a. | n.a. | 0.29 | n.a. | 0.1 | n.a. | n.a. |
| Y | n.a. | n.a. | n.a. | n.a. | n.a. | n.a. | n.a. | n.a. | n.a. | n.a. | 29 | n.a. | n.a. | n.a. | n.a. |
| S | n.a. | n.a. | n.a. | n.a. | n.a. | 10440 | 2690 | 2810 | 130 | 1740 | 773 | n.a. | n.a. | n.a. | n.a. |
| Cu | n.a. | n.a. | n.a. | n.a. | n.a. | 2919 | 110 | 156 | 4 | 0 | 1.4 | n.a. | n.a. | n.a. | n.a. |
| Sr | n.a. | n.a. | n.a. | n.a. | n.a. | 34 | 31 | 59 | 37 | 389 | 145 | n.a. | n.a. | n.a. | n.a. |
| Ba | 43.9 | 107 | 73.4 | 46.1 | 878 | 31 | 19 | 20 | 25 | 167 | 127 | 44.8 | 190 | 43.2 | 42.4 |
| Rb | 8.5 | 8.5 | 10 | 9 | 44.1 | 6.5 | 6.3 | 8.1 | 6.0 | 10.4 | 21 | 9.0 | 9.3 | 7.8 | 9.5 |

constant in olivine cumulates with a value close to that of the parental magma (Fig. 58). The same ratio is also observed in whole rock analyses of peridotites containing disseminated ore as shown in Fig. 58 by the low-Al samples from the base of the ore-bearing Kammikivi sill. In ultramafic cumulates, olivine-incompatible elements in general show ratios similar to those observed in ferropicritic metavolcanites as demonstrated by the chondrite-normalized REE patterns in Fig. 59. In pyroxenites, REE profiles from La to Sm are flat. This is consistent with the low crystal/liquid parti-

Table 14. (*Continued*)

| Intrusion$ | 16 Or | 17 Or | 18 Or | 19 Pi | 20 Pi | 21 Pi | 22* Pi | 23* Pi | 24* Pi | 25* Pi | 26* Pi | 27* Pi | 28* Pi | 29 Pi | 30* Pi |
|---|---|---|---|---|---|---|---|---|---|---|---|---|---|---|---|
| $SiO_2$ | 36.72 | 36.31 | 40.62 | 37.16 | 37.62 | 36.08 | 36.81 | 36.74 | 41.23 | 41.32 | 42.42 | 43.73 | 45.48 | 47.86 | 52.80 |
| $TiO_2$ | 0.82 | 0.96 | 3.18 | 0.74 | 0.64 | 0.66 | 0.81 | 0.86 | 4.88 | 3.68 | 3.12 | 4.93 | 4.08 | 3.20 | 1.50 |
| $Al_2O_3$ | 2.68 | 2.74 | 4.80 | 2.14 | 2.29 | 2.56 | 2.97 | 2.69 | 5.40 | 7.28 | 13.34 | 13.49 | 12.93 | 14.32 | 13.68 |
| $Fe_2O_3$ | n.a. | n.a. | n.a. | n.a. | n.a. | n.a. | 5.12 | 7.45 | 7.93 | 5.38 | 5.07 | 2.62 | 4.84 | n.a. | 2.27 |
| FeO | n.a. | n.a. | n.a. | n.a. | n.a. | n.a. | 13.26 | 11.51 | 11.25 | 12.06 | 10.79 | 12.02 | 10.38 | n.a. | 9.15 |
| $FeO_{tot}$ | 15.40 | 16.50 | 14.99 | 17.02 | 16.54 | 18.14 | 17.86 | 18.21 | 18.38 | 16.90 | 15.35 | 14.38 | 14.73 | 13.31 | 11.19 |
| MnO | 0.20 | 0.21 | 0.18 | 0.20 | 0.20 | 0.21 | 0.19 | 0.23 | 0.20 | 0.14 | 0.18 | 0.17 | 0.12 | 0.18 | 0.19 |
| MgO | 30.46 | 28.92 | 10.80 | 33.87 | 33.30 | 31.03 | 30.05 | 28.86 | 10.31 | 9.82 | 6.97 | 5.71 | 5.13 | 3.79 | 1.99 |
| CaO | 2.83 | 2.06 | 14.58 | 2.35 | 2.13 | 2.98 | 2.02 | 2.60 | 15.37 | 15.71 | 11.85 | 9.52 | 11.26 | 7.38 | 4.94 |
| $Na_2O$ | 0.10 | 0.00 | 0.46 | 0.19 | 0.10 | 0.14 | 0.14 | 0.17 | 0.36 | 0.96 | 1.94 | 2.72 | 2.93 | 3.56 | 4.45 |
| $K_2O$ | 0.26 | 0.09 | 0.01 | 0.11 | 0.12 | 0.22 | 0.31 | 0.29 | 0.17 | 0.07 | 0.50 | 1.33 | 0.24 | 1.60 | 2.76 |
| $P_2O_5$ | 0.22 | 0.10 | 0.17 | 0.06 | 0.05 | 0.04 | 0.05 | 0.06 | 0.03 | 0.51 | 0.07 | 0.09 | 0.15 | 0.33 | 0.45 |
| $H_2O$ | n.a. | n.a. | n.a. | n.a. | n.a. | n.a. | 6.53 | 7.42 | 2.13 | 1.96 | 3.12 | 3.44 | 2.01 | n.a. | 3.17 |
| $CO_2$ | n.a. | n.a. | n.a. | n.a. | n.a. | n.a. | 0.13 | 0.11 | 0.12 | 0.20 | 0.04 | 0.23 | 0.14 | n.a. | 2.33 |
| L.O.I. | 4.00 | 2.86 | 2.97 | n.a. | n.a. | n.a. | n.a. | n.a. | n.a. | n.a. | n.a. | n.a. | n.a. | 3.80 | n.a. |
| Cr | 3500 | 4580 | 570 | 4039 | 4122 | 3774 | 4826 | 4768 | 501 | 270 | 50.0 | 15.2 | 22.8 | 32.4 | 24.7 |
| Ni | 1500 | 1690 | 142 | 2140 | 1748 | 2480 | 1414 | 1635 | 159 | 67.2 | 77.8 | 65.8 | 71.7 | 38.7 | 0 |
| Co | 140 | 146 | 105 | n.a. | n.a. | n.a. | 170 | 168 | 65.9 | 72.9 | 82.5 | 41.7 | 56.9 | 40.2 | 16.5 |
| Sc | 11 | 15.2 | 90.2 | 12.8 | 16.6 | 14.4 | 13.6 | 15.0 | 61.1 | 64.0 | 41.0 | 30.3 | 38.1 | 37.8 | 12.6 |
| V | 130 | n.a. | n.a. | 119 | 126 | 132 | n.a. | n.a. | n.a. | n.a. | n.a. | n.a. | n.a. | n.a. | n.a. |
| Zr | 50 | n.a. | n.a. | 38.5 | 47.5 | 49.1 | n.a. | n.a. | n.a. | n.a. | n.a. | n.a. | n.a. | n.a. | n.a. |
| Ta | 0.46 | 0.56 | 0.97 | n.a. | n.a. | n.a. | 0.22 | 0.28 | 0.44 | 0.38 | 0.92 | 1.02 | 1.00 | 2.72 | 2.70 |
| Nb | n.a. | n.a. | n.a. | 7.1 | 8.9 | 8.5 | n.a. | n.a. | n.a. | n.a. | n.a. | n.a. | n.a. | n.a. | n.a. |
| Th | 0.83 | 0.81 | 1.38 | 3.1 | 3.1 | 3.2 | 0.68 | 0.60 | 0.59 | 0.62 | 1.76 | 1.44 | 1.52 | 3.58 | 7.61 |
| U | 0.15 | 0.43 | 0.95 | 3.3 | 2.5 | 2.6 | 0.19 | 0.11 | 0.30 | 0.26 | 0.44 | 0.34 | 0.36 | 1.9 | 1.63 |
| La | 5.6 | 6.3 | 14.1 | n.a. | n.a. | n.a. | 4.41 | 5.36 | 6.59 | 6.21 | 11.23 | 10.97 | 12.43 | 29.5 | 56.71 |
| Ce | 13 | 16.7 | n.a. | n.a. | n.a. | n.a. | 11.24 | 13.16 | 15.45 | 13.90 | 25.91 | 25.55 | 30.82 | n.a. | 128.1 |
| Nd | 7 | 11.5 | n.a. | n.a. | n.a. | n.a. | 5.75 | 7.66 | 12.28 | 10.17 | 14.01 | 13.11 | 17.71 | n.a. | 58.52 |
| Sm | 1.4 | 2.2 | 4.75 | n.a. | n.a. | n.a. | 1.65 | 2.00 | 3.70 | 3.38 | 4.05 | 4.00 | 4.58 | 7.77 | 12.89 |
| Eu | 0.5 | 0.73 | n.a. | n.a. | n.a. | n.a. | 0.48 | 0.58 | 1.28 | 1.15 | 1.56 | 1.45 | 1.68 | n.a. | 3.72 |
| Tb | 0.3 | 0.38 | n.a. | n.a. | n.a. | n.a. | 0.24 | 0.28 | 0.49 | 0.55 | 0.55 | 0.49 | 0.66 | n.a. | 1.51 |
| Yb | 0.4 | 0.54 | n.a. | n.a. | n.a. | n.a. | 0.48 | 0.52 | 0.93 | 0.77 | 1.10 | 0.84 | 1.46 | n.a. | 3.34 |
| Lu | 0.06 | 0.08 | n.a. | n.a. | n.a. | n.a. | 0.06 | 0.07 | 0.13 | 0.12 | 0.15 | 0.13 | 0.22 | n.a. | 0.45 |
| Y | 8 | n.a. | n.a. | 3.8 | 3.4 | 3.0 | n.a. | n.a. | n.a. | n.a. | n.a. | n.a. | n.a. | n.a. | n.a. |
| S | n.a. | n.a. | n.a. | 4460 | 3280 | 11000 | 3900 | 2900 | 4400 | 7900 | 1700 | n.a. | 2000 | n.a. | n.a. |
| Cu | 490 | n.a. | n.a. | 431 | 303 | 875 | 170 | 120 | 230 | n.a. | 200 | 30 | n.a. | n.a. | n.a. |
| Sr | 20 | n.a. | n.a. | 25.4 | 35.0 | 73.4 | n.a. | n.a. | n.a. | n.a. | n.a. | n.a. | n.a. | n.a. | n.a. |
| Ba | 70 | 31.5 | 70.1 | 32.5 | 34.1 | 63.5 | 43.7 | 41.3 | 21.6 | 44.7 | 90.9 | 297 | 74.3 | 331 | 619 |
| Rb | n.a. | 8.7 | 4.6 | 6.6 | 7.9 | 11.8 | 9.1 | 11.5 | 6.0 | 3.1 | 26.9 | 45.0 | 11.0 | 24.2 | 72.5 |

n.a. = not analysed
* = major element analyses taken from Smolkin (1991).
$ = U, Kaula-Kammikivi region, exact location unknown; Ka, Kammikivi, NK = Northern Kotselvaara; Or, Ortoaivi; Pi, Pilgujärvi.
Rock types (protoliths):
1-4, 6-8, 12, 15-23, peridotites; 9, 13-14, pyroxenites; 5, 24-30, gabbros; 10-11, quench gabbros.
Samples:
**1**, 9F; **2**, 3395-UJ-1935; **3**, 3410-UJ-1935; **4**, 3434-UJ-1935; **5**, 2616-UJ-1935; **6**, Pet1/33.10; **7**, Pet1/15.35; **8**, Pet1/20.35; **9**, Pet1/5.40; **10**, Pet1/1.00; **11**, Pet1/0.30; **12**, 700/60 S; **13**, 880/90S; **14**, 140/160 S; **15**; 57.1-HV-28; **16**, OA-HV-28; **17**, 61.1-HV-28; **18**, 62.2-HV-28; **19**, PJ 3B; **20**, PJ 3C; **21**, PJ 8; **22**, SA-14; **23**, SA-40; **24**, SA-22; **25**, SA-13; **26**, SA-8; **27**, SA-19; **28**, SA-5; **29**, Pilgunjunne 9; **30**, SA-3.

tion coefficient of clinopyroxene for LREE (e.g., Frey et al., 1978). In gabbroic rocks, the REE patterns are again straight and LREE-enriched. In general, no significant Eu anomalies are observed in gabbroic rocks. The analysis of the lower chilled margin of the Northern Kotselvaara intrusion presented in Fig. 59 displays a REE pattern which is typical of ferropicritic volcanic rocks.

Figures 23, 24, and 28 illustrate variations in major and some trace elements across the Pilgujärvi layered intrusion and the Kammikivi layered sill. Table 14 lists geochemical data from these

Table 15. Average chemical compositions of ultramafic rocks from gabbro-wehrlite intrusions.

| | 1 | 2 | 3 | 4 | 5 | 6 | 7 | 8 | 9 | 10 |
|---|---|---|---|---|---|---|---|---|---|---|
| $SiO_2$ | 36.29 | 36.96 | 37.85 | 35.00 | 37.20 | 39.54 | 39.77 | 36.40 | 37.13 | 39.53 |
| $TiO_2$ | 0.79 | 0.83 | 1.14 | 0.67 | 1.09 | 1.13 | 1.34 | 0.72 | 0.95 | 1.35 |
| $Al_2O_3$ | 3.05 | 2.97 | 3.88 | 2.52 | 4.14 | 4.31 | 3.99 | 2.46 | 3.16 | 4.58 |
| $Fe_2O_3$ | - | - | - | - | - | - | - | 9.16 | 8.42 | 7.25 |
| FeO | - | - | - | - | - | - | - | 7.41 | 8.58 | 8.84 |
| $FeO_{tot}$ | 17.05 | 15.51 | 15.54 | 16.71 | 16.51 | 14.94 | 16.20 | 15.65 | 16.15 | 15.36 |
| MnO | 0.20 | 0.19 | 0.19 | 0.19 | 0.18 | 0.17 | 0.18 | 0.20 | 0.20 | 0.19 |
| MgO | 29.48 | 29.51 | 26.50 | 30.39 | 24.54 | 25.34 | 25.54 | 32.09 | 28.20 | 23.02 |
| CaO | 2.85 | 2.63 | 3.35 | 0.19 | 2.73 | 2.69 | 2.15 | 1.82 | 2.65 | 5.13 |
| $Na_2O$ | 0.14 | 0.09 | 0.09 | 0.17 | 0.09 | 0.09 | 0.09 | 0.10 | 0.10 | 0.13 |
| $K_2O$ | 0.22 | 0.11 | 0.07 | 0.13 | 0.08 | 0.08 | 0.04 | 0.11 | 0.11 | 0.09 |
| $Cr_2O_3$ | - | - | - | - | - | - | - | 0.51 | 0.50 | 0.40 |
| NiO | - | - | - | - | - | - | - | 0.36 | 0.28 | 0.36 |
| $H_2O$ | - | - | - | - | - | - | - | 8.00 | 9.00 | 6.24 |
| n* | 124 | 102 | 19 | 23 | 31 | 23 | 17 | 51 | 42 | 19 |

* number of analyses
1,2,3, serpentinized peridotites from ore-bearing, potentially ore-bearing, and barren intrusions, respectively; 4, serpentinized olivinites from ore-bearing intrusions; 5,6,7, chlorite-talc-serpentine rocks from ore-bearing, potentially ore-bearing, and barren intrusions, respectively; 8, serpentinized pyroxene-bearing olivinites; 9, serpentinized peridotites (wehrlites); 10, serpentine-chlorite-talc rocks. 1-7 taken from Zak et al. (1982), 8-10 from Smolkin (1991).

Table 16. Correlation matrix of olivine- and sulfide-incompatible element abundances in 26 samples from the Kammikivi ore-bearing sill.

| | $Al_2O_3$ | $TiO_2$ | $P_2O_5$ | V | Zr | La | Sm | Ta | Th |
|---|---|---|---|---|---|---|---|---|---|
| $TiO_2$ | 0.973 | | | | | | | | |
| $P_2O_5$ | 0.975 | 0.967 | | | | | | | |
| V | 0.940 | 0.926 | 0.876 | | | | | | |
| Zr | 0.981 | 0.982 | 0.991 | 0.897 | | | | | |
| La | 0.964 | 0.966 | 0.980 | 0.881 | 0.986 | | | | |
| Sm | 0.981 | 0.986 | 0.968 | 0.933 | 0.982 | 0.975 | | | |
| Ta | 0.948 | 0.968 | 0.968 | 0.854 | 0.973 | 0.971 | 0.972 | | |
| Th | 0.950 | 0.927 | 0.972 | 0.844 | 0.968 | 0.962 | 0.945 | 0.961 | |
| U | 0.914 | 0.878 | 0.903 | 0.848 | 0.913 | 0.915 | 0.899 | 0.893 | 0.948 |

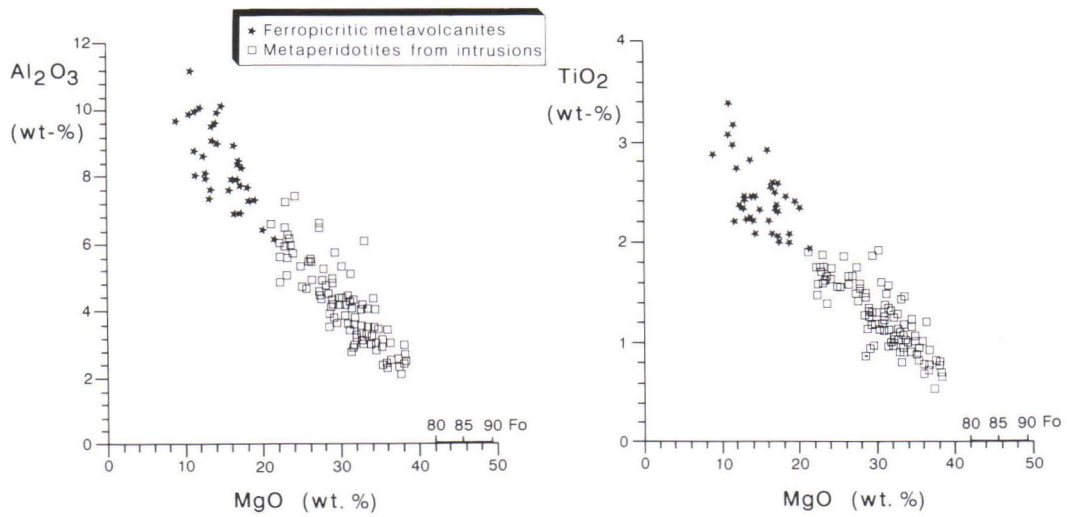


Fig. 57. $Al_2O_3$ and $TiO_2$ against MgO for metaperidotites from gabbro-wehrlite intrusions and ferropicritic metavolcanites. Also shown is the compositional range of olivines with $Fo_{80-90}$.

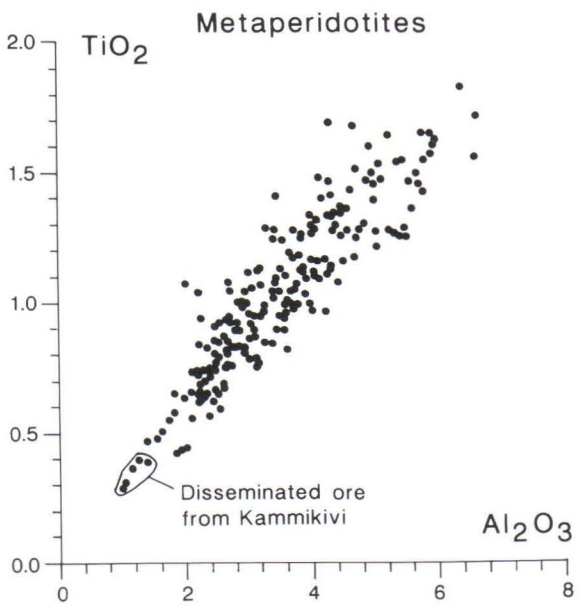


Fig. 58. $Al_2O_3$ against $TiO_2$ (wt. %) for metaperidotites from intrusions including ore-bearing varieties from the Kammikivi sill.

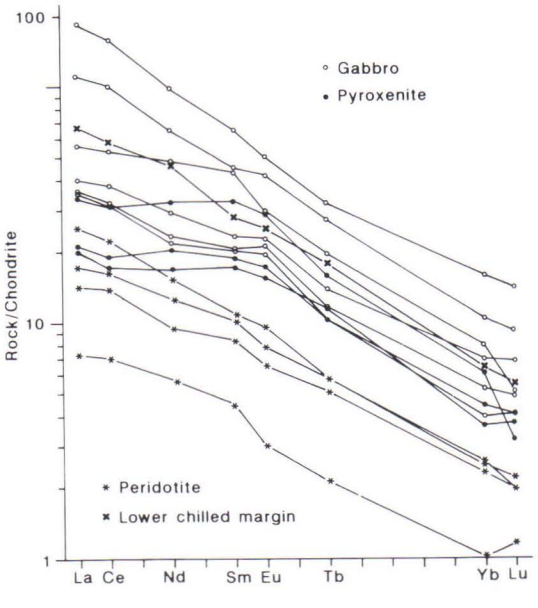


Fig. 59. Chondrite-normalized REE profiles for various rock types from gabbro-wehrlite intrusions.

bodies. The behavior of different components in the Pilgujärvi section reflects well the crystallization of the cumulus phases (cf. Fig. 23). Alkalies and silica are strongly enriched in the last differentiates close to the roof. Iron enrichment in the residual magma was prevented by the early appearance of titanomagnetite as a cumulus phase. In this respect, the differentiation of the Pilgujärvi intrusion is more akin to the evolution of a calc-alkaline magma than a tholeiitic magma. However, the general features of the ferropicritic magma do not favor its classification as calc-alkaline. Sulfur is concentrated in the lower part of the intrusion but it is noteworthy that relatively sulfur-rich levels are also present in the middle or upper part of the intrusion.

The cross section of the Kammikivi sill in core Pet1 is not complete, for the core begins from the gabbroic part (Fig. 28). Nevertheless, the texture of this part of the sill, indicating a high cooling rate, suggests that the upper contact was not far from the place where drilling was started. The general pattern of variation of the components is reminiscent of what is observed in thick layered lava flows and differs from the pattern of the Pilgujärvi intrusion. This is not surprising in view of the diverse sizes and conditions of crystallization within these two bodies. The Kammikivi sill is dominated by ultramafic rocks which attain their highest MgO content in the middle part of the section. The low CaO content and $CaO/Al_2O_3$ value in cumulates of the lower half of the Kammikivi body are obvious signs of marked CaO loss. Also the extremely low alkali contents in ultramafic rocks indicate a significant migration of alkalies out of the sill. Despite the serpentinization processes and the loss of the above mentioned components, the immobile elements that are incompatible with the olivine lattice or are not captured by the sulfide liquid have retained their mutual relations unchanged. As shown in Table 16, they display highly significant correlation coefficients with each other in 26 analyses from the Pet1 drill core. The phenomenon is reflected in Fig. 28 by the similarity of the curves of $TiO_2$ and Sm.

Sulfides are concentrated at the bottom of the sill, forming a layer with a rather sharp upper boundary. Sulfur contents reach values of about 16% and the maximum nickel and copper contents are about 5 wt. %. As was noted in the case of the Pilgujärvi intrusion, sulfur abundances may also attain significant levels higher up in the section.

## Parental magma of ferropicritic rocks

One of the most important goals of igneous petrology is to elucidate problems of mantle composition and evolution as well as magma genesis. For this purpose, it is essential to recognize which of the primitive volcanic rocks are primary, mantle-derived magmas that have not been modified by crystal fractionation or other processes after their segregation from the mantle source. An important step in this direction is to identify the parental magma composition of a given rock suite and to evaluate whether it is representative of a primary magma.

The ferropicritic liquid composition can be estimated using several different approaches. Direct measurements can be made on pillow and massive lavas, spinifex-textured rocks, and chilled margin samples from layered lava flows and intrusions. A hypothetical liquid composition can be obtained by calculating weighted average compositions of lava flows and intrusions. Each of these methods has disadvantages. The presence of olivine phenocrysts in pillow lavas and massive lavas could cause an overestimation of the MgO content and an underestimation of the contents of olivine-incompatible elements. Intratelluric olivine phenocrysts may be also present in chilled margin samples. Alteration by seawater or metamorphism may produce complications in the

Table 17. Lower chilled margin and weighted average compositions of gabbro-wehrlite intrusions (calculated to 100 % on an anhydrous basis, $Fe^{2+}$ and $Fe^{3+}$ adjusted as $Fe^{2+}=0.9Fe_{tot}$).

| | 1 | 2 | 3 | 4 | 5 | 6 | 7 | 8 | 9 |
|---|---|---|---|---|---|---|---|---|---|
| $SiO_2$ | 45.07 | 41.69 | 44.26 | 44.69 | 45.04 | 44.84 | 43.73 | 43.25 | 44.36 |
| $TiO_2$ | 2.05 | 2.70 | 2.85 | 1.95 | 2.07 | 3.08 | 1.88 | 1.43 | 2.04 |
| $Al_2O_3$ | 7.50 | 10.26 | 9.56 | 6.48 | 7.19 | 10.23 | 6.53 | 6.72 | 6.87 |
| $Fe_2O_3$ | 1.85 | 1.92 | 1.66 | 1.94 | 1.86 | 1.86 | 1.97 | 1.77 | 1.90 |
| FeO | 15.00 | 15.53 | 13.44 | 15.69 | 15.07 | 15.02 | 15.92 | 14.33 | 15.41 |
| MnO | 0.21 | 0.29 | 0.25 | 0.18 | 0.23 | 0.27 | 0.23 | 0.15 | 0.20 |
| MgO | 17.75 | 16.98 | 18.79 | 19.40 | 18.63 | 13.01 | 21.06 | 22.97 | 20.62 |
| CaO | 9.13 | 9.28 | 8.32 | 8.62 | 8.94 | 8.23 | 6.84 | 7.51 | 6.92 |
| $Na_2O$ | 0.71 | 0.55 | 0.19 | 0.17 | 0.27 | 2.19 | 0.96 | 1.34 | 0.92 |
| $K_2O$ | 0.06 | 0.09 | 0.05 | 0.02 | 0.09 | 0.79 | 0.45 | 0.23 | 0.39 |
| $P_2O_5$ | 0.20 | 0.26 | 0.29 | 0.19 | 0.19 | 0.21 | n.a. | 0.03 | n.a. |
| $Cr_2O_3$ | 0.26 | 0.26 | 0.24 | 0.41 | 0.28 | 0.16 | 0.27 | 0.26 | 0.22 |
| NiO | 0.21 | 0.18 | 0.09 | 0.25 | 0.15 | 0.10 | 0.17 | n.a. | 0.15 |
| Mg # | 0.679 | 0.661 | 0.714 | 0.688 | 0.688 | 0.607 | 0.702 | 0.741 | 0.705 |
| Fo(0.30) | 87.6 | 86.7 | 89.3 | 88.0 | 88.0 | 83.7 | 88.7 | 90.5 | 88.8 |
| Fo(0.33) | 86.5 | 85.5 | 88.3 | 87.0 | 87.0 | 82.4 | 87.7 | 89.7 | 87.8 |

n.a. = not analysed.
Mg # is atomic $Mg/(Mg+Fe^{2+})$, Fo(0.30) and Fo(0.33) are calculated equilibrium olivine compositions obtained using $K_D$ values 0.30 and 0.33, respectively.
**1**, pyroxenite from lower marginal zone, Pilgujärvi intrusion, sample SA-49 (Smolkin, 1977); **2**, pyroxenite from lower marginal zone, Pilgujärvi intrusion, sample SA-48 (Smolkin, 1977); **3**, pyroxenite from lower marginal zone, Northern Kotselvaara intrusion, sample SA-243 (Smolkin, 1991); **4**, pyroxenite from lower marginal zone, Northern Kotselvaara intrusion, sample SA-245 (Smolkin, 1991); **5**, average of 23 lower chilled zone samples from the Kaula, Kotselvaara, Mirona, Kierdzhipori, Raisoaivi, Pilgujärvi, Lammas and Onki intrusions (Smolkin, 1991); **6**, weighted average composition of the Pilgujärvi intrusion (Smolkin, 1977); **7**, weighted average composition of the Pechenga intrusions (Zhangurov and Predovskii, 1974); **8**, weighted average composition of the Pechenga intrusions (Smolkin, 1974); **9**, weighted average composition of the Pechenga intrusions (Rabinovich, 1978).

interpretation of rock compositions. This is particularly true for chilled margin samples which may have reacted with country rocks, either during emplacement or at a later, postcrystallization stage through metasomatic processes. Contact zones are apt to deform as shear zones during tectonic movements and serve as channels for metasomatic fluids. Owing to these processes, lower chilled margins of many intrusions at Pechenga are not preserved or do not correspond chemically to the primary composition of the rock. When calculating a weighted average composition, the proportions of each rock type should be known and therefore drill cores should provide the best material. Even if a representative section were available in this respect, there is still some uncertainty in how closely the calculated composition would match the liquid composition. This stems from the fact that during emplacement, the magma may have carried an extra component of olivine phenocrysts or the flow or the intrusion may have not behaved as a closed system but as a channel through which magma flowed and continuously precipitated olivine crystals and, in some cases, segregated sulfide droplets. For example, the section along core Pet1 across the Kammikivi layered sill (excluding the ore zone) shows a weighted average MgO content of 26.6% which is excessive when compared with the most likely ferropicritic parental liquid composition.

Table 18. Compositions of selected rock types and weighted averages of layered ferropicritic flows (calculated to 100 % on an anhydrous basis, $Fe^{2+}$ and $Fe^{3+}$ adjusted as $Fe^{2+}=0.9Fe_{tot}$).

| | 1 | 2 | 3 | 4 | 5 | 6 | 7 | 8 |
|---|---|---|---|---|---|---|---|---|
| $SiO_2$ | 47.44 | 46.45 | 48.83 | 49.81 | 46.03 | 46.45 | 46.94 | 44.93 |
| $TiO_2$ | 2.21 | 2.29 | 2.86 | 3.35 | 2.27 | 2.29 | 1.98 | 2.31 |
| $Al_2O_3$ | 9.58 | 10.14 | 9.68 | 12.18 | 7.69 | 10.14 | 8.19 | 6.39 |
| $Fe_2O_3$ | 1.57 | 1.72 | 1.64 | 1.78 | 1.67 | 1.72 | 1.67 | 1.75 |
| FeO | 12.69 | 13.91 | 13.31 | 14.40 | 13.51 | 13.91 | 13.53 | 14.15 |
| MnO | 0.19 | 0.20 | 0.19 | 0.19 | 0.21 | 0.20 | 0.19 | 0.20 |
| MgO | 13.98 | 14.80 | 9.04 | 5.89 | 17.42 | 14.80 | 17.35 | 19.90 |
| CaO | 10.19 | 8.62 | 11.40 | 9.35 | 10.52 | 8.62 | 8.48 | 9.47 |
| $Na_2O$ | 0.80 | 0.40 | 2.61 | 2.65 | 0.17 | 0.40 | 1.06 | 0.40 |
| $K_2O$ | 0.93 | 1.03 | 0.09 | 0.13 | 0.07 | 1.03 | 0.08 | 0.07 |
| $P_2O_5$ | 0.21 | 0.21 | 0.29 | 0.26 | 0.24 | 0.21 | 0.22 | 0.22 |
| $Cr_2O_3$ | 0.15 | 0.16 | 0.07 | 0.00 | 0.10 | 0.16 | 0.21 | 0.10 |
| NiO | 0.08 | 0.08 | 0.00 | 0.01 | 0.10 | 0.08 | 0.11 | 0.11 |
| Mg # | 0.663 | 0.655 | 0.548 | 0.422 | 0.697 | 0.655 | 0.696 | 0.715 |
| Fo(0.30) | 86.7 | 86.3 | 80.1 | 70.8 | 88.5 | 86.3 | 88.4 | 89.3 |
| Fo(0.33 | 85.6 | 85.2 | 78.6 | 68.8 | 87.4 | 85.2 | 87.4 | 88.4 |

**Mg # is atomic $Mg/(Mg+Fe^{2+})$, Fo(0.30) and Fo(0.33) are calculated equilibrium olivine compositions obtained using $K_D$ values 0.30 and 0.33, respectively.**
**Rock types and samples:**
**1-2, randomly oriented olivine spinifex-textured rock, S-VI/410.0, S-VI/412.7, Shuljärvi; 3, pyroxene spinifex-textured rock, S-3R/731.4, Kaula; 4, Parallel olivine spinifex-textured rock, S-2986-A, Kierdzhipori; 5, average of 4 lower chilled margin samples (Sharkov and Smolkin, 1989); 6, weighted average composition of the Shuljärvi flow; 7, weighted average composition of the Kierdzhipori flow; 8, weighted average composition of the Lammas flow (Sharkov and Smolkin, 1989).**

In spite of the uncertainties considered above, some constraints can be placed on the ferropicritic liquid composition. Table 17 lists measured chilled margin compositions and calculated weighted average compositions of intrusions reported previously in the literature. They have been normalized to 100% on a volatile-free basis assuming $Fe^{2+}/(Fe^{2+}+Fe^{3+})=0.9$. Also shown are Mg numbers $[Mg/(Mg+Fe^{2+})]$ and equilibrium olivine compositions calculated by using the olivine-liquid equilibria (Roeder and Emslie, 1970). Two sets of olivine compositions are listed based on the Fe-Mg exchange coefficients ($K_D$) of 0.30 and 0.33, respectively. Table 18 shows similarly processed data for spinifex-textured samples, chill zone samples, and weighted averages of layered lava flows.

If the Kammikivi sill is excluded, the MgO content in the weighted average compositions of intrusions varies between 14.6-23.0% while the range for the lower chill zone samples is between 13.5-20.0%. One analysis of the upper chill zone from the Pilgujärvi intrusion is available, and shows an MgO content of 14.3%. The analyses of the lower chill zone of layered lava flows and their weighted average compositions have a relatively restricted variation in MgO between 17.0-19.9% (Table 18). One upper chill sample from the Kierdzhipori flow was analysed in this study (Table 12, anal. 10). This rock contains many cal-

cite-pyrrhotite filled amygdules and therefore its composition may not be truly representative of the liquid. The MgO content is 11.6% in the analysis normalized to 100% on an anhydrous basis. The most magnesian rock with a randomly oriented olivine spinifex texture contains 14.8% MgO.

The forsterite contents of olivines calculated from the lower chilled margin analyses and weighted average compositions are in most cases higher (up to 90.6%) than that of the most magnesian olivine (Fo 84.2%) so far encountered at Pechenga. The reason for this may be that the most magnesian olivine has not yet been discovered in the region. However, the analyses of peridotites plotted in Fig. 57 suggest that a more probable reason for the discrepancy is an overestimate of MgO in the analyses due to the effect of intratelluric olivine grains which were suspended in the magma during the emplacement of the magma. Petrographical evidence shows that the modal olivine content increases rapidly upwards from the few millimeter or centimeter wide aphanitic chill zone, and therefore it is not always possible to avoid the accumulated olivines in sampling. Also the analysis from the lower chill sample from a layered flow in Table 18 indicates a relatively large forsterite content between 87.4-88.4% depending on the $K_D$. The randomly oriented olivine spinifex samples also indicate an olivine composition slightly more magnesian than $Fo_{84.2}$.

The accurate estimation of the MgO content of a liquid in equilibrium with $Fo_{84.2}$ depends on several factors. One of these is the assumption of the oxidation state of iron which here is taken to correspond approximately to the FMQ buffer. Other variables which are demonstrated in Fig. 60 are the iron content of the liquid and the adopted $K_D$ value. The variable $FeO_{tot}$ content of rocks at a constant MgO content produce changes in Mg number and thus a vertical scatter for the trend in Fig. 60. Tables 17 and 18 show that rocks with an equilibrium olivine composition approaching $Fo_{84}$ may have MgO from 13.5% to 17% depending on the iron content of the rock. The lower chilled margin analyses from intrusions tend to have somewhat higher $FeO_{tot}$ contents than, for

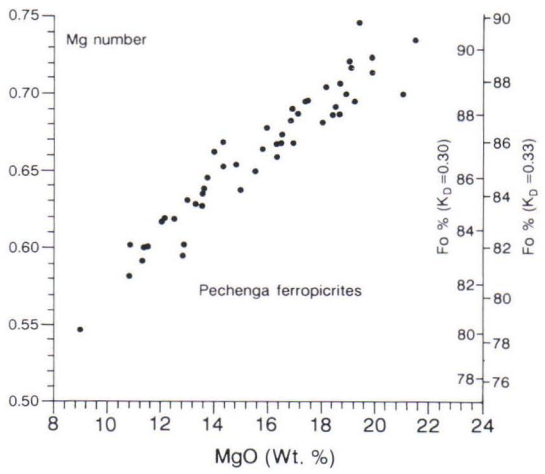


Fig. 60. MgO (wt. %) of ferropicritic rocks plotted against Mg number [atomic Mg/(Mg+Fe)] of the same rocks and calculated equilibrium olivine composition using $K_D$ values of 0.30 and 0.33.

example, pillow lavas or massive lavas. This results in a higher MgO content for a liquid in equilibrium with a given olivine composition for estimates based on chilled margin samples. Changing $K_D$ from 0.30 to 0.33 causes a difference of about 1.5% in the MgO content of the equilibrium liquid or about 1% in the Fo content of the equilibrium olivine (Fig. 60).

On the basis of the analyses in Tables 17 and 18, it can be inferred that the minimum MgO of the parental ferropicritic magma was about 15% MgO. The most reliable evidence in terms of direct measurement is provided by the analysis of an olivine spinifex sample with 14.8% MgO. Markedly higher MgO values observed in some weighted average analyses or analyses of lower chilled margins are probably a consequence of an extra olivine component. The figure of 15% MgO agrees well with analyses of ferropicritic pillow lavas, massive lavas, and tuffs (Tables 10 and 11). The observed complete gradation of textures from olivine porphyritic to randomly oriented olivine spinifex without any appreciable change in the bulk composition of the rock suggests that most pillow and massive lavas closely approach the

composition of the ferropicritic parental magma (cf. Figures 4, 5, and 9).

An accurate estimation of the original $CaO/Al_2O_3$ value of the ferropicritic magma is not easy to obtain because of the mobile character of CaO. The general alteration trend has been loss of CaO during serpentinization, amphibolization, and albitization. Nevertheless, on the basis of the high modal abundance of Ca-rich pyroxene in almost all rock types, the weighted average compositions of intrusions and layered flows, and analyses of the best-preserved metavolcanites, it can be concluded that $CaO/Al_2O_3$ is higher than 1 in the parental ferropicritic magma. Because of its relatively high $TiO_2$ and low $Al_2O_3$ content, the ferropicritic magma possesses a low $Al_2O_3/TiO_2$ value, falling between 3-4. This ratio can be used as a fingerprint for olivine cumulates formed by ferropicrite magmas, to distinguish them from those derived from komatiitic liquids.

It is not possible to directly measure the $Na_2O$ and $K_2O$ contents of the parental ferropicritic magma because, as was deduced earlier, the ubiquitously low levels of alkalies in ultramafic ferropicrites are an artifact of postmagmatic alteration processes. The same is true for other mobile alkali and alkali earth elements such as Rb, Cs, Ba, and Sr. The presence of alkalies in the parental magma is demonstrated by the crystallization of kaersutitic amphibole and phlogopitic mica both in intrusive and extrusive ferropicritic rocks. A rough indirect estimation of alkali contents can be made utilizing the best-preserved olivine cumulates from intrusions that still contain abundant brown interstitial mica and amphibole. These rocks have $K_2O/Al_2O_3$ and $Na_2O/Al_2O_3$ values of about 0.05-0.1 and 0.04-0.06, respectively. Given an $Al_2O_3$ content of 7-8%, these ratios yield values of 0.8% for $K_2O$ and 0.5% for $Na_2O$. Bearing in mind the tendency of ultramafic rocks to lose alkalies during alteration processes, the above mentioned figures probably represent the minimum alkali content of the parental magma.

Iron enrichment in a basic to ultrabasic volcanic rock can be caused by the abundance of olivine phenocrysts in a liquid with a more normal iron content. Alternatively, if it can be shown that the high iron content of a basalt is not a result of the presence of intratelluric olivines but is a real feature of the liquid, there are several explanations for the origin of high FeO. Given a mantle source peridotite with a normal Fe-Mg ratio, a basalt produced by partial melting of this source may assimilate some iron-rich rock like BIF en route to or at the surface and thereby acquire an iron-rich composition. Fractional crystallization of low-Fe phases including clinopyroxene and plagioclase is an effective means of raising the iron content of the residual liquid but this option can be discarded because olivine was the liquidus phase in ferropicrites during eruption. Also olivine fractionation at high temperatures results in iron enrichment in the residual liquid. Of course, the high iron content may also be a primary feature of the parental magma attributable either to the mantle source composition or conditions of partial melting.

In Fig. 61, ferropicritic rock compositions in cation mole proportions are plotted together with calculated olivine fractionation curves on an FeO vs. MgO diagram. Ninety per cent of the total Fe is assumed to be ferrous iron in the ferropicritic analyses in this diagram. The olivine fractionation curves were computed by subtracting small increments of the equilibrium olivine from the various model melt compositions. At each point on the fractionation curves, the composition of olivine coexisting with the melt is obtained from the intercept of the tangent of the curve and the olivine compositional line on the right side of the diagram. Also shown are lines with constant MgO/FeO, the uppermost of which was computed using a $K_D$ value of 0.31. This line represents liquids that are in equilibrium with the most magnesian olivine encountered in the Pechenga area and therefore tangents of the olivine fractionation curves along this line project to $Fo_{84.2}$. Because this value is the minimum forsterite content of olivine in equilibrium with the parental ferropicritic liquid, all potential parental magma compositions should locate to the right of this line. As is evident from Fig. 61, this fact confines the MgO content of the parental magma to a value higher

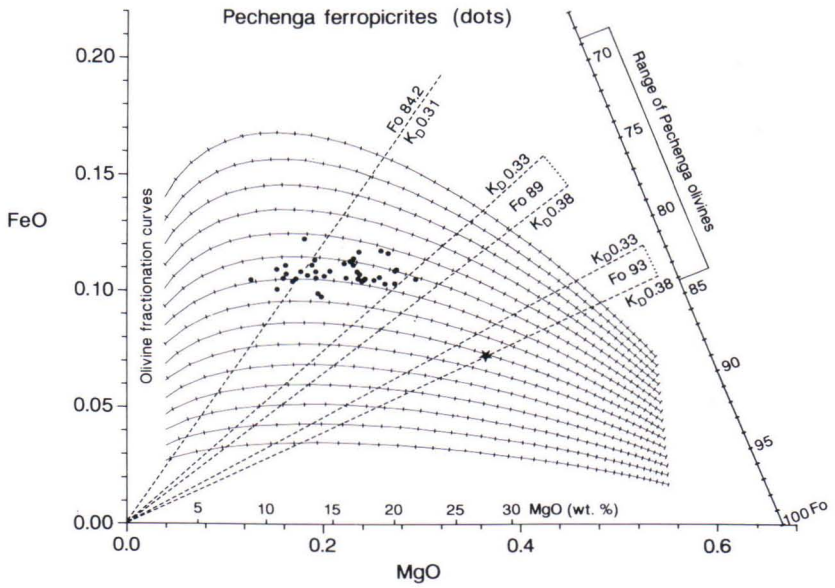


Fig. 61. FeO against MgO in cation mole proportions for ferropicritic rocks (dots) and the parental magma of the Alexo komatiites (star) (Arndt, 1986b). FeO is assumed to be $0.9 \times FeO_{tot}$. Also shown are olivine fractionation paths for various magma compositions calculated employing a $K_D$ value of 0.31. Each tick represents 5% fractionation with respect to the previous tick. Dashed lines indicate FeO/MgO values of liquids in equilibrium with a given olivine composition for given $K_D$ (Tangents of olivine fractionation curves along these lines project to given olivine composition).

than 13%. As was pointed out previously, using a higher $K_D$ value would shift the line to the right and result in a higher MgO content for the liquid.

Figure 61 demonstrates that it is in principle possible to achieve a ferropicritic composition by mixing a low MgO liquid and its equilibrium olivines. The high iron content of, for example, spinifex textured ferropicrites negates such a process as a general mechanism for producing iron-rich picrites at Pechenga. The $K_d$ of iron oxide between olivine and basic to ultrabasic liquid is lower than unity at high temperatures (higher than about 1300°C at 1 atm, Roeder and Emslie, 1970) thus making olivine fractionation a potential factor for iron enrichment. From Fig. 61, it can be seen that if the high FeO content of the ferropicritic magma was the result of olivine fractionation, a very extensive fractionation process would be required. For example, an increase in FeO content from 10 to 14 wt. % is equivalent to a decrease in MgO content from higher than 32 to 15 wt. %. The high nickel content of ferropicrites is not consistent with such a fractionation scenario.

There is no evidence for contamination of the ferropicritic magma by any iron-rich material. If the iron enrichment is a result of assimilation of some iron-rich rock, the contaminant should have had an $FeO_{tot}$ content much higher than that observed in ferropicrites, but such rocks, such as for example iron formations, are absent from the Pechenga sequence. In general, the geochemistry of ferropicrites including low $Al_2O_3/TiO_2$, Al/V, high HFSE/REE, and HFSE/Th compared with crustal rocks does not permit extensive amounts of assimilation of common sialic crustal rocks.

Furthermore, the relatively uniform composition of ferropicrites in an area extending at least 250 km from Pechenga to Imandra Varzuga (Hanski and Smolkin, 1989) renders random crustal contamination processes unlikely as a mechanism for producing such consistently iron-rich picritic compositions.

From the above considerations, it can be concluded that the high iron content is an intrinsic feature of the ferropicritic parental liquid and therefore mantle processes must be invoked to explain it. This question will be addressed further in the last part of this study.

Several criteria have been utilized in the identification of primary magmas (e.g., Frey et al., 1978). One widely adopted criterion employs the comparison of Mg numbers of presumed primary liquid compositions and liquids in equilibrium with Group I spinel peridotite xenoliths. The latter are estimated using Fe-Mg liquid-residual olivine partitioning data. The Mg number in olivines from spinel peridotites generally ranges between 0.88 and 0.92 (Arai, 1987). Using a $K_D$ value of 0.33 which is appropriate under upper mantle conditions (Takahashi and Kushiro, 1983), a basaltic liquid derived from the least refractory peridotite should have an Mg number of about 0.71. Liquids with Mg numbers clearly less than this are generally interpreted as derivatives from more primitive magmas mainly through (polybaric) olivine fractionation (e.g., O'Hara, 1968; Frey et al., 1978).

Figure 60 shows that the MgO content of a ferropicritic magma should be higher than 18 wt. % to satisfy the above mentioned criterion for a primary magma. Ferropicrites with an MgO content about 15 wt. % possess Mg numbers less than 0.68. A standard interpretation would be that these rocks represent fractionated liquids that are no longer in equilibrium with mantle olivines. This is, however, in conflict with the high MgO content of ferropicrites. A preferred interpretation is, as will be discussed in more detail later, that the source of ferropicrites was more iron-rich than normally inferred from upper mantle xenoliths.

The other criterion for identifying primary magmas is the high concentration of compatible elements, particularly nickel. Because of olivine's high mineral/liquid partition coefficient for nickel, this element is a sensitive indicator of olivine fractionation and can be used to identify magmas that have undergone very little or no olivine removal. For example, Frey et al. (1978) noted that basalts having more than 320 ppm Ni also fulfill other criteria for primary partial melts of peridotites. Figure 55 demonstrates that ferropicritic rocks with MgO around 15% commonly have nickel contents above this level. On the other hand, ferropicritic rocks with MgO less than 10%, including pyroxene spinifex-textured rocks, show Ni abundances commonly less than 200 ppm. This implies that olivine fractionation has taken place to reduce the nickel content of the liquid, and hence, the parental magma had an MgO content higher than 10%.

## Pechenga ferropicrites compared with other primitive magmas

Hanski and Smolkin (1989) performed a comparative study of high-magnesian, nonkomatiitic metavolcanites in the Kola Peninsula and concluded that analogous rocks to those of the Pechenga ferropicrites are found in the Tominga suite in the Imandra-Varzuga greenstone belt. Picrites from the Umba and Panarechka Suites in the Imandra-Varzuga belt, minor picrites from the Kuetsjärvi Suite in the Pechenga area, and picrites from the South Pechenga Series differ from ferropicrites in being slightly lower in $FeO_{tot}$ (commonly 12-14%), $TiO_2$, and presumably other incompatible trace elements. They most closely resemble Suisaarian picrites from the Onega region in southern Karelia (Russia).

In the following discussion, the Pechenga fer-

ropicrites are compared with primitive magmas outside the Kola Peninsula mostly using geochemical data collected from the literature. Figure 62 shows a MgO vs. $FeO_{tot}$ plot for nonkomatiitic primitive magma compositions while Fig. 63 presents the same diagram for compositions which have been classified as belonging to a komatiite suite. $FeO_{tot}$ is the total iron content expressed as FeO in the analysis which is calculated to 100% on a volatile-free basis. As was shown in Fig. 61, olivine fractionation does not have a dramatic influence on the iron content of liquid. Therefore, reasonable conclusions can be drawn from a comparison of the iron contents of rocks having widely varying MgO contents, as is the case with data in Figures 62 and 63.

Nonkomatiitic primitive magmas display a rather wide range in $FeO_{tot}$ which in some cases may even reach values close to 20% (Fig. 62). In most cases, however, the total iron oxide content falls below 14%, which was regarded by Hanski and Smolkin (1989) as the lowest level for a typical ferropicritic composition. In komatiitic metavolcanites, $FeO_{tot}$ is mostly around 11-12% but, as discussed below, some high-iron varieties have also been reported in the literature. Thus, iron-rich magnesian volcanic rocks like those occurring in the Pechenga area represent only a minority among the primitive volcanic rocks on earth, but their occurrence is not restricted to the Pechenga area. Representative analyses of iron-rich volcanic rocks from outside the Pechenga area are listed in Table 19. In order to evaluate how well the iron-rich samples in Figures 62 and 63 represent the corresponding rock types, histograms were constructed for those magma suites which contain iron-rich members with $FeO_{tot}$ in excess of 14% (Fig. 64).

Although the $FeO_{tot}$ content in alkaline lavas is commonly less than 14%, nepheline melilitites (Fig. 64A) and basanites (Fig. 64C) contain high abundances of iron in some areas, for example in Hawaii (Clague and Dalrymple, 1988). This is compatible with the suggestion that the mantle source of Hawaiian volcanites is relatively iron-rich (Wilkinson, 1985). The $FeO_{tot}$ contents of olivine nephelinites range from 10.0 to 16.3% (Fig. 64B). According to Le Bas (1987), the world average is 12.8%. As shown in Fig. 64B, several iron-rich nephelinites have been reported in the literature from, for example, Australia (Frey et al., 1978) and Canada (Francis & Ludden, 1990).

Meimechites and related high-Mg volcanic rocks form an early Mesozoic, primitive, alkaline rock suite in the Maymecha-Kotuy Province in northern Siberia (Gladkikh et al., 1987). According to Sobolev et al. (1991), meimechites or al-

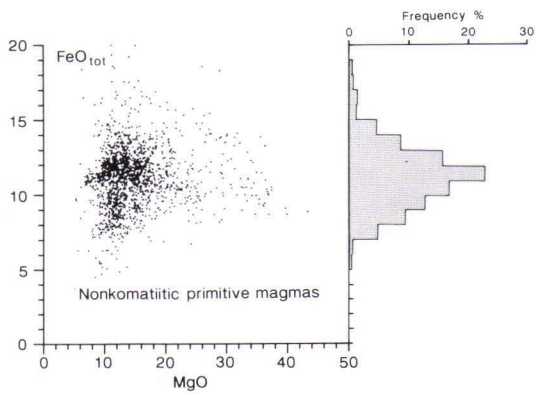


Fig. 62. MgO and $FeO_{tot}$ contents (wt. %) of nonkomatiitic primitive magmas from the literature.

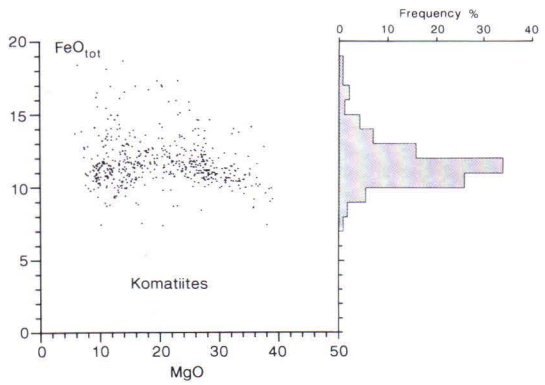


Fig. 63. MgO and $FeO_{tot}$ contents (wt. %) of komatiitic primitive magmas from the literature.

**Table 19. Iron-rich primitive magmas from the literature (major elements normalized to 100% on an anhydrous basis).**

| | 1 | 2 | 3 | 4 | 5 | 6 | 7 | 8 | 9 | 10 | 11 | 12 |
|---|---|---|---|---|---|---|---|---|---|---|---|---|
| $SiO_2$ | 39.56 | 41.14 | 43.23 | 41.32 | 40.00 | 40.60 | 40.57 | 50.84 | 44.55 | 46.89 | 39.47 | 49.80 |
| $TiO_2$ | 3.40 | 3.24 | 2.83 | 3.61 | 3.43 | 4.00 | 3.47 | 1.81 | 4.15 | 1.34 | 1.18 | 1.41 |
| $Al_2O_3$ | 10.23 | 10.29 | 11.94 | 10.32 | 9.63 | 4.20 | 5.86 | 11.88 | 9.54 | 8.83 | 10.34 | 8.61 |
| $FeO_{tot}$ | 14.59 | 14.07 | 14.16 | 14.82 | 15.50 | 15.80 | 17.59 | 14.82 | 16.03 | 14.11 | 14.89 | 14.77 |
| MnO | 0.22 | 0.20 | 0.21 | 0.19 | 0.20 | n.a. | 0.21 | 0.25 | 0.26 | 0.19 | 0.24 | 0.27 |
| MgO | 14.46 | 14.09 | 12.04 | 12.44 | 14.15 | 24.50 | 13.20 | 10.88 | 12.86 | 19.69 | 21.73 | 12.32 |
| CaO | 12.91 | 12.45 | 12.04 | 10.17 | 11.40 | 9.00 | 16.42 | 7.61 | 10.24 | 7.79 | 11.81 | 10.46 |
| $Na_2O$ | 2.58 | 2.82 | 2.78 | 3.88 | 3.04 | 0.30 | 1.16 | 1.57 | 1.37 | 0.81 | 0.18 | 2.09 |
| $K_2O$ | 1.26 | 1.07 | 0.37 | 1.74 | 1.55 | 1.10 | 0.93 | 0.17 | 0.61 | 0.22 | 0.04 | 0.18 |
| $P_2O_5$ | 0.79 | 0.64 | 0.40 | 1.53 | 1.10 | 0.50 | 0.59 | 0.15 | 0.40 | 0.13 | 0.11 | 0.13 |
| Mg # | 0.663 | 0.665 | 0.627 | 0.624 | 0.644 | 0.754 | 0.598 | 0.593 | 0.614 | 0.734 | 0.743 | 0.620 |
| Cr | 475 | 498 | 414 | 385 | 410 | n.a. | 580 | 1030 | 486.7 | n.a. | 2081 | 1065 |
| Ni | 290 | 345 | 273 | 312 | 366 | n.a. | 300 | 641 | 550 | n.a. | 1164 | 364 |
| Co | n.a. | n.a. | n.a. | 54.2 | 66 | n.a. | 72 | 62.3 | n.a. | n.a. | n.a. | 69.1 |
| Sc | n.a. | n.a. | n.a. | 12.5 | 18.7 | n.a. | 53 | 23.1 | n.a. | n.a. | n.a. | 39.1 |
| V | n.a. | n.a. | n.a. | 290 | 194 | n.a. | 210 | 267 | n.a. | n.a. | n.a. | 220 |
| Zr | 234 | 202 | 174 | 433 | 320 | n.a. | 320 | 122 | n.a. | n.a. | 57 | 130 |
| Ta | 4.3 | n.a. | n.a. | 7.4 | n.a. | n.a. | 4.8 | 0.47 | n.a. | n.a. | n.a. | 0.53 |
| Nb | 74 | 67 | 39 | 105 | 97 | n.a. | 100 | 9.7 | n.a. | n.a. | 6 | n.a. |
| Th | 5.2 | n.a. | n.a. | n.a. | 6.6 | n.a. | n.a. | 1.34 | n.a. | n.a. | n.a. | 2.25 |
| U | n.a. | n.a. | n.a. | n.a. | 2.3 | n.a. | n.a. | n.a. | n.a. | n.a. | n.a. | 0.91 |
| La | 59 | n.a. | n.a. | 72.7 | 62.2 | n.a. | 120 | 11.8 | n.a. | n.a. | n.a. | 5.55 |
| Ce | 92 | n.a. | n.a. | 139.0 | 140 | n.a. | 210 | 26.6 | n.a. | n.a. | n.a. | n.a. |
| Nd | 39 | n.a. | n.a. | 61.0 | 57.2 | n.a. | n.a. | n.a. | n.a. | n.a. | n.a. | n.a. |
| Sm | 9.9 | n.a. | n.a. | 14.85 | 11.9 | n.a. | 12 | 3.87 | n.a. | n.a. | n.a. | 3.27 |
| Eu | 2.77 | n.a. | n.a. | 4.09 | 3.9 | n.a. | 3.6 | 1.37 | n.a. | n.a. | n.a. | n.a. |
| Tb | 1.2 | n.a. | n.a. | 1.32 | 1.5 | n.a. | 1.2 | 0.57 | n.a. | n.a. | n.a. | n.a. |
| Ho | n.a. | n.a. | n.a. | 1.2 | 1.16 | n.a. | n.a. | n.a. | n.a. | n.a. | n.a. | n.a. |
| Yb | 1.4 | n.a. | n.a. | 1.8 | 1.42 | n.a. | 1.8 | 1.33 | n.a. | n.a. | n.a. | n.a. |
| Lu | 0.20 | n.a. | n.a. | 0.19 | 0.175 | n.a. | 0.36 | 0.19 | n.a. | n.a. | n.a. | 0.22 |
| Y | 24 | 24 | 20 | 30 | n.a. | n.a. | n.a. | 19.2 | n.a. | n.a. | 16 | n.a. |
| Sr | n.a. | n.a. | n.a. | 1373 | n.a. | n.a. | 1880 | 183 | n.a. | n.a. | 199 | 45 |
| Ba | n.a. | n.a. | n.a. | 446 | n.a. | n.a. | 840 | 50.4 | n.a. | n.a. | 32 | 92 |
| Rb | n.a. | n.a. | n.a. | 10 | n.a. | n.a. | 39 | 4.6 | n.a. | n.a. | 4 | 11 |

kaline komatiites, as they also called these rocks, represent the most magnesian volcanites found in Phanerozoic formations, with liquid compositions of up to 29% MgO. These really seem to comprise a distinct high-Fe rock class, since almost all analyses compiled from the literature contain a total FeO content greater than 13% with many having $FeO_{tot}$ values around 16% or even higher (Fig. 64D).

High-Fe, magnesian volcanic rocks are found in some flood basalt provinces. Figures 64E and 64F show analyses of Karoo picrites from South Africa and Deccan picrites from India. Iron-rich varietes occur in these areas (Duncan et al., 1984; Beane and Hooper, 1988), but as is evident from the histograms, they constitute only rare exceptions in these rock suites. High-iron picrites are more characteristic of the Norilsk flood basalt province in Siberia. As is evident from Fig. 64H, the $FeO_{tot}$ content of the picrites from the Norilsk area displays a wide range from less than 10% up to 16%. A closer examination reveals that there are differences between different stratigraphic units in the area. The total FeO content in picrites

Table 19. (*Continued*)

| | 13 | 14 | 15 | 16 | 17 | 18 | 19 | 20 | 21 | 22 | 23 | 24 |
|---|---|---|---|---|---|---|---|---|---|---|---|---|
| $SiO_2$ | 45.89 | 46.75 | 46.12 | 45.58 | 43.58 | 48.07 | 46.69 | 45.18 | 47.06 | 48.78 | 44.88 | 45.35 |
| $TiO_2$ | 2.66 | 1.77 | 1.01 | 0.85 | 1.52 | 1.19 | 1.09 | 1.51 | 0.96 | 1.25 | 1.74 | 1.15 |
| $Al_2O_3$ | 7.52 | 9.71 | 10.28 | 7.71 | 11.59 | 8.96 | 8.95 | 9.36 | 8.46 | 5.64 | 5.23 | 6.58 |
| $FeO_{tot}$ | 16.93 | 15.25 | 14.95 | 15.10 | 15.02 | 14.31 | 14.84 | 14.90 | 16.11 | 16.54 | 17.29 | 18.67 |
| MnO | 0.17 | 0.18 | 0.25 | 0.43 | 0.18 | 0.31 | 0.22 | 0.27 | 0.23 | 0.28 | 0.31 | 0.21 |
| MgO | 18.35 | 16.11 | 13.06 | 23.51 | 18.71 | 13.32 | 18.83 | 17.48 | 13.41 | 14.22 | 19.67 | 14.00 |
| CaO | 7.85 | 8.77 | 12.22 | 5.79 | 8.20 | 12.36 | 9.10 | 10.54 | 11.82 | 13.21 | 9.84 | 13.17 |
| $Na_2O$ | 0.13 | 1.07 | 1.98 | 0.82 | 0.95 | 1.12 | n.a. | 0.63 | 1.62 | n.a. | 0.34 | 0.56 |
| $K_2O$ | 0.12 | 0.21 | 0.08 | 0.14 | 0.12 | 0.21 | 0.04 | 0.12 | 0.14 | n.a. | 0.51 | 0.22 |
| $P_2O_5$ | 0.39 | 0.18 | 0.06 | 0.06 | 0.14 | 0.16 | 0.22 | n.a. | 0.18 | 0.08 | 0.18 | 0.09 |
| Mg # | 0.682 | 0.677 | 0.634 | 0.755 | 0.712 | 0.648 | 0.715 | 0.699 | 0.622 | 0.630 | 0.693 | 0.598 |
| Cr | n.a. | 1120 | 1130 | 2090 | n.a. | 1750 | 1982 | 2254 | n.a. | 389 | 1820 | 1270 |
| Ni | n.a. | 573 | 315 | 1060 | n.a. | 751 | 1241 | 1141 | n.a. | 736 | 1200 | 1100 |
| Co | n.a. | 84.6 | 75.7 | 72.6 | n.a. | 136 | n.a. | 94 | n.a. | 105 | 110 | 90 |
| Sc | n.a. | 40.6 | 53.2 | 30.4 | n.a. | n.a. | n.a. | n.a. | n.a. | n.a. | n.a. | n.a. |
| V | n.a. | 310 | 320 | 200 | n.a. | 278 | 200 | 264 | n.a. | 277 | 190 | 180 |
| Zr | n.a. | 130 | 60 | 50 | n.a. | 67 | 84 | 86 | n.a. | 29 | 70 | 20 |
| Ta | n.a. | 1.38 | 0.124 | .174 | n.a. | 0.25 | 5 | 5 | n.a. | n.a. | n.a. | n.a. |
| Nn | n.a. | n.a. | n.a. | n.a. | n.a. | n.a. | n.a. | n.a. | n.a. | n.a. | 20 | 20 |
| Th | n.a. | 1.77 | 0.158 | .268 | n.a. | n.a. | n.a. | n.a. | n.a. | n.a. | n.a. | n.a. |
| U | n.a. | 0.48 | 0.07 | 0.15 | n.a. | n.a. | n.a. | n.a. | n.a. | n.a. | n.a. | n.a. |
| La | n.a. | 17.1 | 5.39 | 1.52 | 6.7 | n.a. | n.a. | n.a. | n.a. | n.a. | n.a. | n.a. |
| Ce | n.a. | n.a. | n.a. | n.a. | 14 | n.a. | n.a. | 13.3 | n.a. | n.a. | n.a. | n.a. |
| Nd | n.a. | n.a. | n.a. | n.a. | 11.2 | n.a. | n.a. | 11.9 | n.a. | n.a. | n.a. | n.a. |
| Sm | n.a. | 4.4 | 2.33 | 1.71 | 3.1 | n.a. | n.a. | 3.5 | n.a. | n.a. | n.a. | n.a. |
| Eu | n.a. | n.a. | n.a. | n.a. | 1.03 | n.a. | n.a. | 1.19 | n.a. | n.a. | n.a. | n.a. |
| Gd | n.a. | n.a. | n.a. | n.a. | n.a. | n.a. | n.a. | 3.9 | n.a. | n.a. | n.a. | n.a. |
| Tb | n.a. | n.a. | n.a. | n.a. | 0.31 | n.a. | n.a. | n.a. | n.a. | n.a. | n.a. | n.a. |
| Yb | n.a. | n.a. | n.a. | n.a. | 1.3 | n.a. | n.a. | 1.64 | n.a. | n.a. | n.a. | n.a. |
| Lu | n.a. | .355 | 0.239 | .311 | 0.25 | n.a. | n.a. | n.a. | n.a. | n.a. | n.a. | n.a. |
| Y | n.a. | n.a. | n.a. | n.a. | n.a. | 15 | 16 | 20 | n.a. | 4 | 10 | 10 |
| Sr | n.a. | n.a. | n.a. | n.a. | n.a. | n.a. | 33 | 37 | n.a. | 67 | n.a. | n.a. |
| Ba | n.a. | n.a. | n.a. | n.a. | n.a. | n.a. | 67 | 24 | n.a. | 40 | n.a. | n.a. |

n.a.= not analysed.
Mg # is atomic $Mg/(Mg+Fe^{2+})$ calculated assuming $Fe^{2+}=0.9*Fe_{tot}$.

**1**, Nepheline melilitite, Hawaii (Clague and Dalrymple, 1988); **2**, nephelinite, Hawaii (Clague and Dalrymple,1988); **3**, basanite, Hawaii (Clague and Dalrymple, 1988); **4**, olivine nephelinite, Yukon, Canada (Francis and Ludden, 1990); **5**, olivine nephelinite, Victoria, Australia (Frey et al., 1978); **6**, meimechite, Maymecha Kotuy, Siberia (Sobolev and Slutskii, 1984); **7**, olivine melilitite, Maymecha Kotuy, Siberia (Gladkikh, 1991); **8**, Keweenawan picrite, Ontario (Klewin and Berg, 1991); **9**, Morongovsky picrite, Norilsk, Siberia (Fedorenko and Dyuzhikov, 1981); **10**, Gudchikhinsky picrite, Norilsk, Siberia (Fedorenko and Dyuzhikov, 1981); **11**, Scecofennian picrite, Uusimaa, Finland (Peltonen, 1990); **12**, chilled margin of dike from gabbro-wehrlite association, Kuhmo, Finland (this study); **13**, picrite from the Oskol Group, the Ukraine (Krestin and Yudina, 1988); **14**, picrite, Sattasvaara area, Finnish Lapland (this study); **15-16**, komatiitic basalt and komatiite, Sattasvaara area, Finnish Lapland (this study); **17**, komatiite, Karasjok, northern Norway (Krill et al., 1985); **18**, komatiitic basalt, Barberton Mountain Land, South Africa (Jahn et al., 1982); **19**, komatiite, Ventersdorp Group, South Africa (McIver et al., 1982); **20**, amphibolite (komatiitic basalt), Kolar Schist Belt, India (Rajamani et al., 1985); **21**, basaltic komatiite, Minnesota (Green and Schulz, 1977); **22**, basal border pyroxenite of the Boston Creek Flow, northeastern Ontario (Stone et al., 1987); **23**, average of pyroclastic komatiites of the Dismal Ashrock, northwestern Ontario (Schaefer and Morton, 1991); **24**, average of green komatiitic pyroclastics, Grassy Portage Bay area, northwestern Ontario (Schaefer and Morton, 1991).

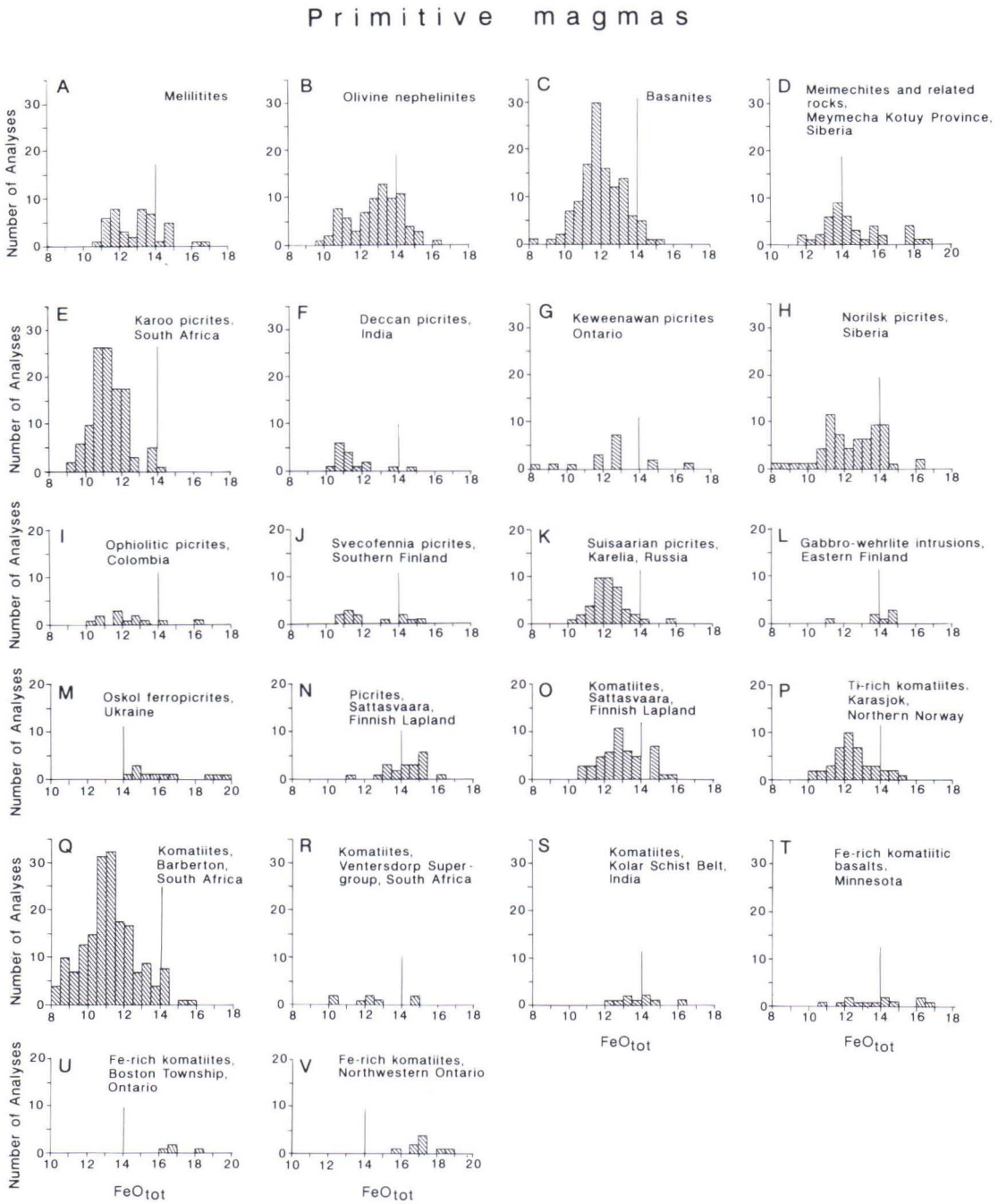


Fig. 64. Histograms of $FeO_{tot}$ (wt. %) for primitive magma suites having members with $FeO_{tot}$ higher than 14%. List of literature references available from the author.

from the Triassic Tuklonsky Suite is everywhere less than 12%, in MgO-rich volcanic rocks from the Permian Gudchikhinsky Suite commonly more than 12%, and in picrites from the Triassic Morongovsky Suite generally higher than 13% (Fedorenko, 1983). In the latter two suites, $FeO_{tot}$ exceeds 14% in many cases.

Some Fe-rich picrites have also been documented from the base of the middle Proterozoic sequence of the Keweenawan flood basalts (Fig. 64G) (Klewin and Berg, 1991). Of the three samples with $FeO_{tot}$ higher than 14% in Fig. 64G, two possess relatively low $TiO_2$ (<1%) and only one has the high $TiO_2$ (1.8%) typical of iron-rich volcanites. This feature, coupled with a rather large spread in $FeO_{tot}$, render the significance of the published Fe-rich analyses unclear.

Figure 64I presents $FeO_{tot}$ analyses of high-Ti picrites from the Romeral zone ophiolite in the southwestern Colombian Andes (Spadea et al., 1989). Some of them show elevated total iron contents but most have an $FeO_{tot}$ content less than 13.5%. The variation is too large to be explained by simple petrogenetic processes, and therefore their significance is difficult to assess.

In Fig. 64J, analyses of Svecofennian picritic metavolcanites from South Finland are displayed (Peltonen, 1990; Schreurs et al., 1986). They come from three separate areas, each of which contain iron-rich varieties as well as those with a normal iron oxide level of less than 12%. Thus, the available scarce analytical data do not reveal any consistent patterns and the iron content of these rocks needs further examination.

The Suisaarian picrites are Ludicovian (early Proterozoic) picrites in the Onega region, southern Karelia (Russia) and have commonly been correlated with the Pechenga ferropicritic rocks in stratigraphic schemes. As was mentioned previously, Hanski and Smolkin (1989) showed that these two picritic rock types have slight but significant differences in their chemical composition. This is also evident in Fig. 64K which presents data for the Suisaarian picrites. Only in some exceptional cases does $FeO_{tot}$ exceed 14%, mostly being within the range of 11.5-13.0% (e.g., Kulikov, 1988).

2.2-Ga-old gabbro-wehrlite intrusions occur widely in eastern and northern Finland as sills and dikes in Jatulian metasediments and in the underlying Archean basement. On the basis of analyses of chilled margins and incompatible element ratios of olivine cumulates, Hanski (1986) concluded that the parental magma of these intrusions is close to the Suisaarian picrite type. According to Fig. 64L, $FeO_{tot}$ in the parental magma of these intrusions is close to 14%.

Krestin and Yudina (1988) have studied early Proterozoic picritic metavolcanites from the Ukrainian Shield. These rocks are found in the Ekaterinovskaya Formation of the Oskol Group in the Tim-Yastrebovo graben-syncline. It is interesting that they occur in the upper part of a sequence comprising quartzites, carbonate rocks, carbonaceous pelitic metasediments, and picritic-tholeiitic metavolcanites, i.e., in a tectonic setting reminiscent of that of the Pechenga ferropicrites. Compositionally, the Oskol metavolcanites are real ferropicrites, for in all analyses published by Krestin and Yudina (1988), $FeO_{tot}$ exceeds 14.5% (Fig. 64M).

Over the past eigth years, a large amount of geochemical data has been collected on early Proterozoic volcanic rocks occurring in Finnish Lapland within the framework of the Lapland Volcanite Project (Lehtonen, 1989). One result is the recognition of an association of two types of ultramafic metavolcanites in the Sattasvaara area in Central Lapland, i.e., LREE-enriched, high-Ti varieties classified as picrites and LREE-depleted, low-Ti varieties classified as komatiites. The distribution of $FeO_{tot}$ in the Sattasvaara komatiites and picrites is illustrated in Figures 64N and 64O, respectively. Most of the picritic samples have an $FeO_{tot}$ content higher than 14% and high-Fe types also occur among the komatiites. Iron enrichment in the Sattasvaara komatiites appears to be coupled with enrichment in $TiO_2$, since these komatiites possess higher $TiO_2$ contents than typical Munro-type komatiites, as will be demonstrated later.

Figure 64P shows a histogram for analyses of MgO-rich metavolcanites from the Karasjok greenstone in northern Norway. This belt is a

northerly continuation of the Central Lapland greenstone belt which accounts for the similarity of the magnesian metavolcanites in the Karasjok and Sattasvaara areas. Barnes and Often (1990) called the Karasjok rocks Ti-rich komatiites. The $TiO_2$ content in these rocks is higher than in typical komatiites but it varies within wide limits. No distinction between picritic and komatiitic varieties has been applied to these rocks, and therefore, Fig 64P includes data from both types. Most commonly $FeO_{tot}$ values range between 11.5-13.0% but Fe-rich samples are also found among both relatively low-Ti and high-Ti types.

Analyses of komatiitic rocks from the classical komatiite area, the Barberton Mountain Land in South Africa are plotted in Fig. 64Q. A large spread is evident with the bulk of the analyses having $FeO_{tot}$ between 9.5-12.0%. There exists a distinct subpopulation of low-Mg komatiites with $FeO_{tot}$ clustering toward the 14% boundary. These rocks, reported by Jahn et al. (1982) and Glikson (1979), occur in the Sandspruit Formation and differ from other komatiitic metavolcanites from Barberton in being higher in $TiO_2$ at an equivalent MgO content. Limited geochemical data published by McIver et al. (1982) for younger komatiites occurring in the Ventersdorp Supergroup in South Africa is shown in Fig. 64R. The authors give two analyses of iron-rich komatiites ($FeO_{tot}$ 14.8% and 15.0%). These samples have higher $TiO_2$ than komatiites in general at an equivalent MgO level. However, their significance is unclear owing to an unexpected strong positive correlation between MgO and $FeO_{tot}$ in the rock suite while $TiO_2$ remains approximately constant (see Fig. 5.3 in McIver et al., 1982).

Evidence for the existence of Fe-rich komatiites in India is given in Rajamani et al. (1985). These rocks are situated in the Kolar schist belt and are about 2.7 Ga old. Their $FeO_{tot}$ contents range between 12-16%, but the majority of the analyses plot between 13 and 15%. These magnesian metavolcanites are not ordinary komatiites, because those rocks having high $FeO_{tot}$ (>14%) also possess abnormally high $TiO_2$ contents (1.2-1.5%). A few analyses of iron-rich komatiites have also been published by Jahn et al. (1982) from the Holenarsipur area.

So-called iron-rich basaltic komatiites have been described by Green and Schulz (1977) from the Vermilion district in Minnesota. The published analyses represent magnesian basalts and layered sills from a 2.7-Ga-old greenstone belt and amphibolites from an older gneiss terrain (3.6 Ga). These rocks form a chemically heterogenous group. As is shown in Fig. 64T, $FeO_{tot}$ varies within wide limits. This concerns all rock types: flows 10.8-16.9%, chilled margins and bulk analyses of sills 11.6-14.7%, and amphibolites 12.9-16.5%. Besides having a higher $FeO_{tot}$ content, most of the Minnesota rocks show a somewhat elevated $TiO_2$ content when compared with typical komatiitic basalts.

Further examples of rock types described as komatiites but typically possessing high iron contents are found in the Archean Abitibi greenstone belt in Ontario. Stone et al. (1987) have studied a single, thick, layered basaltic komatiite lava flow in the Boston Township area. $FeO_{tot}$ attains high values of between 16.1-18.4% in the spinifex and basal pyroxenite samples from this Boston Creek Flow (Fig. 64U). Schaefer and Morton (1991) have recently documented two occurrences of exceptionally iron-rich komatiitic pyroclastic rock units in northwestern Ontario (Fig. 64V). Both the Boston Creek Flow and the komatiite units from northwestern Ontario are also rich in $TiO_2$.

Apart from the ferropicrites described by Krestin and Yudina (1988), there are also occurrences of Fe-rich komatiites in the Ukrainian Shield. These occur in the Kosivtsevskaya greenstone belt as layered lava flows (Bobrov and Malyuk, 1991). Analyses of spinifex-textured rocks suggest that the $FeO_{tot}$ content of the parental magma was slightly higher than 14%. It is significant that, in contrast to most other so-called high-Fe komatiites, the Kosivtsevskaya komatiites are low in $TiO_2$ (<0.50%).

The above considerations attest to the fact that Fe-rich magmas have erupted on the earth's surface over a time period covering most of the earth's history, i.e., at least from the late Archean to the Quaternary. Lower Proterozoic, Fe-rich primitive magmas are wide-spread in the northern

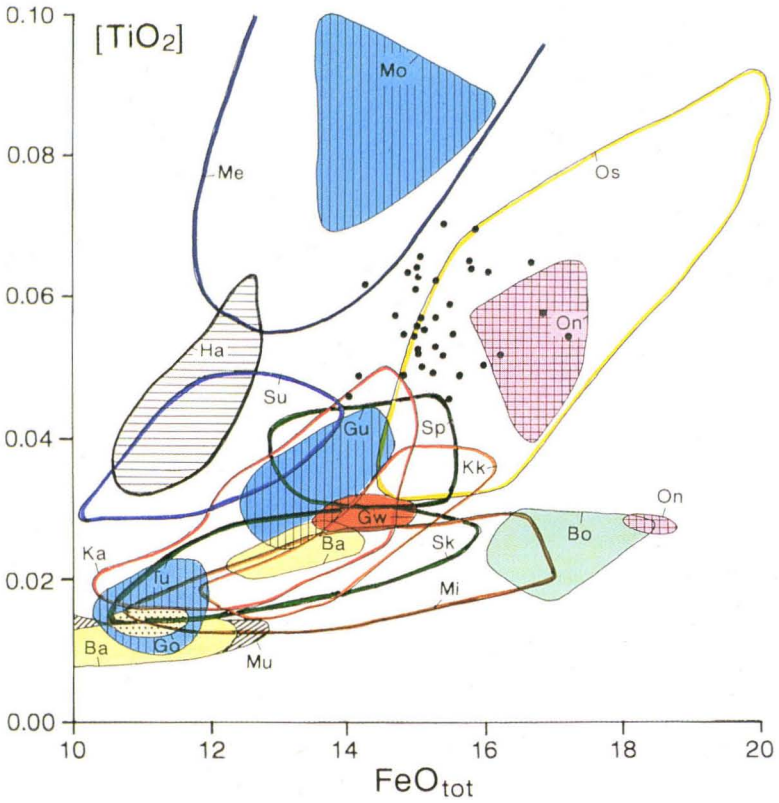


Fig. 65. [$TiO_2$] plotted against $FeO_{tot}$ (wt. %) for primitive magma suites. [$TiO_2$] is $TiO_2$ corrected for olivine fractionation and accumulation and is calculated as [$TiO_2$] = $TiO_2$/(2/3 - MgO - FeO) in mole proportions (see Appendix 1). Black dots are Pechenga ferropicrites. Fields: Ba=Barberton komatiites, Mu=Munro komatiites, Go=Gorgona komatiites, Mi=Minnesota Fe-rich basaltic komatiites, Bo=Boston Township Fe-rich basaltic komatiites, Tu=Tuklonsky picrites (Norilsk), Gu=Gudchikhinsky picrites (Norilsk), Mo=Morongovsky picrites (Norilsk), Kk=komatiites from Kolar Schist Belt (India), Ka=Karasjok komatiites (northern Norway), Gw=parental magma of gabbro-wehrlite intrusions (Finland), Sk=Sattasvaara komatiites (Finnish Lapland), Sp=Sattasvaara picrites, Su=Suisaarian picrites (Russian Karelia), Ha=Hawaiian picrites, Me=meimechites (Siberia), Os=Oskol picrites (Ukraine), On=Fe-rich komatiites from northwestern Ontario.

part of the Fennoscandian Shield and they are also found in the Ukrainian Shield. It is also evident from the rock types considered above that low silica activity is a typical feature of many Fe-rich magma suites. This is consistent with the observation that the addition of FeO contracts the primary phase field of olivine, resulting in the lowering of the silica content of a liquid at an isobaric invariant melting point (Herzberg, 1992).

In contrast to FeO, the abundance of $Al_2O_3$ and $TiO_2$ in a volcanic rock is strongly affected by olivine fractionation or the presence of phenocrystal olivine. To eliminate the effects of these processes, the $Al_2O_3$ and $TiO_2$ contents are recalculated by projecting the rock compositions from the olivine composition. This is done by comput-

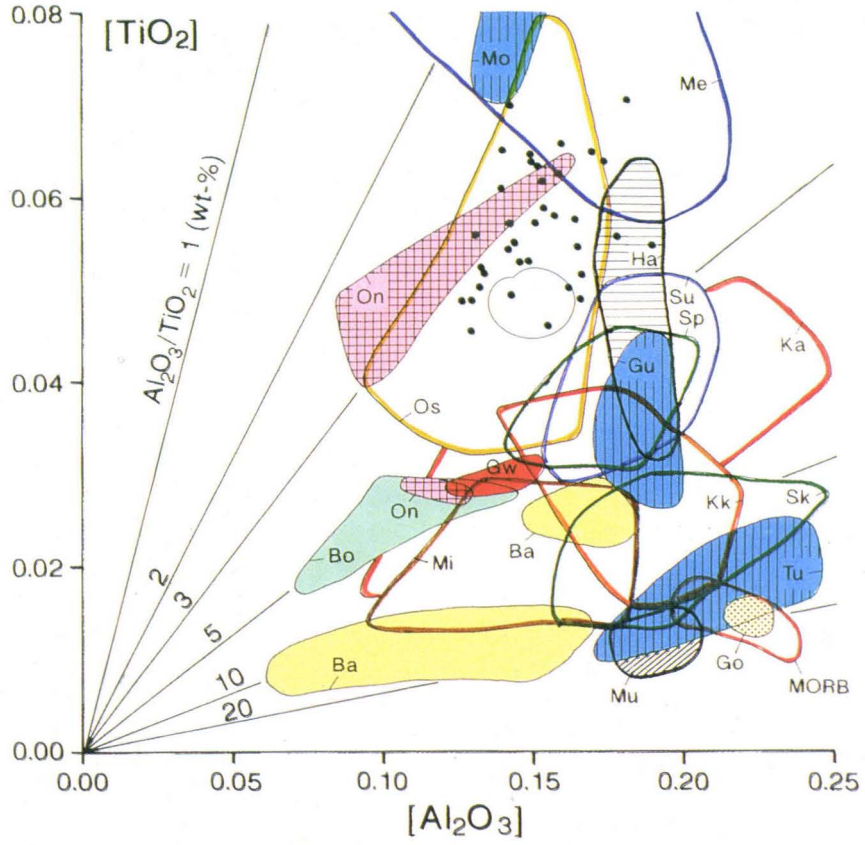


Fig. 66. $[TiO_2]$ against $[Al_2O_3]$ for primitive magma suites. $[TiO_2]$ and $[Al_2O_3]$ are $TiO_2$ and $Al_2O_3$ corrected for olivine fractionation and accumulation and are calculated as $[TiO_2] = TiO_2/(2/3 - MgO - FeO)$ and $[Al_2O_3] = Al_2O_3/(2/3 - MgO - FeO)$ (mol. prop.) (see Appendix 1). Black dots represent Pechenga ferropicrites. Abbreviations for the fields same as in Fig. 65.

ing the functions $[Al_2O_3] = Al_2O_3/(2/3 - MgO - FeO_{tot})$ and $[TiO_2] = TiO_2/(2/3 - MgO - FeO_{tot})$ in molecular proportions (see Appendix 1). For simplicity, all iron is taken as ferrous. The use of the above mentioned functions also makes the comparison of $Al_2O_3$ or $TiO_2$ between rocks with varying iron contents more meaningful than if the comparison were made by considering these components solely as a function of MgO. In Fig. 65, $[TiO_2]$ is plotted against $FeO_{tot}$ (wt. %) for various magma suites. In terms of iron and $TiO_2$ enrichment, the Pechenga ferropicrites most closely resemble some analyses of the Oskol picrites from Ukraine and the so-called Fe-rich komatiites from northwestern Ontario. A positive correlation between $[TiO_2]$ and $FeO_{tot}$ is observed in most individual rock suites. There are, however, large differences in the relations between

these components. The $TiO_2$ enrichment is weakest in the Minnesota and Boston Township komatiites, intermediate in the Pechenga ferropicrites, Oskol picrites, and komatiites from northwestern Ontario, and most pronounced in meimechites and the Morongovsky picrites from Siberia.

The relationship between $[Al_2O_3]$ and $[TiO_2]$ in various picrites and komatiites is explored in Fig. 66. This diagram permits a direct evaluation as to whether a difference in $Al_2O_3/TiO_2$ is related to a variation in the abundance of $Al_2O_3$ or that of $TiO_2$. Also it can be seen that despite similar $Al_2O_3/TiO_2$ values, the $Al_2O_3$ and $TiO_2$ contents may differ between separate magma suites. The similarity between the Oskol and Pechenga picrites and the komatiites from northwestern Ontario is again highlighted in Fig. 66. This figure also shows that even though the most Al-depleted volcanic rocks belong to the Barberton-type komatiites, many other rock types, including ferropicrites from Pechenga plot, in terms of their $[Al_2O_3]$ values, within the range of the Barberton komatiites.

As a final point, the REE chemistry of the Pechenga ferropicrites and other primitive magmas will be briefly reviewed. On the basis of the data files collected in this work (Fig. 62-63), some generalizations can be made concerning the REE, $TiO_2$, and $FeO_{tot}$ contents of primitive magmas. Many iron-rich magma suites are also enriched in LREE over HREE, but LREE-enrichment may occur in other suites without concomitant elevated iron contents. High La/Yb values and moderately high $TiO_2$ contents have been measured even in rock types low in iron such as high-Mg ultrapotassic rocks (Foley and Venturelli, 1989). Primitive magmas with low $TiO_2$ may be enriched or depleted in LREE but those with elevated $TiO_2$ contents invariably have high REE contents and sloping chondrite-normalized REE patterns. The enrichment of LREE and MREE over HREE appears to correlate more strongly with $TiO_2$ than $FeO_{tot}$, since among high-Fe rock suites, this enrichment is most pronounced in those rocks having highest $TiO_2$ contents. At the $[TiO_2]$ level of the Pechenga ferropicrites, primitive magmas generally show $(LREE/MREE)_N > 1$ and $(MREE/HREE)_N > 2.5$. With regard to the average $[TiO_2]$ of 0.057 and $(Sm/Yb)_N$ of 4.5, the Pechenga ferropicrites most closely resemble certain basanites. It should be added that REE data are lacking for the Oskol picrites and the komatiites from northwestern Ontario which in other respects mimic the Pechenga ferropicrites.

## Ore deposits

A detailed study of the geochemistry of ore deposits is beyond the scope of this paper. Only a short review is given on the salient features of the different ore types and some new data on trace chalcophile elements are presented. In their review on the geochemistry of the Pechenga Ni-Cu deposits, Zak et al. (1982) published statistical parameters, such as variation coefficients, correlations, and ratios, of the Ni and Cu distribution in various ore deposits and ore types but absolute concentrations for Cu and Ni were not given. In fact, bulk rock analyses of ore samples from Pechenga have rarely been tabulated in the literature. Table 20 shows examples of chemical data on disseminated ore from the Kammikivi deposit analysed in this study and massive and breccia ores taken from Gorbunov (1968).

According to Gorbunov et al. (1985b), the Ni concentrations in deposits hosted by metaperidotites range from 1 wt. % in low-grade disseminated ore to 6 wt. % in densely disseminated ore. Ni attains values up to 10-12 wt. % in massive and breccia ores. Mineralized phyllites contain from traces up to 2 wt. % Ni. In massive ores, the Cu content ranges from less than 1 to 13 wt. % while high-grade disseminated and breccia ores

Table 20. Whole rock analyses of disseminated (#1-3), breccia (#4-6), and massive Ni-Cu ores (#7-8).

| | 1 | 2 | 3 | 4 | 5 | 6 | 7 | 8 |
|---|---|---|---|---|---|---|---|---|
| Fe | 29.91 | 33.37 | 34.41 | 44.20 | 47.41 | 30.75 | 55.18 | 50.76 |
| S | 10.94 | 12.36 | 13.46 | 32.70 | 32.75 | 16.25 | 36.56 | 31.61 |
| Ni | 3.73 | 4.66 | 5.07 | 2.54 | 5.37 | 2.53 | 4.64 | 5.41 |
| Cu | 1.20 | 1.55 | 2.03 | 0.39 | 2.04 | 4.01 | 1.32 | 10.00 |
| Co | 0.06 | 0.07 | 0.07 | 0.07 | 0.12 | 0.08 | 0.07 | 0.12 |
| $SiO_2$ | 22.90 | 18.92 | 17.54 | 14.61 | 9.22 | 20.24 | 0.99 | 0.46 |
| $TiO_2$ | 0.39 | 0.37 | 0.31 | 0.59 | 0.41 | 0.19 | 0.00 | 0.00 |
| $Al_2O_3$ | 1.27 | 1.16 | 1.05 | 1.02 | 1.56 | 5.51 | 2.14 | 0.00 |
| MnO | 0.17 | 0.17 | 0.18 | 0.04 | 0.05 | 0.17 | 0.00 | 0.00 |
| MgO | 20.14 | 17.02 | 15.44 | n.d. | 3.82 | 11.68 | 0.08 | 0.11 |
| CaO | 0.12 | 0.12 | 0.10 | 0.75 | 4.96 | 0.71 | 0.44 | 0.14 |
| $Na_2O$ | 0.00 | 0.00 | 0.00 | 0.00 | - | - | 0.10 | 0.00 |
| $K_2O$ | 0.00 | 0.00 | 0.00 | 0.00 | - | - | 0.00 | 0.00 |
| $P_2O_5$ | 0.04 | 0.03 | 0.03 | 0.00 | 0.00 | 0.00 | 0.16 | 0.00 |
| $H_2O$ | n.a. | 6.03 | 5.55 | 0.35 | 0.30 | 0.13 | 0.08 | 0.10 |

1-3, Kammikivi sill (samples Pet1/41.55, Pet1/42.75, Pet1/44.00); 4-8 taken from Gorbunov (1968).

have on average 4-6 wt. % Cu. In low-grade disseminated ores, the Cu content is tenths of a per cent. The most Cu-rich ore type is represented by mineralized phyllites which contain up to 10 wt. % Cu. Cobalt values are highest in massive ores where they may attain 0.25 wt. %.

Gorbunov et al. (1985b) and Zak et al. (1982) emphasize the large variations within each ore type. Ni and Cu behave most coherently in disseminated ores in peridotites and serpentinites. In these ores, Ni/Cu varies slightly in different deposits, falling between 1.75-2.86 with an average value close to 2 (Zak et al., 1982). The relatively high abundance of Cu compared to Ni clearly separates ferropicrite-related Ni deposits from those generated from komatiite magmas. The latter are typically poor in copper (Naldrett, 1989b). According to Gorbunov et al. (1985b), the average ratios of nickel, copper, and cobalt in various Ni-ore types at Pechenga are:

1) Disseminated ore 55:24:1
2) Breccia ore 56:22:1
3) Massive ore 48:19:1
4) Ore in phyllite 47:48:1

Yakovlev et al. (1968) have published a great number of Se and S analyses for various ore types from Pechenga. In this study, these were supplemented by Se, Te, and S analyses for some ore samples as well as S-poor samples including peridotites and gabbros from intrusions, rock types from layered flows, unfractionated ferropicrites, and S-rich phyllites.

The highest Se contents are measured in rocks rich in sulfur but there is a large variation of the Se content in each ore type (Fig. 67). It follows that the Se/S value is predominantly controlled by the Se abundance of the rock. The Se-S ratio varies between $40\text{-}280\times10^{-6}$ in massive ores and $20\text{-}160\times10^{-6}$ in breccia ores. Disseminated ores which are expected to most reliably represent

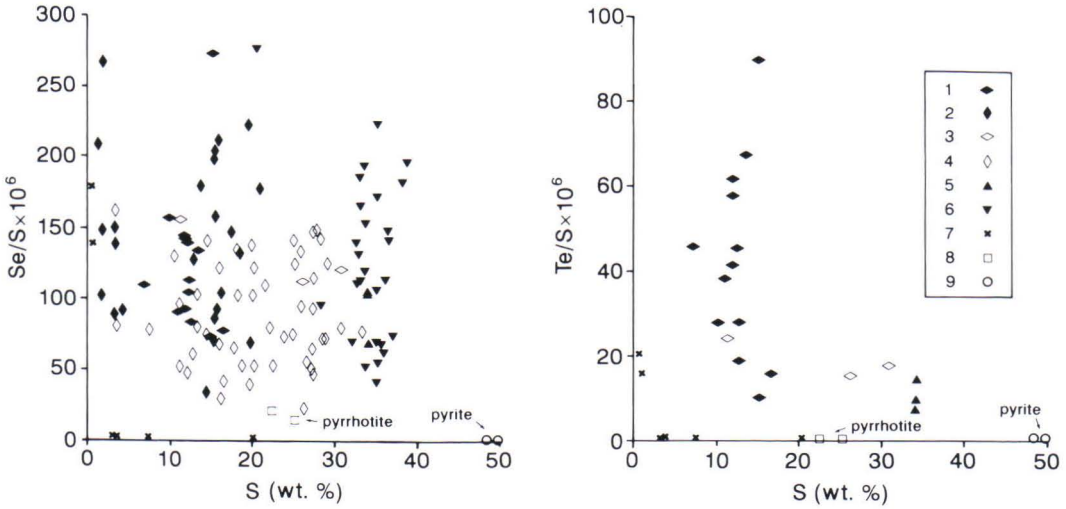


Fig. 67. Se/S and Te/S against sulfur for disseminated (1,2), breccia (3,4) and massive Ni-Cu ores (5,6), sulfide-poor and -rich metasediments (7), and pyrrhotite (8) and pyrite (9) fractions from phyllites. 2, 4 and 6 taken from Yakovlev et al. (1968).

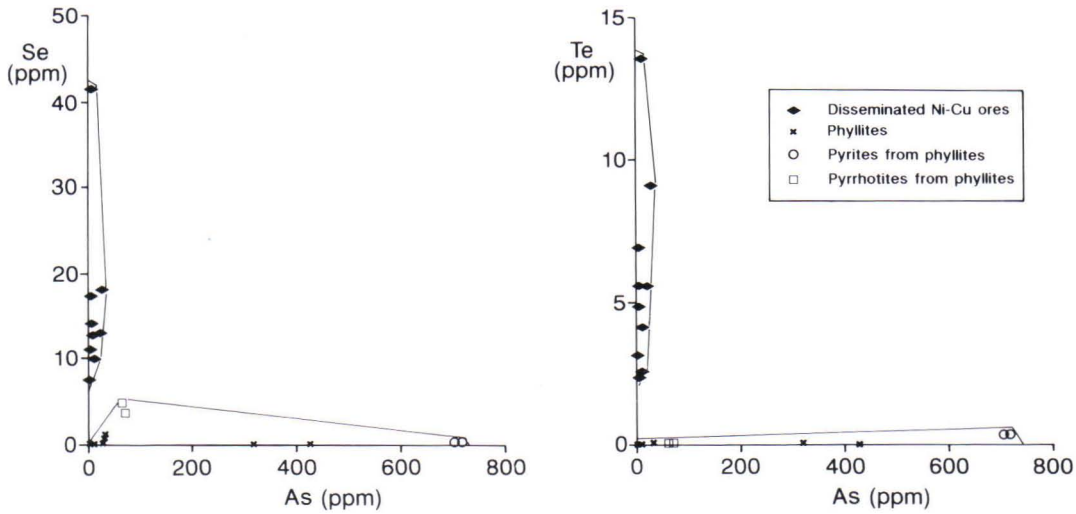


Fig. 68. Se and Te against As for disseminated Ni-Cu ores, sulfide-poor and -rich metasediments, and pyrite and pyrrhotite fractions from phyllites.

Table 21. Metal concentrations and sulfur isotope compositions in phyllites and separated sulfides.

| Sample | Rock/ Mineral | Location | $\delta^{34}S$ | S (wt. %) | Se (ppm) | Te (ppm) | As (ppm) | Zn (ppm) | Mo (ppm) | Ni (ppm) | Cu (ppm) | Co (ppm) |
|---|---|---|---|---|---|---|---|---|---|---|---|---|
| Kotsel 3 | Phyllite | Kotselvaara | n.a. | 20.2 | 0.03 | 0.08 | 349 | 611 | 58 | 236 | 362 | 24 |
| Kotsel 4 | Phyllite | Kotselvaara | n.a. | 20.2 | 0.02 | 0.09 | 361 | 629 | 59 | 228 | 311 | 33 |
| Kotsel 5 | Phyllite | Kotselvaara | n.a. | 3.59 | 0.11 | 0.01 | 7 | 192 | 4 | 136 | 150 | 40 |
| Kotsel 6 | Phyllite | Kotselvaara | n.a. | 3.30 | 0.11 | 0.01 | 2 | 196 | 6 | 126 | 128 | 39 |
| Kotsel 7 | Phyllite | Kotselvaara | n.a. | 6.50 | 0.24 | 0.02 | 25 | 181 | 7 | 192 | 198 | 69 |
| Pet1/47.50 | Phyllite | Kammikivi | n.a. | n.a. | 96 | 0.11 | 32 | 49 | 6 | 125 | 1740 | 30 |
| Pet1/48.40 | Phyllite | Kammikivi | n.a. | 0.88 | 1.22 | 0.14 | 34 | 51 | 3 | 103 | 714 | 30 |
| Kv-12A | Pyrite | Kotselvaara | 15.3 | n.a. | 0.26 | 0.40 | 707 | 437 | 13 | 456 | 513 | 1030 |
| Kv-12B | Pyrite | Kotselvaara | 15.3 | n.a. | 0.29 | 0.41 | 717 | 351 | 10 | 407 | 438 | 875 |
| Kv-13A | Pyrrhotite | Kotselvaara | 11.2 | n.a. | 3.82 | 0.02 | 72 | 303 | 17 | 983 | 390 | 232 |
| Kv-13B | Pyrrhotite | Kotselvaara | 11.9 | n.a. | 4.92 | 0.04 | 65 | 381 | 16 | 877 | 361 | 213 |
| Kv-14 | Pyrite | Kotselvaara | 12.2 | n.a. | n.a. | n.a. | n.a. | n.a. | n.a. | n.a. | n.a. | n.a. |

n.a. = not analysed.
Sulfur isotope compositions determined by J. Tammenmaa at the Laboratory of Ingeneering Geology and Geophysics of the Institute of Technology, Espoo, Finland.

magmatic Se/S values, also exhibit a considerable spread in Se/S, varying between 35-275×$10^{-6}$ (Fig. 67). In general, Se/S does not have any correlation with Ni/(Ni+Cu).

The cosmic Se/S value is about 300×$10^{-6}$ (Anders and Grevesse, 1989). Data on mantle nodules indicate that the pristine upper mantle has a Se/S value close to that in chondrites. Partial melting appears to deplete the mantle residue more in Se than S resulting in a decrease in Se/S (Morgan, 1986). Thus a primary magma generated from a depleted mantle can have a Se/S value considerably less than 300×$10^{-6}$. According to Thompson and Naldrett (1984), the minimum magmatic value is approximately 100×$10^{-6}$. From Fig. 67, it is evident that most of the disseminated ore samples possess a Se/S value higher than 100×$10^{-6}$.

Tellurium behaves in a fashion similar to that of selenium. As shown in Fig. 67, there is a large spread in Te abundances over a limited range of S, resulting in large variations in Te/S. In disseminated ores, this ratio is mostly between 20-60×$10^{-6}$, encompassing the chondritic ratio of 37×$10^{-6}$ (Anders and Grevesse, 1989). Massive and breccia ores are rich in Se relative to Te compared with disseminated ores. In the ore samples analysed for Te, this element shows good correlation with Pd, indicating that Pd mostly resides in tellurides. Arsenic concentrations were determined for some disseminated ore samples. In all of these samples, the As content is very low (1.6-29 ppm), resulting in very high Se/As and Te/As (Fig. 68).

S-rich phyllite samples (3.8-22.4% S) were analysed from the Kotselvaara area (Table 21). They have low concentrations of Se (<0.25 ppm) and Te (<0.1 ppm) compared with Ni-Cu ores (Fig. 67) and therefore these phyllites display extremely low values of Se/S and Te/S (Se/S 0.07-3.28×$10^{-6}$, Te/S 0.28-0.38×$10^{-6}$). Analyses of pyrite and pyrrhotite separates show that Se and Te are selectively concentrated in these minerals; pyrite is relatively rich in Te (about 0.4 ppm) and low in Se (0.26-0.29 ppm) while pyrrhotite is rich in Se (4-5 ppm) and very poor in Te (0.02-0.04 ppm). Two S-poor siltstone samples (0.5, 0.9% S) from the Kammikivi area were also analysed for Se and Te. These components appeared to occur in relatively high concentrations (Se 0.96 and 1.22 ppm, Te 0.11 and 0.14 ppm), resulting in high Se/S and Te/S compared with S-rich sedimentary samples. Arsenic contents in phyllites are variable but may attain values of several hundred ppm. Arsenic obviously resides in pyrite as demonstrated by analyses of pyrite separates containing more than 700 ppm As (Fig. 68).

# ISOTOPE GEOCHEMISTRY

## Pb-Pb

Since the late 1950's, the Pb-Pb isotopic system has been used in the attempt to solve the age and genesis of the Pechenga Ni-Cu deposits (Vinogradov et al., 1959). The most recent studies include those by Pushkarev et al. (1988), Hanski et al. (1990), and Abzalov et al. (1991b). Hanski et al. (1990) obtained a Pb-Pb isochron age of 2004±55 Ma for ferropicritic rocks. Following this study, some additional Pb-Pb isotope analyses for volcanic and intrusive ferropicritic rocks as well as S-rich phyllites have been performed at the Geological Survey of Finland in Espoo by M. Vaasjoki (for methods, see Vaasjoki, 1989). The analytical results together with the earlier measurements from Hanski et al. (1990) are listed in Table 22. The new samples are as follows. Sample **A1083D** is an evolved ferropicritic metavolcanite from the Kotselvaara area. **SA-14**, **SA-36**, and **SA-21** represent, respectively, peridotitic, pyroxenitic, and gabbroic cumulates from the Pilgujärvi intrusion. Also two pyrite separates (**Kv-12**, **Kv-14**) and one pyrrhotite separate (**Kv-13**) from S-rich phyllites and one whole rock phyllite sample (**Kotsel 7**) were analysed.

Figure 69 presents a $^{207}Pb/^{204}Pb$ vs. $^{206}Pb/^{204}Pb$ diagram for all the analyses reported in Table 22. The data for ferropicritic rocks display a large spread in the isotopic ratios, i.e., $^{206}Pb/^{204}Pb$ ranges from 17.16 to 39.10 with the highest values observed in the gabbroic rocks and the apatite from the Pilgujärvi intrusion. Excluding one anomalous sample (1684/1) from the serpentinized ultramafic part of a layered lava flow, the ferropicritic metavolcanites together with the whole rock samples and the apatite from the Pilgujärvi intrusion define a moderately good Pb-Pb isochron with an age of 1988±39 Ma. All the ages reported in this study are given with a $2\sigma$ error. Taking the metavolcanite and intrusive samples separately, an age of 1957±24 Ma is obtained for the metavolcanites and 1977±48 Ma for the Pilgujärvi intrusion. These results are in agreement with the conclusion drawn earlier by Hanski et al. (1990) that the gabbro-wehrlite intrusions and the ferropicritic metavolcanites have the same age within analytical error. In the $^{207}Pb/^{204}Pb$ vs. $^{206}Pb/^{204}Pb$ diagram, the whole rock sample of S-rich phyllite and the pyrite fractions lie close to the isochron with the pyrrhotite fractions plotting somewhat above it. The sedimentary samples show more scatter than the volcanic and intrusive samples. This is understandable because of the potential variation in the initial Pb isotopic ratios in sedimentary rocks.

In Fig. 69, the isochron lies clearly below the average global lead evolution curve of Stacey and Kramer (1975). This means that for a long period before the ferropicritic volcanism, lead evolution took place in a reservoir which had a U-Pb ratio lower than the global average. This is also shown by the low $\mu(^{238}U/^{204}Pb)$ values of 7.9-8.0 obtained from the ferropicritic data in Fig. 69, as calculated from the Canyon Diablo lead using a single stage evolution model and $T_o$=4570 Ma. The initial Pb isotope compositions for ferropicritic metavolcanites can not be directly measured or inferred from Figures 69 and 70. However, these initial compositions can be estimated from magmatic sulfides generated from ferropicritic magma. According to Pushkarev et al. (1978), the most primitive sulfide Pb composition has a value of about 15.0 for both $^{207}Pb/^{204}Pb$ and

**Table 22. Pb isotope data for Pechenga rocks.**

| Sample | Rock type/ Mineral | Location | Pb (ppm) | U (ppm) | $^{206}Pb/^{204}Pb$ | $^{207}Pb/^{204}Pb$ | $^{208}Pb/^{204}Pb$ |
|---|---|---|---|---|---|---|---|
| 1684/1 | Ol cumulate | Kotselvaara | 0.76 | 0.25 | 20.639 | 15.930 | 43.507 |
| 1684/5 | Spinifex zone | Kotselvaara | 1.42 | 0.38 | 22.404 | 15.954 | 43.033 |
| 1685a-G | Globule | Kotselvaara | 11.83 | 1.35 | 17.984 | 15.470 | 37.859 |
| 1685a-M | Matrix | Kotselvaara | 5.58 | 1.57 | 21.002 | 15.813 | 40.854 |
| 1748/9 | Spinifex zone | Kotselvaara | 6.26 | 0.52 | 17.258 | 15.359 | 36.926 |
| 1748/10 | Spinifex zone | Kotselvaara | 1.72 | 0.84 | 33.693 | 17.346 | 55.081 |
| A1083D | Evolved rock | Kotselvaara | n.a. | n.a. | 21.217 | 15.837 | 41.204 |
| SA-14 | Peridotite | Pilgujärvi | n.a. | n.a. | 17.849 | 15.457 | 36.821 |
| SA-36 | Pyroxenite | Pilgujärvi | n.a. | n.a. | 18.581 | 15.608 | 37.103 |
| SA-21 | Gabbro | Pilgujärvi | n.a. | n.a. | 39.097 | 18.051 | 56.129 |
| 149 | Apatite | Pilgujärvi | n.a. | n.a. | 37.41 | 17.88 | 54.81 |
| Kotsel 7 | Phyllite | Kotselvaara | n.a. | n.a. | 19.274 | 15.668 | 35.555 |
| Kv-12 | Pyrite | Kotselvaara | n.a. | n.a. | 16.992 | 15.413 | 35.129 |
| Kv-14 | Pyrite | Kotselvaara | n.a. | n.a. | 23.974 | 16.094 | 35.149 |
| Kv-13 | Pyrrhotite | Kotselvaara | n.a. | n.a. | 24.503 | 16.401 | 36.295 |

**n.a. = not analysed. Errors in measured ratios are 0.15%.**

$^{206}Pb/^{204}Pb$.

Also shown in Fig. 69 is the Pb isotopic evolution of a model upper crust ($\mu_2$=13), calculated according to the two-stage model of Huhma (1986). As was noted above, the sedimentary samples approximately follow the isochron defined by the ferropicritic samples and hence plot clearly below the crustal lead evolution curve. This implies that lead in S-rich phyllites does not have a major Archean upper crustal component.

In the $^{208}Pb/^{204}Pb$ vs. $^{206}Pb/^{204}Pb$ diagram, ferropicrites are also reasonably well aligned along a line passing through the field of Ni-Cu sulfide ores (Fig. 70). The samples from the Pilgujärvi intrusion appear to be shifted slightly towards the right away from the array of the ferropicrites. In contrast, mineral and whole rock samples from phyllites deviate drastically from the ferropicritic rocks in having low $^{208}Pb/^{204}Pb$ values at the same $^{206}Pb/^{204}Pb$ level. The position of phyllites in the diagram is consistent with their low measured Th/U of between 0.3-1.1. Figure 70 indicates a considerable difference in the Th-U ratio between the ferropicritic magma and the phyllites. The Th-U ratio can be calculated by using the following equation:

$$\frac{^{232}Th}{^{238}U} = m \left[ \frac{(e^{\lambda 238\tau} - 1)}{(e^{\lambda 232\tau} - 1)} \right]$$

where $\tau$ is the age of the samples, m is the slope of the regression line in the $^{208}Pb/^{204}Pb$ vs. $^{206}Pb/^{204}Pb$ diagram, $\lambda 238 = 0.155125 \times 10^{-9}$ $y^{-1}$, and $\lambda 232 = 0.049475 \times 10^{-9}$ $y^{-1}$. Th/U can also be calculated for individual samples if the initial $^{208}Pb/^{204}Pb$ and $^{206}Pb/^{204}Pb$ value can be estimated, for example, from the associated sulfides (Dupre et al., 1984). For ferropicritic metavolcanites plotted in Fig. 70 (excluding sample 1684/1), this procedure gives a mean $^{232}Th/^{238}U$ value of 3.84±0.14. This value is lower than the value of 4.2 for the Bulk Earth (Allègre et al., 1986) and indicates a moderately depleted mantle source for ferropicrites. In terms of $^{232}Th/^{238}U$, the mantle source of ferropicrites was not so ex-

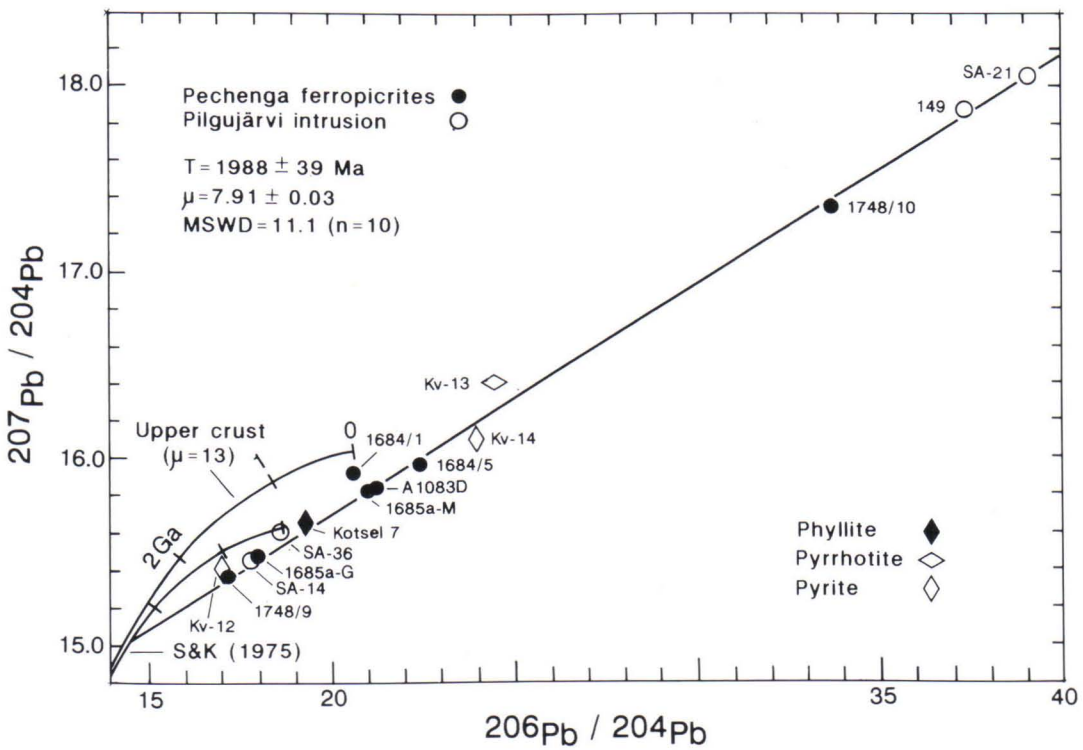


Fig. 69. $^{207}Pb/^{204}Pb$ vs. $^{206}Pb/^{204}Pb$ diagram for ferropicritic metavolcanites, cumulates and apatite from the Pilgujärvi intrusion, and whole rock phyllite and separated sulfides from the productive pile. Model upper crust evolution curve taken from Huhma (1987). S&K (1975) designates the average global lead evolution curve of Stacey and Kramer (1975).

tensively depleted as the source of many komatiite suites (Allègre et al., 1986). Allègre et al. (1986) observed a good negative correlation between $^{232}Th/^{238}U$ and $^{147}Sm/^{144}Nd$ in komatiites from various regions of the earth. This is conceivable because Th/U decreases and Sm/Nd increases with the degree of depletion of the source mantle. In the $^{232}Th/^{238}U$ vs. $^{147}Sm/^{144}Nd$ diagram (not shown), the Pechenga ferropicrites plot considerably away from the komatiite trend because of the decoupling of the Sm-Nd isotope composition and the REE chemistry in ferropicrites (see below).

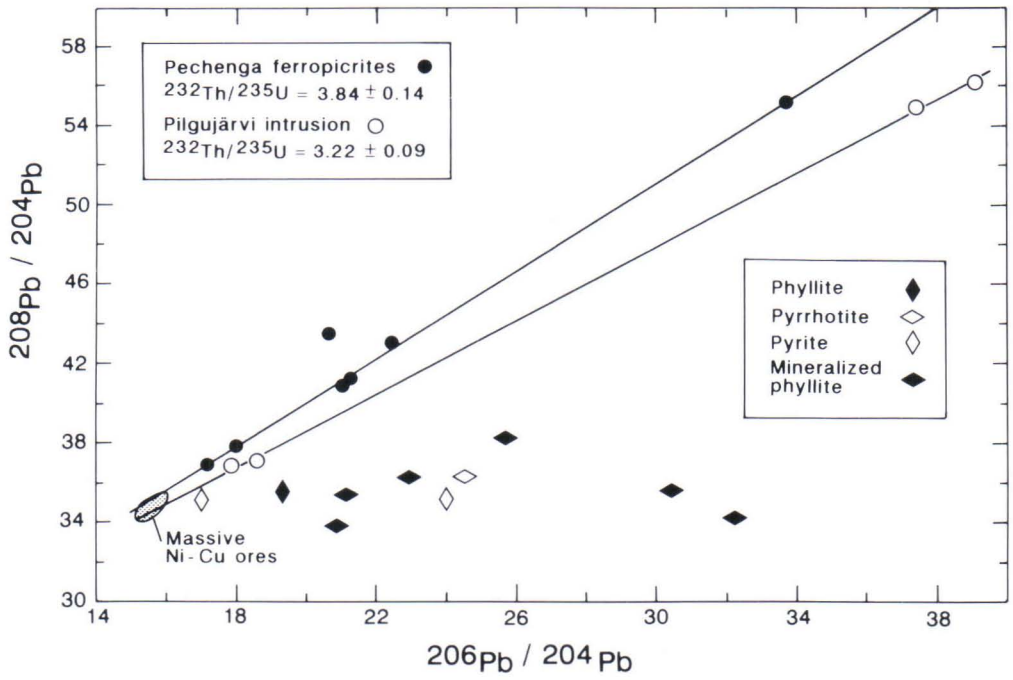


Fig. 70. $^{208}Pb/^{204}Pb$ vs. $^{206}Pb/^{204}Pb$ diagram for ferropicritic metavolcanites, cumulates and apatite from the Pilgujärvi intrusion, and whole rock phyllites and separated sulfides from the productive pile. Phyllite data from this study and Pushkarev et al. (1988). Field of Ni-Cu ores based on data from Pushkarev et al. (1988).

## Sm-Nd

Hanski et al. (1990) analysed nine samples for Sm-Nd isotopes including whole rocks and clinopyroxene separates from ferropicritic layered lava flows and clinopyroxene and apatite separates from the Pilgujärvi intrusion. The data from the ferropicrites yielded an age of 1990±60 Ma with an initial $\varepsilon_{Nd}$ value of +1.6±0.4. The clinopyroxene and apatite fractions from the Pilgujärvi intrusion resulted in an indistinguishable age. Eight new Sm-Nd isotopic analyses on ferropicritic samples and single analyses on an ultrafelsic tuff and a tholeiitic lava have been performed by H. Huhma at GSF in Espoo. They have been listed in Table 23 together with the results from Hanski et al. (1990). The analytical techniques have been described elsewhere (Huhma, 1986).

The new samples reported in this study are as follows. **1748/3** is a cumulate metaperidotite from the base of the Lammas layered lava flow while **1684/4** is a pyroxenitic cumulate from the middle

Table 23. Sm-Nd results for Pechenga rocks.

| Sample | Rock/ Mineral | Location | Sm (ppm) | Nd (ppm) | $^{147}Sm/^{144}Nd$ | $^{143}Nd/^{144}Nd$ |
|---|---|---|---|---|---|---|
| 1684 | Ol cumulate | Kotselvaara | 2.99 | 9.23 | 0.1962 | 0.512715±30 |
| 1684/1 | Ol cumulate | Kotselvaara | 3.81 | 18.67 | 0.1234 | 0.511746±26 |
| 1684/4 | Cpx from 1684/4 | Kotselvaara | 3.09 | 13.72 | 0.1362 | 0.511896±52 |
| 1684/4 | Cpx cumulate | Kotselvaara | 4.83 | 20.20 | 0.1443 | 0.512024±10 |
| 1684/5 | Spinifex zone | Kotselvaara | 3.12 | 9.58 | 0.1968 | 0.512713±26 |
| 1684/5 | Cpx from 1684/5 | Kotselvaara | 4.65 | 14.06 | 0.2001 | 0.512787±40 |
| 1748/9 | Spinifex zone | Lammas | 6.89 | 31.84 | 0.1309 | 0.511862±25 |
| 1748/6 | Cpx cumulate | Lammas | 4.65 | 18.73 | 0.1502 | 0.512124±21 |
| 1748/3 | Olivine cumulate | Lammas | 3.01 | 13.60 | 0.1338 | 0.511936±12 |
| S-2986/76.5 | Spinifex zone | Kierdzhipori | 7.51 | 33.76 | 0.1346 | 0.511900±10 |
| S-3077/322.5 | Pillow lava | Shuljärvi | 5.47 | 22.00 | 0.1499 | 0.512062±10 |
| S-3R/731.4 | Spinifex zone | Kaula | 7.45 | 33.90 | 0.1329 | 0.511874±10 |
| PS4 | Spinifex zone | Kaula | 8.77 | 42.62 | 0.1243 | 0.511779±10 |
| Pet1/1.00 | Quench gabbro | Kammikivi | 9.55 | 41.36 | 0.1396 | 0.511959±10 |
| SA-41 | Cpx from pyroxenite | Pilgujärvi | 4.50 | 19.81 | 0.1373 | 0.511950±21 |
| 149 | Apatite | Pilgujärvi | 296 | 1322 | 0.1353 | 0.511947±24 |
| S-2986/70.0 | Tholeiitic lava | Kierdzhipori | 3.06 | 9.74 | 0.1899 | 0.512719±17 |
| 1825-1A | Ultrafelsic tuff | Kuorpukas | 12.84 | 67.24 | 0.1156 | 0.511576±10 |

Error in $^{147}Sm/^{144}Nd$ is 0.4%. The concentrations were determined from liquid aliquots.
$^{143}Nd/^{144}Nd$ ratios normalized to $^{146}Nd/^{144}Nd=0.7219$.

part of a thick lava flow south of Kaula. **PS4** was taken from the same area. This sample is an evolved rock with a parallel olivine spinifex texture. **S-2986/76.5** also represents an evolved ferropicritic variant taken from the S-2986 layered lava flow (Kierdzhipori). In addition, one clinopyroxene separate (**S-2986/84.1**) from the central part of same lava flow was analysed. **S-3R/741.3** is a pyroxene spinifex-textured rock from Kaula. **Pet1/1.00** comes from the upper, gabbroic part of the Kammikivi sill while **S-3077/322.5** represents a pillow lava from the Shuljärvi area in the southern part of the Pilgujärvi Suite. **S-2986/70.0** is a tholeiitic lava above the ferropicritic S-2986 lava flow from Kierdzhipori. The ultrafelsic tuff sample **1825-1A** has been collected from the Kuorpukas Mountain area. The sampling sites are marked in Fig. 3. The other samples listed in Table 23 have been described by Hanski et al. (1990).

The Sm-Nd isotopic results are presented as a $^{143}Nd/^{144}Nd$ vs. $^{147}Sm/^{144}Nd$ diagram in Fig. 71. The ferropicritic samples display a moderately good spread in $^{147}Sm/^{144}Nd$ from 0.12 to 0.20 by virtue of the fractionation effect of clinopyroxene. Regression analysis of the data for ferropicritic metavolcanites and their minerals, treated as a single population, yields an age of 1960±87Ma. One of the samples, S-3077/322.5, lying somewhat below the regression line, belongs to those ferropicrites which have exceptionally flat chondrite-normalized profiles for LREE (see Fig. 53). Although the rare earth elements are generally considered to be relatively refractory elements in hydrothermal and metamorphic alteration processes, the anomalous features of sample S-3077/322.5 in both the Sm-Nd isochron diagram and the REE diagram can be explained by post-

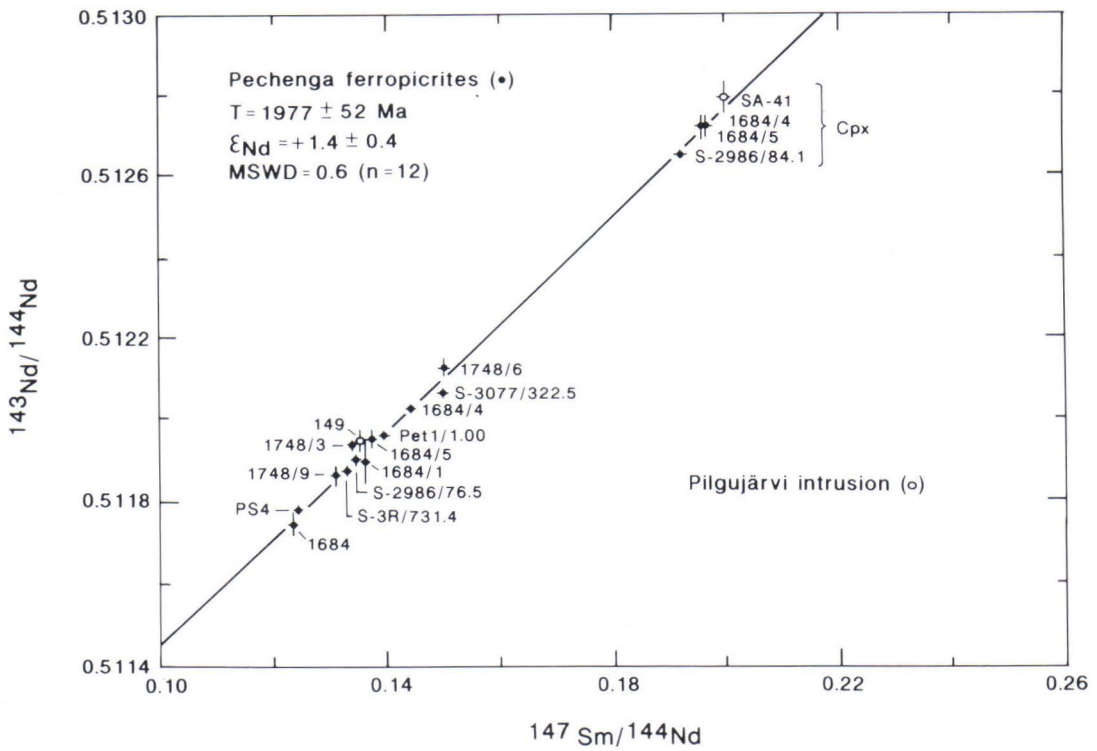


Fig. 71. $^{143}Nd/^{144}Nd$ vs. $^{147}Sm/^{144}Nd$ diagram for whole rock samples and mineral separates from ferropicritic metavolcanites and the Pilgujärvi intrusion. Open symbols refer to samples from the Pilgujärvi intrusion.

crystallization loss of Nd and other LREE. The calculated Nd isotopic evolution line of this sample transects the lines of the other samples at about 1700 Ma (not shown) suggesting that Nd loss occurred during a metamorphic event at that time. Omitting S-3077/322.5 and two serpentinite samples (1684/1, 1748/3) from the bottom part of layered flows which probably also have disturbed Sm-Nd isotope systems, the remaining 12 volcanic samples define an isochron with an age of 1977±53 Ma and an initial $^{143}Nd/^{144}Nd$ value of $0.5101512\pm20\times10^{-6}$ corresponding to an $\varepsilon_{Nd}$ value of +1.4±0.4. The two-point isochron of the mineral fractions from the Pilgujärvi intrusion yields a slightly higher initial Nd isotope ratio of +2.1 and an age of 1969 Ma. The Sm-Nd ages are in excellent agreement with the Pb-Pb ages reported above. They also concur well with the minimum age of 1970±5 Ma documented by Hanski et al. (1990) for a zircon fraction from an ultrafelsic tuff.

The initial $\varepsilon_{Nd}$ of +1.4±0.4 obtained for ferropicrites indicate a depleted mantle source with a time-averaged Sm-Nd ratio distinctly higher than that in chondrites. The depletion was, however, not so strong as in a model MORB source mantle

which would have had an $\varepsilon_{Nd}$ value of about 4-6 at 2.0 Ga ago (Smith and Ludden, 1989). The positive $\varepsilon_{Nd}$ value contrasts with the strong LREE enrichment observed in ferropicrites and indicates a relatively recent enrichment event in the mantle source (Hanski et al., 1990).

A single Sm-Nd isotope analysis on a tholeiite from the Pilgujärvi Suite suggests that these rocks have an $\varepsilon_{Nd}$ value of about +3.3. This value deviates clearly from the initial ratio of ferropicrites. This provides additional evidence for independent mantle sources for the ferropicrites and tholeiites of the Pilgujärvi Suite. The Sm-Nd data suggest a strongly depleted source mantle for the Kolosjoki tholeiites. This is consistent with results obtained for other noncontaminated Karelian basaltic rocks (Huhma et al., 1990, Huhma, 1986).

When the $^{143}Nd/^{144}Nd$ value of 0.511576±10 measured for the felsic tuff sample (1825-1A) is corrected to an initial ratio at 1.97 Ga, an $\varepsilon_{Nd}$ value of -0.3±0.4 is obtained. This implies, assuming a volcanic origin for this rock, that the source had a time-integrated Sm/Nd value close to that of chondrites. While bearing in mind the scarcity of data, some conclusions can still be drawn from this result. The difference in the initial Nd isotope ratios between ultrafelsic tuffs, ferropicrites, and tholeiites rules out the possibility that the felsic rocks are products of direct fractional crystallization of a ferropicritic or tholeiitic parental magma. It also negates a potential genetic link between the felsic rocks and ferropicrites or tholeiitic basalts through silicate liquid immiscibility. The source material was unlikely to be Archean upper sialic crust which has commonly developed distinctly negative $\varepsilon_{Nd}$ values through time (e.g., Huhma, 1986). The nonfractionated REE character of the source suggests that it consisted of some mafic rock type such as amphibolite. Given the existence of Archean zircons and gneiss fragments in the felsic tuffs (Borisov and Smolkin, 1992), the source was located most probably in the basement complex below the Pechenga supracrustal sequence. Alternatively, felsic tuffs could be derived from a Proterozoic upper mantle source. In that case, the chemical and isotope composition of felsic tuffs indicate, respectively, that the liquid evolved through a large degree of fractional crystallization and was contaminated with crustal material.

## Re-Os

### General features of the Re-Os isotopic systematics

Because the Re-Os isotopic system has only recently been applied to terrestrial igneous rocks and is unfamiliar to most geologists not actively working in the field of isotope geology, it is prudent here to present the most pertinent aspects of the system and its potential applications. Reviews of the Re-Os systematics have recently been published by Luck (1989) and Shirey (1991).

Osmium is one of the platinum-group elements and rhenium is situated just before it in the periodic table of the elements. The Re-Os isotope system is based on the beta decay of $^{187}Re$ to $^{187}Os$. The most recent experimental determination of the decay constant ($\lambda$) of $^{187}Re$ is that performed by Lindner et al. (1989) with a result of $1.639\pm0.05 \times 10^{-11}y^{-1}$. This value is somewhat higher than their previous experimental estimate of $1.59\pm0.04 \times 10^{-11}y^{-1}$ (Lindner et al., 1986) and the value of $1.52\pm0.04 \times 10^{-11}y^{-1}$ obtained by Luck and Allègre (1983) by analysing Re and Os isotopes in iron meteorites that have been dated precisely by other methods. The half life of $^{187}Re$ is 43.5 billion years, about ten times the age of the earth, thus being close to the half life of $^{87}Rb$. The long half life of $^{187}Re$ enables the Re-Os method to be utilized in the dating of rocks ranging in age from the generation of the solar system to less than 100 Ma (Luck et al., 1980; Walker et al., 1991b).

The decay equation is expressed as

$$(^{187}Os/^{186}Os)_m$$

$$= (^{187}Re/^{186}Os)_m (e^{\lambda t} - 1) + (^{187}Os/^{186}Os)_i$$

where m and i denote measured and initial isotope ratios, respectively. As for the analogous ε parameter used in the Sm-Nd systems, the γ parameter for the Re-Os system is defined as follows (Walker et al., 1989):

$$\gamma_{Os}(T) = \left[ \frac{^{187}Os/^{186}Os)_{sample}}{(^{187}Os/^{186}Os)_{mantle}} - 1 \right] \times 100.$$

$\gamma_{Os}(T)$ describes the percentage difference between the Os isotopic compositions of a sample at any time (T) and a reference mantle value at that time. $(^{187}Os/^{186}Os)_{sample}$ is obtained using the Re-Os decay equation as expressed above and the osmium isotopic ratio of the mantle at any time is calculated from the relation:

$$(^{187}Os/^{186}Os)_{mantle} = 1.06 - 3.3(e^{\lambda t} - 1),$$

where 1.06 and 3.3 are respectively the average $^{187}Os/^{186}Os$ and $^{187}Re/^{186}Os$ values of chondrites today (Walker et al., 1989).

The Re-Os isotope system is not a new radioactive decay scheme in studing geological objects (Herr et al., 1961), but its employment has been difficult until about a decade ago owing to technical problems. The application of thermal ionization mass spectrometry (TIMS) to the Re-Os system has been severely hindered by the high ionization potentials of these elements (Os 8.7 eV, Re 7.9 eV) coupled with the extremely low concentrations of Re and particularly Os in common igneous rocks. In most igneous rocks, osmium abundances fall below 1 ppb (Morgan and Lovering, 1967).

A major advancement was achieved by J.-M. Luck and C.J. Allègre from the University of Pierre and Marie Curie in Paris by employing secondary ion mass spectrometry (SIMS) in Re-Os isotope analysis (Luck et al., 1980; Allègre and Luck, 1980). Their pioneering studies initiated more widespread application of Re-Os isotope systematics to terrestrial and extraterrestrial rocks. One of the advantages of the SIMS technique is that it allows direct analysis by ion microprobe of high-Os samples such as PGE minerals (Allègre and Luck, 1980; Hart and Kinloch, 1989). Subsequent progress in Re-Os isotope analysis was based on the realization that Re and Os can be efficiently ionized when subjected to resonance excitation by laser light of an appropriate wavelength. This led to the development of resonance ionization mass spectrometry (RIMS) by Walker and Fassett (1986) at the National Bureau of Standards (Gaithersburg, Maryland, USA). RIMS has proven to be sensitive and precise in measuring silicate rocks with low Re and Os abundances and it has been successfully applied to meteorites, komatiites and ultramafic xenoliths (Walker and Morgan, 1989; Walker et al., 1988, 1989, 1991b).

The most recent fundamental improvement in Re-Os isotope analysis has been the development of negative thermal ion mass spectrometry (NTIMS) by Creaser et al. (1991) at the California Institute of Technology. One of the advantages of this technique is that it permits the use of the conventional thermal ionization mass spectrometer. This equipment is modified by reversing the polarities of the magnet to produce negatively charged oxides of osmium and rhenium. The technique allows determination of the isotopic ratios with a precision of better than ±2 ‰ and the optimum detection limit for osmium is below $10^{-14}$ g. The ionization efficiency for Os is also superior (2-6%) compared to other techiques, such as RIMS which achieves an efficiency of about $5\times10^{-7}$ (Shirey et al., 1990). Negative thermal ion mass spectrometry has now been developed in several laboratories and will probably supercede SIMS, RIMS, and other techniques

previously used in Os isotope analysis, including accelerator mass spectrometry (AMS; Fehn et al., 1986), inductively coupled plasma mass spectrometry (ICP-MS; Masuda et al., 1986; Russ et al., 1987), and laser microprobe mass analysis (LAMMA; Lindner et al., 1986).

Like the other platinum group elements, osmium and rhenium both possess a strong siderophile and chalcophile character and are therefore concentrated in metallic phases such as iron meteorites and magmatic sulfides. During partial melting of the mantle, Re is an incompatible element (D=0.001-0.3) and is concentrated in the melt fraction, while Os is compatible to highly compatible (D=2-400) and is enriched in mantle residues (Walker et al., 1988, 1989, 1991b). Because of these unique geochemical characteristics, rhenium and osmium can provide petrogenetic information which would otherwise be unattainable by utilizing the radioactive decay systems of lithophile elements.

As with the Rb-Sr or Sm-Nd isotope decay schemes, the Re-Os isotope can be employed both as a geochronometer and as a petrogenetic tracer. Age determinations using the $^{187}Re/^{187}Os$ system can be obtained in principle in three different ways, namely by directly comparing the absolute abundances of $^{187}Re$ and $^{187}Os$ in a rhenium-rich mineral, constructing an isochron, and calculating 'model ages'. A mineral that is ideal for dating using the first method is molybdenite (Luck and Allègre, 1982). Because molybdenite is commonly rich in rhenium but free of "common" osmium, osmium in this mineral is purely radiogenic and the mineral can be dated in an analogous fashion to zircon using U-Pb isotopes.

Because significant Re/Os fractionation in magmatic processes can be caused by metals and sulfides as well as silicates, the systems that are potentially capable of being dated by the Re-Os isochron method are more numerous than those to which other common geochronometers can be applied. The most important processes that can be dated include planetary differentiation processes, such as the core formation (Luck and Allègre, 1983; Bennett and Esat, 1991), crystallization of basic to ultrabasic magmas as intrusions or lava flows (Walker et al., 1988; Lambert et al., 1989), and various ore forming processes (Horan et al., 1991).

A model age can be calculated for a single sample if the initial $^{187}Os/^{186}Os$ value can be estimated. By analogy with the $T_{DM}$ model ages used in Nd isotopic systematics, Re-Os model ages can be calculated assuming that the initial ratios followed the (chondritic) Os isotope evolution of the mantle. In such cases, a model age $T_{MA}$, as defined by Luck and Allègre (1984), is obtained using the equation:

$$T_{MA} = 1/\lambda \times \ln \left[ \frac{(^{187}Os/^{186}Os)_{sample} - (^{187}Os/^{186}Os)_{mantle}}{(^{187}Re/^{186}Os)_{sample} - (^{187}Re/^{186}Os)_{mantle}} + 1 \right]$$

where $(^{187}Os/^{186}Os)_{mantle}=1.06$ and $(^{187}Re/^{186}Os)_{mantle}=3.3$. These mantle values are average present-day values of carbonaceous chondrites after Walker and Morgan (1989). Particularly, rocks with a high Re/Os value such as basic volcanic rocks are promising for model age calculations because the higher the $^{187}Re/^{186}Os$ value, the less critical is the accuracy of the initial-ratio estimate to the accuracy of an age determination. The absolute maximum age ($T_{max}$) for a sample can also be calculated by extrapolating the growth curve back in time until the initial ratio decreases down to 0.802, which was the initial ratio of meteorites 4.55 Ga ago.

Figure 72 schematically represents the Os isotopic evolution lines for a chondritic mantle, a komatiitic and basaltic melt, and the corresponding residues produced from this mantle from 30% and

10% partial melting 3.5 Ga ago (after Walker et al., 1989). The largest deviation from the chondritic evolution line in the residue results after a high degree of partial melting when all Re is partitioned into the melt fraction. In this case, as shown by the horizontal line in Fig. 72, the difference in $^{187}Os/^{186}Os$ with respect to the chondritic line is only about 8% after an evolution of 3.5 Ga. In contrast, basic and ultrabasic melts with high Re/Os will rapidly attain high $^{187}Os/^{186}Os$ values. This strong fractionation of Re and Os during partial melting renders the Re/Os isotopic system ideal for studying the evolution of the earth's crust and mantle.

The first estimate of the Os isotope evolution of the earth's mantle over geologic time was made by Allègre and Luck (1980) by determining the $^{187}Os/^{186}Os$ of osmiridium alloys of estimated age. These minerals are extremely low in Re and hence their present-day $^{187}Os/^{186}Os$ composition is the same as that at the time of crystallization. On an age vs. $^{187}Os/^{186}Os$ diagram, Allègre and Luck (1980) obtained a straight line passing through the initial ratio of meteorites. The conclusion from this and their later study (Luck and Allègre, 1991) was that the upper mantle is similar to the bulk silicate earth since both have a present-day $^{187}Os/^{186}Os$ value around 1.05-1.06, corresponding to an evolution with a $^{187}Re/^{186}Os$ value of 3.33. The latter figure is close to the average value of carbonaceous chondrites (Walker and Morgan, 1989). The chondritic Re-Os ratio of the bulk mantle is compatible with the chondritic noble metal patterns observed in primitive mantle xenoliths (e.g., Jagoutz et al., 1978).

As more Os isotope data are obtained, some heterogeneity has appeared among mantle-derived materials. Walker et al. (1989) reported low $^{187}Os/^{186}Os$ values in the range of 0.905-1.070 ($\gamma_{Os}$ from -14 to 0) for peridotite xenoliths from South Africa, which represent subcontinental lithospheric mantle beneath the old Kaapvaal craton. These nonradiogenic compositions are attributed to long-term evolution with low Re/Os most likely resulting from a depletion due to one or more ancient partial melting events and isolation from chemical exchange with the underlying sublithospheric mantle.

Compared to subcontinental mantle, oceanic peridotites and MOR basalts have higher $^{187}Os/^{186}Os$ values, ranging between 1.003-1.083 while ocean island basalts record still higher values (1.079-1.174; Martin, 1991; Martin et al., 1991). These results led Martin (1991) to suggest that the bulk silicate earth has today's $^{187}Os/^{186}Os$ value of 1.10 (corresponding to $^{187}Re/^{186}Os$ of 4.1). This figure is higher than the average for analysed carbonaceous chondrites but still falls within their range. The lower values of oceanic mantle are thought to be due to long-term Re depletion at least partly related to extraction of continental crust through geological time (Martin et al., 1991).

It is now well established that the Os isotope evolution of the earth's mantle is close to the chondritic growth curve and is remarkably homogeneous compared to the evolution of lithophile radioactive systems like Sm-Nd and Rb-Sr. In addition, large differences in geochemical characteristics between the above mentioned isotopic tracers may lead to decoupling of the Re-Os system from other isotopic systems. For example, in

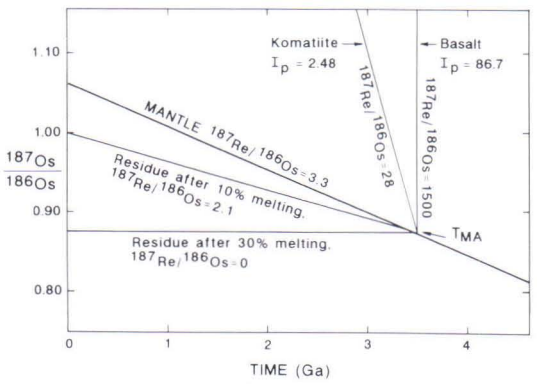


Fig. 72. Schematic representation of the Os isotopic evolution of mantle and its residues and melts after 10% and 30% partial melting (modified after Walker et al., 1989). $I_p$ denotes Y-axis intersection, i.e., present-day $^{187}Os/^{186}Os$.

some mantle xenoliths, kimberlites, and picrites, Sm-Nd systematics reveal a long-lived LREE enrichment in their mantle sources whereas Re-Os systematics display negative $\gamma_{Os}$ values indicative of an ancient melt removal from the mantle (Pearson et al., 1991; Walker et al., 1989; Ellam et al., 1991). Thus, the agent that caused the LREE enrichment in these cases did not have a notable effect on the Re-Os isotopic systematics of the mantle. Neither did Reisberg et al. (1991) observe any relationship between $^{187}Os/^{186}Os$ and $^{143}Nd/^{144}Nd$ in peridotites of the Ronda Ulramafic Complex, where a recent metasomatic event has strongly affected the Nd isotope systematics but has had little effect on the Os isotope systematics.

The relative inertness of the Re-Os system with respect to fluids causing mantle enrichment processes, the slow evolution of the $^{187}Os/^{186}Os$ in the mantle in time, and the high Re/Os in basaltic rocks contribute to the assessment that calculated model $T_{MA}$ ages of basalts can in many cases be reasonably close to their crystallization ages, provided the system has remained closed after crystallization. It should, however, be remembered that crustal contamination, either by assimilation of sialic material by basalt during ascent or at the surface or incorporation of recycled sediment or oceanic crust back to the mantle, can result in considerable deviations of the initial $^{187}Os/^{186}Os$ value of basalt with respect to the chondritic value. The average upper continental crust has a present-day $^{187}Os/^{186}Os$ of about 10 which is ten times higher than the value in primary melts from the mantle (Martin et al., 1991).

The sensitivity of the Re-Os system for reflecting crustal interactions can be utilized in the investigations of layered intrusions and related ore deposits. For example, Walker et al. (1991a) obtained a surprising result when studing the Re-Os isotope composition of Ni-Cu deposits from the Sudbury Igneous Complex. They found that the major proportion of Os (from 50 to nearly 100%) and probably other PGE as well was derived from crustal melts. Other studies of large layered intrusions, such as the Stillwater and Bushveld Complexes, also indicate the involvement of a component of radiogenic osmium from crustal sources (Lambert et al., 1989; Martin, 1989; McCandless and Ruiz, 1991; Hart and Kinloch, 1989; Allègre and Luck, 1980).

## Re-Os isotopes in Pechenga rocks

Only a few Precambrian volcanic rocks have so far been studied using Re-Os isotopic systematics. Preliminary results on the Pechenga rocks were presented in Walker et al. (1991c). Re-Os isotopic analysis have been applied to 18 samples, ten of which are ferropicritic volcanic rocks. The remaining eight samples were taken from the ore-bearing Kammikivi layered sill (Table 24). Samples **1748/3**, **S-3077/322.5**, **S-2986/76.5**, **S-3R/731.4**, **Pet1/1.00** have also been analysed for Sm-Nd and are described in the corresponding section. Four of the Kammikivi samples (**Pet1/43.95, Pet1/45.05, Pet2/25.65, Pet2/27.70**) are disseminated Ni-Cu ores from the basal part of the sill. Pet2/25.65 is a sulfide concentration of an ore sample from which gangue minerals, consisting mainly of chlorite, were eliminated using heavy liquids. Samples **Pet1/25.66** and **Pet1/33.10** represent the olivine cumulate and **Pet1/5.40** the pyroxene cumulate part of the sill (see Fig. 28). Pet1/33.10 have a weak sulfide dissemination resulting in a relatively high S content of 1.2%. Volcanic samples come from four different areas. Sample series 1748 and S-2986 exemplify various rock types from two layered lava flow, the former occurring in the Lake Lammas area and the latter in the Kierdzhipori area (see Figures 6 and 73). Samples **1748/9**, **1748/8A**, and **S-2986/76.0** were collected from the spinifex zone of the flows while **1748/6** and **S-2986/84.1** represent pyroxene cumulates in the middle part and **S-2986/93.5** an olivine cumulate in the lower part of the flows.

Re and Os isotopic compositions were determined by R. Walker at the National Institute of Standards (Gaitherburg, Maryland) using resonance ionization mass spectrometry (RIMS) (Walker and Fassett, 1986). Rhenium and osmium concentrations were measured by isotope dilution using $^{185}Re$ and $^{190}Os$ spikes. Before ana-

lysis, Re and Os were separated following HCl-HF-$H_2SO_4$-ethanol digestion by distillation for Os and solvent extraction for Re, a technique specifically developed by Walker (1988) for use with RIMS. Uncertainties for Re and Os concentrations and Os isotopic ratios are generally between 1-4% (2σ), primarily limited by counting statistics (Walker and Fassett, 1986). The rhenium and osmium concentrations and $^{187}Re/^{186}Os$ and $^{187}Os/^{186}Os$ values are listed in Table 24.

In accordance with the behavior of so-called iridium PGEs, Os is most abundant in olivine cumulates (up to 2.54 ppb) and sulfide ores (2.33-23.4 ppb). In evolved rocks, the Os concentration is extremely low, with the minimum measured value being 0.0048 ppb. Re is also high in ore samples (15.6-58.8 ppb) but, in contrast to Os, it is not strongly fractionated with respect to different silicate rock types. The sulfide fraction of sample Pet2/25.65 possesses the highest measured Os and Re concentrations of 51.3 and 121 ppb, respectively. Figure 73 presents variations in Re and Os abundances and $^{187}Re/^{186}Os$ across two layered lava flows while Fig. 74 exhibits the same data for the Kammikivi ore-bearing sill. Proceeding upwards from the base of the layered bodies, Os decreases systematically, falling to extremely low levels in the most evolved rocks. In pyroxenites, the abundance of Os has already diminished to less than 0.02 ppb. The rise of Os in the upper part of the Lammas flow is caused by the unfractionated character of sample 1748/9 (MgO 14.4%). The low Os abundance of 0.09 ppb in sample Pet1/25.66, representing an olivine cumulate from the ore-bearing Kammikivi sill, is noteworthy. The olivine cumulates with similar MgO and Ni contents from the S-poor Kierdzhipori and Lammas flows have Os values of 2.54 and 1.66 ppb, respectively (Table 24). The difference may be attributed to the fractionation

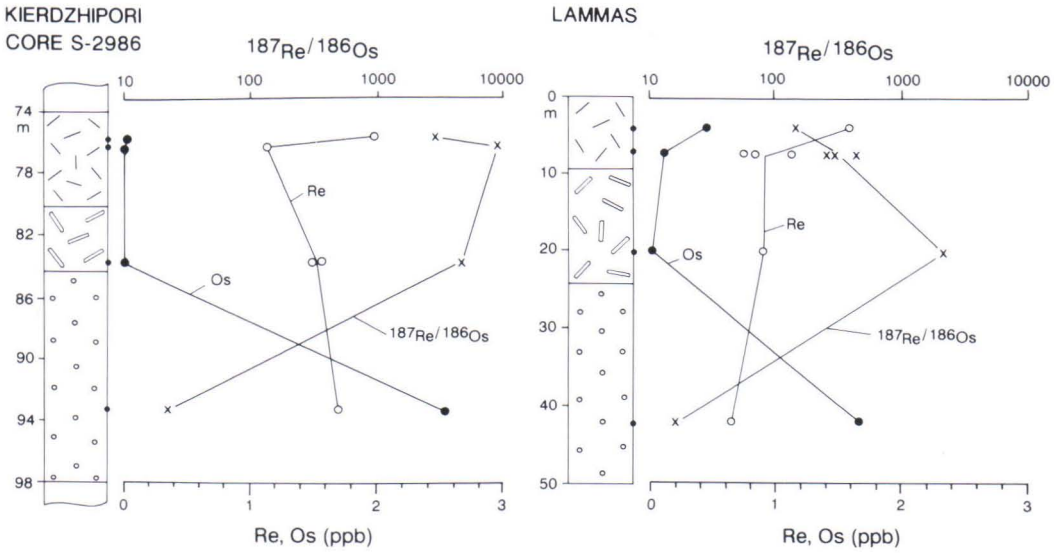


Fig. 73. Variation in Re and Os abundances and $^{187}Re/^{186}Os$ across the Kierdzhipori and Lammas flows.

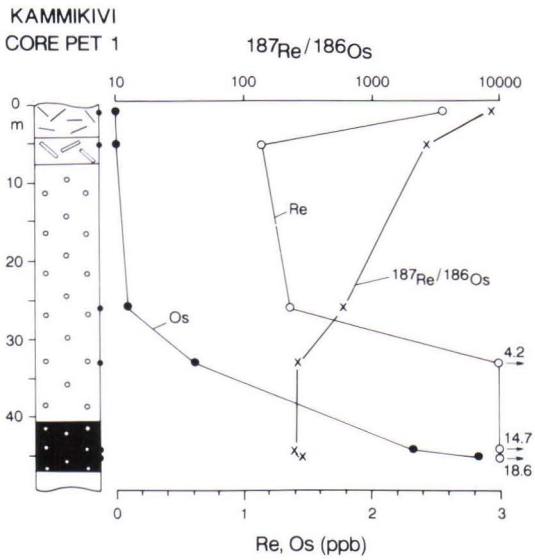


Fig. 74. Variation in Re and Os abundances and $^{187}Re/^{186}Os$ across the Kammikivi sill.

effect of sulfide liquid in the Kammikivi sill. In that case, however, the same effect should also be seen in the behavior of rhenium but no Re depletion is observed in sample Pet1/25.66 compared with the Re values in the lower part of the Kierdzhipori and Lammas flows.

The chalcophile nature of Re is confirmed by its high abundances in the disseminated ore samples from the Kammikivi sill. The accumulation of sulfide liquid at the bottom of the sill may have caused depletion of the residual magma in Re and other chalcophile elements. However, contrary to expectations, rhenium is not depleted in the gabbroic part of the Kammikivi sill when compared with the evolved parts of the unmineralized Lammas and Kierdzhipori flows. In fact, the highest Re concentration of the silicate samples (2.74 ppb) was measured on sample Pet1/1.00, taken from the S-poor upper part of the Kammikivi body.

**Table 24. Re-Os isotopic data for Pechenga ferropicrites and associated Ni-Cu ores.**

| Sample | Rock type | Location | Re (ppb) | Os (ppb) | $^{187}Os/^{186}Os$ | $^{187}Re/^{186}Os$ |
|---|---|---|---|---|---|---|
| 1748/9 | Spinifex zone | Lammas | 1.63±0.02 | 0.449±0.005 | 6.26±0.08 | 146±3 |
| 1748-8A | Globular rock | Lammas | 0.856±0.025 | 0.111±0.003 | 19.6±0.8 | 309±3 |
| 1748-8A(rep) | Globular rock | Lammas | 0.757±0.014 | 0.113±0.002 | 20.7±0.5 | 268±7 |
| 1748-8A(rep) | Globular rock | Lammas | 1.15±0.02 | 0.104±0.002 | 19.9±0.3 | 440±10 |
| 1748-6 | Cpx cumulate | Lammas | 0.918±0.014 | 0.0153±0.004 | 78.0±1.5 | 2260±60 |
| 1748-3 | Ol cumulate | Lammas | 0.658±0.014 | 1.66±0.02 | 1.62±0.02 | 15.9±0.3 |
| S-2986/76.0 | Spinifex zone | Kierdzhipori | 1.98±0.04 | 0.0280±0.0011 | 107±5 | 2850±140 |
| S-2986/76.5 | Spinifex zone | Kierdzhipori | 1.14±0.02 | 0.00478±0.00019 | 318±12 | 9370±400 |
| S-2986/84.1 | Cpx cumulate | Kierdzhipori | 1.58±0.03 | 0.0119±0.0004 | 189±9 | 5260±250 |
| S-2986/84.1(rep) | Cpx cumulate | Kierdzhipori | 1.51±0.02 | 0.0125±0.0005 | 166±7 | 4790±200 |
| S-2986/93.5 | Ol cumulate | Kierdzhipori | 1.70±0.05 | 2.54±0.04 | 1.70±0.03 | 22.4±0.5 |
| S-3077/322.5 | Massive lava | Shuljärvi | 0.516±0.009 | 0.782±0.008 | 1.83±0.03 | 26.5±0.5 |
| S-3R/731.4 | Spinifex zone | Kaula | 1.42±0.02 | 0.134±0.002 | 15.0±0.2 | 427±11 |
| Pet1/1.00 | Quench gabbro | Kammikivi | 2.58±0.03 | 0.0112±0.0006 | 336±8 | 9050±530 |
| Pet1/5.40 | Cpx cumulate | Kammikivi | 1.16±0.02 | 0.0163±0.0004 | 83.8±2 | 2840±90 |
| Pet1/25.66 | Ol cumulate | Kammikivi | 1.38±0.02 | 0.0902±0.0013 | 20.7±0.3 | 614±13 |
| Pet1/33.00 | Ol cumulate | Kammikivi | 4.20±0.06 | 0.624±0.009 | 13.5±0.2 | 270±6 |
| Pet1/43.95 | Diss. ore | Kammikivi | 14.7±0.2 | 2.33±0.03 | 11.0±0.2 | 252±5 |
| Pet1/45.05 | Diss. ore | Kammikivi | 18.6±0.2 | 2.83±0.04 | 11.4±0.2 | 263±6 |
| Pet2/25.65 | Diss. ore | Kammikivi | 121±4 | 51.3±1.0 | 5.37±0.06 | 94.8±3.0 |
| Pet2/27.70 | Diss. ore | Kammikivi | 55.3±0.8 | 23.4±0.3 | 6.50±0.10 | 94.9±3.0 |

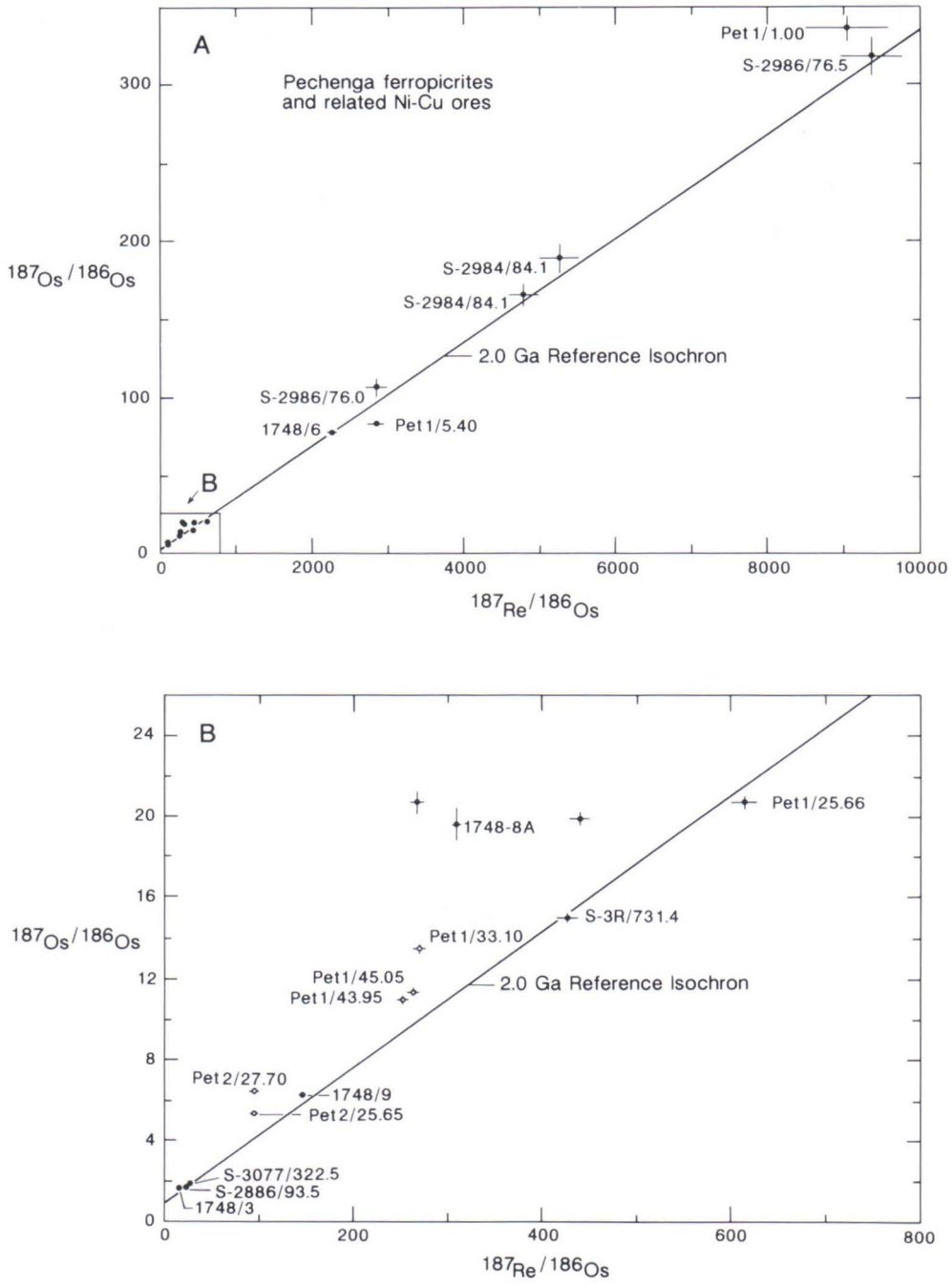


Fig. 75. A. $^{187}Re/^{186}Os$ versus $^{187}Os/^{186}Os$ isochron diagram for ferropicritic metavolcanites and silicate rocks and Ni-Cu ores from the Kammikivi sill. B. Detail of Re-Os isochron diagram of Fig. 75A. Open symbols mark sulfide-rich samples from Kammikivi with more than 1 wt. % S.

Isotopic data are plotted on $^{187}Re/^{186}Os$ vs. $^{187}Os/^{186}Os$ diagrams (Fig. 75). Included in Fig. 75 is a 2.0 Ga reference isochron with a chondritic Os initial ratio of 0.94 (using a decay constant of $1.639\times10^{-11}$ $y^{-1}$, Lindner et al., 1989). From the diagram, it is apparent that ferropicrites exhibit an extremely large variation in $^{187}Re/^{186}Os$, from less than 20 up to 10,000. Although there is an overlap between different rock types, a general rule is that the chemically most evolved samples from the spinifex zone or the gabbroic part of the differentiated bodies display highest $^{187}Re/^{186}Os$ and $^{187}Os/^{186}Os$ values while olivine cumulates and undifferentiated ferropicrites have the lowest values, and pyroxene cumulates lie in an intermediate position. As shown in Fig. 75, the large spread in $^{187}Re/^{186}Os$ values is primarily a consequence of the large variation in the abundance of Os during differentiation of the ferropicritic magma. The effective fractionation of Re from Os within ferropicritic lava flows demonstrates the suitability of this method for dating single differentiated lava flows. The Pechenga rocks display a truly huge variation in $^{187}Re/^{186}Os$ when compared with the variation reported previously for komatiite lava flows. Luck and Arndt (1985) measured values ranging from 10 to 50 for whole rock samples from a komatiite lava flow in Alexo. Walker et al. (1988) obtained a similar range for komatiite flows in Munro Township.

Using the $^{187}Re$ decay constant of $1.639 \times 10^{-11}$ $y^{-1}$ (Lindner et al., 1989), the Re-Os data can be regressed to give an age of 2035±60 Ma for the Kierdzhipori flow and an age of 2027±64 Ma for the Lammas flow. These ages are somewhat older than those obtained by the Sm-Nd and Pb-Pb methods but still overlap with them within the limits of uncertainty. The Y-axis intercepts of the isochrons for the Kierdzhipori and Lammas flows yield initial $^{187}Os/^{186}Os$ values of 0.913±0.02 and 1.16±0.11, respectively. These values are equivalent to $\gamma_{Os}$ values of -3.0±2.1 and +23±12. The initial ratio is most reliably estimated on the basis of samples with low $^{187}Re/^{186}Os$ because these are most insensitive to the error in the age determination. With an age of 1.97 Ma, the following initial Os ratios are obtained for such samples: 1748/3 1.098, S-2986/93.5 0.965, S-3077/322.5 0.960, and S-3R/731.4 0.987 corresponding to $\gamma_{Os}$ values between +1.6 and +16. Although the initial Os ratio is not yet precisely constrained, the available data with the exception of the Lammas flow indicate that ferropicritic rocks and presumably the mantle source of ferropicritic rocks had a $^{187}Os/^{186}Os$ value close to that of bulk earth at the time of the ferropicritic magmatism.

Although the Os isotopes for the metavolcanite samples define a moderately good isochron, many points do not fall on the regression line. One problematic sample, which was omitted when calculating the ages and initial ratios above, is 1748/8A, which represents the matrix portion of a globular rock. As will be discussed later, the globular structure is interpreted to have been generated through secondary processes, which partly accounts for the deviation of this sample from the regression line. The wide scatter in $^{187}Re/^{186}Os$ at approximately constant $^{187}Os/^{186}Os$ could be a result of recent loss of Re but no particular weathering effects can be seen in this sample. Furthermore, the disparate analytical results were obtained for aliquots of the same powdered sample and therefore it is difficult to find any geological reason for the scatter in $^{187}Re/^{186}Os$.

Other samples that deviate from the reference isochron in Fig. 75 include silicate rocks and sulfide ores from Kammikivi. The olivine cumulate Pet1/25.66 straddles on the isochron but the pyroxene cumulate (Pet1/5.40) and the gabbroic rock (Pet1/1.00) plot, respectively, beneath and above the reference line. All of the disseminated sulfide ore samples and the S-rich olivine cumulate Pet1/33.10 show radiogenic Os isotope compositions and clearly lie above the array formed by the silicate samples. The significance of these results will be discussed later in the section concerning the genesis of the Ni-Cu sulfide ores.

## Rb-Sr

The previous Rb-Sr isotopic data on ferropicritic rocks are restricted to those provided by Smolkin (1991), who analysed whole rock samples and single fractions of apatite and clinopyroxene from the Pilgujärvi intrusion. Because of the mobility of alkali and alkali earth elements, whole rock samples may give ambiguous isotope results. Therefore, Sr isotope analyses were restricted to mineral separates in this study. Three clinopyroxene fractions were separated from one lava flow and two intrusions. One of the pyroxenes (**S-2986/84.1**) from the S-2986 lava flow was also analysed for Sm-Nd isotopes. Sample **Pet1/5.40** is a pyroxene fraction from the pyroxenite unit of the Kammikivi sill while **Pet10/2.40** was separated from a pyroxenite from a drill core penetrating the Ortoaivi intrusion.

Two of the pyroxene fractions (Pet1/5.40, S-2986/84.1) were cleaned by hand-picking but this was not done for sample Pet10/2.40, since it seemed pure enough after heavy liquid separation. The Rb-Sr isotope analyses were performed at GFS in Espoo by H. Huhma. Mineral fractions were washed in very dilute HCL using ultrasonic bath. Chemical separation of Rb and Sr were performed using standard chromatographic methods. The isotope determinations were carried out on a VG-SECTOR 54 mass-spectrometer which was also used in producing new Pb and Nd isotope data. During this study, the mean $^{87}Sr/^{86}Sr$ of eight measurements of SRM987 Sr standard was 0.710235. $^{87}Sr/^{86}Sr$ was normalized to $^{86}Sr/^{88}Sr=0.1194$. The Rb-Sr results are shown in Table 25 together with the mineral analyses from Smolkin (1991).

The concentrations of Rb (0.108-1.29 ppm) and Sr (34.4-52.5 ppm) for the separated clinopyroxenes are clearly higher than the values measured for clinopyroxenes from Archean komatiitic and tholeiitic lava flows and sills (Fig. 82). For the Archean pyroxenes, Zindler (1982) and Hart and Brooks (1977) reported abundances ranging between 0.02-0.09 ppm for Rb and between 3.65-21.1 ppm for Sr. The relatively high concentrations of these elements in pyroxenes from the Pechenga rocks suggest that the negative anomalies at Rb and Sr, observed in the spidergram in Fig. 54, are artifacts of postmagmatic leaching of alkalies from the ferropicritic metavolcanites. Applying a pyroxene/melt partition coefficient of 0.1 for strontium (Irving, 1978), the equilibrium melt can be deduced to have contained more than 300 ppm Sr.

Pyroxenes display low $^{87}Rb/^{86}Sr$ values (0.01-0.07) thus being well suited for estimating an initial Sr isotope ratio. The calculated initial $^{87}Sr/^{86}Sr$ values at 1980 Ma are as follows: 0.70218 for Pet1/5.40, 0.70268 for Pet10/2.40, and 0.70255 for S-2986/84.1. The apatite fraction from the Pilgujärvi intrusion is high in Sr (809

**Table 25. Rb-Sr isotopic data for mineral separates from Pechenga (Pilgujärvi data taken from Smolkin, 1991).**

| Sample | Mineral | Location | Rb* (ppm) | Sr* (ppm) | $^{87}Rb/^{86}Sr$ | $^{87}Sr/^{86}Sr$ |
|---|---|---|---|---|---|---|
| Pet1/5.40 | Clinopyroxene | Kammikivi | 0.276 | 39.93 | 0.0200 | 0.702747±20 |
| Pet10/2.40 | Clinopyroxene | Ortoaivi | 1.29 | 52.53 | 0.07093 | 0.704704±20 |
| S-2986/84.1 | Clinopyroxene | Kierdzhipori | 0.108 | 34.39 | 0.00906 | 0.702810±20 |
| SA-22 | Clinopyroxene | Pilgujärvi | - | - | 0.08750 | 0.704900±158 |
| 149 | Apatite | Pilgujärvi | - | - | 0.0001 | 0.704810±100 |

* not corrected for blank.

ppm) and low in Rb (0.25 ppm), resulting in very low $^{87}Rb/^{86}Sr$ (0.0001) (Smolkin, 1991). As a result, the measured $^{87}Sr/^{86}Sr$ value of 0.70299 is representative of the initial Sr isotope ratio for the gabbro pegmatite from which the apatite separate was extracted. This value is slightly higher than those obtained for pyroxenes in this study. On the other hand, the initial ratio (0.70240) reported by Smolkin (1991) for the pyroxene from the Pilgujärvi intrusion falls between the values obtained for the Kammikivi and Kierdzhipori pyroxenes.

## Sulfur

Grinenko et al. (1967) have published a great number of sulfur isotope determinations on many Ni-Cu ore deposits from the Kola Peninsula. Figure 76 shows the results obtained by Grinenko et al. (1967) for Pechenga ores supplemented by a few analyses from Pushkarev et al. (1988) and Grinenko and Smolkin (1991). As pointed out earlier, the central zone of the Pechenga ore field is divided into eastern and western parts, where the intrusions occur at different stratigraphic levels in the productive pile. The same division is also reflected in the sulfur isotope data in Fig. 76. The western region, containing the Kaula, Kotselvaara, and Kammikivi deposits, is characterized by near chondritic $\delta^{34}S$ compositions, while the eastern region, represented by the Southwestern (Zdanov) deposit from the Pilgujärvi intrusion, yields heavier sulfur isotope values. A further significant feature in Fig. 76 is that there are no essential differences in the S isotope composition between disseminated (syngenetic), massive, and breccia (epigenetic) nickel-copper ores at Pechenga. This implies a common source of sulfur for the main ore types. These ore types in individual deposits display a limited range of variation, but in the case of vein-impregnation ores in phyllites close to the lower contact of the intrusions, the spread is greater.

Genkin et al. (1987) have analysed $\delta^{34}S$ for sulfides from Ni-mineralization discovered in a peridotite unit in the superdeep drill core. The $\delta^{34}S$ values in disseminated and conjugated brecciated and veinlet ores vary from +0.65 to +2.92 per mil and are relatively close to meteoritic in composition. Grinenko and Smolkin (1991) have analysed two samples of massive ore from the base of a 11.5-m-thick ultramafic-mafic body recovered in drill core S-2904 near the Kierdzhipori ore-bearing intrusion. According to Gorbunov et al. (1989), this unit is a lava flow but Grinenko and Smolkin (1991) regard it as a thin sill. The

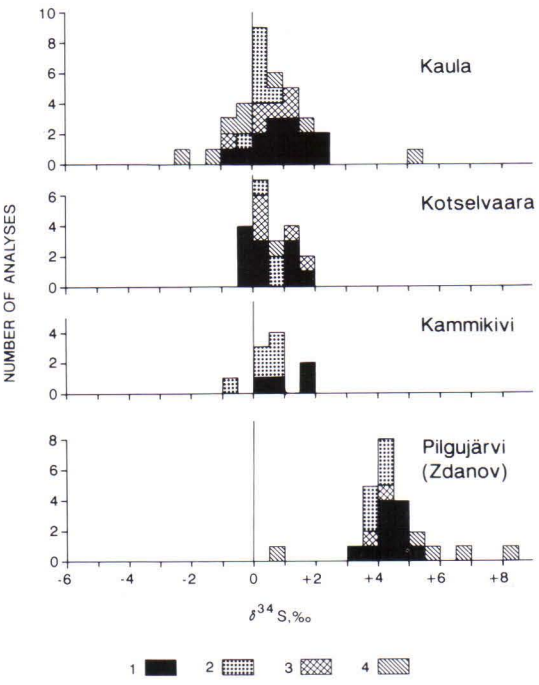


Fig. 76. Sulfur isotope composition of different types of Ni-Cu ores from various ore deposits. Data from Grinenko et al. (1967), Pushkarev et al. (1988) and Grinenko and Smolkin (1991). 1) disseminated ore in metaperidotite, 2) massive ore, 3) breccia ore, 4) Ni-Cu ore in footwall phyllites.

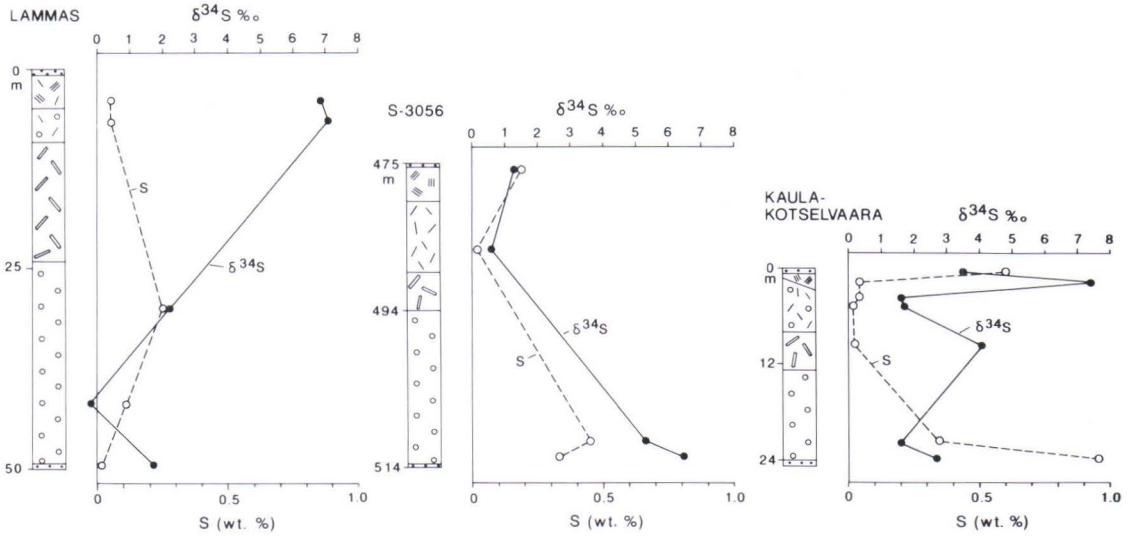


Fig. 77. Variation in concentration and isotopic composition of sulfur across three differentiated lava flows. Data are from Grinenko and Smolkin (1991).

samples yield near-chondritic $\delta^{34}S$ values of +0.4 per mil.

Recently, Grinenko and Smolkin (1991) have examined the S isotope composition of ferropicritic metavolcanites and silicate rocks from barren and ore-bearing intrusions. In contrast to the relative constant $\delta^{34}S$ composition of the sulfide ores, these display variable S isotope compositions. In layered ferropicritic lava flows, $\delta^{34}S$ ranges from -0.2‰ to +7.4 ‰ . Figure 77 illustrates three examples of the internal variation of the S isotope composition and the S concentration within individual lava flows. Common features in these sections include the heterogeneity of $\delta^{34}S$ and the enrichment of heavy sulfur in samples located close to the upper or lower contacts.

In the barren Northern Kotselvaara intrusion, Grinenko and Smolkin (1991) observed a systematic decrease of $\delta^{34}S$ from +8.7‰ to zero over a distance of ten meters upwards from the lower contact. Similar behavior of $\delta^{34}S$ is also seen in the mineralized Pilgujärvi intrusion as shown in Fig. 23. The lower margin of the intrusion has a $\delta^{34}S$ value of +8.7‰ , but $\delta^{34}S$ rapidly decreases upwards to values of less than +5‰ in the lower part of the ultramafic zone. Grinenko and Smolkin (1991) suggested that local assimilation of country rock sulfur during emplacement of the flow or intrusion caused the high $\delta^{34}S$ at the margins. Owing to the low sulfur contents of these rocks, their isotopic composition can be readily changed by exposure to reagents with a different S isotope composition. Fault zones are common at the contacts of many intrusions and flows. As these contact zones could have acted as channelways for circulating hydrothermal fluids, secondary alteration processes might also explain the heterogeneous S-isotopic composition close to the contacts of the lava flows and intrusions.

In order to clarify the provenance of sulfur in Ni-Cu deposits, it is crucial to know the S isotope composition of the S-rich metasediments occurring in the productive pile. According to Genkin et al. (1987), the sulfur isotope composition of pyrrhotite from productive pile metasediments in the superdeep drill core show rather heavy values: this composition reaches +20.97 per mil in tuffaceous sandstones and +19.46 per mil in phyllites.

In this study, three pyrite and two pyrrhotite fractions were separated from S-rich phyllites from the Kotselvaara area. S isotopic results for these minerals are shown in Table 21. The values, varying between +11.2‰ and +15.3‰ , are distinctly heavier than those of Ni-Cu sulfides in the Kotselvaara deposit (Fig. 76). Grinenko and Smolkin (1991) have also published two S isotope analyses for S-rich metasediments near the Kotselvaara intrusion. Their results of -4‰ and -5‰ deviate significantly from those obtained in this study. Grinenko and Smolkin (1991) also performed some S isotope measurements on host metasediments of the Kierdzhipori ore-bearing intrusion. Sulfide-rich phyllites exhibit $^{\delta 34}$S values heavier than +10 per mil while siltstones very poor in sulfur show a near chondritic $\delta^{34}$S composition. Akhmedov and Krupenik (1990) have recently measured sulfur isotope compositions of pyrites from different types of iron sulfide mineralizations in phyllites at various levels of the productive pile. They report a relatively restricted range from +1.2‰ to +3.2‰ with little lateral or vertical variation within the productive pile. These results are in conflict with the considerably heavier values measured in this work and Genkin et al. (1987), and they also deviate from the results of Grinenko and Smolkin (1991). From the review presented above, it is obvious that more data are needed to better understand the S isotopic systematics of the S-rich sedimentary rocks in the productive pile.

In summary, the S isotope composition of the S-rich Ni-Cu ore samples, including disseminated, massive and breccia ores, display relative homogeneous values, not deviating substantially from the chondritic composition in most deposits. The Zdanov deposit from the Pilgujärvi intrusion seems to be an exception showing slightly heavier values. The variation is larger in S-poor samples of ferropicritic metavolcanites and rock types from gabbro-wehrlite intrusions. Samples close to or at contact zones commonly show the heaviest S isotope compositions. There are many indications that S-rich tuffaceous and phyllitic metasediments in the productive pile are enriched in heavy sulfur with $\delta^{34}$S values varying between +10‰ and +20‰. Some investigators have, however, presented results that are closer to the chondritic value or even negative. The extent of the heterogeneity of sulfur isotopes in sedimentary sulfides is thus still open to question.

## ORIGIN OF THE GLOBULAR FERROPICRITIC ROCKS

The globular structures in ferropicritic rocks at Pechenga have previously been regarded as products of silicate liquid immiscibility (SLI) (Smolkin et al., 1987), by analogy with explanations proposed for mesoscopically similar structures in some Archean ocellar komatiites (Ferguson and Currie, 1972; Cawthorn et al., 1979). Other mechanisms, however, can also account for the generation of these structures. This question has been examined in detail by Hanski (in press) and the results are briefly summarized below.

The globular structures are indeed superficially reminiscent of features attributed to liquid immiscibility, including for example light-colored spheroidal aggregates, present at all stages of coalescence, in a darker matrix. The iron-rich nature of the parental magma also makes ferropicrites favourable candidates for SLI. However, several lines of field, microscopical, mineralogical, and chemical evidence argue against the immiscibility hypothesis, as discussed below.

The large size of the globules and the relatively similar chemical compositions between the

globules and matrix suggest low surface tension at the interface of the alleged conjugate liquids. However, no signs of distortion due to the influence of a gravitational field or shear during flow have been observed. On the other hand, the relatively large size of the globules (even close to the margin of narrow dikes) renders the possibility of the nucleation and growth of the globules *in situ* from a melt unlikely.

The globular rocks are composed of phenocrystal to microcrystal phases (olivine, clinopyroxene, kaersutite, magnetite, and ilmenite) with a large range in grain size, set in a fine-grained mesostasis. In all cases, the adjacent globule and matrix possess identical modal proportions, grain sizes, morphologies, and orientations of all these phases, as strikingly demonstrated, for example, by the spinifex-textured varieties of globular rocks (Fig. 20). The only mineralogical dissimilarity is in the originally glassy mesostasis which is composed of chlorite in the matrix and alkali feldspar, quartz, and chlorite in the globules. It is extremely difficult to envisage how the crystallization of the identical minerals in the same proportions could have led to the formation of such dramatically different mesostasis compositions in the globules and their matrix. When a textural zonation, such as variation in the grain size or crystal habit of clinopyroxene, is observed in a sample, the zonation is independent of the globule-matrix boundaries. This would not be expected for conjugate immiscible liquids which have different structures and solidus temperatures and should therefore respond differently to the cooling regime.

Microprobe analyses do not reveal any differences in the compositional ranges of the crystalline phases between the globules and matrix. This also applies to the rapidly crystallized late-stage microlites which should reflect the diverging chemical compositions of the conjugate liquids if SLI is responsible for the globular structures.

Geochemically, the globules and the matrix differ most clearly with respect to those components which are generally regarded as mobile during alteration processes. Immobile trace element characteristics are similar in the globules and the matrix. No preferential partitioning of high field strength elements into the matrix or volatile partitioning, as reflected by modal kaersutite, into the globules has been observed, contrary to what would be expected according to the immiscibility model. The high sulfur content of the low-iron globules relative to that in the high-iron matrix is not compatible with a magmatic partitioning of sulfur between two immiscible liquids because the solubility of sulfur in silicate melt is positively correlated with the iron content of the melt (e.g., Poulson and Ohmoto, 1990).

The most important chemical components of a silicate liquid which control the stability of igneous amphibole are water and alkalies (Gilbert et al., 1982). Given the substantial differences in total alkali contents of the globules and matrix (Fig. 51), it is difficult to understand the similar modal amphibole contents in both without invoking substantial postcrystallization mobility of alkali elements in the globular rocks.

The data presented above rule out the involvement of all known magmatic models in the formation of the globular structures in the Pechenga ferropicrites. A solid-state hydrothermal/metamorphic diffusional process that affected the originally glassy mesostasis is inferred to be the only feasable mechanism which can account for the observed characteristics of the globular rocks. Although the elimination of a magmatic origin by itself implies a secondary origin for the globules, the exact alteration mechanism that produced rounded light-weathering segregations in a dark matrix remains unclear. One reason is that it is not easy to say which part of the rock, the globules or the matrix, is more representative of the rock's original composition. All that can be said for certain, without further research, is that both of them are mineralogically and chemically altered.

## AMPHIBOLE AS A PALEODEPTH INDICATOR?

Kaersutitic amphibole is a characteristic mineral of ferropicritic intrusive and extrusive rocks. Its mode of occurrence as overgrowths on spinifex pyroxenes, groundmass needles, or poikilitic grains and its Ti-rich composition rule out a xenocrystic, phenocrystic, subsolidus, or metamorphic origin. Instead, these features undoubtedly argue for *in situ* crystallization from a hydrous magma after the emplacement of the lava flows and intrusions.

The coexistence of hydrous amphibole with silicate melt requires that a considerable amount of water was dissolved in this melt. The solubility of water in silicate melt is strongly pressure-dependent, decreasing to negligible when pressure is reduced to 1 atm. It follows that the existence of hydrous igneous amphibole can in principle be utilized to constrain the pressure of crystallization of a magmatic body. Specifically, the occurrence of *in situ* crystallized amphibole in a volcanic rock may give an indication of the water depth of eruption of the volcanic unit.

Figure 78 presents phase diagrams of water-bearing systems relevant to this study. These diagrams illustrate the principal features of hydrous systems including negative dT/dP values of the solidus and liquidus as opposed to the positive slope of the amphibole-out curve at low to moderate pressures. Amphibole is stable with a silicate liquid under the P-T conditions between the solidus and the amphibole-out curve. A significant feature in the diagrams is the point where the amphibole-out curve is transected by the solidus of the system (Fig. 78A-C). This point marks the minimum pressure at which amphibole is stable with a silicate liquid. There are only a few experimental determinations of this point in the literature but it is generally thought that hydrous phases are not stable with a silicate liquid under P conditions less than 0.5 kbar (Burnham, 1979).

Spulber and Rutherford (1983) determined liquidus phase relations of two oceanic tholeiites and found that the crossing of the solidus and amphibole liquidus occurs at 1.5 kbar in both systems when $P_{H2O}$ is about $0.7P_{total}$ (Fig. 78A,B). Because the thermal stability of amphibole increases with increasing water fugacity at pressures below about 4 kbar (Holloway, 1973), the minimum pressure of 1.5 kbar obtained by Spulber and Rutherford would be lowered if the experiments had been performed under water-saturated conditions. Condliffe (1976) conducted experiments on an olivine gabbro under $H_2O$-saturated conditions and obtained a lower limit of 1.5 kbar for the amphibole stability field (Fig. 78C).

Because the maximum thermal stability of amphibole is expected in melts that are closest to amphibole in bulk composition, recent experiments by Johnson (1990) on a mixture of equal proportions of Fe-Ti basalt and natural kaersutite are particularly pertinent when discussing the stability of kaersutite. Under water-saturated conditions, she obtained kaersutite at 1 kbar pressure but could not synthesize this mineral at 0.5 kbar pressure (Fig. 78F). She also conducted experiments on a basanite and transitional basalt with $P_{H2O} < P_{total}$. These starting materials yielded amphibole at 1.0 and 1.5 kbar, respectively (Fig. 78D,E). Some other hydrothermal experimental investigations also exist where amphibole has been observed to be stable with a silicate liquid at 1 kbar pressure but runs were not extended to lower pressures (Ford, 1976; Gibb and Henderson, 1976; Luhr, 1990; Sisson et al., 1991; Beard and Lofgren, 1991). Extrapolations of these results to lower pressures is not easy because of the strong pressure-dependence of the thermal stability of amphibole at low pressures.

When applying diagrams such as those in Fig. 78 to ferropicritic metavolcanites, it is worth remembering that amphibole commenced crystal-

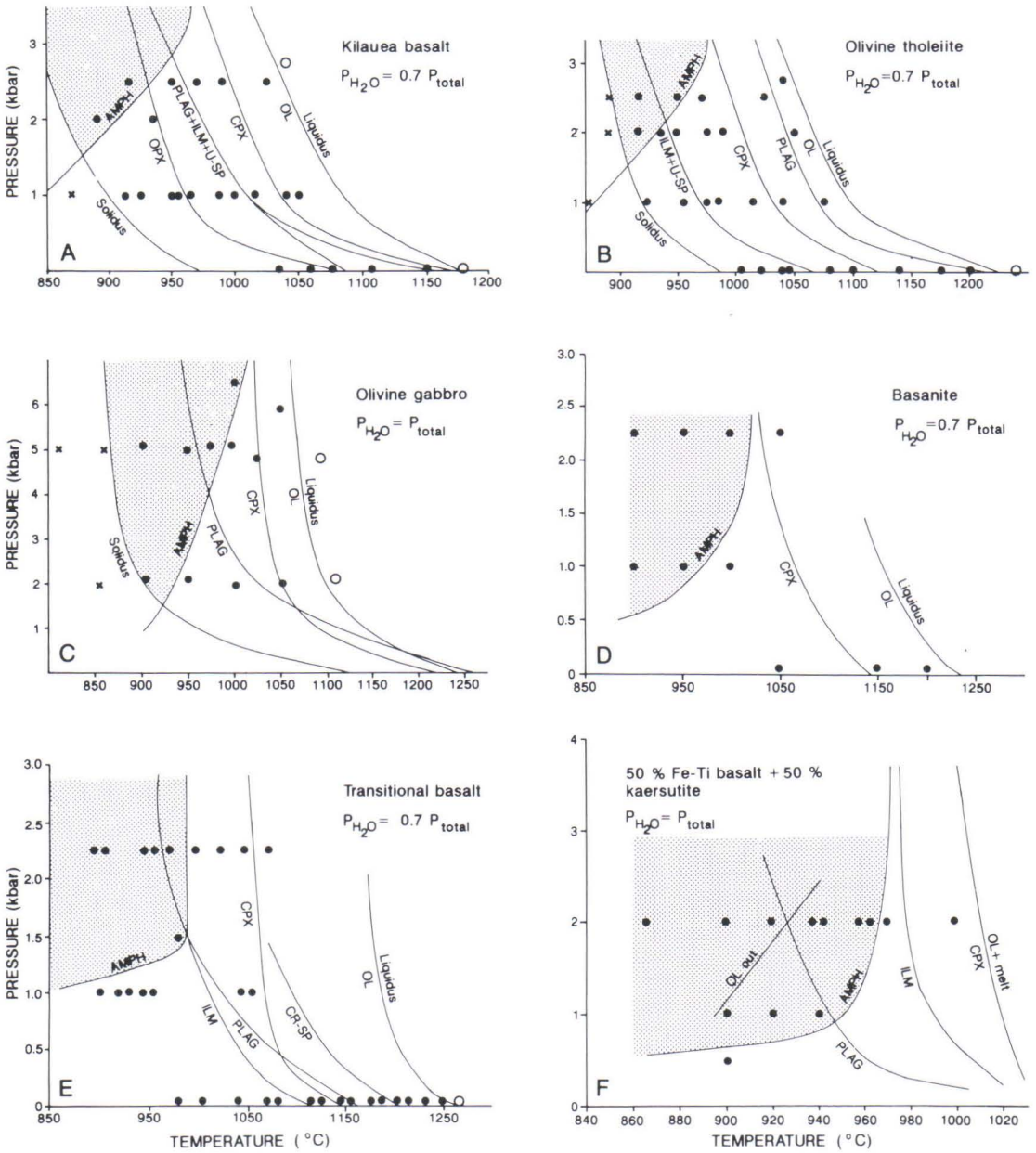


Fig. 78. Experimentally determined liquidus phase relations for hydrous basaltic systems. Data sources: A-B, Spulber and Rutherford (1983); C, Condliffe (1976); D-F, Johnson (1990). Circles, above silicate liquidus; dots, glass+crystals; crosses, below solidus; shaded area, stability field of igneous amphibole.

lizing around clinopyroxene crystals at temperatures far above the solidus because, in many kersutite-bearing samples, the onset of amphibole crystallization took place while there was still up to 50% of melt which subsequently quenched to form glassy groundmass. This means that the crystallization took place at a water pressure higher than indicated by the crossing point of the solidus and the amphibole-out curve.

Experimental studies on water-bearing systems show that at total pressures of at least up to 15 kbar, the liquidus temperature of amphibole increases as $P_{H2O}$ increases. In contrast, the liquidus temperature of plagioclase is strongly suppressed by the increase of water pressure (Fig. 78). As a result, when $P_{H2O}$ increases enough, the liquidus curves of amphibole and plagioclase transect each other and eventually amphibole's liquidus temperature becomes higher than that of plagioclase. Thus, if amphibole is observed to precede plagioclase in a crystallization sequence, as is the case in ferropicritic metavolcanites, a relatively large $P_{H2O}$ can be deduced to have prevailed during the solidification of the rock. The water pressure at which the amphibole-plagioclase liquidus crossover takes place has been determined in many experimental studies. It commonly varies between 1-4 kbar depending on the melt composition and water fugacity (see Fig. 78).

In summary, the experimental data suggest that a water pressure of at least 0.5 kbar is required to stabilize hydrous amphibole with a silicate liquid. Provided that the load pressure is caused by the overlying water column, as is the case with submarine volcanic rocks, this pressure corresponds to a water depth deeper than 5 km under water-saturated conditions and even larger depths under water-undersaturated conditions.

The occurrence of *in situ* crystallized primary amphibole in ferropicritic volcanic rocks therefore suggests eruption and crystallization on the floor of a deep ocean basin. The sedimentary and volcanic record of the Pechenga Series records evolution from shallow-water to deeper-water conditions. However, such a huge water depth as indicated by the experimental data is difficult to reconcile with the proposed tectonic evolution of the Pechenga basin. Evidence for this is provided by the ultrafelsic tuffs which occur together with ferropicrites in the Pilgujärvi Suite and form a marker horizon within this unit. These tuffs contain granite and granite-gneiss fragments and a zircon population with an Archean age (Borisov and Smolkin, 1992). These features indicate an old crustal source for these rocks or at least their ascent through such rocks and hence the existence of an Archean sialic basement under the basin during the ferropicritic volcanism and probably during the deposition of other sedimentary and volcanic rocks of the Pechenga Series as well.

According to Stromov (1985), the interlayering of thin units of pelitic, arenaceous and silty metasediments, the well-sorted character of sedimenary material, and the presence of intraformational conglomerates and ripple marks in the productive pile are evidence for the formation of these rocks in a shallow-water environment. Additional evidence against a very deep-water regime comes from the low boron content of pelitic metasediments in the Pilgujärvi Suite, indicating low water paleosalinity (Melezhik, 1987), as well as from nonmarine Sr isotopic compositions of carbonate rocks in the same formation (V. Melezhik, pers. comm., 1992). Furthermore, Ivanova et al. (1988) reported the finding of coccoid microphytofossils in cherts in the middle part of the Kolosjoki Suite. These fossils indicate a relatively shallow water depth at that time because sunlight is essential for phototrophic algae.

One solution to the kaersutite problem could be the stabilization of amphibole due to internal overpressuring in the inner parts of the flows. In principle, this overpressure can be caused by resurgent boiling of a cooling melt that becomes saturated with water due to crystallization of anhydrous phases. The maximum overpressure that gas exsolution can generate in a magmatic body is dependent on the tensile strength of the overlying rocks. Failure takes place when the overpressure reaches a value of about twice the tensile strength (Tait et al., 1989). Touloukian et al. (1981) have experimentally determined a tensile strength of about 90 bar for basalt. This result was obtained

for a pristine sample of small size and therefore can be regarded as an upper limit. In lava flows having fractured flow tops, the tensile strength is expected to be much lower. Consequently, internal overpressuring is not a likely explanation for the crystallization of magmatic amphibole in lava flows.

One possibility is that the amphiboles which crystallized in the Pechenga rocks are close to pure oxy-amphiboles, where the OH site is filled with $O^{2-}$. Substitution of OH for O is accompanied by oxydation of ferrous iron to ferric iron. According to Aoki (1963), $Fe^{3+}/Fe^{2+}$ in oxykaersutites is greater than 2. In the Pechenga amphiboles, the averages of the stoichiometrically-acceptable lower and upper limits of the ferric iron content calculated using the method of Spear and Kimball (1984) result in $Fe^{3+}/Fe^{2+}$ values mostly between 0.2-0.3 (Table 4). This result, coupled with the coexistence of kaersutite with titanian phlogopite in the Pechenga ultramafic rocks, indicate the hydrous nature of the amphibole. It should be mentioned that because oxy-amphiboles have not been produced experimentally in dry silicate systems, it is uncertain whether they can crystallize as primary magmatic phases. Instead, oxy-amphiboles have been shown to be the products of dehydration-oxidation of hydrous magmatic amphiboles (Aoki, 1963).

It is well known that substitution of OH by halogens in the amphibole structure increases the thermal stability of amphibole (Holloway and Ford, 1975; Foley, 1991). Pure F-end member amphiboles can be stable at high temperatures even at atmospheric pressure (Troll and Gilbert, 1974). However, the effect of halogens on amphibole stability have rarely been studied at magmatic temperatures. Mahood and Baker (1986) produced a small amount of kaersutite in an experimental crystallization study of an alkali basalt under anhydrous conditions at 1 atm pressure. They suggested that after about 70% crystallization, concentrating the F of the original rock powder into the remaining liquid might have stabilized amphibole. Also Bailey and Cooper (1978) synthesized amphibole in dry experiments on a pantellerite and ascribed it to the effects of halogens.

Microprobe analyses of kaersutites from the Pechenga rocks reveal a maximum fluorine content of less than 0.6% (Table 4) which leads to the inference that the composition of these amphiboles is dominated by the hydrous end-member. In the absence of relevant experimental data, the effect of such an amount of fluorine on amphibole stability is difficult to estimate precisely. Nevertheless, a rough assessment may be obtained from the solubility data of water in silicate melt.

Water solubility in basaltic liquid is modelled by using the experimental solubity measurements of Hamilton et al. (1964). Their data in the pressure range of 1-6 kbar is regressed to the following equation:

$$X(H_2O)\ (\text{mol. }\%) = C_1 P^{1/2}(\text{bar}) - C_2$$

where $C_1$=0.336 $bar^{-1/2}$ and $C_2$=0.614. Extrapolation of the solubility to zero at zero pressure results in the coefficients $C_1$=0.316 $bar^{-1/2}$ and $C_2$=0 at pressures below 1 kbar pressure. The solubility of water in a basaltic melt as a function of pressure, as calculated by the above equation, is shown in Fig. 79A. As the experiments by Johnson (1990) and others indicate, the lower pressure limit of the stability field of hydrous amphibole is somewhere between 0.5 and 1 kbar. In the following calculations, it is assumed that the pressure is 0.7 kbar. At this pressure, the solubity limit of water is about 8.3 mol. %. Because hydrous amphibole has a fixed amount of water in its lattice, one can calculate the partition coefficient of water between amphibole and silicate liquid as a function of pressure by using the water solubility curve in Fig. 79A. This coefficient $K_d$(Sat) varies antipathetically with water solubility and represents the minimum value of the partition coefficient at pressures higher than 0.7 kbar.

The maximum thermal stability of amphibole at pressures less than 4 kbar is achieved under water-saturated conditions (Holloway, 1973). It is therefore assumed that $P_{H2O}=P_{total}$ at 0.7 kbar. At

higher pressures, however, kaersutite can also coexist with a silicate liquid under water-undersatured conditions. This does not, however, mean that the minimum water content of liquid to stabilize amphibole is lower at higher pressures. To estimate the minimum water abundance, it is expedient to use bulk compositions close to amphibole in order to minimize the possible destabilizing effects of other components in the liquid. Merrill and Wyllie (1975) carried out high-pressure experiments on a bulk composition of kaersutite + 0.9 wt. % $H_2O$. They discovered that this amount of water was insufficient to bring amphibole to the liquidus of the system even at pressures of up to 20 kbar. Holloway (1973) used pargasite+$H_2O$ as a starting material. In experiments with $X_{H2O}$ 0.3 in the fluid phase, he calculated water contents of 3.2 and 3.8 wt. % in the liquid phase at pressures of 5 and 8 kbar, respectively. Jakobsson and Holloway (1986) in turn obtained kaersutite as a liquidus phase at 15 kbar in a basanite with about 4 wt. % $H_2O$. By using these experimental data and the water saturation point at 0.7 kbar as constraints, a line depicting the minimum water content to stabilize amphibole at pressures 0.7-5 kbar is drawn in Fig. 79A. This line can be used to calculate the maximum partition coefficient $K_d$(Max) of water between amphibole and silicate liquid (Fig. 79A).

An estimation is required for the distribution of water between amphibole and liquid below 0.7 kbar for use in calculations determining the minimum fluorine content in amphibole that is necessary to complement the water defiency in the amphibole lattice, below the stability limit of pure hydrous amphibole. The partition coefficient $K_d$ of water below 0.7 kbar is probably lower than 0.48, the value at 0.7 kbar, as deduced from the negative temperature-$K_d$ relationship and the increasing liquidus temperature of amphibole with decreasing pressure. However, when attempting to determine the minimum fluorine content of amphibole, it is expedient to use high $K_d$ values of water, such as the extrapolated $K_d$ values given by the $K_d$(Max) curve.

By using the extrapolated $K_d$(Max) values and the solubility of water in silicate melt, the water content of amphibole can be calculated. The result is shown in Fig. 79B. Because the sum of OH and F in the amphibole lattice is constant, it is easy to calculate the fluorine content that is necessary to saturate liquid with amphibole at low pressures (Fig. 79B). It is emphasized that the fluorine content of amphibole here obtained is the minimum value that is needed to stabilize amphibole at a given pressure. From Fig. 79B, it can be seen that in order to suppress the lower pressure stability limit of igneous amphibole from 0.7 kbar to 0.2 kbar, amphibole should be composed of about half of the fluorine component which is a

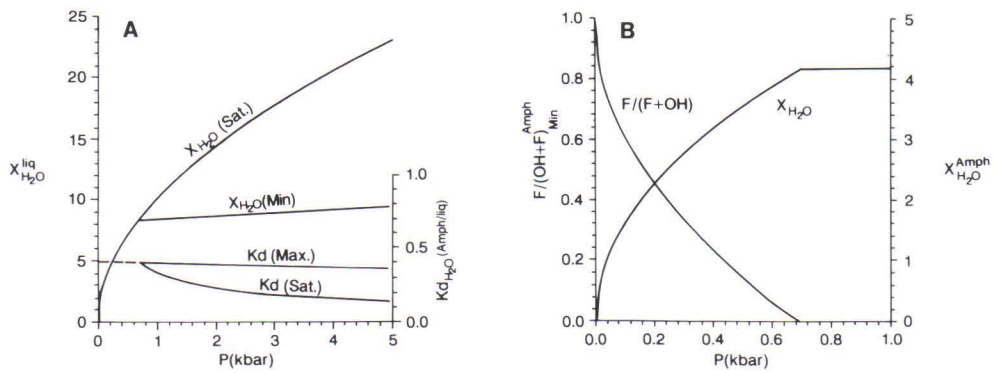


Fig. 79. A. Calculated distribution ($K_d$) of water between amphibole and silicate liquid based on the water solubility data [$X_{H2O}$(Sat.)] of Hamilton et al. (1964) and experimental phase equilibrium data on hydrous systems. B. Estimated minimum F/(F+OH) in amphibole for stability with silicate liquid at very low lithostatic load pressures (for more details, see text).

much higher value than observed in the Pechenga kaersutites. However, there are many uncertainties in the calculations discussed above and more experimental investigations with mixed $H_2O$-halogen fluids are needed concerning the effects of halogens on amphibole stability at low pressures.

Kaersutitic amphibole commonly occurs in volcanic rocks as phenocrysts or xenocrysts and often displays resorption effects. In the literature, there are, however, some descriptions of such amphiboles, occurring in both ancient and modern volcanic rocks, which can be deduced to have been crystallized *in situ* after the emplacement of the host volcanic rock. Brown magmatic amphibole as an interstitial phase has been reported in some Archean thick lava flows in the Abitibi greenstone belt. These include komatiitic and tholeiitic flows such as the Fred's and Theo's Flows at Munro Township (Arndt et al., 1977) and the Boston Creek Flow at Boston Township (Stone et al., 1987). Arndt (1986a) described an amphibole-bearing komatiite lava lake at Munro Township and argues that it was erupted in a relatively shallow water environment.

More recent examples of lavas containing *in situ* crystallized kaersutite are provided by alkaline metavolcanites from the Forties Field in the Mesozoic North Sea Basin (Fall et al., 1982; Latin et al., 1989). A characteristic feature of ankaramite and hawaiite lavas in this area is the presence of groundmass kaersutite and biotite. Microprobe analyses were made on kaersutites in an ankaramite sample from the Forties region, kindly donated by F.G.F. Gibb. These contain 0.44%-0.845% F and 0.05-0.09% Cl, and are thus far from pure halogen end-members. The North Sea volcanites were deposited on Triassic red beds and are overlain by a 2-3 km thick sequence of Mesozoic and Cainozoic metasediments. They occur at the triple junction of three graben structures generated during a continental rifting episode and are interpreted to have erupted under shallow water to even subaerial conditions (Gibb and Kanaris-Sotiriou, 1976).

More recent amphibole-bearing volcanic rocks have also been described in the literature. These include boninites which are relatively silica-rich, primitive volcanites erupted in submarine trenches associated with island arcs. Their hydrous nature is shown by the presence of pargasitic amphibole which occurs in a similar fashion as kaersutite in ferropicrites, viz. fringes around pyroxenes and discrete groundmass needles (Crawford et al., 1988). Hekinian (1974) reported the first occurrence of magmatic amphibole on the floor of the Indian Ocean at DSPD Site 211, close to the Christmas Islands. Here at a water depth of 5535 m, the drill core begins with a 400-m-thick pile of sediments which are underlain by a succession of slightly nepheline-normative basic lavas. Hekinian (1974) named these amphibole-bearing basalts and amphibolites. They contain up to 80% modal amphibole which occurs as radiating clusters of arborescent crystals indicative of rapid *in situ* crystallization.

Recently, Hekinian et al. (1991) reported an occurrence of kaersutite-bearing nephelinetephrites from the Ra Seamount in the Austral hot spot region in the South Pacific. These volcanites form highly vesiculated pillow lavas and are composed of quenched kaersutite, clinopyroxene, glass, and sparse olivine. Tephrites were recovered from the flank of the seamount at 1310-1480 m depth. The depth of eruption was probably not this deep, because the summit of the seamount at a depth of 1040 m is covered with coralline material and coarse-grained foraminiferal sand, suggesting that it was formerly near or at the surface.

Another location worth mentioning in the Pacific Ocean is the intraplate region SW of Hawaii. Bass et al. (1973) and Morawski et al. (1975, 1976) described kaersutite-bearing alkali basalts recovered at deep sea drilling site 165A. Kaersutite occurs as rims around prismatic titanaugites and also as a groundmass phase, particularly in more coarse-grained patches in the groundmass. The basalts were penetrated at a depth of about 450 m below the sea floor and about 5,500 m below the sea surface. However, according to R. Moberly (pers. comm., 1991), the water depth was less, about 3,400 - 3,800 m during the time of emplacement at the assumed eruption site on the upper part of the flank of the mid-ocean ridge.

The above examples of natural, *in situ* crystallized amphiboles from modern ocean floor environments indicate that amphibole can crystallize from alkaline magmas at pressures less than 0.5 kbar, perhaps even at 0.1 kbar. However, because the halogen contents of the amphiboles in these lavas have not been documented, it is difficult to judge their significance.

Kaersutitic amphibole is a typical mineral in some alkaline hypabyssal dikes. In general, the depth of crystallization of dikes is not easy to determine precisely and therefore can seldom be used to infer stabilities of minerals. However, according to Philpotts (1972), field evidence suggests that a kaersutite-bearing camptonite dike in the Monteregian region was emplaced at a depth corresponding to a load pressure of 0.3 kbar. A similar pressure was estimated by Henderson and Gibb (1987) for the Lugar theralite sill which contains poikilitic, *in situ* crystallized kaersutites.

As a final point, it should be noted that the crystal habit of amphibole in many of the volcanic rocks discussed above, including ferropicrites from Pechenga, is evidence of rapid crystallization. Laboratory experiments on hydrous rock compositions have demonstrated that amphibole readily nucleates as a quench phase (Green, 1973; Graham, 1981). On the other hand, with increasing cooling rate of a basic melt, the nucleation temperature of feldspar has been observed to decrease more than that of mafic anhydrous silicates (Walker et al., 1976). The cooling rate may thus greatly affect the relative crystallization temperatures of amphibole and plagioclase and the indiscriminate application of crystallization sequences from equilibrium phase diagrams, like those in Fig. 78, to natural rapidly crystallized rocks may result in erroneous estimations of intensive parameters. The influence of disequilibrium crystallization of amphibole on its lower pressure stability limit is difficult to assess because controlled cooling rate experiments of water-bearing systems at low pressures are extremely rare (Baker and Grove, 1982). In any case, the occurrence of amphibole in the inner parts of thick lava flows, for example at Pechenga and Munro Township, indicate that quench crystallization does not provide a satisfactory solution to the enigmatic occurrence of amphibole in submarine volcanites.

In conclusion, there seems to be an apparent discrepancy between the interpreted eruption conditions of some ancient and modern, amphibole-bearing lava flows and the huge water depth (>5 km) inferred from the experimentally determined low-pressure stability of magmatic amphibole. More low-pressure experimental studies with mixed halogen-$H_2O$ fluids and empirical data on compositions of amphiboles from modern submarine environments are needed before magmatic amphibole can be used as a paleodepth indicator of ancient volcanic rocks.

## GENESIS OF THE Ni-Cu SULFIDE DEPOSITS

Since the first studies of the Pechenga Ni-Cu deposits, a primary magmatic model of ore formation, in which sulfide liquids segregated through immiscibility from a mafic or ultramafic magma, has been the most favored explanation for the deposits (Väyrynen, 1938). Hydrothermal models have also been proposed, but these were decisively refuted by Gorbunov (1968). He presented several microscopic and mesoscopic arguments for the existence of premetamorphic, syngenetic sulfides. These include the presence of sulfide droplets within olivine and pyroxene crystals, the sideronitic texture of disseminated ores where sulfide remained between silicate minerals

in the form of interstitial liquid, the strata-bound nature of the Ni-Cu sulfide mineralizations and their concentration in the lower peridotitic parts of the hosting intrusions, the distinctly asymmetric structure of the sheet-like ore bodies, and their sharper contacts with the lower wall in comparison the hanging wall. These features, in conjunction with the chemical composition of the ores, which suggests equilibration with a basic-ultrabasic magma, demonstrate that sulfides were accumulated in a liquid state near the basal parts of magma chambers under the influence of gravity.

Although the primary magmatic origin of the disseminated ores is no more in doubt, there still exist important, incompletely resolved questions, including the timing of sulfide separation and the source of sulfur. The occurrence of sulfur-rich metasediments in the productive pile has led some authors to propose models in which the ores result from the interaction of picritic magma with the enclosing country rocks and scavenging of sulfur from the sediments to combine with chalcophile elements from the magma. Stromov (1985) made a paleogeological reconstruction of the productive pile and distinguished five stratigraphic levels which appear to control the location of the ore-bearing intrusions. He also noted that sedimentary rocks at these horizons are rich in iron sulfides and have a S content varying between 5-24%. Stromov (1985) interpreted this regularity in terms of a model involving the injection of ultrabasic intrusions into unconsolidated, gently dipping sediments, in which some intrusions invaded sulfide-bearing layers and became enriched with assimilated sulfur, resulting in essentially *in situ* segregation of syngenetic Ni-Cu sulfides.

Gorbunov (1968) regarded the interaction of the ore-forming magmas with silica-rich country rocks as a potential cause of the formation of an immiscible sulfide phase but according to him, the magma was originally rich in sulfur. The results of isotopic studies have also led to inferences of a juvenile sulfur source. According to Grinenko et al. (1967) and Pushkarev et al. (1988), sulfur and lead isotopic data suggest a predominantly mantle origin for sulfur in the Ni-Cu sulfide deposits. Only in rare cases, such as the Zdanov deposit, is a component of crustal sulfur possible (Grinenko et al., 1967).

There are also different opinions concerning the timing and mode of formation of the breccia and massive ores. However, two things are sure: the chemical and isotope data show unequivocally that these ore masses share the same ultimate source for sulfur and ore metals as the associated primary disseminated ores, while field and microscopic data attest that massive and breccia ores have been affected by intensive tectono-metamorphic transformations. Zak et al. (1982) concluded that epigenetic massive and breccia ores were generated from preexisting magmatic disseminated ores in fault zones during regional metamorphism. However, they noted that the degree to which concentration of ore material took place during the magmatic stage proper is not fully understood. In the light of the 'billiard-ball model' put forward to explain massive Ni deposits in mineralized komatiite lavas (Usselman et al., 1979), it is possible that some parts of the massive ores are the result of pooling of sulfides at the base of the intrusions during the magmatic stage. Abzalov et al. (1991b) suggested on the basis of Pb-Pb isotope analyses of massive ores that these segregated during the emplacement of the ore-bearing intrusions and were later remobilized during a tectono-metamorphic event. According to Smolkin (1991), it is possible that segregation of sulfides already took place during the ascent of ferropicritic magma and rich massive ores in some deposits were generated by independent injection of a sulfide melt. The limited field and analytical data gathered in this study do not permit any thorough examination of questions concerning the origin of the massive and breccia ores. However, the available data can be used to evaluate the provenance of sulfur in the Pechenga ore deposits.

## Geochemical evidence

When making a geochemical comparison between ore-bearing intrusions and barren ferropicritic metavolcanites, the question arises as to whether there exist any differences that might be attributed to contamination of the magma of ore-bearing intrusions with material from the surrounding sulfide-rich sediments. Relevant elements, which are appropriate for revealing such contamination, should be nonchalcophile, in order to avoid the effects of sulfide fractionation and accumulation, olivine-incompatible because of the possible effects of olivine fractionation or accumulation, and relatively immobile due to the possible effects of alteration. The following elements fulfill these requirements: Al, Ti, P, V, Sc, Zr, REE, Th, U, Ta, Nb. Analyses of these elements for one S-rich phyllite from the Kotselvaara area and one S-poor phyllite from the Kammikivi area are presented in Fig. 80 as a spidergram normalized to a typical ferropicrite. The most striking features are the high uranium and low phosphorous contents of the metasediments giving rise, for example, to high U/Sm and Al/P values. It follows that if a significant amount of assimilation has taken place, it should be detected by comparing ratios involving U or P.

As an example, Fig. 81 illustrates Sm and U contents for ferropicritic metavolcanites, ore-bearing gabbro-wehrlite intrusions, and phyllites. In the phyllites, Sm/U is extremely low compared to that in metavolcanites and intrusions and no clear distinction can be made between Ni-bearing and barren magmatic bodies. This does not, however, rule out a small amount of assimilation of country rocks, as is shown by the mixing calculations. Figure 81 demonstrates how the Sm/U value of the ferropicritic magma changes with a bulk assimilation of 5% of phyllitic material compositionally equivalent to samples A and B. It is obvious that such a small degree of contamination is difficult to detect by using whole rocks analyses of Sm and U. The reason for this is that the ferropicritic magma has relatively high concentrations of many incompatible elements whose ratios are therefore not easily affected by assimilation processes.

Although there is some uncertainty in to what extent the measured Se/S and Te/S values represent the original magmatic values of the sulfide liquid, the preponderance of Se/S values greater than $100\times10^{-6}$ and close to chondritic Te/S values in disseminated ores from the western ore field suggest that sulfur is mostly magmatic in origin. Figure 68 compares phyllites and sulfides separated from them with disseminated Ni-Cu ores in terms of their Se, Te, and As contents. Although the As concentration of the sedimentary samples is highly variable, it is obvious that their As/Se and As/Te values exceed cosmic values (0.1 and 8, respectively; Anders and Grevesse, 1989) by many orders of magnitude and differ drastically from ratios observed in the Kotselvaara, Kammikivi, and Ortoaivi Ni-Cu deposits. As/Se in these disseminated ores is slightly higher than the cos-

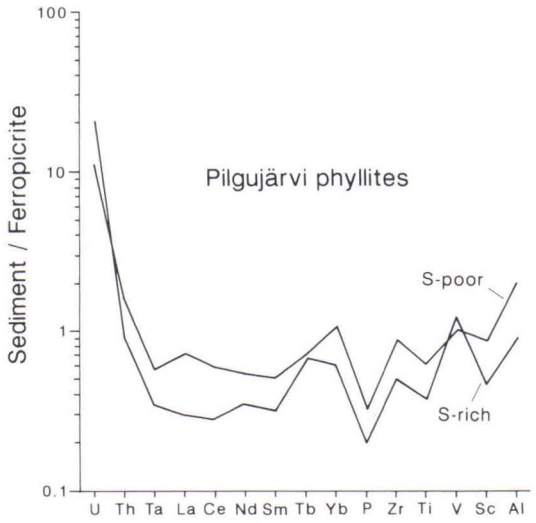


Fig. 80. Compositions of sulfide-rich phyllite from the Kotselvaara area and sulfide-poor phyllite from the Kammikivi area, normalized to typical ferropicrite.

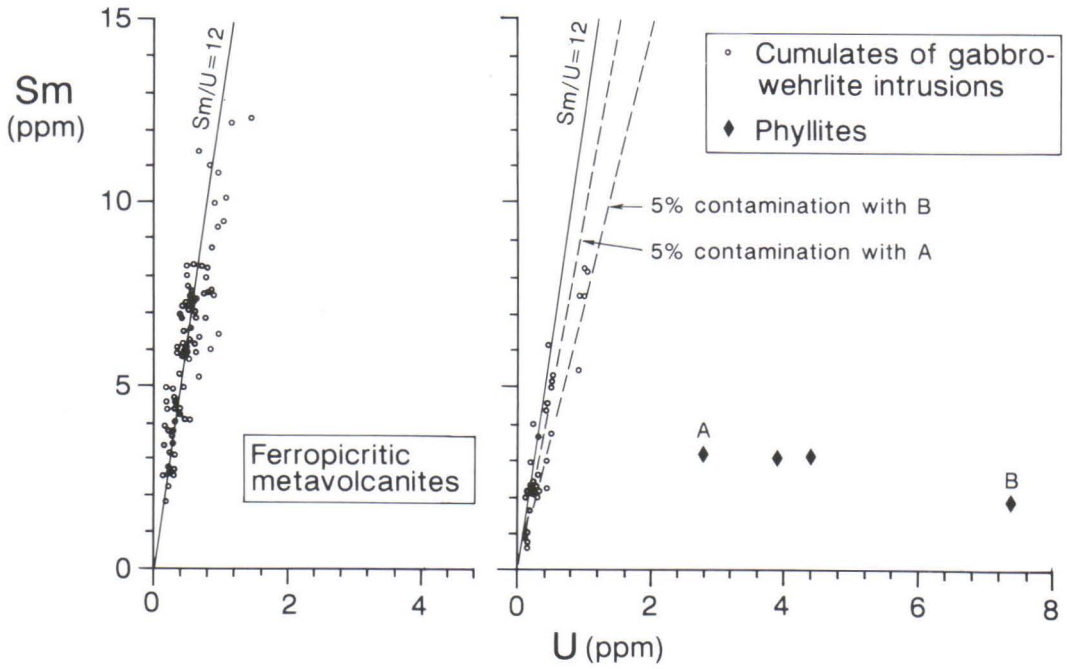


Fig. 81. U and Sm contents of ferropicritic metavolcanites, cumulates of Ni-bearing gabbro-wehrlite intrusions and phyllites from the productive pile.

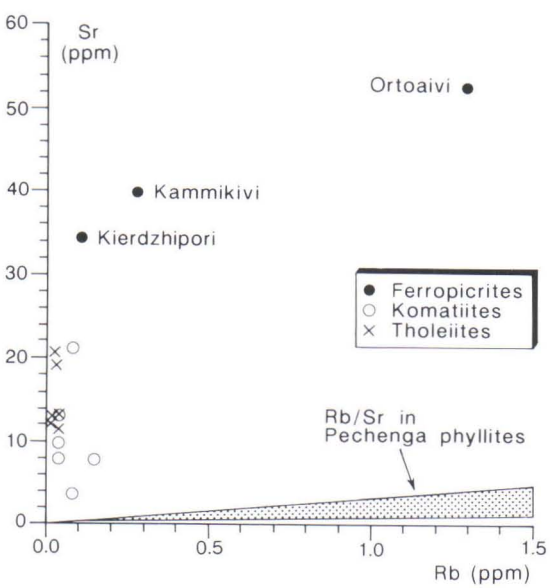


Fig. 82. Rb and Sr contents of pyroxene separates from the Kammikivi and Ortoaivi sills and the Kierdzhipori flow and from Archean komatiitic and tholeiitic flows and sills from Canada. Data on komatiites and tholeiites taken from Hart and Brooks (1977) and Zindler (1982). Also shown is range of Rb/Sr in phyllites from the productive pile according to Gorokhov et al. (1982) and this study.

mic ratio but As/Te in turn falls below the cosmic value. If a significant amount of pyritic sulfide was assimilated from enclosing sediments by the ore-forming magma, this should be revealed as elevated As/Se and As/Te values for the segregated sulfide phase. No geochemical evidence for such a process is observed in the deposits in the western ore field. This is compatible with the near chondritic S isotope composition of the Ni-Cu ores in that region. Unfortunately, As/Te and As/Se data are not available for ore samples from the Pilgujärvi intrusion.

Pelitic metasediments of the productive pile have high Rb contents ranging between 25-110 ppm. These result in high Rb/Sr values (0.3-1.1) clearly exceeding that of the primitive mantle (0.03). Thus, it can be deduced that if a primitive magma with relatively low contents of Rb and Sr is contaminated with this kind of pelitic material, the Rb-Sr ratio of the magma would readily increase. As was noted before, Rb and Sr have been mobile in ferropicrites and therefore their primary contents can not be directly measured. The Rb-Sr ratio can, however, be assessed by using the analytical data from the separated clinopyroxenes. In Fig. 82, Rb and Sr contents of the Pechenga clinopyroxenes are compared with those obtained for pyroxenes from uncontaminated Archean komatiites and tholeiites from Canada. It is apparent that the Rb/Sr value of the Pechenga pyroxenes fall within the range of komatiitic pyroxenes and differ considerably from the ratio for phyllites from Pechenga. Low Rb/Sr in pyroxenes from the Kierdzhipori lava flow and the ore-bearing Kammikivi sill provides little evidence for significant assimilation of country rock sediments during the emplacement of these bodies. The highest Rb/Sr value is observed in pyroxene from the ore-bearing Ortoaivi intrusion. This could be related to an excess of Rb due to impurities, since this pyroxene fraction was not cleaned by hand-picking.

## Isotopic evidence

The Se-S ratio together with S isotopes have been used to distinguish between different sources of sulphur (e.g., Eckstrand et al., 1989). Because phyllites in the productive pile have very low Se and Te abundances and Se/S and Te/S values compared with typical magmatic sulfides, both these ratios are expected to decrease and $\delta^{34}S$ to increase in proportion to the degree of contamination of the magma with sedimentary sulfur. Ideal mixing curves were calculated by using average Te and Se abundances and S isotope compositions of pyrite and pyrrhotite from S-rich phyllites for the sedimentary sulfur end member. The magmatic end member was assigned a chondritic Te/S and two alternative values for Se/S ($100\times10^{-6}$, $300\times10^{-6}$). The mixing curves show that if the large variation in Se/S and Te/S observed in disseminated sulfides (Fig. 67) is a consequence of mixing of sulfur from these two sources with homogeneous Se/S and Te/S, large changes in the sulfur isotope composition should be expected. For example, a decline of Se/S from 300 to 75 would mean an increase of the sedimentary sulfide component up to 80% and a change in $\delta^{34}S$ from zero to about +10. Yakovlev et al. (1968) did not give information on which particular deposits their abundant Se and S data belong to. Therefore, available data for making a comparison between the S isotope and Se/S values for individual deposits are limited. Nevertheless, the relatively constant and low $\delta^{34}S$ values observed in deposits of the western ore field are in striking contrast with the generally large variation in Te/S and Se/S.

The reported S isotope compositions for sedimentary rocks of the productive pile have a large spread, from at least -7.0‰ to +21.0 ‰, but the extent of heterogeneity in $\delta^{34}S$ of sedimentary sulfides is currently poorly constrained. In any case, if the sulfur in the Ni-Cu

ores contained a major sedimentary component, a heterogenous distribution of $\delta^{34}S$ in magmatic sulfides would be observed. The restricted range of variation and close to chondritic values of the S isotope composition in Ni-Cu ores at Kaula, Kotselvaara, and Kammikivi indicate that the bulk of sulfur is juvenile in origin (Fig. 76).

An important and intriguing problem is the difference in S isotope compositions between deposits in the eastern and western ore fields (Fig. 76). There are no indications that the magmas that formed the ore-bearing intrusions were different with respect to major or trace elements in these two areas. However, the areas differ with regard to the stratigraphic level at which the ore-bearing bodies occur. The eastern intrusions were emplaced as relatively large intrusions in the lower part of the productive pile, whereas the western intrusions, which are generally smaller in size, occur in the upper part of the productive pile and seem to have been emplaced closer to the earth's surface, in some cases possibly even on the sea floor. Thus there is a difference in the pressure conditions of emplacement. It is well known that degassing of sulfur as $SO_2$ from a magma alters the sulfur isotope composition of the remaining sulfur towards a lighter composition (Sakai et al., 1982). On the basis of the presence of magmatic amphibole in the ferropicritic lavas and intrusions, the pressure of emplacement was probably high enough to preclude notable degassing of sulfur in the early magmatic stage, during which the Ni-Cu sulfide ores segregated.

The large size of the Pilgujärvi intrusion could have provided sufficient thermal energy to assimilate a considerable amount of country rock phyllite. Figure 23 shows that there is an increase in $\delta^{34}S$ of the rocks towards the lower contact of the intrusion indicating some interaction with country rocks. However, the sulfur isotope composition of other rocks higher up in the section are closer to the values measured for ores than the values in the contact zone. According to Grinenko and Smolkin (1991), the relatively homogeneous S isotope composition of the Pilgujärvi intrusion indicates that the shift of $\delta^{34}S$ from a meteoritic value to a value averaging $+4.2‰$ is a result of contamination that took place before the emplacement of the intrusion into the productive pile. Grinenko and Smolkin (1991) presented a model according to which the magma that produced intrusions in the western ore field (Kaula, Kotselvaara, Kammikivi) received an input of crustal sulfur in a magma chamber located in the Archean crust where metasediments possessed S isotopic compositions close to that of chondrites. On the other hand, the magma that produced the ore-bearing intrusions in the eastern ore field (Pilgujärvi) was only marginally contaminated with sulfur from the present country rocks and was instead more strongly contaminated in a magma chamber located in underlying Proterozoic metasediments, prior to emplacement into the productive pile.

Two problems arise with this model. Firstly, the nature and location of potential S-rich metasedimentary contaminants in the metavolcanite-dominated Pechenga Series below the productive pile is unknown. Secondly, the basement complex is mainly composed of granite gneisses and different granites which are compositionally similar to other Archean basement areas, being characterized, for example, by low Ta/La, Ti/Zr and high $Al_2O_3/TiO_2$ and $Al_2O_3/V$. If ferropicritic magma resided in a magma chamber in the Archean crust for a sufficiently long period in order to assimilate significant amounts of crustal sulfur, it would also have had the opportunity to become contaminated with Archean granitoid material. The above mentioned ratios in ferropicritic rocks are not consistent with any substantial degree of contamination by Archean crustal material. Neither is there evidence for it in the Sr, Nd, Pb, or Os isotope compositions of ferropicrites.

Grinenko and Smolkin (1991) observed an increase of $\delta^{34}S$ towards the lower contact of the Northern Kotselvaara intrusion as well as in the Pilgujärvi intrusion. They also pointed out that high $\delta^{34}S$ values are observed in the lower contact zones of ferropicritic lava flows (Fig. 77). According to these authors, this feature, together with the general heterogeneous distribution of $\delta^{34}S$ suggest that assimilation of isotopically heavy sulfur from underlying metasediments has

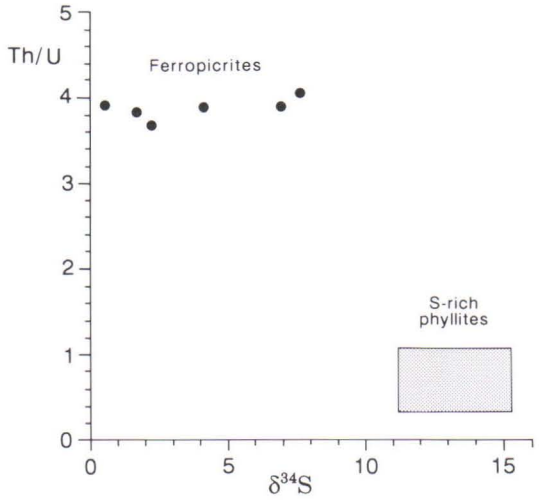


Fig. 83. Th-U ratio against sulfur isotope composition for samples from layered ferropicritic lava flows. Th-U ratio was calculated from Pb isotope data of this study. $\delta^{34}S$ data from Grinenko and Smolkin (1991) and Smolkin (pers. comm., 1992).

taken place at the site of extrusion of the ferropicritic lava flows. Data given by Grinenko and Smolkin (1991) show that relatively heavy $\delta^{34}S$ values (up to 7.4 per mil) occur not only near the lower contact of lava flows but also close to their upper contact. If the high sulfur isotope values are caused by assimilation of underlying sedimentary material, it is hard to explain why some lava flows have high $\delta^{34}S$ in the upper part while $\delta^{34}S$ stays low in the middle and lower part of the same lava flows. Because phyllitic metasediments appear to have low Th/U (Fig. 80) and high $\delta^{34}S$ compared with ferropicritic magma, bulk assimilation of these sediments would cause a decrease in Th/U and an increase in $^{\delta 34}S$ in the ferropicritic magma with an increasing degree of assimilation and thus create a negative correlation between Th/U and $\delta^{34}S$.

Th/U for ferropicritic samples can be calculated from the $^{208}Pb/^{204}Pb$ and $^{206}Pb/^{204}Pb$ data using the procedure outlined earlier in the section on Pb isotopes. In Fig. 83, Th/U is plotted against sulfur isotope composition for samples from layered ferropicritic lava flows. Also shown is the field of S-rich phyllites based upon whole rock analyses of Th and U and $\delta^{34}S$ measurements of pyrite and pyrrhotite separates. The expected negative correlation between Th/U and $\delta^{34}S$ is not observed; Th/U remains approximately constant while $\delta^{34}S$ varies from +0.5‰ to +7.4‰ . The observed relationship between Th/U and $\delta^{34}S$ is thus not easy to explain by a contamination process but it is understandable if the variation in sulfur isotopic composition is a result of postmagmatic processes. It is therefore suggested that the elevated $\delta^{34}S$ compositions in the marginal parts of the lava flows were generated through the introduction of isotopically heavy sulfur from country rocks during metamorphic processes. This was also regarded by Grinenko and Smolkin (1991) as a potential reason for high $\delta^{34}S$ in the upper part of the lava flows but it applies to the lower contact zones as well. A general observation in the Pechenga region is that sulfur isotope compositions show rather constant values in sulfur-rich rocks such as Ni-Cu ores but vary within wider limits in rocks that are low in sulfur. This seems plausible because postcrystallization exchange reactions with country rocks would more easily affect the isotopic composition of rocks having a low sulfur content. The preceding discussion does not exclude the possibility that the elevated $\delta^{34}S$ values observed in the lower marginal parts of some intrusions resulted from interaction with country rocks at the magmatic stage. However, the potential postmagmatic migration of sulfur should also be taken into account.

In the diagram plotting thorogenic $^{208}Pb/^{204}Pb$ against uranogenic $^{206}Pb/^{204}Pb$, analyses of ferropicritic metavolcanites and whole rock and apatite samples from the Pilgujärvi intrusion appear to be aligned along lines with slightly different coefficients (Fig. 70). The points for the Pilgujärvi samples are shifted towards the phyllitic samples, indicating some contamination by sedimentary material having a low Th/U value. The array of the Pilgujärvi samples yields a $^{232}Th/^{235}U$ value of 3.22±0.09. Based upon limited trace element data for phyllitic metasediments, simple mass balance calculations suggest that the decrease of $^{232}Th/^{235}U$ from a value of

3.8, calculated for ferropicritic metavolcanites, to 3.2 can be explained by bulk contamination of a ferropicrite magma with 2 to 6% of sediment depending on the Th/U value of the sedimentary component. This is qualitatively consistent with the S-isotope data for the Pilgujärvi intrusion (Fig. 23).

Assuming a $\delta^{34}S$ value from 0 to +1 per mil for a ferropicritic magma and from +12 to +15 per mil for the crustal source of sulfur, the average $\delta^{34}S$ value of 4.2 per mil for the Pilgujärvi Ni-Cu sulfide ores corresponds to an amount of 23-35% of sedimentary sulfur of these ores. Using these figures as constraints, together with the percentage of bulk assimilation of 2-6%, deduced from the Pb isotopic data, and assuming that the ferropicritic magma was close to sulfur saturation during emplacement and contained 0.2% sulfur, the sedimentary contaminant should have contained 2.8-5.3% sulfur. If the ferropicritic magma had a sulfur content half the value stated above, the sulfur content of the contaminant can also be reduced to a half. Sulfur-rich metasediments with a sulfur content within the above mentioned range are not uncommon in the productive pile (Stromov, 1985).

The calculations thus imply that the Pb and S isotope data for ores and silicate rocks of the Pilgujärvi intrusion are also quantitatively consistent with a contamination hypothesis. Interaction between the Pilgujärvi intrusion and enclosing sediments is also supported by the existence of country rock xenoliths in the middle part of the intrusion (Smolkin, 1977). It should, however, be borne in mind that there are other explanations for the observed difference in the $^{208}Pb/^{204}Pb$-$^{206}Pb/^{204}Pb$ relations between ferropicritic metavolcanites and the Pilgujärvi intrusion. Namely, lower Th/U may be attributed to a more depleted mantle source for the magma batch that formed the Pilgujärvi intrusion. Some support for this idea is provided by the initial Nd isotope composition which is slightly higher for the Pilgujärvi intrusion than for ferropicritic metavolcanites. However, it must be pointed out that there are very few Nd data for the Pilgujärvi intrusion and none at all for the sedimentary rocks. Therefore Nd isotopes cannot be used to evaluate the extent of interaction between ore-forming magmas and sedimentary rocks. The available REE data from phyllites reveal that these rocks possess lower Nd concentrations than the potential ferropicritic parental magma and hence any contamination effects they cause might not be readily apparent in the Nd isotope composition of the crystallization products of the ferropicritic magma.

The radiogenic Os isotope composition of ore samples from the Kammikivi deposit were noted earlier. This can be interpreted in several ways. The preliminary explanation was that the radiogenic Os was a result of remobilization and homogenization of ore material within the lower part of the host intrusion during a metamorphic event (Walker et al., 1991c). It is well known that ore material has been mobile at different scales in the Pechenga area. This phenomenon is seen under the microscope as a "negative" texture where sulfide pseudomorphs have replaced earlier olivine or at outcrop scale, for example, as the formation of stringer ores in footwall metasediments. The two-stage model involving magmatic and metamorphic fractionation was based upon three ore analyses which appeared to be aligned along an isochron with an age of about 1720 Ma and an initial $^{187}Os/^{186}Os$ value at that time of about 3.5. In the 250 Ma interval from the time of igneous crystallization to the time of ore mobilization, the $^{187}Os/^{186}Os$ of a whole-rock system with an average $^{187}Re/^{186}Os$ of 650 would grow from chondritic to 3.5.

As is shown in Fig. 75, Re-Os isotope data for the five S-rich samples analysed to date from Kammikivi do not form a simple linear array and therefore this hypothesis of remobilization within the ore-bearing part of the sill does not adequately explain the position of the ore samples in the diagram (Fig. 75). Furthermore, the average $^{187}Re/^{186}Os$ of 650 for ore seems to be too high, since the maximum measured value is 260. If the sill remained as a closed system during remobilization, ore samples should show values on both sides of 650.

When the initial $^{187}Os/^{186}Os$ composition is calculated for each ore sample at 2.0 Ga, values

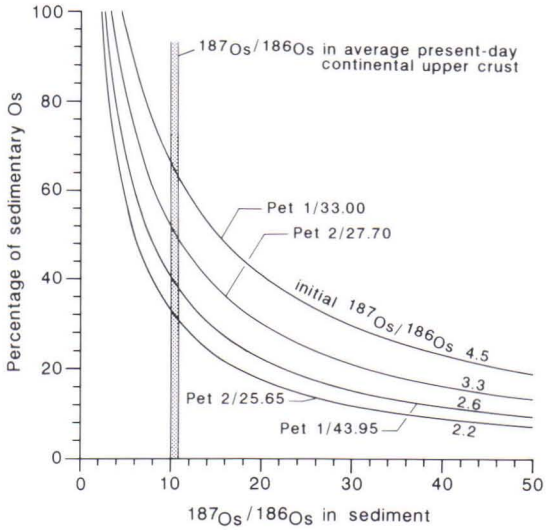


Fig. 84. Calculated percentages of bulk contamination and $^{187}Os/^{186}Os$ in sedimentary contaminant which explain observed initial Os isotopic ratios in individual S-rich samples from Kammikivi. It is assumed that magma, from which ore samples crystallized, had a chondritic initial Os isotopic ratio.

ranging from 2.21 to 4.50 are obtained, corresponding to $\gamma_{Os}$ values between 133-375. If these are magmatic values, at least two osmium sources are required, one being the mantle-derived ferropicritic melt and the other some crustal rock with a high $^{187}Os/^{186}Os$. Os isotope data are not yet available for sedimentary rocks of the productive pile, but on the basis of high Os isotope values recorded for recent black shales and other marine sediments (Esser and Turekian, 1988; Ravizza and Turekian, 1989, Ravizza et al., 1991), it is conceivable that the high $^{187}Os/^{186}Os$ value in the ore samples could be due to assimilation of country rock sediment by the ore-forming magma.

If this were the case, some difficulties would arise. For example, it would mean that some degree of Os isotopic disequilibrium exists between the sulfides and the silicate rocks in the Kammikivi sill, because the silicate rocks plot closer to the 2.0 Ga reference isochron. In other words, the isotopic effects of assimilation are restricted to the sulfide portion of the sill. This would indicate that the sulfide-bearing rocks and the overlying barren rocks crystallized from separate magma batches. The change from radiogenic to non-radiogenic Os isotope composition takes place within the olivine cumulate unit between samples Pet1/33.10 and Pet1/25.66. The former has the highest calculated initial $^{187}Os/^{186}Os$ value of 4.5 while the latter nearly follows the chondritic $^{187}Os/^{186}Os$ evolution.

The initial Os isotope composition of the ore samples can in principle be used to infer the amount of crustal Os in ores if the initial ratio and the concentration of Os in the crustal component can be measured or estimated. Archean upper crust can be eliminated as a potential contaminant because to cause the initial Os isotope ratio of the ferropicritic magma to increase from 0.94 to 2.5, more than 80% assimilation of crustal material with 0.015 ppb Os and a $^{187}Os/^{186}Os$ value of 10 would be required. This is so because of the low abundance of Os in typical crustal rocks relative to values of 0.45-0.78 ppb measured in primitive ferropicritic rocks. Sedimentary rocks of the productive pile are probably more effective contaminants, since black shales are known to possess high Os contents (Ravizza and Turekian, 1989, Ravizza et al., 1991). Assuming Os concentrations of 0.6 ppb and 0.2 ppb for the ferropicritic magma and the sedimentary component, respectively, and chondritic initial $^{187}Os/^{186}Os$ for the ferropicrite magma, binary mixing calculations were performed to examine which combinations of $^{187}Os/^{186}Os$ in the sediment and the percentage of bulk contamination could account for the initial ratios in individual ore samples.

The results are graphically portrayed in Fig. 84. They indicate that if the contaminant had an $^{187}Os/^{186}Os$ value lower than the present-day average continental upper crust, a large proportion of osmium contained in the ore samples could have been derived from country rocks (Fig. 84). As the Pb-Pb isotope analyses of pelitic sediments of the productive pile suggest that the Archean basement rocks are not a dominant component in these rocks, the major proportion of osmium is presumably derived from seawater and volcanic rocks. It follows that $^{187}Os/^{186}Os$ in

phyllites was likely to have been lower than 8-9, which are the values measured for recent organic-rich marine sediments (Ravizza and Turekian, 1992). The curves in Fig. 84 are only tentative until actual Os data are obtained for sedimentary rocks of the productive pile. In any case, the calculations suggest that a considerable amount of crustal Os must be involved if the radiogenic composition of the ore samples is due to contamination by crustal material. Furthermore, assuming a constant $^{187}Os/^{186}Os$ value and a constant Os content for the contaminant, a large variation in the extent of contamination is recorded by separate samples (Fig. 84). For example with a $^{187}Os/^{186}Os$ value of 10 in a sediment, samples Pet2/25.65 and Pet2/27.70, which are located only 2 m apart from each other, would contain 32% and 51% of sedimentary Os, respectively. Equally enigmatic is the heterogeneity in the initial Os ratios of closely spaced ore samples because this would suggest limited homogenization of Os isotopes in interstitial sulfide liquid at the magmatic stage.

The S isotope data (Fig. 76) and the chalcophile element composition of ore together with major element (Fig. 58) and trace element data of silicate rocks argue against strong interaction with country rocks in the case of the Kammikivi layered sill. These results in conjunction with other problems discussed above demand that other explanations should be found for the radiogenic Os isotope composition of the ore samples.

Turning back to the hypothesis of reworking of sulfides during a metamorphic event, this model is modified below as follows. Instead of assuming closed system behavior, it is considered that there was a possible change in the content of ore metals in the lower part of the intrusion. One way for a sample to acquire a high calculated initial $^{187}Os/^{186}Os$ value at about 2.0 Ga is to undergo a loss of Re in a subsequent mobilization event. For each sample, it is possible to calculate the change in $^{187}Re/^{186}Os$ that is needed for its $^{187}Os/^{186}Os$ evolution line to project from the initial ratio at a given time of metamorphism to a chondritic value at 2.0 Ga. If the reworking event took place 1720 Ma ago, the radiogenic compositions of ore samples at Kammikivi are explained by a Re loss varying between 59-85%. The loss would be even larger if the time interval between the magmatism and the metamorphism was shorter. In the case of a recent Re loss, the percentages of Re leaching would vary between 13-43%.

The high Os initial ratios could also be produced by the introduction of radiogenic osmium from country rocks during metamorphism. This process is, however, more difficult to model because $^{187}Os/^{186}Os$ of the potential hydrothermal fluid is poorly constrained. If the fluid phase had a $^{187}Os/^{186}Os$ value of 10, an Os addition from 16% to 65% is needed to explain the radiogenic Os isotope compositions of the ore samples. The calculated percentage of the nonmagmatic Os is not significantly affected by the timing of the enrichment event.

The perturbation of the Re-Os isotope system is evident for silicate sample Pet1/5.40, which clearly plots beneath the reference isochron, indicating either a loss of Os or a gain in Re (Fig. 75). The initial Os isotopic ratio of this sample calculated at 2.0 Ga has a negative value. The rock contains rather fresh-looking clinopyroxenes but they are set in a chloritic mass replacing magmatic interstitial phases. Assuming a simple two-stage model and an input of Re, the resetting of the system can be inferred to be younger than the time at which the $^{187}Os/^{186}Os$ evolution of the sample transects the chondritic $^{187}Os/^{186}Os$ evolution line. In this way, a maximum resetting time of 1750 Ma is obtained for sample Pet1/5.40.

The time of metamorphism has not yet been precisely dated in the Pechenga region. According to Pushkarev et al. (1988), a Pb-Pb isotopic age of 1810±25 Ma has been obtained for a garnet-vesuvianite dike cutting the Pilgujärvi intrusion. Gorokhov et al. (1982) reported a Rb-Sr isochron age of 1650±75 Ma for pelitic metasediments of the Pilgujärvi Suite and interpreted it to correspond to an episode of low-grade metamorphism. A recent Rb-Sr isotope study by Balashov et al. (1991) on volcanic rocks from various levels of the Pechenga Group yields ages of 1770±43 Ma, 1770±110 Ma, 1790±42 Ma, and

about 1780 Ma. For the Litsa-Araguba granites located east of Pechenga, Pushkarev et al. (1978) reported a U-Pb zircon age of 1810±50 Ma and a younger Rb-Sr age of 1720±25 Ma. Zwicky (1991) has carried out a K-Ar isotope study on rocks of the Opukasjärvi greenstone belt less than 100 km west of Pechenga. He obtained closure ages between 1695-1733±22 Ma for biotite, 1723-1774±22 Ma for muscovite, and 1745-1811±22 Ma for hornblende.

It should be emphasized that the hypotheses considered above involving either loss of Re or gain of Os during metamorphism are end-member models and are not valid if the fluid phase transported both Re and Os. In the latter case, the change in the isotope composition of sulfides during the remobilization event would be still larger. It is thus evident that irrespective of whether the high radiogenic osmium values in ore samples is of magmatic or metamorphic origin, substantial changes in the Re-Os systematics of the magma or sulfides must have occurred. This study and those of Luck and Arndt (1985) and Walker et al. (1988) have shown that the Re-Os isotope system is stable in silicate rocks under low-grade metamorphic conditions but some literature data exist concerning unstable behavior of this system in metamorphosed sulfides. It is interesting to note that Luck and Arndt (1985) reported radiogenic Os isotope compositions for two magmatic sulfide samples from a komatiite flow in Alexo, Abitibi belt. These sulfides lie distinctly to the left of the isochron defined by genetically related komatiite samples and show initial $^{187}Os/^{186}Os$ compositions of about 1.5 and 3.1. Luck and Arndt (1985) suggested that the ore samples have lost Re during recent leaching. Luck and Allègre (1984) published a single analysis of sulfide ore associated with the Cape Smith komatiites and calculated a model of 1740±60 Ma for this sample. If the U-Pb zircon age of 1918±8 Ma obtained for the Kattiniq sill is taken as the emplacement age of the Chukotat Group komatiites (Parrish, 1989), the initial Os ratio of the sulfide ore falls considerably below the chondritic evolution line and acquires a $\lambda_{Os}$ value as low as -21.5 ($\lambda=1.639\times10^{-11}$ $y^{-1}$). It is noteworthy that sulfide fractions from the Ultramafic series (UMS) of the Stillwater intrusion have initial $^{187}Os/^{186}Os$ values (2701 Ma) of 1.36 and 1.75 which are clearly higher than the range obtained for silicate and chromitite samples from this intrusion (0.88-1.18) (Lambert et al., 1989). Resetting of the Re-Os system has been documented by Beneteau et al. (1991) in chalcopyrite samples in the Falconbridge East Ni-Cu deposit (Sudbury) and also in pyrrhotite-pentlandite samples at the contacts of the same deposit. On the other hand, Walker et al. (1991a) analysed whole rock sulfide ore samples from the Levack West and Falconbridge mines and obtained isochrons with ages within the uncertainty limits of the accepted age of the Sudbury Complex. This suggest closed-system behavior for the Re-Os system in these ores.

Clearly, additional Os isotope data are needed in order to place more strict constraints on the role of country rocks in the Ni-Cu ore formation and the timing of mobilization and recrystallization of ore material. The Re-Os method potentially allows one to study the timing of (re)crystallization of ores by constructing mineral isochrons based on analyses of ore mineral separates. Pb-Pb isotope analyses on rocks of the Kammikivi sill as well as Re-Os isotope analyses of sulfide and primary silicate mineral fractions from the same sample could also shed light on the question of contamination versus mobility of Re and Os.

The interpretation of the Sr isotope data in terms of potential interaction of magmas with country rocks is hampered by limited knowledge of the initial $^{87}Sr/^{86}Sr$ value of the sediments at the time of the ferropicritic magmatism. The only available Sr isotope data on the sedimentary rocks of the productive pile are the six analyses of pelitic rocks published by Gorokhov et al. (1982). As was mentioned earlier, five of them plot on an isochron with a proposed metamorphic age of 1650±75 Ma and give an initial ratio of 0.7077±0.0015 at that time. On the basis of the present study and analyses of Gorokhov et al. (1982), pelitic metasediments can be calculated to have an average Rb/Sr of 0.56. This would mean a change in $^{87}Sr/^{86}Sr$ of 0.0022 per 100 Ma. When

going back in time from 1.65 Ga to 2.O Ga, the initial ratio of 0.7077 thus diminishes to 0.6999, i.e., clearly below the bulk earth evolution curve. Although this value is unrealistically low for a pelitic sediment, it may indicate that there is no significant component of Archean upper crustal detritus in the analysed pelitic samples. This is also consistent with the Pb isotope data. It must be stressed, however, that these calculations are imprecise for many reasons. For example, it is uncertain whether the homogenization during metamorphism took place within the scale of sampling, a problem which was not addressed by Gorokhov et al. (1982). If it is assumed that the Rb-Sr system of the sediment samples was not disturbed after the time of deposition, their calculated initial $^{87}Sr/^{86}Sr$ values would vary between 0.6959-0.7125 at 2.0 Ga.

It is significant that the initial Sr isotope ratios obtained from clinopyroxene separates show no significant differences between the barren Kierdzhipori flow and the mineralized Kammikivi and Ortoaivi sills. In fact, the lowest value indicating a chondritic evolution was measured for pyroxenite from the ore-bearing Kammikivi sill. The data of Smolkin (1991) for the Pilgujärvi apatite suggest a slightly higher initial ratio (0.703) for this intrusion but even this value is relatively close to the chondritic value about 2.0 Ga ago (Fig. 103).

New geochemical and isotopic data obtained during recent years strongly argue for the generation of the Pechenga ore-bearing intrusions from a ferropicritic magma and their emplacement contemporaneously with ferropicritic volcanism (Hanski and Smolkin, 1989; Hanski et al., 1990). These results are compatible with the classification of the Pechenga Ni-Cu deposits as synvolcanic ore deposits (Naldrett, 1989b). In this respect, the Pechenga ores are analogous to komatiite-related Ni-deposits in Western Australia. The difference between these two areas is that the economic deposits are concentrated in the intrusive subvolcanic facies at Pechenga while the Kambalda-type deposits occur mainly at the basal parts of volcanic sequences. Petrographic features indicate, however, that some of the ore-bearing bodies such as the Kammikivi layered 'sill' crystallized, if not on the sea floor, at least very close to it.

Key elements in recent genetic models that have been proposed to explain Ni-Cu deposits in komatiites, include a dynamic flow regime of volcanism, thermal erosion of underlying sedimentary rocks and basalts by a hot, turbulent magma, and consequent sulfide assimilation (Lesher, 1989). A dynamic subvolcanic environment is also applicable to the Pechenga area. An excessive modal olivine component in intrusions constitutes one piece of evidence for an open system behavior of magma chambers feeding overlying volcanism. It also explains why differences have not been found in olivine compositions between barren and ore-bearing intrusions, for silicate liquids did not necessarily solidify in the same place as the sulfides with which they equilibrated. Also the high proportion of sulfides in some magmatic units suggests that the unit acted as a channel through which a considerable amount of ferropicritic magma migrated, precipitating sulfides. Alternatively, the sulfide liquid segregated earlier from a greater volume of magma and was emplaced as an independent sulfide liquid. Particularly striking in this respect is a recently discovered Ni-Cu deposit in the Kierdzhipori area. Here a 3.2 m thick magmatic unit which has been regarded as a flow by Gorbunov et al. (1989) and a sill by Grinenko and Smolkin (1991), contains a 0.45 m thick massive ore overlain by a 1 m thick disseminated ore at its base.

The effects of thermal erosion by ferropicritic magma have not been described from the Pechenga area. Although some assimilation during the magmatic stage may have occurred, for example in the Pilgujärvi intrusion, major and trace element data and S, Sr, Nd and Pb isotope results suggest that country rock sulfides seem not to have played a significant role in the formation of economic Ni-Cu sulfide deposits in the western ore field, neither at the magmatic nor at the metamorphic stage. Instead, sulfur can be regarded as predominantly juvenile in these deposits. In contrast to this interpretation, radiogenic Os isotope

compositions of S-rich samples from the Kammikivi sill imply a considerable component of crustal Os in the ores. However, this feature could also be explained by postmagmatic disturbance of the Re-Os system in sulfides, although this would require a considerable loss of Re or gain of Os. Clearly, more isotope measurements are needed to reconcile the Re-Os results with other data.

## MANTLE SOURCE OF FERROPICRITIC MAGMAS

### Residual mineralogy

Knowledge of the residual mineralogy is critical in assessing the trace element characteristics of the mantle source from which a basaltic melt segregated. In particular, establishing the presence or absence of residual garnet is important, because this mineral can strongly influence the relative abundances of rare earth elements in the liquid due to its high partition coefficients for heavy REE (e.g., Harrison, 1981). The LREE enrichment of volcanic rocks such as alkali basalts has been commonly ascribed to a garnet-bearing residue in the mantle (e.g., Kay and Gast, 1973; Lanphere and Frey, 1987). In a similar way, the high La/Yb values in ferropicritic rocks may be a result of the preferential retention of heavy REE by residual garnet, in which case the degree of melting was not sufficiently high to eliminate all the garnet from the garnet peridotite source. Because the near solidus partial melts of a mantle peridotite become more magnesian and even approach komatiitic compositions with increasing pressure (Takahashi, 1986), the high MgO abundance of ferropicrites does not rule out a model invoking a low degree of melting at a relatively high pressure with a garnet-bearing residuum. On the other hand, geochemical data from mantle xenoliths demonstrate that many peridotites, and particularly those that have a depleted major element composition, possess high La/Yb values compared with chondrites (see McDonough and Frey, 1989). Therefore, the possibility that the source region of the ferropicritic magma was enriched in light REE should seriously be considered. If the mantle source possesses inherently high La/Yb, then the resultant melt is LREE-enriched irrespective of the degree of melting.

From the above discussion, it is evident that it should be possible to evaluate the potential saturation of a ferropicritic liquid in residual garnet at the time of melt segregation without making any assumptions concerning the degree or depth of melting. This will be attempted in the following discussion by employing major element analyses of ferropicrites and the results of high-pressure experimental petrology derived from the literature.

Hanson and Langmuir (1978) defined three types of elements with respect to their partitioning behavior between crystalline and liquid phases, viz. essential structural constituents, trace elements, and intermediate elements. An essential structural constituent (ESC) is an element which completely fills one structural site in a mineral and for which there is little solid solution. Because the abundance of an ESC in the mineral is stoichiometrically constrained to a constant value, a mineral-melt partition coefficient $K_d$ of this element, which is a function of P and T, completely determines the concentration of this element in the liquid. Conversely, given an abundance of an ESC in the liquid under certain P-T conditions, the $K_d$ of a mineral specifies whether the liquid is saturated with this mineral or not. Examples of ESCs are respectively Si, Ca, and Al in olivine,

clinopyroxene, and garnet.

The concentration of an essential structural constituent in minerals and melt is independent of the abundance of this element in the system or the proportions of minerals. Thus, if the concentration of an ESC in the system is changed under fixed conditions, the proportions of minerals and melt will vary, but the compositions of the phases remain unchanged. In contrast, trace elements which, by definition, follow Henry's Law and have constant $K_d$'s irrespective of their concentrations in the system will have variable concentrations in mineral and liquid phases, depending on the proportions of these phases and the abundances of trace elements in the system. In addition, trace elements occur at such low concentrations in silicate liquids that they cannot significantly affect the stability of solid phases. For example, the saturation of a liquid with garnet is not dependent on the Yb content of the liquid, but when the Al content diminishes to a sufficiently low level in the liquid, garnet will no longer be in equilibrium with this liquid.

An intermediate element shares the properties of both ESC and a trace elements. For a given $K_d$, the abundance of an intermediate element in minerals and melt can vary, but only within the limits imposed by stoichiometry. The abundance of this element is also influenced by the relative proportions of the mineral and liquid phases. Typically, intermediate elements have a wide range of solid solution with each other in a given structural site in a mineral, such as Mg and Fe in the olivine lattice.

As mentioned above, essential structural constituents are elements that completely determine

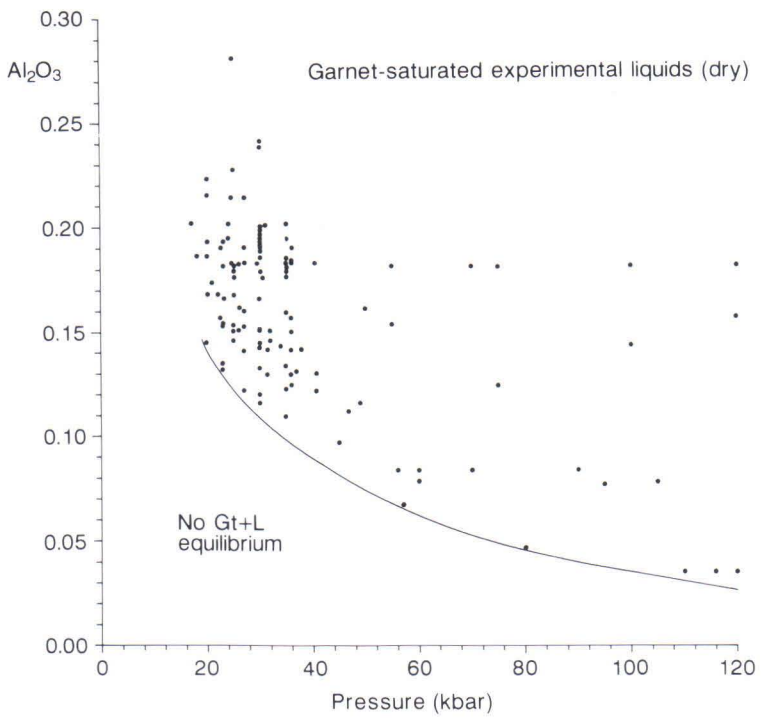


Fig. 85. $Al_2O_3$ (cation mole proportion) vs. pressure diagram for dry silicate liquids that have been shown experimentally to be in equilibrium with garnet ± other phases. For data sources, see Appendix 2.

the stability of a mineral under given P-T conditions. In the case of garnet, the $Al_2O_3$ content of a liquid can potentially be used to constrain the garnet stability. Figure 85 shows the $Al_2O_3$ content (in cation mole proportions) of experimentally studied liquids that have garnet as a liquidus phase, with or without other phases, at various pressures under dry conditions. The curve in the diagram delineates a region where a liquid has an $Al_2O_3$ content that is too low to allow garnet to be in equilibrium with this liquid. The curve shows that the minimum $Al_2O_3$ content of liquid needed to saturate garnet increases with decreasing pressure. This means that the maximum $K_d$(gt-liq) for $Al_2O_3$ increases with increasing pressure. From the $Al_2O_3$ vs. P diagram, one can infer that if a parental magma has an $Al_2O_3$ content, for example, of less than 0.09, the pressures during segregation must have been higher than about 40 kbar, provided garnet was one of the residual phases. This diagram alone, however, does not yet tell whether garnet actually was left in the residue if the pressure of segregation cannot be independently constrained.

In most current theories of basalt petrogenesis, the source material for primary basalt magmas is olivine-rich lherzolite or harzburgite (e.g., Basaltic Volcanism Study Project, 1981; Ringwood, 1989). Because the source region of highly magnesian ferropicritic magma most probably consisted of peridotite, olivine was one of the phases remaining in the crystalline residue. One potential way of determining the existence of residual garnet is to establish whether ferropicritic magma

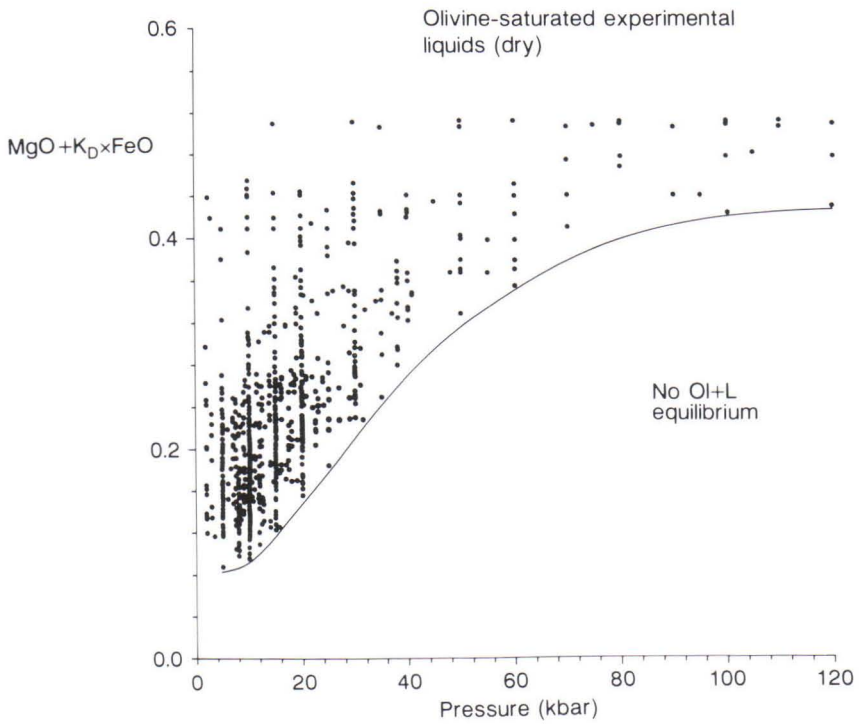


Fig. 86. Plot of MgO+$K_D$×FeO (cation mole proportion) against pressure for experimentally studied dry silicate liquids that are saturated in olivine ±other phases. $K_D$ is the Fe-Mg exchange reaction distribution coefficient between olivine and liquid (see text). For data sources, see Appendix 2.

fulfills the compositional criteria of a liquid that is simultaneously in equilibrium with olivine and garnet. This is done by testing whether there are conditions under which the $Al_2O_3$ content of a ferropicritic liquid is sufficiently high to be saturated in garnet while at the same time MgO and FeO contents are sufficiently high to be saturated in olivine.

Because MgO and FeO are not essential structural constituents in olivine, their abundances in the liquid as such cannot strictly be used as a criterion for olivine saturation. However, since molecular MgO+FeO in olivine is constant (0.667), this sum can be treated as an essential structural constituent. One complicating factor is the differing partition behavior of iron and magnesium between olivine and silicate liquid ($K_d$ for MgO is about three times that of $K_d$ for FeO). This means that the sum of MgO and FeO in liquids with varying MgO/FeO is not sufficient to determine the stability of olivine. The difference in partition coefficients means that approximately three times more iron is needed in the liquid compared to that of magnesium to bring about the same stabilizing effect. This difficulty can be circumvented if FeO is multiplied by $K_D$, the Fe-Mg exchange reaction distribution coefficient of olivine. The function $MgO+K_D \times FeO$ is then used in a similar fashion as $Al_2O_3$ in Fig. 85.

$MgO+K_D \times FeO$ of olivine saturated liquids from anhydrous experiments from the literature are plotted against pressure in Fig. 86. Because $K_D$ has been observed to be slightly pressure-dependent (Takahashi and Kushiro, 1983; Agee and Walker, 1988; Ulmer, 1989), the relation $K_D=0.30 + 0.002 \times P(kbar)$ from 0 to 40 kbar and a constant $K_D$ value of 0.38 at higher pressures has been used in Fig. 86 for those runs in which $K_D$ has not been measured. The simplest synthetic systems were excluded when constructing the diagram: all the liquids contain iron and almost all also contain sodium and/or potassium (Fig. 92). In Fig. 86, olivine-saturated liquids show a wide spread in $MgO+K_D \times FeO$ at low pressures, depending on temperature, but this variation becomes smaller and the minimum $MgO+K_D \times FeO$ value larger with increasing pressure. This feature is compatible with the well-known fact that the normative olivine content of an initial liquid during mantle melting increases with increasing pressure because of the contraction of the primary phase volume of olivine (e.g., O'Hara, 1968). It is also consistent with the convergence of the solidus and liquidus curves of peridotite with increasing pressure (Takahashi, 1986). A curve has been drawn in Fig. 86 which delineates a "forbidden" region where a silicate liquid has never been observed to be stable with an olivine-bearing mineral assemblage under dry conditions.

The minimum olivine stability curve in Fig. 86 permits an estimation to be made of the maximum pressure of segregation for a magnesian silicate melt from an olivine-bearing source. If the ferropicritic parental magma had about 15 wt. % MgO and 14 wt. % FeO, which is equivalent to an $MgO+K_D \times FeO$ value of 0.265, the pressure of segregation is restricted to less than about 38 kbar. On the other hand, if the ferropicrites erupted on the surface are regarded as derivatives of a more primitive parental magma, such as one containing about 20% MgO ($MgO+K_D \times FeO$ about 0.32), segregation could have taken place at pressures as high as 50 kbar. In any case, the maximum depth of generation of the ferropicritic magma occurs well within the stability field of garnet lherzolite (Takahashi, 1986).

When the curves of the minimum $Al_2O_3$ and minimum $MgO+K_D \times FeO$ contents of liquids from Figures 85 and 86, respectively, are combined by plotting $MgO+K_D \times FeO$ against $Al_2O_3$, an Ol+Gt saturation curve as a function of P is obtained (Fig. 89). All liquid compositions that are relatively low in $Al_2O_3$ or $MgO+K_D \times FeO$ and which therefore plot beneath the curve in Fig. 89, can be saturated in either olivine or garnet but not simultaneously in both of these minerals. Instead, for liquid compositions that plot above the curve, Ol+Gt+L equilibrium is possible. Along most of its length, the saturation curve is close to a straight line which can be approximated with the equation $Al_2O_3 = -0.355 \times (MgO+K_D \times FeO) + 0.190$. From this equation, it follows that if a natural liquid with $MgO+K_D \times FeO$ between 0.2-

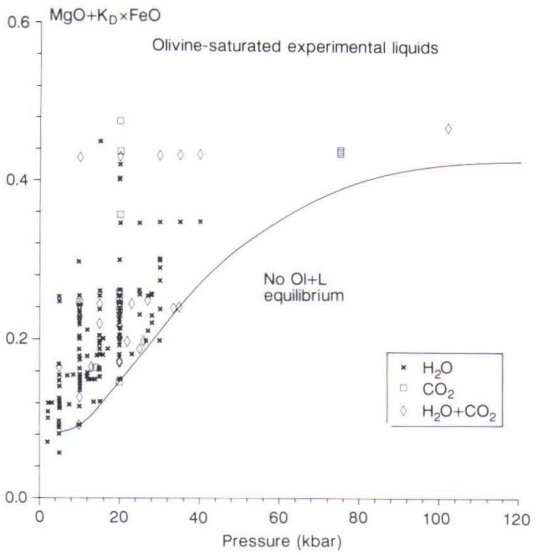


Fig. 87. MgO+$K_D$×FeO (cation mole proportion) vs. pressure diagram for hydrous, $H_2O+CO_2$- or $CO_2$-bearing silicate liquids that have been experimentally shown to be in equilibrium with olivine ± other phases. Liquid compositions plotted on a volatile-free basis. $K_D$ is the Fe-Mg exchange reaction distribution coefficient between olivine and liquid (see text). Curve for olivine stability under dry conditions taken from Fig. 86. For data sources, see Appendix 2.

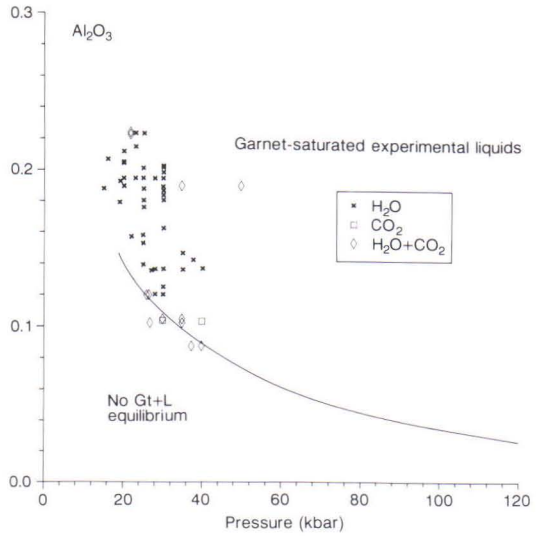


Fig. 88. $Al_2O_3$ (cation mole proportion) vs. pressure diagram for hydrous, $H_2O+CO_2$- and $CO_2$-bearing silicate liquids experimentally shown to be saturated in garnet ± other phases. Liquid compositions plotted on a volatile-free basis. Curve for garnet stability under dry conditions taken from Fig. 85. For literature sources, see Appendix 2.

0.4 (corresponding MgO contents about 12-30% in wt. %) has a value greater than 2.82 for the function (0.534 - MgO+$K_D$×FeO)/$Al_2O_3$, it falls below the Ol+Gt+L stability curve in Fig. 89.

It should be emphasized that not all liquids situated above the Ol+Gt+L stability curve are necessarily saturated in Ol+Gt. The reason is that not all liquid compositions plotting above the olivine stability curve in Fig. 86 are saturated in olivine and not all liquid compositions plotting above the garnet stability curve in Fig. 85 are in equilibrium with garnet. This is because in the simple diagrams of $Al_2O_3$ vs. P and MgO+$K_D$×FeO vs. P, compositions of liquids are projected from the sum of all other components. The presence of other major components makes it difficult to obtain detailed phase equilibrium data above the curves in these diagrams (cf. O'Hara, 1976). Nevertheless, the diagrams in Figures 85, 86 and 89 have not been designed to give detailed phase equilibrium data but to delineate the forbidden Ol+L, Gt+L, Ol+GT+L equilibrium regions, which, taking into account the wide range of compositions used in experimental runs, are thought to be generally applicable (see below). In summary, the $Al_2O_3$ vs. MgO+$K_D$×FeO diagram cannot be used to establish phase equilibria for a given melt composition, but instead can provide information for the elimination of certain mineral-liquid equilibria. The latter information is useful from the point of view of trace elements, particularly if we can deduce the absence of Gt+L equilibria.

A literature survey reveals that surprisingly few iron-bearing, dry liquid compositions have been experimentally verified to be simultaneously

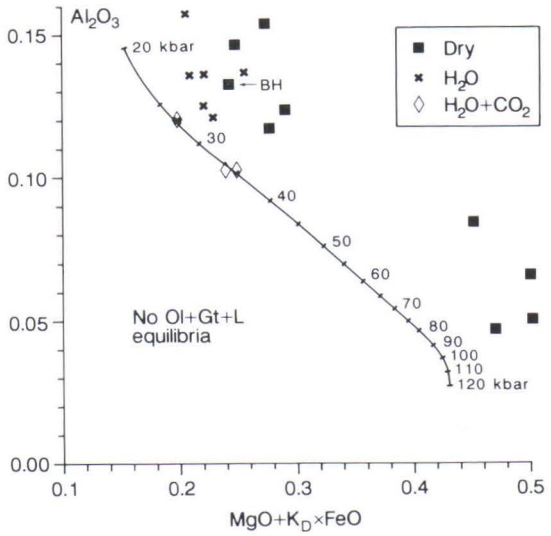


Fig. 89. $Al_2O_3$ vs. $MgO+K_D \times FeO$ diagram (cation mole proportion) constructed by combining garnet and olivine stability curves from Fig. 85 and 86. For liquid compositions plotting beneath the curve, olivine+garnet+liquid equilibrium is not permitted and for those liquids plotting above the curve, this equilibria is possible (under dry conditions). Also shown are liquid compositions that have been experimentally verified to be multiply saturated in olivine+garnet±other phases under dry or volatile-bearing conditions (for references see text). BH denotes iron-rich (23.3 wt. % FeO) melt from Bertka and Holloway (1988).

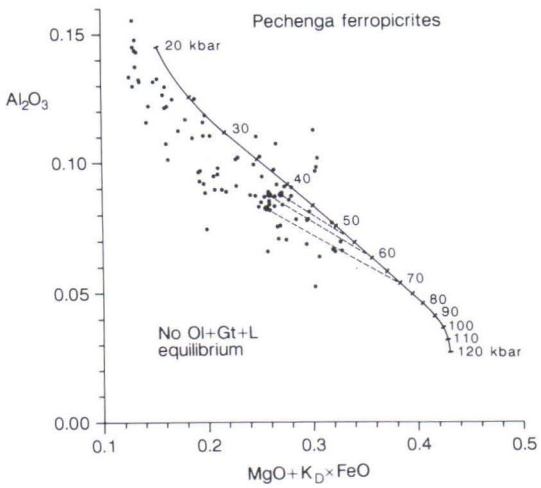


Fig. 90. Pechenga ferropicrites and their low-MgO derivatives on the $Al_2O_3$ vs. $MgO+K_D \times FeO$ diagram. Dashed lines are olivine fractionation paths.

saturated both in olivine and garnet. These compositions are plotted in Fig. 89 (solid squares) and include those reported by Elthon and Scarfe (1984), Bertka and Holloway (1988), Falloon and Green (1988), Maaløe and Jakobsson (1980), Takahashi (1986), and Kato et al. (1988). They are all located well inside the field where the Ol+Gt+L equilibria is allowed. It should be noted that, according to Falloon and Green (1988, p. 393), the composition reported by Elthon and Scarfe (1984) is probably not multiply saturated in Ol+Opx+Cpx+Gt, but rather only in olivine and orthopyroxene, with clinopyroxene and garnet being quench phases.

When analyses of ferropicrites and their derivative liquids are projected on the $Al_2O_3$ vs. $MgO+K_D \times FeO$ diagram (Fig. 90), the majority of them fall below the Ol+Gt saturation curve, indicating that they did not leave a garnet-bearing residue when segregating from the mantle. Also shown in Fig. 90 are olivine fractionation lines from some ferropicrite analyses thought to be close to the parental liquid in composition. They demonstrate that olivine fractionation may cause the residual liquid to cross the Ol+Gt stability curve but the degree of this fractionation should be large. In the latter case, a highly magnesian liquid generated at a pressure range of 55-70 kbar could in principle fractionate to a ferropicritic composition by an extensive amount of olivine separation. However, this alternative is highly implausible not only because of the problem of high Ni in ferropicrites, as discussed earlier, but also because of the difficulty of segregation of ferropicritic liquid owing to the predicted density crossover of the liquid and its residue at very high pressures (Hanski, 1989). Moreover, melting at very high pressures would produce liquids with

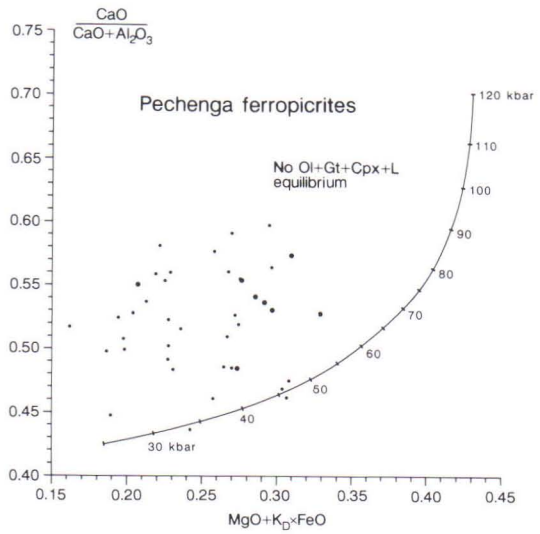


Fig. 91. $CaO/(CaO+Al_2O_3)$ vs. $MgO+K_D \times FeO$ diagram (cation mole proportion) for evaluating olivine-garnet-clinopyroxene-liquid equilibria. Curve shows $CaO/(CaO+Al_2O_3)$ values and minimum $MgO+K_D \times FeO$ value as a function of pressure for a liquid in equilibrium with an Ol+Gt+Cpx-bearing mineral assemblage. $MgO+K_D \times FeO$-pressure relation taken from Fig. 86. CaO and $Al_2O_3$ (wt. %) were calculated by using the equation $a + bP + cP^2 + dP^3$ where P is pressure in kbar and coefficients a=18.60, b=-0.2699, c=2.299, d=-6.80 for CaO and a=26.04, b=-0.4775, c=3.677, d=-10.86 for $Al_2O_3$ (Herzberg, 1992). Small symbols represent individual analyses and larger ones average values of several samples and weighted averages of flows.

$CaO/Al_2O_3$ values larger than those observed in ferropicrites (see below).

It has long been known that, with increasing pressure, the liquidus field of garnet is expanded against that of clinopyroxene thereby causing liquids in equilibrium with Gt and Cpx to acquire higher $CaO/Al_2O_3$ with increasing pressure (O'Hara, 1968). Using high-pressure and ultra-high-pressure experimental data on the system $CaO-MgO-Al_2O_3-SiO_2$, Herzberg (1992) found that $CaO/(CaO+Al_2O_3)$ increases systematically as a function of pressure in liquids multiply saturated in garnet and clinopyroxene. He was also able to demonstrate that the same relation holds equally for iron-bearing systems, since the addition of iron neither expands nor contracts the crystallization field of garnet with respect to that of clinopyroxene. According to Herzberg's data, $CaO/(CaO+Al_2O_3)$ (wt. %) of an initial melt from a peridotite with the residual mineral assemblage Ol+Opx+Cpx+Gt increases from 0.44 to 1.0 when pressure increases from 22 kbar to 158 kbar. When Fig. 89, which gives the minimum $Al_2O_3$ content at a given $MgO+K_D \times FeO$ level for a liquid in equilibrium with Ol+Gt, is combined with the $CaO/(CaO+Al_2O_3)$-pressure relation of Herzberg (1992) for the Gt+Cpx+L-P equilibria, a value for $CaO/(CaO+Al_2O_3)$ (and the minimum CaO content) at a given $MgO+K_D \times FeO$ level is obtained for liquids that are in equilibrium with Ol+Cpx+Gt. The result is presented in Fig. 91. Taking into account, firstly, that the curves in Fig. 86 and 91 represent minimum values of $MgO+K_D \times FeO$ at each pressure and, secondly, that $CaO/(CaO+Al_2O_3)$ does not tend to change significantly as the degree of melting increases, as long as the partial melts are buffered by both garnet and clinopyroxene, it can be inferred that the actual liquids segregating from an Ol+Gt+Cpx-bearing residuum will plot on the right-hand side of the curve in Fig. 91. It should be kept in mind that a positive result with respect to the Ol+Gt+Cpx+L equilibria obtained from Fig. 91 is only valid in combination with the $Al_2O_3$ vs. $MgO+K_D \times FeO$ diagram where the same liquid should plot above the Ol+Gt+L stability curve. Also we should remember that Fig. 91 is applicable to dry conditions and $CO_2$ in particular has a strong effect on the $CaO-Al_2O_3$ relations of liquids (Adam, 1988).

In spite of the uncertainty involved in the estimation of $CaO/(CaO+Al_2O_3)$ for the ferropicritic magma, it can be rather confidently stated that this ratio was equal to or higher than 0.48 in cation mole percentages ($CaO/Al_2O_3 \geq 1$ in weight percentages) (Table 17, 18). This value is too high compared with the $MgO+K_D \times FeO$ level of ferropicrites for it to plot in the field of liquids

that can be in equilibrium with the mineral assemblage Ol+Gt+Cpx (Fig. 91). Consequently, provided that the diagrams based on anhydrous experimental high-pressure data are relevant to the melting process generating ferropicrites, it can be concluded that the $Al_2O_3$-MgO+$K_D$×FeO relations of ferropicrites rule out the presence of olivine+garnet among residual minerals while the CaO/$Al_2O_3$-MgO+$K_D$×FeO relations eliminate the possibility of olivine+garnet+clinopyroxene in the residuum. The diagrams in Fig. 89 and 91, however, do not exclude clinopyroxene from being among the residual minerals and hence the potential mineral combinations in the residuum are Ol, Ol+Opx, Ol+Opx+Cpx, and Ol+Cpx.

Before considering the implications of the above conclusions, it is necessary to establish the experimental uncertainties involved in the construction of the diagrams in Figures 85 and 86 and to determine the effects of the compositional parameters, including volatile contents, on the high-pressure mineral equilibria.

Because all the liquid compositions utilized in Figures 85 and 86 are iron-bearing, it is worth discussing the problem of iron loss, which is often encountered in experimental studies of iron-bearing systems. Platinum and its alloys are commonly used as a capsule material in high-T-P experiments due to their appropriate physical properties, but these materials have the disadvantage that they readily form alloys with iron (e.g., Merrill and Wyllie, 1973). In this context, it is useful to note Thompson's (1984) observation that experiments conducted using Pt capsules have yielded olivine-saturated liquids that are higher in normative olivine at a given pressure than liquids produced in graphite, Fe or Pt/Fe alloy capsules. Therefore, the iron loss problem has probably not been responsible for the location of the minimum MgO+$K_D$×FeO curve at too low a level in Fig. 86.

One of the problems involved in experimental petrology is the insufficient attainment of an equilibrium between the liquid and crystalline phases. The partitioning of elements between coexisting phases can be used as a measure of the approach to equilibrium conditions. In particular, Fe-Mg exchange coefficients between olivine and liquid that are too high or too low are indicative of disequilibrium conditions or changes in liquid composition during the run. On the basis of their low $K_D$ values (around 0.20), some liquid compositions, which would plot beneath the minimum MgO+$K_D$×FeO curve in Fig. 86, were rejected.

The composition of partial melts produced in peridotite melting experiments are often elusive owing to the overgrowth of quench crystals on stable residual phases, especially at high pressures and in the cases of low viscosity melts (e.g., Green, 1973a; Jaques and Green, 1979, 1980). The elimination of the quench problem has been attempted using broad beam microprobe analyses, calculations of liquid composition based on the mode and mineral analyses, and employing a sandwich technique (e.g., Jaques and Green, 1980; Takahashi and Kushiro, 1983). The quench problem is not so serious for liquidus experiments, which represent the majority of the experimental runs utilized in Figures 85-86. Saturation in a particular phase, however, can not always be ascertained in these experiments because of the reaction relationship of this mineral with the liquid. Fortunately, amongst the mantle minerals, this problem is not so often encountered in the case of olivine and garnet as it is in the case of orthopyroxene.

As discussed earlier, the presence of magmatic amphibole and mica in ferropicritic rocks suggest a hydrous nature for the magma from which they crystallized. It is therefore essential to establish the possible effects of water on high-pressure phase relations. The major effect of $H_2O$ is to de-polymerize the silicate melt. One consequence of this is that the phase field of olivine is expanded with respect to that of orthopyroxene, leading to the stabilization of olivine with relatively silica-rich liquids (e.g., Kushiro, 1972). The enlargement of the olivine phase field at higher pressures also causes a melt, with a given normative olivine content, to crystallize olivine at higher pressures than would be the case under dry conditions. This means that the addition of water to a system will tend to shift the olivine stability curve in Fig. 86 to a higher pressure (to the right)

and the Ol+Gt saturation curve in Fig. 88 to the left. In Fig. 87, water-undersaturated melt compositions with $H_2O \leq 5\%$ (crosses), which have been experimentally shown to be in equilibrium with olivine, are plotted against pressure and compared with the olivine stability curve taken from Fig. 86. Restriction to water contents of this amount is probably a reasonable assumption because, given a much higher water content of a primitive melt, it would become water-saturated at some depth during its ascent. Further uprise of a hydrous magma to the surface would necessitate subvolcanic degassing and extensive crystallization. Apart from a few exceptional melt compositions reported by Foden and Green (1992) and Thibault et al. (1992), all wet compositions plot above the olivine saturation curve in Fig. 87. This suggests that the minimum $MgO+K_D \times FeO$ value at a given pressure obtained from the curve is a reliable estimate for an anhydrous melt.

Sekine and Wyllie (1973) have studied experimentally the effect of $H_2O$ on liquidus relationships in the system $MgO-Al_2O_3-SiO_2$ at 30 kbar pressure. They found that, with increasing water content, the liquid coexisting with forsterite, orthopyroxene and pyrope is depleted in MgO and enriched in $SiO_2$ and $Al_2O_3$. Adam's (1988) experimental data on the $CaO-MgO-Al_2O_3-SiO_2-H_2O$ system at 28 kbar also clearly show that the garnet lherzolite-liquid invariant point moves to higher $Al_2O_3$ contents with increasing $H_2O$. This is compatible with Fig. 88 in which hydrous melt compositions do not plot below the garnet saturation curve as defined by anhydrous experiments. The available experimental data suggest that, at least at pressures around 30 kbar, the presence of water in a liquid is not capable of moving the olivine-garnet saturation curve towards the origin in Fig. 89. This inference is corroborated by the position of natural hydrous, multiply-saturated silicate liquids in the $Al_2O_3$ vs. $MgO+K_D \times FeO$ diagram on the right hand side of the Ol+Gt+L stability curve. These liquids have been experimentally shown to be in equilibrium simultaneously with olivine and garnet by Nicholls and Ringwood (1973), Green (1973b), Mengel and Green (1989), Ulmer (1988), Ulmer et al. (1990), and Thibault et al. (1992). Thus, experimental evidence suggests that moderate water contents cannot change the Ol+Gt saturation boundary to lower $MgO+K_D \times FeO$ and $Al_2O_3$ contents in Fig. 89, and therefore the position of ferropicrites below the curve can not be an artifact of their hydrous nature.

Phase boundaries at high pressures are also controlled by $CO_2$ abundances of silicate liquids (e.g., Adam, 1988). The major effect of adding $CO_2$-fluids to basaltic systems is an expansion of the orthopyroxene phase volume at the expense of that of olivine. $CO_2$ is therefore not likely to shift the olivine stability curve in Fig. 86 to lower $MgO+K_D \times FeO$ values (see Fig. 87). The solution of $CO_2$ also leads to the expansion of the liquidus phase volume of garnet against that of clinopyroxene. The net effect is that, with increasing $CO_2$ content, liquids in equilibrium with garnet lherzolite will decrease in $SiO_2$ and $Al_2O_3/MgO$ and increase in $CaO/Al_2O_3$. These effects are similar to those caused by increasing pressure. Pure $CO_2$ fluid is, however, not an efficient agent for bringing the olivine and garnet liquidus fields closer to each other (e.g., Adam, 1990). Instead, a solution of mixed $H_2O+CO_2$ fluids in the melt may result in a sufficient lowering of the pressure range of the garnet liquidus field and a sufficient increase in the pressure range of the olivine liquidus field for them to intersect each other (Green, 1973b; Adam, 1990). In Fig. 89, olivine+garnet saturated liquid compositions with mixed $H_2O-CO_2$ fluids studied by Adam (1990) and Brey and Green (1977) are located closest to the Ol+Gt saturation curve. These compositions are low-silica liquids such as olivine basanites, olivine nephelinites, and olivine melilitites. The possibility of the displacement of ferropicritic compositions beneath the curve in Fig. 89 being a result of their high $CO_2$ or $H_2O+CO_2$ concentrations is not supported by any independent evidence for high $CO_2$ in ferropicrites. In addition, chemical and mineralogical data indicate that the ferropicritic parental magma was not silica-undersaturated although silica activity was not high, as can be inferred from the absence of orthopyroxene in ferropicritic rocks.

Finally, the effects of other compositional parameters, namely iron and alkalies, on the phase equilibria are to be considered. Because FeO expands the crystallization field of garnet at the expense of that of olivine (Herzberg, 1992), the addition of iron may lead to the stabilization of a liquid with garnet lherzolite at lower pressures and with lower $Al_2O_3$ contents of the liquid. This is compatible with the observation that the transition from a spinel- to garnet-bearing mantle assemblage occurs at lower pressures in the iron-rich mantle (Patera and Holloway, 1982). Hence, it is pertinent to consider the significance of the high iron content of ferropicrites and their position with respect to the Ol+Gt saturation curve in Fig. 89.

Bertka and Holloway (1988) have experimentally bracketed the initial, multiply-saturated melt composition (23.3 wt. % FeO) of a model iron-rich Martian garnet lherzolite mantle at 23 kbar pressure. This composition plots well above the Ol+Gt saturation curve in the $Al_2O_3$ vs. $MgO+K_D \times FeO$ diagram (Fig. 89). Additional experimental evidence is provided by Agee and Walker (1988) who conducted high-pressure melting experiments on various komatiite-fayalite mixtures saturated in olivine. They did not report liquidus garnet even in the charges richest in iron. These data and other experimental results on high-FeO liquids have been utilized in the construction of the diagrams in Figures 85 and 86. As shown in Fig. 92, there is a wide range in the FeO contents of the liquids studied experimentally, and therefore, it is believed that the diagrams used in this study are suitable for both low- and high-iron liquids.

The high alkali content of a liquid causes the liquidus fields of olivine and orthopyroxene to expand, thereby resulting in lower MgO+FeO contents of multiply saturated liquids (e.g., Kushiro, 1975). As with iron, the alkali content of experimental liquids employed vary within wide limits and their influences have therefore been taken into account (see Fig. 92).

It is apparent that we can ignore the complications discussed above and conclude that the $Al_2O_3$ vs. $MgO+K_D \times FeO$ diagram is applicable to the

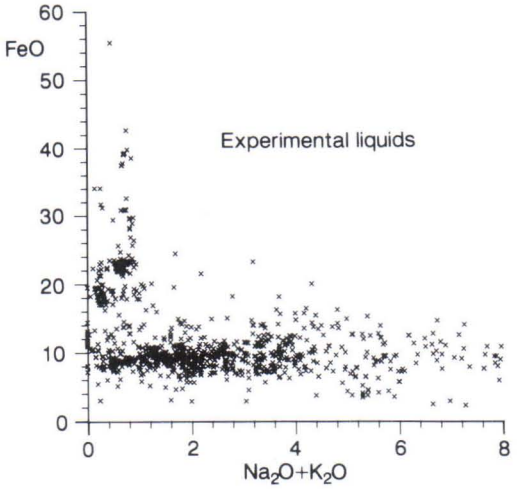


Fig. 92. $FeO_{tot}$ and $Na_2O+K_2O$ (wt. %) contents of experimental liquids utilized in construction of Figures 85-88.

interpretation of the residual mineralogy of the Pechenga ferropicrites. The implication of this is that ferropicrites could not have left a garnet- or garnet+clinopyroxene-bearing residue. Consequently, they are not the products of a low degree of melting at pressures within the stability range of the garnet peridotite facies.

The absence of residual garnet may be the result of its elimination during the partial melting process or because the pressure of melt segregation was lower than the stability of garnet lherzolite mineral assemblage. In the former case, garnet will be totally consumed if the degree of melting is sufficiently large. Garnet lherzolite melting studies by Harrison (1981) at 35 kbar pressure suggest that in a mantle having a composition similar to that of primitive mantle or pyrolite, garnet is totally exhausted when the percentage of the melt fraction is about 10%. The amount of melting is, however, dependent on the pressure and the original modal abundance of garnet in peridotite. The latter is in turn directly proportional to the $Al_2O_3$ content of the source rock.

## Major elements

It was concluded in the chapter on geochemistry that high iron contents are an intrinsic feature of the ferropicritic liquid. It thus remains to be established whether the elevated iron content is an inherited property from an iron-rich mantle or a result of special conditions during mantle melting. Conditions of melting affect the partitioning of iron and magnesium between crystalline and liquid phases. Because the iron content of a basic liquid is a function of the pressure of partial melting in the mantle, and increases with increasing pressure, a source with a relative low Fe/Mg can generate relative iron-rich melts at high pressures (Hanson and Langmuir, 1978).

Also the effects of the volatile content of the liquid on Fe-Mg partitioning should be taken into consideration. Recent high-pressure volatile-bearing experiments by Ulmer (1989), McFarlane and Drake (1990) and Kushiro (1990) have demonstrated that neither moderate contents of $H_2O$ nor $CO_2$ have a significant influence on the exchange coefficient $K_D$. It follows that the high FeO of the ferropicrites cannot be attributed to changing of $K_D$ as a result of a high volatile activity.

Many investigators have observed a slight positive pressure dependence of the exchange $K_D$ (e.g., Takahashi and Kushiro, 1983). The increase of $K_D$ with increasing pressure results in liquids with lower FeO/MgO in equilibrium with olivine of a constant composition. This, however, does not mean lower absolute FeO abundances of the liquid at higher pressures, but in contrast, liquids produced by small extents of partial mantle melting will move towards increasing FeO and MgO content with increasing pressure of melting. The reason for this is the rise in the solidus temperature of the mantle peridotite with increasing pressure which counteracts the opposite effect induced by the increase of olivine-liquid partition coefficients ($K_d$) for both MgO and FeO with increasing pressure at a constant temperature (Hanson and Langmuir, 1978).

If the high FeO of the ferropicrites is regarded as a result of melting at a high pressure, a necessary consequence would be high MgO as well, due to the practically constant $K_D$. For example, using $K_D$ values of 0.33-0.38, a melt with 13% FeO is calculated to have a MgO range of 20-22.5% when equilibrated with olivine of $Fo_{89}$, which is the composition of olivine at the solidus in a pyrolitic mantle. If the residual olivine has a composition of $Fo_{93}$ the MgO content of the melt will be 32-36%.

It is thus impossible to obtain a ferropicritic composition with approximately equal amounts of FeO and MgO (wt. %) from a pyrolitic mantle without violating the concept of the constant exchange $K_D$, which is the cornerstone in petrogenetic studies of primitive magmas. Therefore,

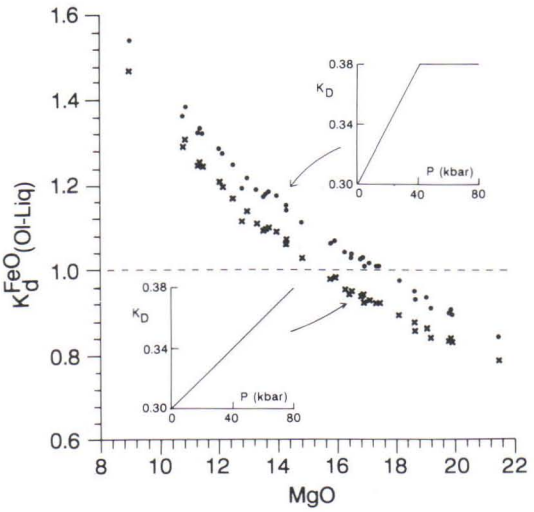


Fig. 93. Partition coefficient of FeO between olivine and liquid as a function of MgO (wt. %) of ferropicritic liquid. Upper curve has been computed using the $K_D$-pressure relation of Takahashi and Kushiro (1983) and lower curve using a linear $K_D$-pressure relation as indicated by the insets.

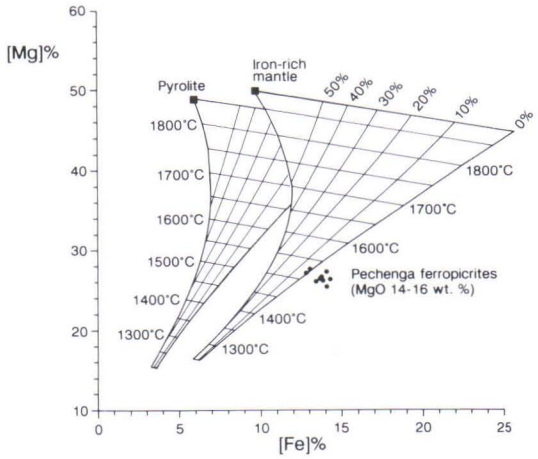


Fig. 94. Pechenga ferropicrites with 14-16 wt. % MgO plotted on an [Mg] vs. [Fe] diagram. [Mg] and [Fe] are compositionally corrected Mg and Fe abundances in cation mole percentages (see Rajamani et al., 1985). Fields with isotherms and melt per cent curves represent permissible compositions of melts produced at 25 kbar from a pyrolitic mantle with MgO 38.1 wt. %, FeO 8.0 wt. %, and Mg/(Mg+$Fe^{2+}$) 0.895 (Ringwood, 1979) and from an iron-rich mantle with 39.1 wt. % MgO, 13.0 wt. % FeO, and Mg/(Mg+$Fe^{2+}$) 0.843. Melt fields and [Fe] and [Mg] values were calculated by using the programs of Rajamani et al. (1989).

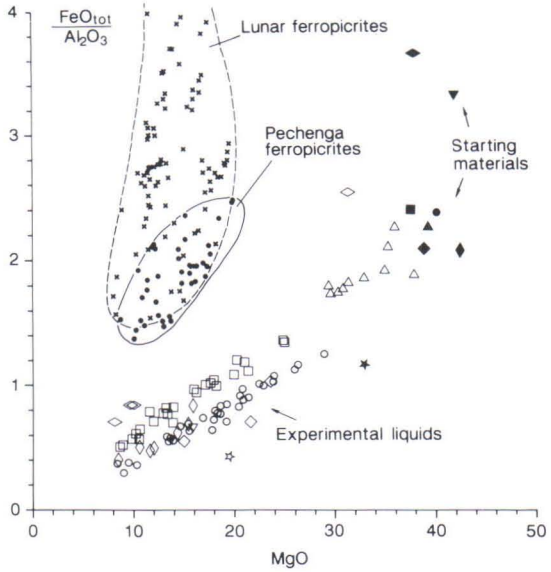


Fig. 95. Variation of $FeO/Al_2O_3$ as a function of MgO in ferropicritic rocks (small dots), lunar ferropicrites (crosses), and liquids produced experimentally in high-pressure melting experiments of terrestrial mantle peridotites. Experimental liquids and corresponding starting materials are marked by open and closed symbols, respectively. Experimental data from Jaques and Green (1980), Sen (1982), Takahashi (1986), Takahashi and Scarfe (1985), Scarfe et al. (1979), McFarlane and Drake (1990), Falloon et al. (1988), Kushiro (1973), and Kushiro et al. (1972). Lunar data taken from Delano (1986), Hughes and Schmitt (1988), Hughes et al. (1988), Ryder and Steele (1987), and Shearer et al. (1990).

the only explanation for the elevated FeO abundance in ferropicrites appears to be an exceptionally high FeO content in their mantle source region.

In the following discussion, an attempt is made to derive constraints that can be imposed on the possible FeO and $Al_2O_3$ abundances in the mantle source of the ferropicrites. Iron is generally regarded as a slightly incompatible element during mantle melting processes. This is evidenced, for example, by compositions of mantle xenoliths and Alpine-type peridotites that have experienced various degrees of melt extraction. They commonly display compositional trends with a gentle decrease in iron with increasing MgO (e.g., Frey et al., 1985). The incompatibility of iron means that the FeO content of the source mantle peridotite can not exceed that of the liquid produced from it. However, iron is not necessarily always an element enriched in the liquid relative to the crystalline residue. The partition coefficient of iron between olivine and liquid ($K_d$) increases with decreasing temperature under isobaric conditions and increases with pressure under isothermal conditions. Figure 61 shows that the tangents of the olivine fractionation curves change their coefficients from negative to positive with the decreasing MgO content (and temperature) of the liquid. This corresponds to a change in the behavior of iron from incompatible to compatible. This transition will shift to more MgO-rich liquid compositions with increasing pressure

Table 26. Analyses of model primitive mantle (#1-2), average mantle xenoliths (#3-5) and iron-rich mantle samples (#6-11).

| | 1 | 2 | 3 | 4 | 5 | 6 | 7 | 8 | 9 | 10 | 11 |
|---|---|---|---|---|---|---|---|---|---|---|---|
| $SiO_2$ | 45.10 | 44.80 | 44.15 | 44.40 | 44.99 | 42.90 | 42.28 | 42.37 | 41.37 | 40.27 | 43.48 |
| $TiO_2$ | 0.20 | 0.21 | 0.07 | 0.13 | 0.06 | 0.25 | 0.28 | 0.28 | 0.30 | 0.47 | 0.13 |
| $Al_2O_3$ | 3.30 | 4.45 | 1.96 | 2.38 | 1.40 | 1.53 | 3.96 | 3.50 | 3.88 | 2.56 | 2.65 |
| $FeO_{tot}$ | 8.00 | 8.00 | 8.28 | 8.31 | 7.89 | 13.00 | 17.44 | 14.82 | 13.69 | 15.93 | 16.22 |
| MnO | 0.15 | 0.14 | 0.12 | 0.17 | 0.11 | 0.14 | 0.28 | 0.20 | 0.21 | 0.24 | 0.25 |
| MgO | 38.50 | 37.20 | 42.25 | 42.06 | 42.60 | 38.40 | 32.01 | 34.71 | 35.07 | 33.08 | 29.40 |
| CaO | 3.10 | 3.60 | 2.08 | 1.34 | 0.82 | 1.90 | 2.59 | 2.39 | 4.55 | 5.19 | 2.95 |
| $Na_2O$ | 0.40 | 0.34 | 0.18 | 0.27 | 0.11 | 0.16 | 0.18 | 0.26 | 0.23 | 0.31 | 0.40 |
| $K_2O$ | - | 0.03 | 0.05 | 0.09 | 0.04 | 0.02 | 0.02 | 0.01 | 0.03 | 0.11 | 0.13 |
| $P_2O_5$ | - | 0.02 | 0.02 | 0.06 | - | - | 0.03 | - | 0.02 | 0.08 | 0.04 |
| $Cr_2O_3$ | 0.40 | 0.38 | 0.44 | 0.44 | 0.32 | 0.11 | 0.34 | 0.29 | 0.16 | 0.30 | 0.25 |
| NiO | - | 0.22 | 0.27 | 0.31 | 0.26 | - | 0.14 | - | 0.11 | 0.12 | 0.22 |
| L.O.I. | - | - | - | - | - | 0.38 | 0.07 | 0.05 | - | 1.50 | 3.50 |
| Total | 99.15 | 99.39 | 99.87 | 99.96 | 98.60 | 98.79 | 99.62 | 98.88 | 99.62 | 100.16 | 99.62 |

**1**, pyrolite (Ringwood, 1979); **2**, primitive mantle (McDonough and Frey, 1989); **3**, average continental spinel lherzolite (Maaløe and Aoki, 1977); **4**, average oceanic spinel lherzolite (Maaløe and Aoki, 1977); **5**, average garnet lherzolite (Maaløe and Aoki, 1977); **6**, garnet lherzolite xenolith, Colorado Plateau (Ehrenberg, 1982); **7**, Al-augite lherzolite xenolith, Arizona (Wilshire et al., 1988); **8**, spinel peridotite adjacent to a pyroxenite vein, Eastern Pyrenees (Bodinier et al., 1988); **9**, spinel lherzolite wall rock of a pyroxenite dike (Irving, 1980); **10**, spinel lherzolite xenolith, Veneto Region, Italy (Morten, 1987); **11**, spinel lherzolite xenolith, New South Wales, Australia (Wilkinson and Binns, 1977).

because of the increase of the exchange coefficient $K_D$ with increasing pressure. The experiments of Takahashi and Kushiro (1983) and Agee and Walker (1988) suggest that $K_D$ increases from about 0.30 at 1 atm to 0.38 at 40 kbar with no essential further changes at higher pressures, while the results of some other investigators indicate a less rapid increase of $K_D$ with pressure (Bickle et al., 1977). Depending on which pressure-$K_D$ relation is adopted, the $K_d$ value for FeO between olivine and liquid varies from 1.0-1.1 for a ferropicritic melt composition with 15 wt. % MgO, as demonstrated in Fig. 93. In any case, $K_d$ of FeO appears to be close to unity for a ferropicritic parental magma.

Because olivine is the most Fe-rich silicate mineral of the possible residual phases, the maximum estimate of the FeO content of the source mantle for ferropicrites is obtained by assuming that they were generated by a large degree of melting leaving olivine as the sole residual mineral. In such a case, $K_d$ values are close to unity and mass balance calculations yield $FeO_{tot}$ contents of 14-15 wt. % for the source mantle region.

Using stoichiometric constraints, mass balance and temperature dependences of iron and magnesium partitioning between olivine and silicate liquids, Hanson and Langmuir (1978) were able to construct an olivine saturation surface on a MgO vs. FeO diagram. This diagram shows permitted melt and residue compositions produced by melting of a given mantle composition under a given pressure. Later Rajamani et al. (1985) modified the diagram by taking into account the compositional dependence of iron and magnesium partitioning as expressed by Ford et al.

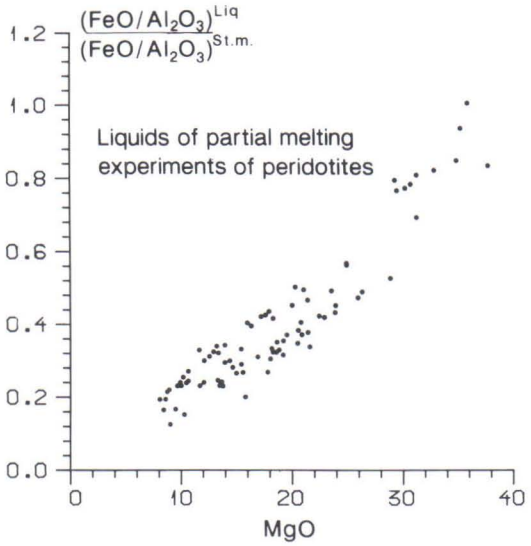


Fig. 96. Ratio of ($FeO/Al_2O_3$) in liquid to ($FeO/Al_2O_3$) in starting material (St.m.) plotted against MgO (wt. %) of liquid from high-pressure partial melting experiments of mantle peridotites. Experimental data sources same as in Fig. 95.

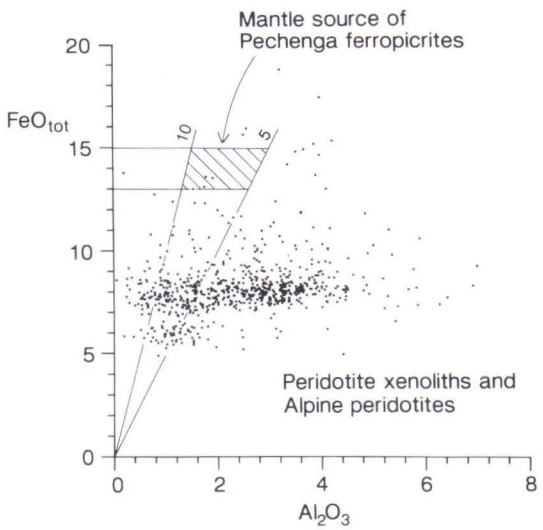


Fig. 97. Plot of $FeO_{tot}$ against $Al_2O_3$ abundances (wt. %) in mantle xenoliths and Alpine peridotites from the literature and the estimated field of the potential source rock composition for the Pechenga ferropicrites (see text).

(1983). They presented melt fields on a diagram plotting compositionally corrected [Fe] and [Mg] in cation mole proportions against each other. The right-hand boundary of the olivine-saturated melt field in the [Mg] against [Fe] diagram represents a solidus melt composition (Fig. 94). With an increasing extent of mantle melting, the MgO content of liquid increases but the FeO content decreases (Langmuir and Hanson, 1980). Thus the solidus melt is the most iron-rich melt produced from a given mantle composition. This means that the minimum iron content for the source of the ferropicrites can be estimated by finding a mantle composition whose initial melt composition approaches the composition of the ferropicritic melt. Figure 94 demonstrates that the calculated initial melt line for a mantle with 39.0 wt. % MgO and 13.0 wt. % FeO [$Mg/(Mg+Fe^{2+})$ 0.842] passes close to the field of ferropicrites with MgO in the range 14-16 wt. %. A melt field for a pyrolitic mantle [MgO 38.1 wt. %, FeO 8.0 wt. %; $Mg/(Mg+Fe^{2+})$ 0.895; Ringwood, 1979] is also shown for comparison in Fig. 94.

The previous discussion suggests that the $FeO_{tot}$ content of the mantle source of ferropicritic magmas falls somewhere between 13-15 wt. %. As is revealed in Table 26, this figure is exceptionally high compared with typical mantle compositions, such as the pyrolite model mantle of Ringwood (1979) or the average garnet and spinel lherzolites of Maaløe and Aoki (1977).

Figure 95 illustrates an $FeO_{tot}/Al_2O_3$ vs. MgO plot where ferropicritic rock compositions are compared with experimentally produced partial melts of mantle peridotites and the compositions of starting materials used in these experiments. The experimental melts display semi-linear trends projecting to the compositions of the corresponding starting materials. Analyses of the Pechenga ferropicrites are clearly displaced to higher $FeO_{tot}/Al_2O_3$ values at a given MgO content compared with experimental liquid compositions from terrestrial peridotites. Instead, the Pechenga rocks straddle the low iron part of the lunar ferropicrite

field. The position of the ferropicritic trend considerably above the field of experimental liquids obviously proves that the source material of the Pechenga ferropicrites had a higher $FeO_{tot}/Al_2O_3$ value than that in common upper mantle peridotites.

In order to obtain a more quantitative estimation of the $FeO_{tot}/Al_2O_3$ value in the source mantle of the Pechenga ferropicrites, this ratio is compared between liquids and the starting peridotites in high-pressure melting experiments as a function of the MgO content of liquid in Fig. 96. With increasing degrees and pressures of melting, the composition of the liquid approaches the composition of the starting material, which accounts for the positive correlation seen in Fig. 96. As shown in the diagram, the $FeO/Al_2O_3$ value of a liquid with 15 wt. % MgO is 0.2-0.4 of the value of the starting material. From this simple relationship and the average $FeO/Al_2O_3$ value of the Pechenga ferropicrites at the same MgO level (Fig. 96), a possible $FeO/Al_2O_3$ range in the source region of the ferropicrites can thus be calculated. This range is expressed as two straight lines diverging from the origin in Fig. 97. Utilizing these lines and the previous estimate on the range of $FeO_{tot}$, a field is delineated for potential source rock compositions. The likely $Al_2O_3$ content of the source of ferropicrites falls within the range of 1.3-3.0 wt. % which is clearly less than the level of the estimated primitive mantle composition (4.45 wt. %, Table 26). Figure 97 also shows compositions of peridotite xenoliths and Alpine-type peridotites collected from the literature. Only very few of these plot inside the field of the potential source compositions of ferropicrites. These include peridotite compositions published by Bodinier et al. (1988), Ehrenberg (1982), Irving (1980), and Morten (1987).

## Trace elements

The absence of residual garnet suggests that the LREE enrichment of the Pechenga ferropicrites was inherited from the mantle source. This suggestion is corroborated by model calculations using the equation of equilibrium batch-melting of Shaw (1970) and a source with chondritic relative abundances of REE. In order to produce a melt with chondrite-normalized La/Yb similar to that of ferropicritic parental magma (≥10), the bulk partition coefficient for Yb between the residue and the liquid should be more than 10 times greater than that for La. None of the likely mineral combinations of olivine, orthopyroxene, clinopyroxene, and spinel can yield such bulk partition coefficients. As shown in Fig. 98, for any combinations of residual olivine, orthopyroxene, and clinopyroxene, the source must have had a chondrite-normalized La-Yb ratio higher than 4. Depending on the degree of melting, this ratio is in the range 6-9 in the case of an olivine-rich (>70%) residue. The inevitable conclusion is that the source region of the ferropicrites was enriched in light REE relative to heavy REE. Also, the elevated concentrations of many other incompatible trace elements, including high field strength elements (HFSE), can most probably be attributed to the high abundances in the source mantle.

It was noted earlier that the Pechenga ferropicrites have abnormally low phosphrous contents compared with other incompatible trace elements (Fig. 54). This could be related to the presence of residual apatite in the mantle source but the saturation of a basic to ultrabasic magma in apatite requires a minimum $P_2O_5$ content of tens of that observed in the ferropicrites (Kogarko et al., 1987). Thus, the relatively low $P_2O_5$ content is most probably a feature inherited from the source mantle composition.

The situation at Pechenga is analogous with that of Hawaiian picrites possessing high MREE/HREE values. Models based on trace ele-

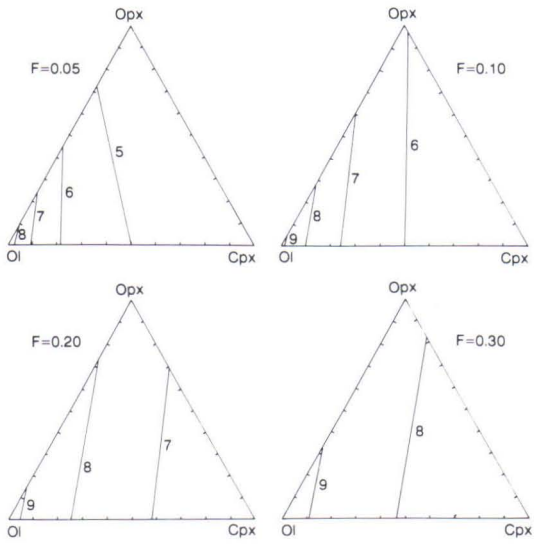


Fig. 98. Calculated chondrite-normalized La/Yb value in the source mantle peridotite of ferropicritic magma with $(La/Yb)_N=10$ as a function of modal composition of the residue and the melt fraction (F). Calculation was performed using the equilibrium batch-melting equation $C_L/C_o=1/(D\times(1-F)+F)$ where $C_L$ is the concentration of the element in the liquid, $C_o$ the initial concentration of the element in the source, D the bulk partition coefficient, and F the melt fraction (Shaw, 1970). Partition coefficients taken from Prinzhofer and Allègre (1985). Ol = olivine, Opx = orthopyroxene, Cpx = clinopyroxene.

ment geochemistry advocate the generation of the Hawaiian picrites within the garnet peridotite stability field (e.g., Lanphere and Frey, 1987). However, high pressure liquidus experiments on proposed parental picritic compositions demonstrate that garnet is not a liquidus phase below about 35 kbar and there is a large pressure gap of about 15 kbar between the Ol+Opx saturation point and the liquidus garnet field (Eggins, 1992a). It should be noted that these experiments are consistent with peridotite melting studies by Falloon et al. (1988) which suggest that Hawaiian picrites equilibrated with harzburgite residues at about 20 kbar. The discrepancy between interpretations based on phase equilibria and geochemical studies implies that either the parental magma for Hawaiian tholeiites was much more MgO-rich than the compositions studied experimentally (MgO 16-19%) and hence was able to equilibrate with garnet lherzolite at high pressures or, alternatively, the melt left behind a harzburgitic residue at moderate pressures, while the Hawaiian mantle source did not possess chondritic relative abundances of middle and heavy rare earth elements. In the latter case, potential origins include the melting of the previously enriched oceanic lithosphere or by dynamic melt segregation processes in an ascending mantle plume as discussed by Eggins (1992a,b).

It is also tempting to apply the $Al_2O_3$ vs. $MgO+K_D\times FeO$ diagram to other primitive volcanic rocks. Figure 99 compares komatiitic rocks from a number of greenstone belts on this diagram. In the Ol+Gt+L-forbidden region, most of the Al-depleted komatiites from South Africa are associated with iron-rich komatiites from Minnesota (Green and Schulz, 1977) and northeastern and northwestern Ontario (Canada) (Stone et al., 1987; Schaefer and Morton, 1991) as well as Al-depleted komatiites from the Pilbara Block (Western Australia) (Gruau et al., 1987) and India (Jahn et al., 1982). The reason for the Al- and HREE-depleted nature of the Barberton-type komatiites has been the subject of much discussion in the literature (e.g., Ohtani, 1990; Gruau et al., 1990). As is indicated by Fig. 99, komatiites from South Africa could not have left a garnet-bearing residue unless the parental magma had a very high MgO content and pressures during segregation were extremely high (about 100 kbar). In this case, variable and in many cases extensive, olivine fractionation would be required to produce low-magnesian komatiites in South Africa.

Figure 100 shows 1840 nonkomatiitic magnesian rock compositions plotted on the $Al_2O_3$ vs. $MgO+K_D\times FeO$ diagram. The majority of them have sufficiently high $Al_2O_3$ and $MgO+K_D\times FeO$ to be capable of coexisting simultaneously with olivine and garnet, but many low-Al compositions plot below the curve. These volcanic rocks include, for example, boninites from various regions (e.g., Cameron, 1989), siliceous high-

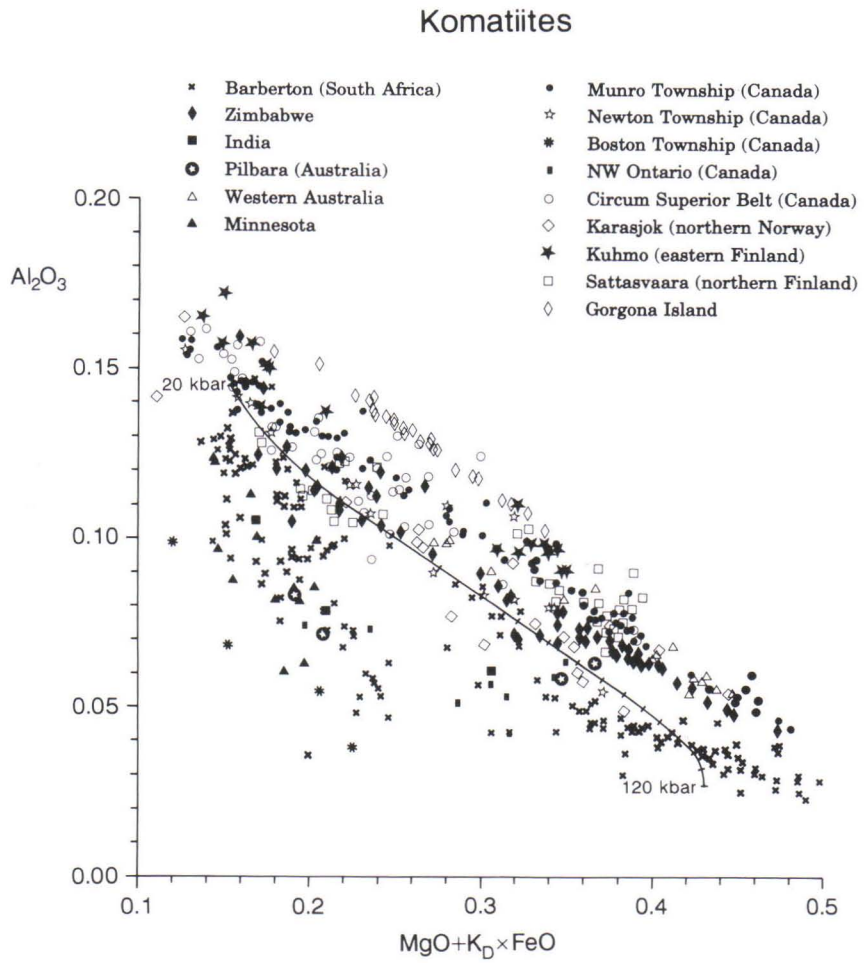


Fig. 99. $Al_2O_3$ vs. $MgO+K_D \times FeO$ diagram for komatiitic metavolcanites. Ol+Gt+L stability curve taken from Fig. 89.

magnesian basalts from Australia (Sun et al., 1989), Karoo picrites from South Africa (Duncan et al., 1984), tholeiitic picrites from Munro Township, Canada (Arndt, 1977a), picrites from the Norilsk area (Fedorenko, 1983), Oskol ferropicrites from the Ukraine (Krestin and Yudina, 1988), the parental magma of the gabbro-wehrlite intrusions in Finland (Hanski, 1986; Vuollo and Piirainen, 1992), some of the Deccan picrites (Krishnamurthy and Cox, 1977), and meimechites and associated olivine melilitites from the Maymecha Kotuy Province in Siberia (Sobolev and Slutskii, 1984). The position of these primitive magmas and also some iron-rich komatiites below the curve is not surprising because, as stated previously, they share many geochemical features with the Pechenga ferropicrites.

It is interesting to note that many of the rock

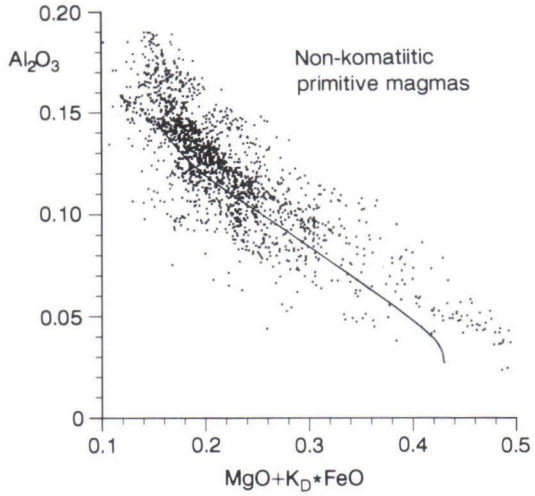


Fig. 100. $Al_2O_3$ vs. $MgO+K_D \times FeO$ diagram for nonkomatiitic primitive magma compositions. Ol+Gt+L stability curve taken from Fig. 89.

types lying below the Ol+Gt saturation curve in Figures 99 and 100 are enriched in LREE elements, a feature which has usually been attributed to the fractionation effect of residual garnet (e.g., Kay and Gast, 1973). This kind of interpretation appears, however, to be in conflict with their position in the Ol+Gt+L-forbidden field in Figures 99 and 100 which indicates that, at least under dry conditions, these magmas could not leave behind a garnet-bearing residue. Instead, geochemical data suggest substantial REE heterogeneity in the mantle region from which these volcanic rocks were derived.

## Isotopic constraints

In Fig. 101, initial Nd isotopic compositions relative to the chondritic uniform reservoir (CHUR) are presented for various mantle-derived rock suites and are compared with the evolution of a model depleted mantle (Smith and Ludden, 1989) and the Archean upper crust (Patchett and Arndt, 1986). The Pechenga ferropicrites with an $\varepsilon_{Nd}$ value of +1.4±0.4 lie below the depleted mantle field and differ in this respect from the uncontaminated komatiites which generally manifest a strong long-term depletion of LREE in their source region (Fig. 101). Jatulian gabbro-wehrlite intrusions in Finland, though sharing many petrographical and geochemical features with the gabbro-wehrlite intrusions at Pechenga (Hanski, 1986), are at least 200 Ma older than the Pechenga ferropicritic rocks. As shown in Fig. 101, they also had a mantle source with a time-integrated Sm-Nd ratio closer to the chondritic value (Huhma et al., 1990; H. Huhma, unpublished data).

It is interesting that in terms of their REE characteristics, the Pilgujärvi tholeiites appear to have had a similarly depleted mantle source as the gabbros in early Proterozoic ophiolites in central Finland. Huhma (1986) reported single Sm-Nd isotopic analyses with initial $\varepsilon_{Nd}$ of +3.1±0.7 and +3.2±1.0 for two 1.97-Ga-old gabbros, one from Jormua and the other from Outokumpu. These values are indistinguishable from the value of +3.3±0.3 obtained for a tholeiite from Pechenga in this study.

Even though it was postulated earlier on the basis of geochemistry that ferropicritic magmas have not been affected by interaction with Archean upper crust, it is worth examining whether the shift of the ferropicrites beneath the depleted mantle field in Fig. 101 is a consequence of contamination with material from the Archean basement. According to Patchett and Arndt (1986),

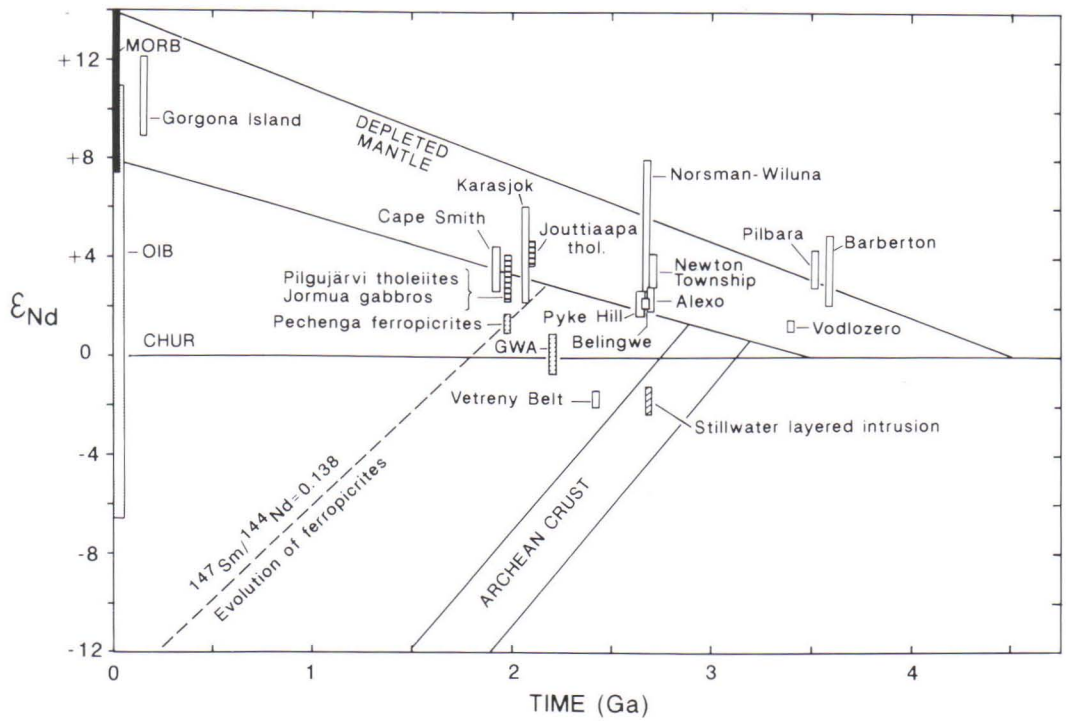


Fig. 101. Variation of initial $\varepsilon_{Nd}$ with time for various mantle-derived rocks and Archean crust. Komatiite suites marked as open columns. Depleted mantle and Archean crust fields after Cousens and Ludden (1991) and Patchett and Arndt (1986), respectively. Literature data for rock suites taken from Cousens and Ludden (1991), Hegner and Bevier (1991), Zindler (1982), Krill et al. (1985), Pukhtel et al. (1991a,b), Huhma (1986), Huhma et al. (1990), DePaolo and Wasserburg (1979), and Morris and Hart (1983). GWA denotes gabbro-wehrlite intrusions in Finland.

the Nd concentration of the Archean crust is about 30-35 ppm on average, thus approaching values of 25-35 ppm measured for primitive ferropicritic rocks. Therefore, a small amount of bulk contamination does not provide an effective means of changing the $^{143}Nd/^{144}Nd$ value of the ferropicritic magma. It can be calculated that in order to diminish $\varepsilon_{Nd}$ from a typical depleted mantle value of +3.6 to the value of +1.4 observed in ferropicrites, 12-20% of bulk assimilation of Archean crust must have occurred. Such an amount of contamination would be recognizable in the geochemistry of ferropicrites, for example, by a decrease in $V/Al_2O_3$ and Nb/Th. However, the $V/Al_2O_3$ values in ferropicrites are exceptionally high and no negative Nb anomalies have been observed. Neither do the Pb isotope data from the ferropicritic rocks support such a high degree of contamination by old continental crust.

It follows that interaction with granitic basement is not a likely explanation for ferropicrites having less radiogenic initial Nd than the depleted mantle at that time. Hence, the calculated initial $^{143}Nd/^{144}Nd$ value can be taken as representative of the value in the source mantle region. The positive initial Nd isotope ratio of the ferropicrites indicate that ferropicritic magma was derived from a mantle source that was previously impoverished in Nd with respect to Sm, presumably by some magma-producing event. The actual ratios of REE in ferropicrites, however, show a strong Nd enrichment over Sm. This implies that either the high incompatible element concentra-

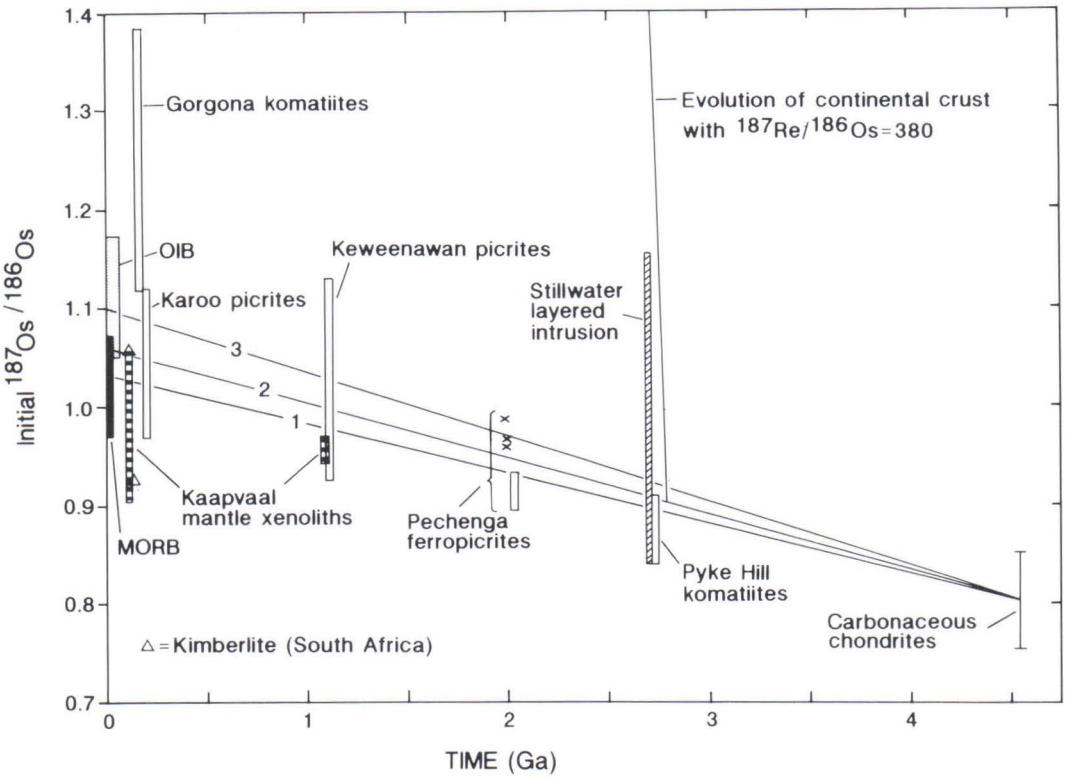


Fig. 102. Variation of initial $^{187}Os/^{186}Os$ with time in mantle derived rocks and continental crust. Range of initial Os in Pechenga ferropicrites based upon the isochron data for the Kierdzhipori flow while individual points mark calculated initial ratios at 1.97 Ga for samples with low Re/Os. Three average terrestrial growth curves are based upon compositions of 1) osmiridium alloys (Allègre and Luck, 1980), 2) carbonaceous chondrites (Walker and Morgan, 1989), and 3) ocean island basalts (Martin, 1991). Other literature data taken from Shirey and Carlson (1991), Walker et al. (1988, 1989, 1991b), Lambert et al. (1989), and Ellam et al. (1991).

tions of the magma were due to the partial melting process and subsequent fractional crystallization, or that the mantle source material was strongly enriched in such elements shortly before partial melting. The possibility of high degree of fractional crystallization causing a change in the relative abundances of REE can be readily eliminated because of the primitive nature of the ferropicrites. The high MgO content of the ferropicrites also argues against the existence of extremely small quantities of partial melting, which would be a prerequisite for fractionation taking place during the melting event, particularly, given the absence of garnet as a residual phase, as deduced earlier in this study.

The only alternative is LIL-element enrichment in the source region shortly before the melting event, so that there was insufficient time for this enrichment process to be reflected by isotope systems. Because of the high-MgO nature of ferropicrites, which suggests a relatively high degree of partial melting, and the inferred absence of residual garnet, it can be concluded that the Sm/Nd value of ferropicrites is close to that of their source region. Consequently, the maximum time interval between the ferropicritic magmatism and the mantle enrichment event can be deduced from the model $T_{DM}$ ages of ferropicrites, i.e., the time

at which the Nd evolution lines of the ferropicrites, calculated on the basis their $^{147}Sm/^{144}Nd$ ratios, transect the evolution line for the model depleted mantle (Fig. 101). Using the depleted mantle evolution of DePaolo (1981), $T_{DM}$ ages of ferropicrites cluster around 2200 Ma. This implies that the mantle source of the ferropicrites underwent a change of its Sm-Nd ratio not earlier than about 200 Ma before the melting event that produced the ferropicritic magmas.

It is interesting that the timing of this isotopic event, namely 2200 Ma, coincides with the emplacement of the gabbro-wehrlite intrusions in eastern and northern Finland (Hanski, 1986). The parental magma of these intrusions is LREE-enriched and their mantle source has probably also undergone an enrichment process. It is therefore reasonable to ask whether the gabbro-wehrlite intrusions both in the Pechenga area and Finland could have had the same mantle source, but while the Finnish intrusions were generated immediately after or during the enrichment event, the melting that produced the Pechenga rocks was postponed to about 200 Ma later. Such a simple picture is not substantiated by the Nd isotope evidence, since it would require that the initial Nd ratio for the older Finnish intrusions is higher than that of the younger Pechenga intrusions. This is in fact contrary to what is observed (Fig. 101).

In Fig. 102, ferropicritic rocks are compared with other mantle-derived rocks in terms of their age and initial $^{187}Os/^{186}Os$ compositions. Also shown are three bulk earth evolution lines based on average Os isotope analyses of osmiridium alloys (Allègre and Luck, 1980), carbonaceous chondrites (Walker and Morgan, 1989), and ocean island basalts (Martin, 1991). For the Pechenga ferropicrites, a range of initial Os values obtained from the 2035 Ma isochron of the Kierdzhipori flow and calculated initial ratios at 1970 Ma for individual samples are marked in Fig. 102. The former indicates an evolution similar to that of the MORB source mantle while the latter values are more reminiscent of the evolution of an OIB source. The age difference of 65 Ma between the two sets of initial values introduces some uncertainty into the calculations but it cannot explain all of the observed scatter. All that can be concluded is that the mantle source of ferropicrites appears to have had an approximately chondritic initial Os isotope ratio.

The initial ratio of $+1.16\pm0.11$ obtained for the Lammas flow lies significantly above the chondritic evolution trend. Figure 102 illustrates a $^{187}Os/^{186}Os$ evolution line for a model Archean continental crust with a $^{187}Re/^{186}Os$ ratio of 380. This kind of crust rapidly develops radiogenic Os isotope compositions and would reach a value of about 6 at 2.0 Ga. It could therefore be argued that the relatively high initial Os of the Lammas flow is a reflection of an interaction with old crustal rocks. However, the low Os concentration in the upper continental crust relative to the osmium content of the ferropicrites renders such a contamination process ineffective. It can be calculated that the extent of assimilation required to raise the initial $^{187}Os/^{186}Os$ value from chondritic to 1.16 would be several tens per cent. No signs of such assimilation are seen in either the Nd and Pb isotope compositions or the geochemistry of the Lammas flow. Hence, the reason for the anomalous initial Os ratio in this flow remains unclear. In general, more analytical work is required to better define the initial $^{187}Os/^{186}Os$ value of the ferropicrites, and this may be possible using the NTIMS technique.

Figure 103 illustrates an initial ratio-time plot for Sr isotope data using the bulk earth, average MORB, and Archean crustal evolutions from Zindler (1982) as a background. The initial $^{87}Sr/^{86}Sr$ values for clinopyroxenes from the Kammikivi and Ortoaivi intrusions as well as from the Kierdzhipori flow lie on or close to the trend of the bulk earth. The apatite from the Pilgujärvi intrusion analysed by Smolkin (1991) plots slightly above the bulk earth field whereas the initial ratio for the Pilgujärvi tholeiites reported by Balashov et al. (1991) plots well inside this field.

The available geochemical and isotope data can be used to evaluate the potential mantle components involved in the generation of the Pechenga ferropicrites and associated tholeiites. Figures 101 and 103 demonstrate that the mantle

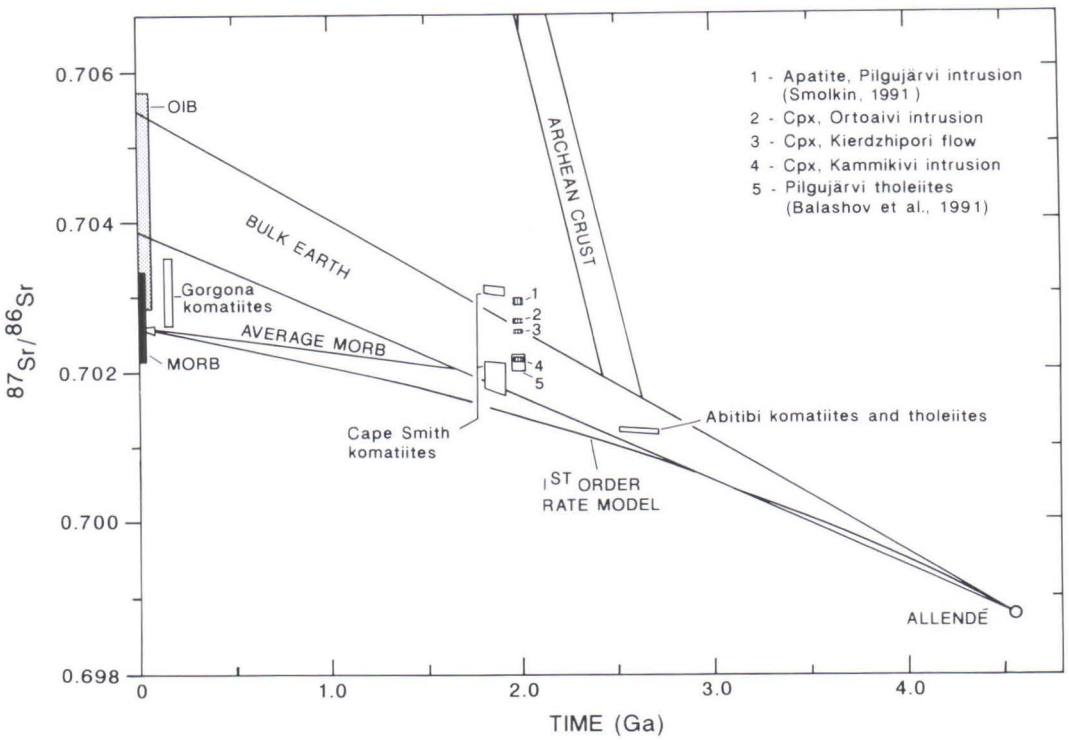


Fig. 103. Sr isotopic evolution diagram. Evolution models of bulk earth, MORB mantle and Archean crust and data on Abitibi and Cape Smith rocks after Zindler (1982) and ranges of $^{87}Sr/^{86}Sr$ for modern MORBs and OIBs after Morris and Hart (1983). Gorgona data from Aitken and Echeverria (1984).

source of ferropicrites had time-averaged Nd/Sm and Rb/Sr values higher than those in the MORB-type mantle. In other words, the former was less depleted than the latter. In this respect, ferropicrites resemble many ocean island basalts which have isotope characteristics similar to the bulk earth or intermediate between the bulk earth and the depleted mantle (e.g., Morris and Hart, 1983). Also the osmium isotope data provide some indications of a source similar to that of OIBs (Fig. 102). On the basis of these isotopic features and the geochemical properties of ferropicrites which mimic those of OIBs (Fig. 54), the generation of ferropicritic magmas could be related to the ascent of a mantle plume from deep parts of the earth's mantle. This is, however, not the only possibility. Because there is no definite evidence for the Pilgujärvi metavolcanites representing outpourings of lavas on an ocean floor, extension of continental crust presumably did not proceed to the formation of oceanic crust and the total elimination of the subcontinental lithospheric mantle. Therefore, the Archean subcontinental lithospheric mantle represents an alternative candidate for producing magmas with relatively unradiogenic Nd and radiogenic Sr isotope compositions compared to the composition of melting products of the convecting asthenosphere. A third possibility is that the ferropicrites were derived from a reservoir consisting of unfractionated primordial mantle material but this option is excluded on the basis of the inferred major and trace element compositions of the source of the ferropicrites.

The Nd isotopic characteristics of the Pilgujärvi tholeiites attest to a long-term depleted mantle reservoir similar to that of the igneous rocks of the Jormua ophiolite and indicate a similar asthenospheric origin. However, the major element composition of tholeiites from the Kolosjoki and Pilgujärvi Suites, in particular their FeO-$TiO_2$ relationships, markedly differ from the composition of the Jormua ophiolitic tholeiites or modern MORBs (Fig. 49). It should be added that no analogies have been found, either among ocean island basalts or flood basalts. The uniformity in the bulk geochemical composition and the large volume of tholeiites of the Kolosjoki and Pilgujärvi Suites fits better with a hypothesis invoking decompression melting of an upwelling mantle plume rather than partial melting of ancient lithosphere.

## A lithospheric model

Mantle xenoliths transported to the surface by kimberlites and other continental magmas demonstrate that the lithospheric mantle beneath old cratons has a complex history (e.g., Menzies and Hawkesworth, 1987). The refractory major element compositions of xenoliths are generally attributed to the participation of this part of the mantle in the formation of Archean continental crust. On the other hand, during its long history, the lithospheric mantle may have been subjected to enrichment processes at various times caused by migration and crystallization of small-volume partial melts or fluids from an underlying MORB-type mantle, or by rising mantle plumes or by the subduction of oceanic lithosphere. As the subcratonic lithospheric keel has remained convectively isolated from the underlying asthenospheric mantle for long periods of time, this has enabled the development of radiogenic isotopic ratios outside the range observed in oceanic magmas. It is thus generally accepted that old subcontinental lithosphere is both geochemically and isotopically heterogenous, with isotopic compositions apparently extending from the field of depleted MORB-type mantle through the field of the source of plume-related OIBs to very radiogenic Sr or unradiogenic Nd isotopic compositions (Menzies and Hawkesworth, 1987). It follows that a subcontinental lithospheric source can only be unequivocally demonstrated in cases where the isotopic composition of a basalt uncontaminated by sialic crust falls outside the mantle array defined by oceanic rocks. This particularly concerns osmium isotopes, since depleted osmium isotope compositions appear to be diagnostic of old, refractory lithospheric mantle (Walker et al., 1989). It should also be pointed out that Re-Os systematics have been observed to record ancient melt depletion events even in mantle rocks that have, according to Sm-Nd isotope systematics, been metasomatically enriched in LIL-elements (Pearson et al., 1991).

The Sr and Nd isotopic compositions of ferropicritic rocks do not allow discrimination between a source located in the ancient refractory subcontinental lithospheric mantle which underwent an enrichment event less than 200 Ma years before its melting, or an OIB-type mantle source that ascended as a plume from the lower mantle. Neither can ferropicrites be shown to have the very low $\gamma_{Os}$ values that would demonstrate a lithospheric origin.

A major difficulty in producing large amounts of basaltic or picritic magma from the subcontinental lithosphere is its refractory nature in terms of major elements and the low temperature, about 300-400 °C below its melting point at a given depth (McKenzie and Bickle, 1988). However, the isotopic data on Karoo picrites, showing radiogenic Sr and unradiogenic Nd isotope compositions together with variable and in many cases low $\gamma_{Os}$ values, indicate that these magnesian rocks contain a major subcontinental lithospheric component (Ellam et al., 1991).

The decoupling of the Nd isotope composition and the REE chemistry of the Pechenga ferropicrites suggests LIL-element enrichment in the source region. Studies of mantle xenoliths show that this can be accomplished by various agents. The most common styles of trace element enrichment are the so-called Fe-Ti enrichment processes, attributed to the effect of infiltration by silicate melts and K-rich metasomatism, thought to be caused by hydrous alkali-rich fluids (Menzies and Hawkesworth, 1987). O'Reilly and Griffin (1988) described modally metasomatized lherzolites from Australia which contain high abundances of many incompatible elements such as Nb, Ta, and Ba but are not particularly rich in titanium or potassium. They ascribed these enrichment patterns to $CO_2$-rich fluids which were also found in fluid inclusions. Lithosperic mantle may also be enriched in certain LIL elements by the introduction of subducted sedimentary material into the mantle. This alternative can, however, be eliminated in the present case on the basis of the relatively low initial Sr ratios of the Pechenga metavolcanites as well as the high titanian nature of the ferropicrites.

As was inferred earlier, the source region of the Pechenga ferropicrites was enriched not only in many incompatible trace elements but also in iron and titanium. Because it has been experimentally shown that $H_2O$ or $CO_2$-rich fluids do not dissolve much iron and titanium at high pressures (Schneider and Eggler, 1986), some other enriching agent is needed to carry iron and titanium to the mantle source of ferropicrites. The most likely candidate for this is an incompatible element-rich silicate melt. Evidence of metasomatic alteration induced by silicate melts is provided by composite mantle xenoliths and orogenic peridotites which are veined by pyroxene or amphibole-rich basic bands and dikes, from a few cm to 1 m thick, interpreted to have crystallized from alkali basalts and other alkalic melts (Bodinier et al., 1988; Whilshire et al., 1988). The material forming the veins is also commonly observed as independent xenoliths. These are assigned to the Al-Ti-augite series or the Group II xenoliths while the host lherzolites or harzburgites have been designated as Cr-diopside series or Group I xenoliths. In many cases, the reaction of the veins with their wall-rocks either via infiltration of melts or diffusional exchange has resulted in enrichment of adjacent peridotite in Fe, Ti, and LREE. It has been suggested that metasomatized peridotites impregnated with Group II rocks may represent a possible source for Fe-rich primary magmas (Goto and Arai, 1987).

Although metasomatic changes are common in peridotite samples from the subcontinental lithosphere, iron enrichment to the $FeO_{tot}$ level required in the inferred ferropicrite source is rare (see Fig. 97). There are also other, more serious problems with this model when applied to the present case. The increase of Fe and Ti due to the interaction of the veins with their surroundings commonly extends for only a short distance from the contact, ranging from a few centimeters to a few decimeters (Dupuy et al., 1986; Bodinier et al., 1988, 1990). This contrasts with the volume of hundreds of cubic kilometers of Fe-rich mantle required to produce the igneous rocks of ferropicritic composition in the Pechenga-Varzuga belt. A typical feature of mantle peridotite affected by metasomatism of the adjacent vein is great heterogeneity in both major and trace element compositions (Bodinier et al., 1990). Upon partial melting of veined mantle, this heterogeneity, coupled with variable density and a varying degree of melting are expected to produce a wide spectrum of melt compositions. Francis and Ludden (1990) explained a suite of rocks ranging in composition from transitional basalt to nephelinite as the products of varying degrees of partial melting of lherzolite penetrated by amphibole-garnet-clinopyroxenite veins. The homogeneity of the composition of ferropicrites encountered in an area of at least 250 km in length is hence difficult to explain by the veined mantle model.

Furthermore, although the injection of alkali basaltic melt into lherzolitic or harzburgitic mantle may cause an increase in the bulk iron content of mantle, it is also accompanied by a concomitant increase in $Al_2O_3$. In fact, $Al_2O_3/FeO_{tot}$ in pyroxenite and hornblendite veins ranges between 0.4-3.0, in most cases being

higher than the primitive mantle value of about 0.56 and in all cases higher than the inferred ratio (0.1-0.2) in the source region of ferropicrites (Fig. 97). A further point to be discussed in connection with the geochemistry of metasomatized peridotites is the observation that Ni behaves in a similar fashion to Mg and is also impoverished, if there is an increase of FeO and decrease of MgO/(MgO+FeO). Figure 55 compares the Ni contents of Pechenga ferropicrites and Munro komatiites and indicates that rather than being depleted in Ni, the source of ferropicrites probably had anomalously high Ni contents.

High Re/Os in basaltic rocks tends to produce high $^{187}Os/^{186}Os$ with time (Fig. 72). Reisberg et al. (1991) have made a direct observation of very radiogenic Os isotope compositions in mafic layers in the Ronda Ultramafic Complex, demonstrating that the layering is an ancient feature. The osmium isotope composition of ferropicrites having a nonradiogenic initial $^{187}Os/^{186}Os$ value can thus be taken as evidence that the trace element or iron enrichment in the source mantle of ferropicrites does not result from the veining of mantle by much older basaltic dikes.

## A plume model

Based upon fluid dynamics calculations and laboratory simulations, the current theory of mantle plumes maintains that plumes originate from a hot, unstable boundary layer deep within the mantle, possibly from the thermal boundary layer above the core-mantle boundary (Griffiths and Campbell, 1990). A newly formed plume driven upwards by buoyancy resulting from thermal expansion consists of two parts: a large bulbous head and a hot, relatively narrow feeder conduit. As the head rises, the adjacent mantle material is heated by conduction and stirred by a circulating flow within the head. Almost all the entrainment takes place in the lower mantle with the source mantle ultimately comprising only 20-40% of the volume of the head. Flow in the plume tail does not entrain significant amounts of the adjacent mantle through which it passes. When the plume head originating from the core-mantle boundary reaches the lithosphere, it flattens out to form a hot disk with a predicted diameter from 1500 to 2500 km and a thickness from 100 to 200 km.

The plume model has been applied to account for the connection between the flood basalt provinces and ocean island chains, which are regarded as products of plume head magmatism and subsequent plume tail-related hot spot tracks, respectively (Campbell and Griffiths, 1990). It has also been invoked to explain the association between high-temperature komatiites and more voluminous lower-temperature tholeiites in Archean greenstone belts (Campbell et al., 1989). Accordingly, partial melting of the bulk of an upwelling and spreading head produces voluminous basaltic volcanism whereas melting of the much hotter material that ascended in the axial conduit gives rise to komatiites. This kind of process could also be envisaged to have operated in the Pechenga area with the tholeiites representing partial melting products of the head and the ferropicrites partial melting products of the the central conduit. The plume model accounts for the anomalously hot mantle needed to produce high-MgO ferropicritic magmas as well as the OIB like geochemistry and isotope composition of ferropicrites. This model is also compatible with the conclusion that ferropicrites and tholeiites come from different mantle sources.

One important factor in evaluating the plume model is the duration of volcanism. The maximum time of volcanic activity caused by a rising plume head is limited to a period of the order of 20 Ma (Campbell and Griffiths, 1990). It is evident that plate tectonic movements will generally not permit a plume to persist in a stationary position with respect to a given point in an overlying continental plate for a long period of time. As

shown by the evidence from the Hawaii-Emperor chain, the plume tail may be active for as much as 200 million years. In such cases, magmatic and tectonic activity produce linear, time-progressive hot-spot tracks. The prolonged magmatic history of the Pechenga Series, starting with the eruption of the volcanic rocks of the Ahmalahti suite more than about 2.3 Ga ago and culminating with the eruption of tholeiites and ferropicrites of the Pilgujärvi suite more than 300 Ma later, is difficult to reconcile with a simple mantle plume model. However, the exact time period over which the upper part of the Pechenga Group was deposited, including the eruption of the tholeiites and ferropicrites of the Kolosjoki and Pilgujärvi Suites, is so far rather poorly constrained.

The buoyancy forces imposed by an ascending plume to the overlying mantle will cause uplift and stretching of the lithosphere (Campbell and Griffiths, 1990). Significant surface uplift is estimated to begin 10-20 Ma before the onset of volcanism and to reach its maximum value of 500-1000 m when the plume is at a depth of 100-200 km. Uplift is succeeded by subsidence. This begins above the axial zone of the plume when the head starts to spread laterally under the lithosphere. Despite the sinking of the basement on which basaltic rocks erupt, the top of the volcanic pile may rise slightly, for the density of basalts is lower than that of the mantle from which they were derived. Regional subsidence will not take place before the decay of the thermal mantle anomaly by conductive heat loss. Because of the large thickness and depth beneath the surface of the hot plume layer, cooling may last hundreds of millions of years, during which the sinking of the crust may lead to the formation of sedimentary basins.

The plume tectonic reworking of the continental crust outlined above raises some problems when applied to the Pechenga region. As was discussed earlier, it is unlikely that the whole Pechenga Group is related to a single upwelling plume. If, however, the upper part of it is assumed to represent plume activity, the preceding period of uplift should be evident in the stratigraphic record of the Pechenga Group. Surface uplift of the order of several hundreds of meters or even one kilometer would cause a period of erosion which would be reflected as discordances and changes in the character of sedimentary sequences. The sedimentary and volcanic formations of the Pechenga Group generally follow each other without any marked discordances and record a gradual transition towards a deeper-water depositional environment. According to Zagorodnyi (1980), there is a minor angular unconformity and evidence for erosion at the contact between the sedimentary rocks of the Kolosjoki Suite and volcanic rocks of the underlying Kuetsjärvi Suite, whereas Zagorodnyi et al. (1964) described a gradual transition from tuffitic metavolcanites to sedimentary rocks at this contact in the eastern and western part of the Pechenga Complex. It is thus highly questionable whether this contact can be interpreted as evidence of extensive uplift. In addition, the most voluminous ferropicritic magmatism took place during and soon after the deposition of the sediments of the productive pile. This can be taken as evidence for ferropicrites having erupted and intruded in a subsiding, relatively deep-water basin. That is, the magmatism would have occurred at a late stage of the plume tectonics when the thermal anomaly in the upper mantle had already subsided.

The striking enrichment of plume-related intra-plate basalts in LIL elements coupled with their Nd and Sr isotopic characteristics, indicating a depleted source or a source similar to bulk earth, poses a problem which has been addressed by invoking a variet of possibilities, including (i) very low degrees of melting, (ii) metasomatic processes similar to those observed in mantle samples from subcontinental lithosphere, and (iii) the recycling of lithospheric material into the lower mantle or at the boundary of the lower and upper mantle. As was pointed out earlier, extremely low degrees of melting or the incorporation of sedimentary material into the source of the ferropicrites can be ruled out on major element and Sr isotopic grounds, respectively. On the other hand, the Os isotope data from the ferropicrites do not support the recycling of old, MORB or other basaltic material in the source region. In

general, the Os isotope data currently available from ocean island basalts are not compatible with OIB being predominantly derived from ancient subducted crustal material (Martin, 1991; Pegram and Allègre, 1992). One solution to the enrichment problem is the suggestion that the enrichment was caused by three-dimensional dynamic melting processes in an ascending mantle plume, as applied by Eggins (1992a,b) to Hawaiian tholeiites. According to this model, small-degree melts in equilibrium with a garnet-bearing residuum migrate from peripheral parts of the plume to the high-temperature core region and there enrich the more or less refractory peridotite in LIL elements. This can occur when the overlying lithosphere deflects the mantle flow away from the plume's central axis while the peripheral melts continue to flow upwards along essentially vertical paths.

Besides high LREE/HREE, the plume model must also explain the high FeO content of ferropicrites. One possibility is the hypothesis that the lower mantle in general has a higher FeO content than the upper mantle. Along with new estimates of solar composition, it has become apparent that chondritic meteorites are not necessarily representative of the solar nebula and that the terrestrial planets may be richer in Fe, Ca, and, Ti than has previously been supposed. Accordingly, Anderson (1989) has calculated that the average FeO content of the mantle is 15.7 wt. %, i.e., much higher than commonly observed in upper mantle lherzolites (Table 26). This suggests a geochemical stratification in the silicate portion of the earth with the lower mantle being enriched in FeO compared with the upper mantle. If this is true, the question arises as to why iron-rich primitive magmas are so rare among volcanic rocks that have been assumed to have been generated by the partial melting of upwelling mantle plumes.

## SUMMARY AND CONCLUSIONS

The early Proterozoic Pechenga Series comprises a 10-km-thick supracrustal sequence deposited on the Archean granite-gneiss basement in the NW part of the Kola Peninsula and is divided into four sedimentary-volcanic cycles. The magmatic history of the series started more than 2.3 Ga ago, with eruptions of amygdaloidal andesites and dacites of the first cycle (Ahmalahti Suite), which contain a strong crustal signature in their chemical composition. These were followed by mildly alkaline lavas representing various stages of fractionation, forming the second cycle (Kuetsjärvi Suite). The bulk of the third (Kolosjoki Suite) and fourth volcanic cycles (Pilgujärvi Suite) are composed of relatively homogeneous tholeiitic metavolcanites which occur mainly as pillow lavas. These possess trace elements characteristics resembling those of MORBs, but their $TiO_2$-$FeO_{tot}$ relationships differ from those of present-day MORBs and most other Phanerozoic magma types as well as the contemporaneous MORB-like magmas of the Jormua ophiolite. A volumetrically minor rock type forming a key horizon in the uppermost volcanic cycle is represented by felsic to ultrafelsic tuffs with an incompatible element-rich, peralkaline rhyolite composition.

Apart from subordinate occurrences in the Kolosjoki Suite, ferropicrites are mainly present at four separate levels in the Pilgujärvi Suite. They comprise tuffs, massive and pillowed lavas, and differentiated lava flows up to 50 m in thickness. Various spinifex types can be distinguished in layered lava flows, including randomly oriented or parallel olivine spinifex and pyroxene spinifex with or without varying amounts of olivine plates. One of the most interesting features of the spinifex rocks is the presence of kaersutite

as fringes around pyroxene grains or as independent needles.

Although the Pechenga rocks are in places fresh by Precambrian standards, they have undergone various alteration processes. Among the manifestations of these processes are globular structures developed in originally glass-rich, evolved ferropicritic rocks. A key piece of evidence which supports this interpretation is provided by spinifex textures passing disturbed through globule-matrix boundaries.

The Pechenga Ni-Cu deposits are genetically and spatially related to gabbro-wehrlite intrusions crystallized from ferropicritic magma. These intrusions were emplaced into the lower, sedimentary part of the fourth cycle comprising a thick sequence of silty and phyllitic metasediments and mafic to picritic tuffs. Two ore-bearing bodies are described in more detail in this work. These are the Pilgujärvi layered intrusion, which is the thickest intrusion found in the area, and the Kammikivi layered sill. The petrographical features of the latter, which mimic those observed in layered ferropicritic flows, suggest an emplacement very close to the earth's surface.

Microprobe analyses are reported for most primary minerals of the ferropicritic rocks. The Fo content of olivines ranges between 68.2-84.2%. The most striking feature of chrome spinel, clinopyroxene, and primary amphibole and mica is their high $TiO_2$ content which is a reflection of a high overall abundance of $TiO_2$ in the magma as well as high crystallization temperatures. The ZnO content of the chrome spinel does not appear to have the same exploration significance as spinels from Western Australian komatiites. The ubiquitous replacement of olivine by secondary minerals in lava flows limits the use of olivine compositions as an indicator of chalcophile element depletion. Instead, the behavior of Ni in barren and mineralized bodies can be potentially monitored with help of Ni analyses of the most magnesian chrome spinels.

Major element analyses of ferropicritic pillow lavas, tuffs, and the most magnesian spinifex-textured rocks as well as chilled margin and weighted average compositions of intrusions and layered flows demonstrate that the ferropicritic parental magma contained about 15 wt. % MgO. This MgO content and the elevated Ni content of several hundreds of ppm are widely accepted geochemical criteria for near-primary and primary mantle-derived magma compositions. The high $FeO_{tot}$ (>14 wt. %) causes the Mg number to fall below 0.70 in the parental ferropicritic magma. Taking 15% MgO as the value for the primary magma, the maximum pressure of melt segregation in the upper mantle is estimated to be about 38 kbar which is equivalent to a depth of about 120 km.

Geochemical comparison with other primitive magmas reported in the literature reveals that, with respect to major elements, the Pechenga ferropicrites most closely resemble the early Proterozoic Oskol picrites in the Ukraine (Krestin and Yudina, 1988) and the so-called Fe-rich komatiites from an Archean greenstone belt in northwestern Ontario (Schaefer and Morton, 1991). In multi-element, primitive mantle-normalized trace element plots, ferropicritic rocks display convex-up patterns with relatively high abundances of elements such as U, Th, Nb, Ta, and LREE. These patterns are reminiscent of those observed in ocean island basalts and other typical intraplate volcanites.

Despite the striking textural resemblance to spinifex-textured komatiites, the Pechenga ferropicrites possess many mineralogical and geochemical features that distinguish them from typical komatiites. These include the presence of abundant primary hydrous phases indicating the hydrous nature of the parental magma and the elevated contents of FeO, $TiO_2$, HFSE, and LREE as well as the chemical characteristics (Ni/Cu) of associated Ni-Cu deposits. The presence of mesoscopic spinifex textures in ferropicritic rocks demonstrate that spinifex textures are not restricted to rocks of komatiitic affinity and therefore cannot be used as a diagnostic feature of komatiites. In the light of the data obtained from komatiites and the Pechenga rocks, spinifex textures may be developed both by dry and volatile-bearing magmas, and there seems to be no reason why, for example, melts similar in composition to

the highly magnesian Hawaiian picrites (Clague et al., 1991) would not be capable of crystallizing as spinifex-textured flows.

The distinction of komatiites from picrites on the basis of their chemical compositions is not straightforward. Namely, there exist magnesium-rich volcanic rocks which have been termed Ti-rich komatiites or Fe-rich komatiites and which chemically approach the Pechenga ferropicrites (Barnes and Often, 1990; Stone et al., 1987; Schaefer and Morton, 1991). Thus, no strict demarcation between komatiites and picrites can be drawn, either on textural or chemical grounds.

Because of the nature of the alteration processes, i.e., the survival of primary magmatic minerals in many places, together with the strong *in situ* fractionation of individual lava flows and intrusions, reasonable age information is obtainable from ferropicritic rocks by using several methods. New Sm-Nd and Pb-Pb isotopic data are used together with those published by Hanski et al. (1990) to place constraints on the timing of the ferropicritic magmatism, with results clustering around about 1970 Ma. Particularly, this work demonstrates the applicability of the Re-Os system in dating ferropicritic and presumably other picritic volcanic rocks. This is by virtue of the huge variation in $^{187}Re/^{186}Os$ observed in ferropicritic layered flows, with values ranging from 20 up to nearly 10,000. The Re-Os method yields somewhat older ages compared to those obtained by the Sm-Nd and Pb-Pb methods but the ages, nevertheless, overlap within analytical uncertainty. There is still some uncertainty in the initial Os isotopic ratio of the ferropicritic magma, but this problem may be overcome in future studies using the negative thermal ionization technique (NTIMS).

The overall geochemical data of ferropicrites coupled with their isotopic characteristics indicating a moderately depleted mantle source in terms of the Nd and Pb isotope composition and a grossly chondritic mantle source with respect to the Sr and Os isotopes, preclude a significant interaction with the Archean upper crust. This lack of crustal involvement can be taken as a direct reflection of the extensional tectonic environment during ferropicritic magmatism, which favors rapid ascent of magmas, minimal residence time in crustal magma chambers, and thinning of the continental lithosphere.

There can be little doubt that the kaersutitic amphibole in the ferropicritic rocks, excluding subsolidus replacements in pyroxenes in thick intrusions, are primary igneous amphiboles, as shown by petrographic criteria and their chemical compositions. Factors that control the low-pressure stability of magmatic amphibole are examined, with particular reference to existent experimental data. It is concluded that the minimum water pressure of about 0.5 kbar suggested by the experiments is not consistent with the occurrence of amphibole in the Pechenga ferropicrites and some other ancient and modern submarine lava flows because such a pressure would require a water depth in excess 5 km. Further research, including laboratory experiments on $H_2O$ and halogen-bearing systems as well as studies of volcanic rocks erupted under known conditions, is needed before amphibole can be used confidently as a paleodepth indicator in ancient volcanic and subvolcanic rocks. Owing to the highly volatile nature of sulfur, a certain load pressure is necessary to prevent sulfur escape and thereby create favorable circumstances for Ni-Cu ore formation. To enable a better understanding of the genesis of the Pechenga Ni-Cu deposits, it would be important to obtain more tightly constrained estimates of the pressure conditions under which the gabbro-wehrlite intrusions and ferropicritic lava flows crystallized.

It is now well established that ore-producing magmas at Pechenga were emplaced contemporaneously with the cogenetic ferropicritic volcanism. Consequently, major fault zones such as the Luotna Fault which developed during later tectonic movements cannot be regarded as channels for transporting ore-bearing magmas as had previously been suggested. The primary Ni-Cu ores were formed in a dynamic subvolcanic environment by gravity-induced segregation of immiscible sulfide droplets which were trapped in mechanically favorable places such as embayments at lower contacts of magma chambers. Sul-

fur isotopic data clearly demonstrate that the massive and breccia ores were generated by reworking and mobilization of magmatic sulfides in shear zones along the lower contacts of ore-bearing peridotites presumably during the regional metamorphism. With regard to ore genesis, the most important incompletely resolved question is the potential interaction of ore-forming ferropicritic magmas with enclosing sulfur-rich sediments.

Sulfur isotope and geochemical evidence, including high Se/S, Te/S, Se/As, and Te/As of Ni-Cu ores, suggest that the bulk of the sulfur in ore bodies of the western ore field is juvenile in origin. A perplexing problem has emerged from the radiogenic Os isotopic compositions of sulfur-rich samples from the Kammikivi sill. If this is attributed to the assimilation of country rock phyllites, then the degree of bulk assimilation required is deduced to be of the order of several tens of per cents, which is not supported by geochemical or other isotopic data. Furthermore, the variable initial $^{187}Os/^{186}Os$ values of ore samples would point to large differences in the extent of contamination and limited Os isotopic homogenization between closely spaced ore samples. One way of accounting for the anomalous Os isotopic compositions of ore samples is to postulate resetting isotopic systems in sulfide minerals during recrystallization and mobilization of sulfides and reactions with hydrothermal fluids transporting metasomatizing agents to and from the enclosing phyllitic metasediments. Radiogenic Os isotope compositions may result from either leaching of Re from sulfides or an introduction of radiogenic Os from country rocks but in both of these processes, the relative amounts of metal migration should have been very extensive. This problem can be potentially clarified by carrying out Re-Os isotopic analyses on carefully separated sulfide and primary silicate fractions from the same samples. If the radiogenic Os were a consequence of country rock assimilation, then the Re-Os system could provide an effective tool for revealing such contamination effects. On the other hand, if metamorphic processes are responsible for high $^{187}Os/^{186}Os$ values, the Re-Os system can supply valuable information concerning the postmagmatic history of ore deposits.

A long known and inadequately understood difference exists between the relatively heavy sulfur isotope composition of ores from the Pilgujärvi intrusion ($\delta^{34}S$ +3.0 ‰ to +5.5 ‰) and the near chondritic values measured for ore bodies from the western ore field. Pb-Pb isotope data on the Pilgujärvi intrusion indicate a slightly lower Th/U than in the ferropicritic metavolcanites which, together with S isotopic data, support the assimilation hypothesis.

High-pressure phase equilibrium data on basic to ultrabasic systems from the literature have been used constructing an $Al_2O_3$ vs. $MgO+K_D \times FeO$ diagram (Fig. 89) in which the chemical components are expressed in cation mole proportions and where $K_D$ symbolizes the Mg-Fe exchange reaction distribution coefficient between olivine and liquid. This diagram can be used to distinguish magma types which are too low in $Al_2O_3$ and/or MgO+FeO to be simultaneously in equilibrium with both olivine and garnet at high pressures, i.e., inconsistent with the retention of a garnet lherzolite residue in the mantle. When applied to the Pechenga ferropicrites, the $Al_2O_3$ vs. $MgO+K_D \times FeO$ diagram shows that most of these rocks plot below the olivine+garnet saturation curve, which indicates the absence of residual garnet during melt segregation. Such an observation has important implications for the interpretation of the rare earth element patterns of ferropicritic rocks. Namely, it can be shown that LREE-enrichment is not the result of fractionation during the melting event but an original feature of the mantle source. It is also likely that the source was enriched in other incompatible trace elements including HFSE.

The inferred high La/Yb in the mantle source of the Pechenga ferropicrites is in conflict with the positive initial $\varepsilon_{Nd}$ value (+1.4±0.4) obtained for these metavolcanites, which indicates a time-integrated depletion of Nd compared to Sm in the source. This is a common problem encountered in alkali basalts and is often resolved by assuming an enrichment event in the mantle source shortly before melt segregation. In the case of the Pe-

chenga ferropicrites, such an enrichment has occurred less than 200 Ma before the generation of the magma.

Olivine-liquid equilibria have been used to show that, without invoking a considerable extent of fractional crystallization, the high iron content of ferropicrites can only be explained by an exceptionally high iron content in the mantle source material. The $FeO_{tot}$ content of the source has been calculated to be somewhere between 13-15 wt. % while the $Al_2O_3$ content is estimated to fall in the range of 1.3-3.0 wt. %. Compared to primitive mantle, the source of the Pechenga ferropicrites was thus clearly richer in iron and poorer in aluminum.

Similarities in the incompatible and isotope chemistry (Sm-Nd, Rb-Sr, Re-Os) of many ocean island basalts and ferropicrites point to common source characteristics. This observation is compatible with a model according to which the Pechenga ferropicrites are partial melting products of an ascending mantle plume generated by a thermal anomaly close to the core-mantle boundary. However, the isotopic data cannot be used to exclude derivation from metasomatized subcontinental lithospheric mantle. Nevertheless, they do eliminate the possibility of significantly older basaltic veins being responsible for trace element and iron enrichment in the mantle. The characteristics of the ultimate mantle source of the ferropicritic magmas is not yet adequately understood because, as was discussed in the previous chapter, both the plume and lithospheric models have certain weaknesses when applied to the Pechenga region.

## ACKNOWLEDGEMENTS

Many people have contributed to the production of this work. I am very grateful to Prof. Tauno Piirainen for his encouragement at the beginning of this study. This research would not have been possible without close collaboration with Russian colleagues, in particular Valery Smolkin. I am most indebted to him for his compliance and patience during the last years as the progress of our joint endeavor sometimes seemed to be too sluggish due to barriers between languages and countries. The field guidance by Valery Smolkin, Peter Skufin, Marat Abzalov, and Anatoly Borisov greatly improved my understanding on many aspects of the geology of the Pechenga area which is thankfully acknowledged. I am grateful to Valery Smolkin and Peter Skufin for generously donating samples, rock powders and analytical results. Fergus Gibb is thanked for kindly supplying volcanite samples from the North Sea Basin.

I am much obliged to Richard Walker, Hannu Huhma, and Matti Vaasjoki for performing isotopic analyses and Gerhard Brügmann for providing INA and PGE analyses. Jan Bitmead and Ian Campbell are thanked for providing spark source mass spectrometric analyses. The sample preparation and analytical work by the staff of the isotope laboratory in Espoo and the geochemical laboratory in Rovaniemi is also appreciated. Microprobe analyses were performed by Lassi Pakkanen and Bo Johansson at the GSF in Espoo and Pirkko Kylmäluoma and Seppo Sivonen at the Oulu University. Mineral separations were carried out by Pentti Kouri. Marjatta Kanste and Soili Ahava drafted the original diagrams and Reino Lampela and Jari Väätäinen assisted in photographical work. Computer programmes for solving some special problems were written by Vesa Tolonen and Hannu Kähkölä.

This study benefited greatly from useful oral

and written discussions with many individuals including Valery Smolkin, Peter Skufin, Richard Walker, Gerhard Brügmann, Nick Arndt, Anthony Philpotts, Viktor Melezhik, Marat Abzalov, Tapani Mutanen, Hannu Huhma, Matti Vaasjoki, Marie Johnson, and Ralph Moberly. Critical comments by Heikki Papunen and Hannu Huhma on early versions of the manuscript are also appreciated. Nick Gardner and Peter Sorjonen-Ward carefully reviewed the English of the manuscript.

I would like to express my warmest thanks to all the above mentioned persons and others who have helped me to bring this study to a succesful end. Last, but most important, I thank my wife and children for their patience when they often had to wait vainly for their father to come home during long, dark evenings spent in the lengthy preparation of this work.

# REFERENCES*


**Abzalov, M.Z., Petrov, V.P., Polezhayev, L.I., 1991a.** Izmenenie Ti-khromshpinelidov pri metamorfizme ultrabazitov Pechengskogo kompleksa (Kolskii poluostrov). Mineralog. Zhurnal, 13, 40-48.

**Abzalov, M.Z., Gorokhovskii, B.M., Turchenko, S.I., 1991b.** Izotopnyi sostav svintsa sulfidov kak indikator polistadiinogo formirovaniya Pechenskikh medno-nikelevykh mestorozhdenii. Dokl. Akad. Nauk SSSR, 320, 1230-1234.

**Adam, J., 1988.** Dry, hydrous, and $CO_2$-bearing liquidus phase relationships in the CMAS system at 28 kb, and their bearing on the origin of alkali basalts. J. Geol., 96, 709-719.

**Adam, J., 1990.** The geochemistry and experimental petrology of sodic alkaline basalts from Oatlands, Tasmania. J. Petrol., 31, 1201-1223.

**Agee, C.B., Walker, D., 1988.** Static compression and olivine flotation in ultrabasic silicate liquid. J. Geophys. Res., 93, 3437-3449.

**Aitken, B.G., Echeverria, L.M., 1984.** Petrology and geochemistry of komatiites and tholeiites from Gorgona island, Colombia. Contrib. Mineral. Petrol., 86, 94-105.

**Akhmedov, A.M., Krupenik, V.A., 1990.** Turbiditnye rezhimy sedimentatsii i kolchedanoobrazovanie v ranneproterozoiskom Pechengskom basseine. Sov. Geol., No. 2, 51-60.

**Alapieti, T., Sivonen, S.J., 1983.** Use of the electron microprobe in the investigation of the Early Proterozoic Koillismaa igneous complex, NE Finland. Geol. Surv. Finland Rep. Invest., 61, 22p.

**Allègre, C.J., Luck, J.-M., 1980.** Osmium isotopes as petrogenetic and geological tracers. Earth Planet. Sci. Lett., 48, 148-154.

**Allègre, C.J., Dupre, B., Lewin, E., 1986.** Thorium/uranium ratio of the Earth. Chem. Geol., 56, 219-227.

**Anders, E., Grevesse, N., 1989.** Abundances of the elements: Meteoritic and solar. Geochim. Cosmochim. Acta, 53, 197-214.

**Anderson, D.L., 1989.** Composition of the Earth. Science, 243, 367-370.

**Aoki, K., 1963.** The kaersutites and oxykaersutites from alkalic rocks of Japan and surrounding areas. J. Petrol., 4, 198-210.

**Arai, S., 1987.** An estimation of the least depleted spinel peridotite on the basis of olivine-spinel mantle array. Neues Jahrb. Miner. Abh., 8, 347-354.

**Arai, S., 1992.** Chemistry of chromian spinel in volcanic rocks as a potential guide to magma chemistry. Mineral. Mag., 56, 173-184.

**Arndt, N.T., 1977a.** Thick, layered peridotite-gabbro lava flows in Munro Township, Ontario. Can. J. Earth Sci., 14, 2620-2637.

**Arndt, N.T., 1977b.** Partitioning of nickel between olivine and ultrabasic and basic komatiite liquids. Carn. Inst. Wash. Yearb., 76, 553-557.

**Arndt, N.T., 1986a.** Spinifex and swirling olivines in a komatiite lava lake, Munro Township, Canada. Precambrian Res., 34, 139-155.

**Arndt, N.T., 1986b.** Differentiation of komatiite flows. J. Petrol., 27, 279-301.

**Arndt, N.T., Fleet, M.E., 1979.** Stable and metastable pyroxene crystallization in layered komatiite lava flows. Am. Mineral., 64, 856-864.

**Arndt, N.T., Nisbet, E.G., 1982.** What is komatiite? *In* N.T. Arndt and E.G. Nisbet (Eds.), Komatiites, p. 19-27. Allen & Unwin, London.

**Arndt, N.T., Naldrett, A.J., Pyke, D.R., 1977.** Komatiitic and iron-rich tholeiitic lavas of Munro Township, northeast Ontario. J. Petrol., 18, 319-369.

**Arndt, N.T., Francis, D., Hynes, A.J., 1979.** The field characteristics and petrology of Archean and Proterozoic komatiites. Can. Mineral., 17, 147-163.

**Arndt, N.T., Nisbet, E.G., Cameron, W.G., 1988.** Geochemistry of extremely fresh komatiites from the Belingwe belt, Zimbabwe. Chem. Geol., 70, p. 140.

**Arndt, N.T., Brügmann, G.E., Lehnert, K., Chauvel, C., Chappel, B.W., 1987.** Geochemistry, petrogenesis and tectonic environment of Circum-Superior Belt basalts, Canada. *In* T.C. Pharaoh and R.D. Beckinsale (Eds.), Geochemistry and Mineralization of Proterozoic Volcanic Suites. Geol. Soc. Spec. Publ. 33, 133-145.

**Bachinski, S.W., Simpson, E.L., 1984.** Ti-phlogopites of the Shaw's Cove minette: a comparison with micas from other lamprophyres, potassic rocks, kimberlites, and mantle xenoliths. Am. Mineral., 69, 41-56.

**Bailey, D.K., Cooper, J.P., 1976.** Comparison of the crystallization of pantelleritic obsidian under hydrous and anhydrous conditions. Progress in Experimental Petrology, 4, 230-233.

**Baker, M.B., Grove, T.L., 1982.** The importance of $H_2O$ in controlling textural development during dynamic crystallization. Eos (Trans. Am. Geophys. Union), 63, p. 451.

**Balashov, Y.A., Sharkov, I.V., Kvashnin, Yu.A., Ulyanenko, N.A., Sherstobitova, G.M., Kravchenko, M.P., Sherstennikova, O.G., Fedotov, Zh.A., Skufin,**


* Except when referred to English translations using some other Russian-English transliteration system, the transliteration system of The Grolier International Dictionary (p. 38, Grolier Inc., Danbury, Connecticut) but with no counterparts for the 'hard sign' and 'soft sign' has been employed in this study.

**P.K., 1991.** Datirovanie protsessov vulkanizma i metamorfizma v Pechengskoi strukture Rb-Sr metodom. *In* Metody Izotopnoi Geologii, p. 19-20. Inst. Geokhimii Anal. Khimii AN SSSR, Inst. Geol. Geokhron. Dokembriya AN SSSR, St. Petersburg.

**Barnes, Sarah-Jane, Often, M., 1990.** Ti-rich komatiites from northern Norway. Contrib. Mineral. Petrol., 105, 42-54.

**Barnes, Sarah-Jane, Boyd, R., Korneliussen, A., Nilsson, L.-P., Often, M., Pedersen, R.B., Robin, B., 1988.** The use of mantle-normalization and metal ratios in discriminating between the effects of partial melting, crystal fractionation and sulfide segregation on platinum-group elements, gold, nickel and copper: Examples from Norway. *In* H.M. Prichard, P.J. Potts, J.F.W. Bowles, S.J. Cribbs (Eds.), Geo Platinum 87, p. 113-143. Elsevier, London.

**Barnes, Steven, J., 1986.** The distribution of chromium among orthopyroxene, spinel and silicate liquid at atmospheric pressure. Geochim. Cosmochim. Acta, 50, 1889-1909.

**Barnes, Steven, J., Gole, M.J., Hill, R.E.T., 1988.** The Agnew nickel deposit, Western Australia: Part II. Sulfide geochemistry, with emphasis on the platinum-group elements. Econ. Geol., 83, 537-550.

**Barton, M., 1979.** A comparative study of some minerals occurring in the potassium-rich alkaline rocks of the Leucite Hills, Wyoming, the Vico Volcano, western Italy, and the Toro-Ankole region, Uganda. Neues . Jahrb. Miner. Abh., 137, 113-134.

**Barton, M., Hamilton, D.L., 1978.** Water-saturated melting relations to 5 kilobars of three Leucite Hills lavas. Contrib. Mineral. Petrol., 66, 41-49.

**Basaltic Volcanism Study Project, 1981.** Basaltic Volcanism on the Terrestrial Planets. Pergamon Press, Inc., New York, 1286 p.

**Bass, M., Moberly, R., Rhodes, M.J., Shih, C., Church, S.E., 1973.** Volcanic rocks cored in the central Pacific, Leg 17, Deep Sea Drilling Project. Initial Reports of the Deep Sea Drilling Project, 17, 429-503.

**Beane, J,E., Hooper, P.R., 1988.** A note on the picrite basalts of the Western Ghats, Deccan Traps, India. *In* K.K. Subbarao (Ed.) Deccan Flood Basalts, Memoir Geol. Soc. India, 10, 117-133.

**Beard, J.S., Lofgren, G.E., 1991.** Dehydration melting and water-saturated melting of basaltic and andesitic greenstones and amphibolites at 1, 3 and 6.9 kb. J. Petrol., 32, 365-401.

**Bèdard, J.H.J., Francis, D.M., Ludden, J., 1988.** Petrology and pyroxene chemistry of Monteregian dykes: the origin of concentric zoning and green cores in clinopyroxenes from alkali basalts and lamprophyres. Can. J. Earth Sci., 25, 2041-2058.

**Beneteau, S.B., Richardson, J.M., Dickin, A.P., McNutt, R.H., Coats, C.J., 1991.** Re-Os isotopic systematics of the Falconbridge East mine, Sudbury, Ontario. GAC-MAG-SEG Joint Annual Meeting, Progr. with Abstr., 16, p. A10.

**Bennett, V.C., Esat, T.M., 1991.** Potential of high precision Re-Os isotopic measurements for determining the ages of planetary differentiation. Eos (Trans. Am. Geophys. Union), 72, p. 528.

**Bertka, C.M., Holloway, J.R., 1988.** Martian mantle primary melts: An experimental study of iron-rich garnet lherzolite minimum melt composition. Proc. Lunar Planet. Sci. Conf., 18th, 723-739.

**Bickle, M.J., Ford, C.E., Nisbet, E.G., 1977.** The petrogenesis of peridotitic komatiites: evidence from high-pressure melting experiments. Earth Planet. Sci. Lett., 37, 97-106.

**Bobrov, A.B., Malyuk, B.I., 1991.** Petrologiya rassloennykh potokov komatiitov Kosivtsevskoi zelenokamennykh struktury (Ukrainskii shchit). Geokhimiya, No. 11, 1573-1585.

**Bodinier, J.L., Dupuy, C., Dostal, J., 1988.** Geochemistry and petrogenesis of eastern Pyrenean peridotites. Geochim. Cosmochim. Acta., 52, 2893-2907.

**Bodinier, J.L., Vasseur, G., Vernieres, J., Dupuy, C., Fabries, J., 1990.** Mechanisms of mantle metasomatism: geochemical evidence from the Lherz orogenic peridotite. J. Petrol., 31, 597-628.

**Borisov, A.E., Smolkin, V.F. (1992)** O proiskhozhdenii vysokokremnezemistykh obrazovanii chetvertoi vulkanogennoi tolshchi Pechengskoi struktury. Izv. Russian Akad. Nauk, Ser. Geol., No. 7, 66-78.

**Brey, G., Green, D.H., 1977.** Systematic study of liquidus phase relations in olivine melilite + $H_2O$ + $CO_2$ at high pressures and petrogenesis of an olivine melilite magmas. Contrib. Mineral. Petrol., 61, 141-162.

**Brügmann, G.E., Gorton, M.P., Hancock, R.G.V., 1990.** Simultaneous determination of noble metals, Re, Se, As and Sb by radiochemical neutron activation analysis. J. Geochem. Expl., 37, 25-36.

**Burnham, C.W., 1979.** The importance of volatile constituents. *In* Yoder, H.S., Jr., (Ed.), The Evolution of Igneous Rocks: Fiftieth Anniversary Perspectives, p. 439-482. Princeton University Press, Princeton, N.J.

**Cameron,W.E., 1989.** Contrasting boninite-tholeiite associations from New Caledonia. *In* A.J. Crawford (Ed.), Boninites, p. 314-338. Unwin Hyman, London.

**Campbell, I.H., Griffiths, R.W., 1990.** Implications of mantle plume structure for the evolution of flood basalts. Earth Planet. Sci. Lett., 99, 79-93.

**Campbell, I.H., Griffiths, R.W., Hill, R.I., 1989.** Melting in an Archean mantle plume: heads it's basalts, tails it's komatiites. Nature, 339, 697-699.

**Cawthorn, R.G., McIver, J.R., McCarthy, T.S., Wyatt, B.A., Ferguson, J., Barnes, S.J., 1979.** Possible liquid immiscibility textures in high-magnesia basalts from the Ventersdorp Supergroup, South Africa. J. Geol., 87, 105-113.

**Clague, D.A., Dalrymple, G.B., 1988.** Age and petrology of alkalic postshield and rejuvenated-stage lava from Kauai, Hawaii. Contrib. Mineral. Petrol., 99, 202-218.

**Clague D.A., Weber, W.S., Dixon, J., 1991.** Picritic glasses from Hawaii. Nature, 353, 553-556.

**Condliffe, E., 1976.** Melting relationships of selected rocks of dioritic mineralogy. Progress in Experimental Petrology, 3, 54-55.

**Cousens, B.L., Ludden, J.N., 1991.** Radiogenic isotope studies of oceanic basalts: a window into the mantle. *In* L. Heaman and J.N. Ludden (Eds.), Applications of Radiogenic Isotope Systems to Problems in Geology, Min. Assoc. Can. Short Course Handbook, 19, 225-257.

**Crawford, A.J., Falloon, T.J., Green, D.H., 1988.** Classification, petrogenesis and tectonic setting of boninites, *In* A.J. Crawford (Ed.), Boninites, p. 1-49. Unwin Hyman, London.

**Creaser, R.A., Papanastassiou, D.A., Wasserburg, G.J., 1991.** Negative thermal ion mass spectrometry of osmium, rhenium, and iridium. Geochim. Cosmochim. Acta, 55, 397-401.

**Deer, W.A., Howie, R.A., Zussman, J., 1962.** Rock-forming minerals. Vol. 3, Sheet Silicates. Longmans, Green and Co Ltd., London, 270 p.

**Delano, J.W., 1986.** Pristine lunar glasses: criteria, data, and implications. Proc. Lunar Planet. Sci. Conf., 16th, J. Geophys. Res., 91, D201-D213.

**DePaolo, D.J., 1981.** Neodymium isotopes in the Colorado Front Range and crust-mantle evolution in the Proterozoic. Nature, 291, 193-196.

**DePaolo, D.J., Wasserburg, G.J., 1979.** Sm-Nd age of the Stillwater Complex and the mantle evolution curve for neodymium. Geochim. Cosmochim. Acta., 43, 999-1008.

**Distler, V.V., Filimonova, A.A., Grokhovskaya, T.L., Laputina, I.P., 1990.** Platinum-group elements in the copper-nickel ores of the Pechenga ore field. Internat. Geol. Rev., 32, 70-83.

**Duncan, R.A., Erlank, A.J., Marsh, J.S., 1984.** Regional geochemistry of the Karoo igneous province. Spec. Publ. geol. Soc. S. Afr., 13, 355-388.

**Dupre, B., Chauvel, C., Arndt, N.T., 1984.** Pb and Nd isotopic study of two Archean komatiite flows from Alexo, Ontario. Geochim. Cosmochim. Acta, 48, 1965-1972.

**Dupuy, C., Dostal, J., Boivin, P.A., 1986.** Geochemistry of ultramafic xenoliths and their host alkali basalts from Tallante, southern Spain. Mineral. Mag., 50, 231-239.

**Echeverria, L.M., 1980.** Tertiary or Mesozoic komatiites from Gorgona Island, Colombia: Field relations and geochemistry. Contrib. Mineral. Petrol., 73, 253-266.

**Eckstrand, O.R., Grinenko, L.N., Krouse, H.R., Paktunc, A.D., Schwann, P.L., Scoates, R.F.J., 1989.** Preliminary data on sulphur isotopes and Se/S ratios, and the source of sulphur in magmatic sulphides from the Fox River Sill, Molson Dykes and Thompson nickel deposits, northern Manitoba. Geol. Survey Canada, Paper 89-1C, 235-242.

**Eggins, S.M., 1992a.** Petrogenesis of Hawaiian tholeiites: 1, phase equilibria constraints. Contrib. Mineral. Petrol., 110, 387-397.

**Eggins, S.M., 1992b.** Petrogenesis of Hawaiian tholeiites: 2, aspects of dynamic melt segregation. Contrib. Mineral. Petrol., 110, 398-410.

**Ehrenberg, S.N., 1982.** Petrogenesis of garnet lherzolite and megacrystalline nodules from the Thumb, Navajo volcanic field. J. Petrol., 23, 507-547.

**Eliseev, N.A., Gorbunov, G.I., Eliseev, E.N., Maslenikov, V.A., Utkin, K.N., 1961.** Ultraosnovnye i osnovnye intruzii Pechengi. Akad. Nauk SSSR, Moscow, 357 p.

**Ellam, R.M., Carlson, R.W., Shirey, S.B., 1991.** Re-Os isotope constraints on flood basalt genesis. Eos (Trans. Am. Geophys. Union), 72, p. 579.

**Elthon, D., Scarfe, C.M., 1984.** High-pressure phase equilibria of a high-magnesia basalt and the genesis of primary oceanic basalts. Am. Mineral., 69, 1-15.

**Esperanca, S., Holloway, J.R., 1987.** On the origin of some mica-lamprophyres: experimental evidence from a mafic minette. Contrib. Mineral. Petrol., 95, 207-216.

**Esser, B.K., Turekian, K.K., 1988.** Accretion rate of extraterrestrial particles determined from osmium isotope systematics of Pacific pelagic clay and manganese nodules. Geochim. Cosmochim. Acta., 52, 1383-1388.

**Evans, C.A., 1987.** Oceanic magmas with alkalic characteristics; Evidence from basal cumulate rocks in the Zambales ophiolite, Luzon, Phlippine Islands. Geol. Soc. Am. Spec. Paper 215, 139-150.

**Ewart, A., 1989.** Mineralogy and mineral chemistry. *In* R.W. Johnson (Ed.), Intraplate Volcanism in Eastern Australia and New Zealand, p. 197-218. Cambridge Univ. Press, Cambridge.

**Fall, H.G., Gibb, F.G.F., Kanaris-Sotirou, R., 1982.** Jurassic volcanic rocks of the northern North Sea. J. Geol. Soc. London, 139, 277-292.

**Falloon, T.J., Green, D.H., 1988.** Anhydrous partial melting of peridotite from 8 to 35 kb and the petrogenesis of MORB. J. Petrol., Special Lithosphere Issue, p. 379-414.

**Falloon, T.J., Green, D.H., Hatton, C.J., Harris, K.L., 1988.** Anhydrous partial melting of a fertile and depleted peridotite from 2 to 30 kb and application to basalt petrogenesis. J. Petrol., 29, 1257-1282.

**Fedorenko, V.A., 1983.** Sravnitelnaya petrokhimicheskaya kharakteristika vysokomagnesianykh magmaticheskikh obrazovaniya Norilskogo raiona. Dokl. Akad. Nauk SSSR, 273, 1206-1210.

**Fedorenko, V.A., Dyuzhikov, O.A., 1981.** Giperbazit-bazitovyi effuzivnyi vulkanizm Norilskogo raiona. Sov. Geol., No. 9, 98-106.

**Fehn, U., Teng, R., Elmore, D., Kubik, P.W., 1986.** Isotopic composition of osmium in terrestrial samples determined by accelerator mass spectrometry. Nature, 323, 707-710.

**Ferguson, J., Currie, K.L., 1972.** Silicate liquid immiscibility in the ancient "basalts" of the Barberton Mountain Land, Transvaal. Nature, 235, 86-89.

**Fisk, M.R., Bence, A.E., 1980.** Experimental crystallization of chrome spinel in FAMOUS basalt 527-1-1. Earth Planet. Sci. Lett., 48, 111-123.

**Fleet, M.E., MacRae, N.D., 1975.** A spinifex rock from Munro Township, Ontario. Can. J. Earth Sci., 12, 928-939.

**Foden, J.D., Green, D.H., 1992.** Possible role of ampfibole in the origin of andesite: some experimental and natural evidence. Contrib. Mineral. Petrol., 109, 479-493.

**Foley, S., 1991.** High-pressure stability of the fluor- and hydroxy-endmembers of pargasite and K-richterite. Geochim. Cosmochim. Acta, 55, 2689-2694.

**Foley, S.F., Venturelli, G., 1989.** High-$K_2O$ rocks with high-MgO, high-$SiO_2$ affinities. *In* A.J. Crawford (Ed.), Boninites, p. 72-88. Unwin Hyman, London.

**Ford, C.E., 1976.** The stability field of a natural kaersutite. Progress in Experimental Petrology, 3, 285-288.

**Ford, C.E., Russell, D.G., Craven, J.A., Fisk, M.R., 1983.** Olivine-liquid equilibria: temperature, pressure and composition dependence of the crystal/liquid partition coefficients for Mg, $Fe^{2+}$, Ca and Mn. J. Petrol., 24, 256-265.

**Francis, D., Ludden, J.N., 1990.** The mantle source of olivine nephelinites; basanite and alkaline olivine basalt at Fort Selkirk, Yukon, Canada. J. Petrol., 31, 371-400.

**Frey, F.A., Green, D.H., Roy, S.D., 1978.** Integrated models of basalt petrogenesis: a study of quartz tholeiites to olivine melilites from south eastern Australia utilizing geochemical and experimental petrological data. J. Petrol., 19, 463-513.

**Frey, F.A., Suen, C.J., Stockman, H.W., 1985.** The Ronda high temperature peridotite: geochemistry and petrogenesis. Geochim. Cosmochim. Acta., 49, 2469-2491.

**Genkin, A.D., Gorbunov, G.I., Kazansky, V.I., Lanev, V.S., Filimonova, A.A., Yakovlev, Y.N., 1987.** Ore mineralization. *In* Ye.A. Kozlovsky (Ed.), The Superdeep Well of the Kola Peninsula, p. 199-222. Springer-Verlag, Berlin Heidelberg.

**Gibb, F.G.F., Henderson, C.M.B., 1976.** The origin of analcime in a crinanite sill. Progress in Experimental Petrology, 3, 50-53.

**Gibb, F.G.F., Kanaris-Sotirou, R., 1976.** Jurassic igneous rocks of the Forties Field. Nature, 260, 23-25.

**Gilbert, M.C., Helz, R.T., Popp, R.K., Spear, F.S., 1982.** Experimental studies on amphibole stability. *In* D.R. Veblen and P.H. Ribbe (Eds.), Amphiboles: Petrology and Experimental Phase Relations. Rev. in Mineral., 9B, 229-353. Min. Soc. Am.

**Gladkikh, V.S., 1991.** Geokhimiya melilitovykh vulkanicheskikh porod Maimecha-Kotuiskoi provintsii. Geokhimiya, No. 4, 583-592.

**Gladkikh, V.S., Lyapunov, S.M., Solovev, V.A., 1987.** Geokhimicheskie osobennosti i usloviya formirovaniya vulkanicheskikh assotsiatsii Maimecha-Kotuiskoi i Pribaikalskoi provintsii. *In* Geokhimiya kontinentalnogo vulkanizma, p. 65-114. "Nauka", Moscow.

**Glikson, A.Y., 1979.** Siderophile and lithophile trace-element evolution of the Archean mantle. BMR Jour. Austr. Geol. Geophys., 4, 253-279.

**Golubev, A.I., Akhmedov, A.M., Galdobina, L.P., 1984.** Geokhimiya chernoslantsevykh kompleksov nizhnego proterozoya Karelo-Kolskogo regiona. Nauka, Leningrad, 193 p.

**Gorbunov, G.I., 1968.** Geologiya i genezis sulfidnykh medno-nikelevykh mestorozhdenii Pechengi. Nedra, Moscow, 352 p.

**Gorbunov, G.I. (Ed-in-chief), 1982.** Khimicheskie analizy porod bazit-giperbazitovykh kompleksov dokembriya Kolskogo poluostrova. Kolskii Filial Akad. Nauk SSSR, Apatity, 216 p.

**Gorbunov, G.I., Yakovlev, Yu.N., Astafev, Yu.A., Goncharov, Yu.V., Bartenev, I.S., Neradovskii, Yu.N., 1973.** Atlas tekstur i struktur sulfidnykh medno-nikelevykh rud Kolskogo poluostrova. Nauka, Leningrad, 177 p.

**Gorbunov, G.I., Zagorodny, V.G., Robonen, W.I., 1985a.** Main features of the geological history of the Baltic Shield and the epochs of ore formation. *In* H.Papunen and G.I. Gorbunov (Eds.), Nickel-Copper Deposits of the Baltic Shield and Scandinavian Caledonides. Geol. Surv. Finland, Bull. 333, 17-41.

**Gorbunov, G.I., Yakovlev, Yu.N., Goncharov, Yu.V., Gorelov, V.A., Telnov, V.A., 1985b.** The nickel areas of the Kola Peninsula. *In* H.Papunen and G.I. Gorbunov (Eds.), Nickel-Copper Deposits of the Baltic Shield and Scandinavian Caledonides. Geol. Surv. Finland, Bull. 333, 41-109.

**Gorbunov, G.I., Korchagin, A.U., Mednikov, A.I., 1989.** O rudonosnosti pikritov Pechengi. Dokl. Akad. Nauk SSSR, 304, 1205-1208.

**Gorokhov, I.M., Varshavskaya, E.S., Kutyavin, E.P., Melnikov, N.N., 1982.** Rb-Sr dating of low-grade metamorphics in the U.S.S.R. Precambrian Res., 18, 145-156.

**Goto, K., Arai, S., 1987.** Petrology of peridotite xenoliths in lamprophyre from Shingu, southwestern Japan: Implications for origin of Fe-rich mantle peridotites. Mineral. Petrol., 37, 137-155.

**Graham, A.M., 1981.** Melting relations in island arc lavas from Grenada, Lesser Antilles. Progress in Experimental Petrology, 5, 126-132.

**Green, D.H., 1973a.** Experimental melting studies on a model upper mantle composition at high pressure under water-saturated and water-undersaturated conditions. Earth Planet. Sci. Lett., 19, 37-53.

**Green, D.H., 1973b.** Conditions of melting of basanite magma from garnet peridotite. Earth Planet. Sci. Lett., 17, 456-465.

**Green, J.C., Schulz, K.J., 1977.** Iron-rich basaltic komatiites in the early Precambrian Vermilion district, Minnesota. Can. J. Earth Sci., 14, 2181-2192.

**Griffiths, R.W., Campbell, I.H., 1990.** Stirring and structure in mantle starting plumes. Earth Planet. Sci. Lett., 99, 66-78.

**Grinenko, L.N., Smolkin, V.F., 1991.** Isotopic composition and content of sulfur in ferropicrites and gabbro-wehrlite intrusions of the Pechenga zone. Geokhimiya, No. 9, 1250-1261.

**Grinenko, L.N., Grinenko, V.A., Lyakhnitskaya, I.V., 1967.** Isotopnyi sostav cery sulfidov medno-nikelevykh mestorozhdenii Kolskogo P-va. Geol. Rud. Mestorozh., No. 4, 3-17.

**Grove, T.L., Beaty, D.W., 1980.** Classification, experimental petrology and possible volcanic histories of the Apollo 11 high-K basalts. Proc. Lunar Planet. Sci. Conf., 11th, 149-177.

**Grove, T.L., Walker, D., 1977.** Cooling histories of Apollo 15 quartz-normative basalts. Proc. Lunar Planet. Sci. Conf., 8th, 1501-1520.

**Groves, D.I., Barrett, F.M., Binns, R.A., McQueen, K.G., 1977.** Spinel phases associated with metamorphosed volcanic-type iron-nickel sulfide ores from Western Australia. Econ. Geol., 72, 1224-1244.

**Gruau, G., Jahn, B.M., Glikson, A.Y., Davy, R., Hickman, A.H., Chauvel, C., 1987.** Age of the Archean Talga-Talga Subgroup, Pilbara Block, Western Australia, and

early evolution of the mantle: new Sm-Nd isotopic evidence. Earth Planet. Sci. Lett., 85, 105-116.

**Gruau, G., Chauvel, C., Arndt, N.T., Cornichet, J., 1990.** Aluminum depletion in komatiites and garnet fractionation in the early Archean mantle: hafnium isotope constraints. Geochim. Cosmochim. Acta., 54, 3095-3101.

**Hamilton, D.L., Burnham, C.W., Osborn, E.F., 1964.** The solubility of water and effects of oxygen fugacity and water content on crystallization in mafic magmas. J. Petrol., 5, 21-39.

**Hanski, E., 1980.** Komatiitic and tholeiitic metavolcanics of the Siivikkovaara area in the Archean Kuhmo greenstone belt, eastern Finland. Bull. Geol. Soc. Finland, 52, 67-100.

**Hanski, E., 1986.** The gabbro-wehrlite association in the eastern part of the Baltic Shield. *In* G.H. Fiedrich et al. (Eds.), Geology and Metallogeny of Copper Deposits, p. 151-170. Springer-Verlag, Berlin Heidelberg.

**Hanski, E., 1988.** Major element geochemistry of Archean metavolcanic rocks in the eastern part of the Baltic Shield: role of secondary alteration. Geol. Survey Finland, Spec. Paper 4, 53-70.

**Hanski, E., 1989.** Petsamon ferropikriittien petrologian ongelmia. *Julkaisussa* T. Manninen (toim.), Tulivuorenkivet Kolarista Kuusamoon, Lapin vulkaniittiprojektin ekskursio ja esitelmä-seminaari 5.-10.6. 1989. Geologian tutkimuskeskus, Opas 23, 76-78.

**Hanski, E. (in press)** Globular ferropicritic rocks at Pechenga, Kola Peninsula, (Russia): Immiscibility versus alteration. Lithos

**Hanski, E., Smolkin, V.F., 1989.** Pechenga ferropicrites and other early Proterozoic picrites in the eastern part of the Baltic Shield. Precambrian Res., 45, 63-82.

**Hanski, E., Smolkin, V.F., 1990.** Thick, layered ferropicritic flows in the Pechenga area, Kola Peninsula and their relation to associated Ni-Cu deposits. Internat. Volcanol. Congress, 3.-8. Sept. 1990, Mainz (FGR), Abstracts.

**Hanski, E., Smolkin, V.F., 1991.** Spinifex-textured ferropicritic flows in the Pechenga area, Kola Peninsula. GAC-MAG-SEG Joint Annual Meeting, Progr. with Abstr., 16, p. A51.

**Hanski, E., Huhma, H., Smolkin, V.F., Vaasjoki, M., 1990.** The age of the ferropicritic volcanics and comagmatic Ni-bearing intrusions at Pechenga, Kola Peninsula, U.S.S.R. Bull. Geol. Soc. Finland, 62, 123-133.

**Hanson, G.N., Langmuir, C.H., 1978.** Modelling of major elements in mantle-melt systems using trace element approaches. Geochim. Cosmochim. Acta, 42, 725-741.

**Harrison, W.J., 1981.** Partitioning of REE between minerals and coexisting melts during partial melting of a garnet lherzolite. Am. Mineral., 66, 242-259.

**Hart, S.R., Brooks, C., 1977.** The geochemistry and evolution of early Precambrian mantle. Contrib. Mineral. Petrol., 61, 109-128.

**Hart, S.R., Kinloch, E.D., 1989.** Osmium isotope systematics in Witwaterstarnd and Bushveld ore deposits. Econ. Geol., 84, 1651-1655.

**Hawkins, J., Melchior, J., 1983.** Petrology of basalts from Loihi Seamount, Hawaii. Earth Planet. Sci. Lett., 66, 356-368.

**Hegner, E., Bevier, M.L., 1991.** Nd and Pb isotopic constraints on the origin of the Purtuniq ophiolite and Early Proterozoic Cape Smith belt, northern Québec, Canada. Chem. Geol., 91, 357-371.

**Hekinian, R., 1974.** Petrology of igneous rocks from Leg 22 in the northeastern Indian Ocean. Init. Rep. Deep Sea Drilling Project, 22, 413-447.

**Hekinian, R., Bideau, D., Stoffers, P., Cheminee, J.L., Muhe, R., Puteanus, D., Binard, N., 1991.** Submarine intraplate volcanism in the South Pacific: Geological setting and petrology of the Society and the Austral regions. J. Geophys. Res., 96, 2109-2138.

**Helz, R.T., 1973.** Phase relations of basalts in their melting range at $P_{H2O}$ = 5 kb as a function of oxygen fugacity. Part I. Mafic phases. J. Petrol., 14, 249-302.

**Helz, R.T., 1979.** Alkali exchange between hornblende and melt: a temperature-sensitive reaction. Am. Mineral., 64, 953-965.

**Henderson, C.M.B., Gibb, F.G.F., 1987.** The petrology of the Lugar Sill, SW Scotland. Trans. Royal Soc. Edinburgh, Earth Sci., 77, 325-347.

**Herr, W., Hoffmeister, W., Hirt, B., Geiss, J., Houtermans, F.G., 1961.** Versuch zur Datiering von Eisen Meteoriten nach der Rhenium-Osmium Methode. Z. Naturforsch., 16, 1053-1056.

**Herzberg, C., 1992.** Depth and degree of melting of komatiites. J. Geophys. Res., 97, 4521-4540.

**Holloway, J.R., 1973.** The system pargasite-$H_2O$-$CO_2$: a model for melting of a hydrous mineral with a mixed-volatile fluid-I. Experimental results to 8 kbar. Geochim. Cosmochim. Acta, 37, 651-666.

**Holloway, J.R., Burnham, C.W., 1972.** Melting relations of basalt with equilibrium water pressure less than total pressure. J. Petrol., 13, 1-29.

**Holloway, J.R., Ford, C.E., 1975.** Fluid-absent melting of the fluoro-hydroxy amphibole pargasite to 35 kilobars. Earth Planet. Sci. Lett., 25, 44-48.

**Horan, M.F., Morgan, J.W., Foose, M.P., Walker, R.J., Stepanov, V., 1991.** Rhenium-osmium isotope systematics of ores rich in platinum group elements, Noril'sk-Talnakh district, Siberia. Eos (Trans. Am. Geophys. Union), 72, p. 570.

**Hughes, S.S., Schmitt, R.A., 1988.** Chemistry of a unique low-Ti basalt clast extracted from 60255 regolith breccia. Lunar Planet. Sci., XIX, 515-516.

**Hughes, S.S., Delano, J.W., Scmitt, R.A., 1988.** Apollo 15 yellow-brown volcanic glass: Chemistry and petrogenetic relations to green volcanic glass and olivine-normative mare basalts. Geochim. Cosmochim. Acta, 52, 2379-2391.

**Huhma, H., 1986.** Sm-Nd, U-Pb and Pb-Pb isotopic evidence for the origin of the Early Proterozoic Svecokarelian crust in Finland. Geol. Surv. Finland, Bull. 337, 48 p.

**Huhma, H., Cliff, R.A., Perttunen, V., Sakko, M., 1990.** Sm-Nd and Pb-isotopic study of mafic rocks associated with early Proterozoic continental rifting: The Peräpohja Schist Belt in northern Finland. Contrib. Mineral. Petrol., 104, 369-379.

**Irving, A.J., 1974.** Megacrysts from the Newer basalts and other basaltic rocks of southwestern Australia. Geol. Soc. Am. Bull., 85, 1503-1514.

**Irving, A.J., 1978.** A review of experimental studies of crystal/liquid trace element partitioning. Geochim. Cosmochim. Acta., 42, 743-770.

**Irving, A.J., 1980.** Petrology and geochemistry of composite ultramafic xenoliths in alkalic basalts and implications for magmatic processes within the mantle. Am. J. Sci., 280-A, 389-426.

**Ivanova, L.V., Chapina, O.S., Melezhik, V.A., 1988.** Nakhodka kokkoidykh mikrofitofossilii v metamorfirovannykh kremnyakh rannego proterozoya SSSR. Dokl. Akad. Nauk SSSR, 303, 210-211.

**Jagoutz, E., Palme, H., Baddenhausen, H., Blum, K., Cendales, M., Dreibus, G., Spettel, B., Lorenz, V., Wänke, H., 1979.** The abundances of major, minor and trace elements in the earth's mantle as derived from primitive ultramafic nodules. Proc. Lunar Sci. Conf., 10th, 2031-2050.

**Jahn, B.-M., Gruau, G., Glikson, A.Y., 1982.** Komatiites of the Onverwacht Group, S. Africa: REE geochemistry, Sm/Nd age and mantle evolution. Contrib. Mineral. Petrol., 80, 25-40.

**Jakobsson, S., Holloway, J.R., 1986.** Crystal-liquid experiments in the presence of a C-O-H fluid buffered by graphite + iron + wustite: experimental method and near-liquidus relations in basanite. J. Volcanol. Geotherm. Res., 29, 265-291.

**Jaques, A.I., Green, D.H., 1979.** Determination of liquid compositions in high pressure melting of peridotite. Am. Mineral., 64, 1312-1321.

**Jaques, A.L., Green, D.H., 1980.** Anhydrous melting of peridotite at 0-15 kb pressure and the genesis of tholeiitic basalts. Contrib. Mineral. Petrol., 73, 287-310.

**Johnson, M.C., 1990.** Intensive parameters of volcanic magma systems from experimental amphibole/melt equilibria. Ph.D. thesis, Providence, Rhode Island, Brown University, 153 p.

**Jolly, W.T., 1987.** Geology and geochemistry of Huronian rhyolites and low-Ti continental tholeiites from the Thessalon region, central Ontario. Can. J. Earth Sci., 24, 1360-1385.

**Jurewicz, A.J.G., Watson, E.B., 1988.** Cations in olivine, Part 1: Calcium partitioning and calcium-magnesium distribution between olivines and coexisting melts, with petrologic applications. Contrib. Mineral. Petrol., 99, 176-185.

**Kaivosoja, J., Koivumaa, S., 1984.** Hierarkinen standarditietorakenne (HST). Ohjelmien käyttöohje. Arkeeisten alueiden malmiprojekti, Oulun yliopisto, Rap. 18B, 59 s.

**Kato, T., Ringwood, A.E., Irifune, T., 1988.** Experimental determination of element partitioning between silicate perovskites, garnets and liquids: constraints on early differentiation of the mantle. Earth Planet. Sci. Lett., 89, 123-145.

**Karhu, J., Melezhik, V., 1992.** Carbon isotope systematics of early Proterozoic sedimentary carbonates in the Kola Peninsula, Russia: correlation with Jatulian formations in Karelia. *In* V.V. Balagansky and F.P. Mitrofanov (Eds.), Correlation of Precambrian Formations of the Kola-Karelian Region and Finland, p. 48-53. Geol. Inst., Kola Science Centre, Russian Academy of Sciences, Apatity.

**Kay, R.W., Gast, P.W., 1973.** The rare earth content and origin of alkali-rich basalts. J. Geol., 81, 653-682.

**Klewin, K.W., Berg, J.H., 1991.** Petrology of the Keweenawan Mamainse Point lavas, Ontario: petrogenesis and continental rift evolution. J. Geophys. Res., 96, 457-474.

**Kogarko, L.N., Krigman, L.D., Krot, T.V., 1987.** Rastvorimost i geokhimiya fosfora v magmakh. Geokhimiya, No. 7, 915-927.

**Kontinen, A., 1987.** An early Proterozoic ophiolite - the Jormua mafic-ultramafic complex, northern Finland. Precambrian Res., 35, 313-341.

**Kozlovsky, Ye.A. (Ed.), 1987.** The Superdeep Well of the Kola Peninsula. Springer-Verlag, Berlin Heidelberg, 558 p.

**Kravtsov, N.A., 1984.** Razrezy yuzhnopechengskoi serii. *In* Geologiya i istoriya formirovaniya dokembriiskikh struktur Kolskogo Poluostrova, p. 28-32. Kolskii Filial Akad. Nauk SSSR, Apatity.

**Kremenetskii, A.A., Ovchinnikov, L.N., 1986.** Geokhimiya glubinnykh porod. Nauka, Moscow, 262 p.

**Krestin, E.M., Yudina, V.V., 1988.** Ultraosnovnye vulkanity verkhne arkheiskhikh i nizhneproterozoiskikh poyasov KMA. Byul. Mosk. Obshch. Ispyt. Prid. 3, 89-103.

**Krill, A.G., Bergh, S., Lindahl, I., Mearns, E.W., Often, M., Olerud, S., Olesen, O., Sandstad, J.S., Siedlecka, A., Solli, A., 1985.** Rb-Sr, U-Pb and Sm-Nd isotopic dates from Precambrian rocks of Finnmark. Nor. Geol. Unders. Bull., 403, 37-54.

**Krishnamurthy, P., Cox, K.G., 1977.** Picrite basalts and related lavas from the Deccan Traps of western India. Contrib. Mineral. Petrol., 62, 53-75.

**Kulikov, V.S., 1988.** Vysokomagnesialnyi vulkanizm rannego proterozoya (Kareliya). *In* Komatiity i vysokomagnesialnye vulkaniity rannego dokembriya Baltiiskogo shchita, p. 20-88. Nauka, Leningrad.

**Kushiro, I., 1972.** Effects of water on the compositions of magmas formed at high pressures. J. Petrol., 13, 311-334.

**Kushiro, I., 1973.** Partial melting of garnet lherzolites from kimberlite at high pressures. *In* P.H. Nixon (Ed.) Lesotho Kimberlites, p. 294-299. Lesotho National Development Corporation, Maseru, Lesotho.

**Kushiro, I., 1975.** On the nature of silicate melt and its significance in magma genesis; regularities in the shift of the liquidus boundaries involving olivine, pyroxene, and silica minerals. Am. J. Sci., 275, 411-431.

**Kushiro, I., 1990.** Partial melting of mantle wedge and evolution of island arc crust. J. Geophys. Res., 95, 15929-15939.

**Kushiro, I., Shimizu, N., Nakamura, Y., Akimoto, S., 1972.** Compositions of co-existing liquids and solid phases formed upon melting of natural garnet and spinel lherzolites at high pressures: a preliminary report. Earth Planet. Sci. Lett., 14, 19-25.

**Lambert, D.D., Morgan, J.W., Walker, R.J., Shirey, S.B., Carlson, R.W., Zientik, M.L., Koski, M.S., 1989.** Rhe-

nium-osmium and samarium-neodymium isotopic systematics of the Stillwater Complex. Science, 244, 1169-1174.

**Langmuir, C.H., Hanson, G.N., 1980.** An evaluation of major element heterogeneity in the mantle sources of basalts. Phil. Trans. Roy. Soc. Lond., A297, 383-407.

**Lanphere, M.A., Frey, F.A., 1987.** Geochemical evolution of Kohala Volcano, Hawaii. Contrib. Mineral. Petrol., 95, 100-113.

**Latin, D.M., Dixon, J.E., Fitton, J.G., 1989.** Rift related magmatism in the North Sea Basin. *In* D.J. Blundell and A. Gibbs (Eds.), Tectonic evolution of the North Sea Rifts, p. 101-144. Oxford Univ. Press, Oxford.

**Le Bas, M.J., 1987.** Nephelinites and carbonatites. *In* J.G. Fitton and B.G.J. Upton (Eds.), Alkaline Igneous Rocks, Geol. Soc. London, Spec. Publ., 30, 53-83.

**Leake, B.E., 1978.** Nomenclature of amphiboles. Am. Mineral., 63, 1023-1053.

**Leat, P.T., Jackson, S.E., Thorpe, R.S., Stillman, C.J., 1986.** Geochemistry of bimodal basalt-subalkaline/peralkaline rhyolite provinces within the Southern British Caledonides. J. Geol. Soc. London, 143, 259-273.

**Lehtonen, M., 1989.** The Lapland Volcanite Project. *In* S. Autio (Ed.), Geological Survey of Finland, Current Research 1988. Geol. Survey Finland, Special Pap., 10, 19-21.

**Lesher, C.M., 1989.** Komatiite-associated nickel sulfide deposits. *In* J.A. Whitney and A.J. Naldrett (Eds.), Ore deposition associated with magmas. Rev. Econ. Geol., 4, 45-101.

**Leterrier, J., Maury, R.C., Thonon, P., Girard,D., Marchal, M., 1982.** Clinopyroxene composition as a method of identification of the magmatic affinities of paleo-volcanic series. Earth Planet. Sci. Lett., 59, 139-154.

**Libourel, G., 1989.** Systematics of calcium distribution between olivine and melt: an experimental study. Eos (Trans. Am. Geophys. Union), 70, p. 1393.

**Lindner, M., Leich, D.A., Borg, R.J., Russ, G.P., Bazan, J.M., Simons, D.S., Date, A.R., 1986.** Direct laboratory determination of the $^{187}$Re half-life. Nature, 320, 246-248.

**Lindner, M., Leich, D.A., Russ, G.P., Bazan, J.M., Borg, R.J., 1989.** Direct determination of the half-life of $^{187}$Re. Geochim. Cosmochim. Acta, 53, 1597-1606.

**Lipman, S.J., 1984.** Petrology of alkali wehrlite sills in the Oman Mountains. Min. Mag., 48, 13-20.

**Lofgren, G., 1974.** An experimental study of plagioclase crystal morphology: isothermal crystallization. Am. J. Sci., 274, 243-273.

**Lofgren, G.E., Donaldson, C.H., Usselman, T.M., 1975.** Geology, petrology, and crystallization of Apollo 15 quartz-normative basalts. Proc. Lunar Sci. Conf., 6th, 79-99.

**Luck, J.-M., 1989.** The rhenium-osmium system. *In* E. Roth and B. Poty (Eds.), Nuclear Methods of Dating, p. 95-104. Kluwer Academic Publ., Dordrecht, Netherlands.

**Luck, J.-M., Allègre, C.-J., 1982.** The study of molybdenites through the $^{187}$Re-$^{187}$Os chronometer. Earth Planet. Sci. Lett., 61, 291-296.

**Luck, J.-M., Allègre, C.J., 1983.** $^{187}$Re-$^{187}$Os systematics in meteorites and cosmochemical consequences. Nature, 302, 130-132.

**Luck, J.-M., Allègre, C.J., 1984.** $^{187}$Re-$^{187}$Os investigation in sulfide from Cape Smith komatiite. Earth Planet. Sci. Lett., 68, 205-208.

**Luck, J.-M., Allègre, C.J., 1991.** Osmium isotopes in ophiolites. Earth Planet. Sci. Lett., 107, 406-415.

**Luck, J.-M., Arndt, N.T., 1985.** Re/Os isochron for Archean komatiite from Alexo, Ontario. Terra Cognita, 5, p. 323.

**Luck, J.-M., Birck, J.-L., Allègre, C.-J., 1980.** $^{187}$Re-$^{187}$Os systematics in meteorites: early chronology of the Solar System and age of the Galaxy. Nature, 283, 256-259.

**Luhr, J.F., 1990.** Experimental phase relations of water- and sulfur-saturated arc magmas and the 1982 eruptions of El Chichon Volcano. J. Petrol., 31, 1071-1114.

**Mahood, G.A., Baker, D.R., 1986.** Experimental constraints on depths of fractionation of mildly alkalic basalts and associated felsic rocks; Pantelleria, Strait of Sicily. Contrib. Mineral. Petrol., 93, 251-264.

**Maaløe, S., Aoki, K.-I., 1977.** The major element composition of the upper mantle estimated from the composition of lherzolites. Contrib. Mineral. Petrol., 63, 161-173.

**Maaløe, S., Jakobsson, S.P., 1980.** The P-T phase relations of a primary oceanite from the Reykjanes Peninsula, Iceland. Lithos, 13, 237-246.

**Manninen, T., 1991.** Sallan alueen vulkaniitit. Lapin vulkaniitti projekti. Summary: Volcanic rocks of the Salla area, northeastern Finland. A report of the Lapland Volcanite Project. Report of Inverstgation, No. 104, Geol. Survey Finland, 97 p.

**Martin, C.E., 1989.** Re-Os isotopic investigation of the Stillwater Complex, Montana. Earth Planet. Sci. Lett., 93, 336-344.

**Martin, C.E., 1991.** Osmium isotopic characteristics of mantle-derived rocks. Geochim. Cosmochim. Acta, 55, 1421-1434.

**Martin, C.E., Esser, B.K., Turekian, K.K., 1991.** Re-Os isotopic constraints on the formation of mantle and crustal reservoirs. Austr.J. Earth Sci., 38, 569-576.

**Masuda, A., Hirata, T., Shimizu, H., 1986.** Determinations of osmium isotope ratios in iron meteorites and iridosmines by ICP-MS. Geochem. J., 20, 233-239.

**Maurel, C., Maurel, P., 1983.** Influence du fer ferrique sur la distribution de l'aluminium entre bain silicaté basique et spinelle chromiferè. Bull. Minéral., 106, 623-624.

**McCandless, T.E., Ruiz, J., 1991.** Osmium isotopes and crustal sources for platinum-group mineralization in the Bushveld Complex, South Africa. Geology, 19, 1225-1228.

**McDonough, W.F., Frey, F.A., 1989.** Rare earth elements in upper mantle rocks. *In* B.R. Lipin & G.A. McKay (Eds.), Geochemistry and Mineralogy of Rare Earth Elements, Rev. in Mineral., Vol. 21, p. 99-145. Min. Soc. Am.

**McFarlane, E.A., Drake, M.J., 1990.** Element partitioning anf the early thermal history of the Earth. *In* H.E. Newsom and J.H. Jones (Ed.), Origin of the Earth, p. 135-150. Oxford Univ. Press, Oxford.

**McIver, J.R., Cawthorn, R.G., Wyaat, B.A., 1982.** The Ventersdorp Supergroup - the youngest komatiitic sequence in South Africa. *In* N.T. Arndt and E.G. Nisbet (Eds.) Komatiites, p. 81-90. George Allen & Unwin, Lon-

don.

**McKenzie, D.P., Bickle, M.J., 1988.** The volume and composition of melt generated by extension of the lithosphere. J. Petrol., 29, 625-679.

**Melezhik, V.A., 1987.** Composition of waters of Precambrian basins as indicated by geochemical data. Int. Geol. Rev., 29, 1188-1199.

**Mengel, K., Green, D.H., 1989.** Stability of amphibole amd phlogopite in metasomatized peridotite under water-saturated and water-undersatured conditions. *In* J. Ross, A.L. Jaques et al. (Eds.), Kimberlites and Related Rocks, Vol. 1, Their Composition, Occurrence, Origin and Emplacement. Proc. 4th Internat. Kimberlite Conf., Vol. 1, Geol. Soc. Austr. Spec. Publ., 14, 571-581.

**Menzies, M.A., Hawkesworth, C.J., 1987.** Upper mantle processes and composition. *In* P.H. Nixon (Ed.), Mantle Xenoliths, p. 725-738. John Wiley & Sons Ltd., London.

**Merrill, R.B., Wyllie, P.J., 1973.** Absorption of iron by platinum capsules in high pressure rock melting experiments. Am. Mineral., 58, 16-20.

**Merrill, R.B., Wyllie, P.J., 1975.** Kaersutite and kaersutite eclogite from Kakanui, New Zealand - water-excess and water-deficient melting to 30 kilobars. Geol. Soc. Am. Bull., 86, 555-570.

**Mitchell, R.H., Bergman, S.C., 1991.** Petrology of Lamproites. Plenum Press, new York, 447 p.

**Mitrofanov, F.P., Balashov, Yu.A., Balagansky, V.V., 1991.** New geochronological data on lower Precambrian complexes of the Kola Peninsula. *In* F.P. Mitrofanov and V.V. Balagansky (Eds.), Correlation of Lower Precambrian Formations of the Karelian-Kola region, U.S.S.R. and Finland, p. 12-16. Geol. Inst., Kola Science Center of the USSR Academy of Sciences, Apatity.

**Miyamoto, M., McKay, D.S., Lofgren, G.E., Duke, M.B., 1992.** CaO contents in olivine: an experimental study. Lunar Planet. Sci., XXIII, 925-926.

**Morawski, A., Bence, A.E., Papike, J.J., 1975.** Petrology of titaniferous alkali basalt from DSDP Leg 17, Site 165A in the Central Pacific Basin. Eos (Trans. Am. Geophys. Union), 56, p. 468.

**Morawski, A., Bence, A.E., Papike, J.J., 1976.** Mineralogy-petrology of titaniferous basalt from DSDP Leg 17 Site 165A. Eos (Trans. Am. Geophys. Union), 57, p. 413.

**Morgan, J.W., 1986.** Ultramafic xenoliths: clues to Earth's late accretionary history. J. Geophys. Res., 91, 12375-12387.

**Morgan, J.W., Lovering, J.F., 1967.** Rhenium and osmium abundances in some igneous and metamorphic rocks. Earth Planet. Sci. Lett., 3, 219-224.

**Morris, J.D., Hart, S.R., 1983.** Isotopic and incompatible element constraints on the genesis of island arc volcanics from Cold Bay and Amak Island, Aleutians, and implications for mantle structure. Geochim. Cosmochim. Acta., 47, 2015-2030.

**Morten, L., 1987.** Italy: a review of xenolithic occurrences and their comparison with Alpine peridotites. *In* P.H. Nixon (Ed.), Mantle Xenoliths, p. 135-148. John Wiley & Sons Ltd., London.

**Murck, B.W., Campbell, I.H., 1986.** The effects of temperature, oxygen fugacity and melt composition on the behaviour of chromium in basic and ultrabasic melts. Geochim. Cosmochim. Acta, 50, 1871-1887.

**Naldrett, A.J., 1989a.** Sulfide melts: Crystallization temperatures, solubility in silicate melts, and Fe, Ni, and Cu partitioning between basaltic magmas and olivine. *In* J.A. Whitney and A.J. Naldrett (Eds.), Ore deposition associated with magmas. Rev. Econ. Geol., 4, 5-20.

**Naldrett, A.J., 1989b.** Magmatic Sulfide Deposits. Oxford Univ. Press, Inc., 186 p.

**Naldrett, A.J., Barnes, S.-J., 1986.** The behavior of platinum-group elements during fractional crystallization and partial melting with special reference to the composition of magmatic sulfide ores. Fortschritte Mineral., 64, 113-133.

**Neradovskii, Yu.N., 1985.** Nekotorye tipomorfnye svoistva khromshpinelidov v nikelenosnykh ultraosnovnykh porodakh Pechengi. Zap. Vsesoyu. Mineral. Obshch., 6, 698-702.

**Neradovskii, Yu.N., Smolkin, V.F., 1977.** Neobychnye titankhromovye shpineli v porodakh nikelenosnykh massivov Pechengi. *In* Mineraly i paragenezisy mineralov osnovnykh i ultraosnovnykh porod Kolskogo Poluostrova, p. 125-135. Kolskii Filial Akad. Nauk SSSR, Apatity.

**Nesbitt, R.W., 1971.** Skeletal crystal forms in the ultramafic rocks of the Yilgarn Block, Western Australia: Evidence for an Archean ultramafic liquid. Spec. Publ. Geol. Soc. Austr., 3, 331-347.

**Nesbitt, R.W., Hamilton, D.L., 1970.** Crystallization of an alkali-olivine basalt under controlled $P_{O2}$, $P_{H2O}$ conditions. Phys. Earth Planet. Interiors, 3, 309-315.

**Nesbitt, R.W., Sun, S.-S., Purvis, A.C., 1979.** Komatiites: geochemistry and genesis. Can. Mineral., 17, 165-186.

**Nicholls, I.A., Ringwood, A.E., 1973.** Effect of water on olivine stability in tholeiites and the production of silica-saturated magmas in the island-arc environment. J. Geol., 81, 285-300.

**Nicholls, J., Stout, M.Z., 1988.** Picritic melts in Kilauea - evidence from the 1967-1968 Halemaumau and Hiiaka eruptions. J. Petrol., 29, 1031-1057.

**Nwe, Y.Y., 1976.** Electron-probe studies of the early pyroxenes and olivines from the Skaergaard intrusion, east Greenland. Contrib. Mineral. Petrol., 55, 105-126.

**O'Hara, M.J., 1968.** The bearing of phase equilibria studies on the origin and evolution of basic and ultrabasic rocks. Earth Sci. Rev., 4, 69-133.

**O'Hara, M.J., 1976.** Data reduction and projection schemes for complex compositions. Progress in Experimental Petrology, 3, 103-126.

**Ohtani, E., 1990.** Majorite fractionation and genesis of komatiites in the deep mantle. Precambrian Res., 48, 195-202.

**O'Reilly, S., Griffin, W.L., 1988.** Mantle metasomatism beneath western Victoria, Australia: I. Metasomatism processes in Cr-diopside lherzolites. Geochim. Cosmochim. Acta., 52, 433-447.

**Papadakis, A., 1972.** Eine bemerkenewerte Titanomagnetit-Chromit-Zonierung von Petsamo. Neues Jahrb. Mineral. Monatsch., 7, 316-319.

**Papike, J.J., Cameron, K.L., Baldwin, K., 1974.** Amphi-

boles and pyroxenes: characterization of other than quadrilateral components and estimates of ferric iron from microprobe data. Geol. Soc. Am. Abstr. with Progr., 6, p. 1053-1054.

**Papunen, H., Gorbunov, G.I. (Eds.), 1985.** Nickel-copper deposits of the Baltic Shield and Scandinavian Caledonides. Geol. Surv. Finland, Bull. 333, 394 p.

**Parrish, R.R., 1989.** U-Pb geochronology of the Cape Smith belt and Sugluk block, northern Québec. Geosci. Can., 16, 126-130.

**Patchett, P.J., Arndt, N.T., 1986.** Nd isotopes and tectonics of 1.9-1.7 Ga crustal genesis. Earth Planet. Sci. Lett., 78, 329-338.

**Patera, E.S., Holloway, J.R., 1982.** Experimental determination of the spinel-garnet boundary in a Martian mantle composition. Proc. Lunar Planet. Sci. Conf., 13th, J. Geophys. Res., 87, Supplement, p. A31-A36.

**Pearce, T.H., Gorman, B.E., Birkett, T.C., 1977.** The relationship between major element chemistry and tectonic environment of basic and intermediate volcanic rocks. Earth Planet. Sci. Lett., 36, 121-132.

**Pearson, D.G., Shirey, S.B., Carlson, R.W., Boyd, F.R., Nixon, P.H., Pokhilenko, N.P., 1991.** Re-Os and Sm-Nd isotopic constraints on the chronology of lithospheric mantle and enrichment events. Eos (Trans. Am. Geophys. Union), 72, p. 527.

**Pegram, W.J., Allègre, C.-J., 1992.** Osmium isotopic compositions from oceanic basalts. Earth Planet. Sci. Lett., 111, 59-68.

**Peltonen, P., 1990.** Metamorphic olivine in picritic metavolcanics from Southern Finland. Bull. Geol. Soc. Finland, 62, 99-114.

**Philpotts, A.R., 1972.** Density, surface tension and viscosity of the immiscible phase in a basic, alkaline magma. Lithos, 5, 1-18.

**Philpotts, A.R., 1982.** Compositions of immiscible liquids in volcanic rocks. Contrib. Mineral. Petrol., 80, 201-218.

**Plaksenko, A.N., Smolkin, V.F., 1990.** Typomorphism of accessory chromian spinels in highly magnesian volcanics. Int. Geol. Rev., 32, 244-259.

**Poulson, S.R., Ohmoto, H., 1990.** An evaluation of the solubility of sulfide sulfur in silicate melts from experimental data and natural samples. Chem. Geol., 85, 57-75.

**Predovskii, A.A., Fedotov, Zh.A., Zhangurov, A.M., 1974.** Geokhimiya Pechengskogo kompleksa. Nauka, Leningrad, 139 p.

**Predovskii, A.A., Melezhik, V.A., Bolotov, V.I., Fedotov, Zh.A., Basalaev, A.A., Kozlov, N.E., Ivanov, A.A., Zhangurov, A.A., Skufin, P.K. and Lyubtsov, V.V., 1987.** Vulkanizm i sedimentogenez dokembriya severovostoka Baltiiskogo Shchita. Nauka, Leningrad, 185 p.

**Prinzhofer, A., Allègre, C.J., 1985.** Residual peridotites and the mechanism of partial melting. Earth Planet. Sci. Lett., 74, 251-265.

**Pukhtel, I.S., Zhuravlev, D.Z., Kulikov, V.S., Kulikova, V.V., 1991a.** Petrografiya i Sm-Nd-vozrast differentsirovannogo potoka komatiitovykh bazaltov Vetrenogo Poyasa (Baltiiskii Shchit). Geokhimiya, No. 5, 625-634.

**Pukhtel, I.S., Zhuravlev, D.Z., Kulikova, V.V., Samsonov, A.V., Simon, A.K., 1991b.** Komatiity Vodlozerskogo bloka. Dokl. Akad. Nauk SSSR, 317, 197-202.

**Pushkarev, Yu.D., Kravchenko, E.V., Shestakov, G.I., 1978.** Geokhronometricheskie repery dokembriya Kolskogo Poluostrova. Nauka, Leningrad, 136 p.

**Pushkarev, Yu.D., Ryungenen, G.I., Smolkin, V.F., Shurkina, L.K., 1988.** Geokhimiya izotopov svintsa v svyazi s osobennostyami formirovaniya rudoobrazuyushchikh sistem nikelenosnykh bazit-giperbazitov Kolskogo Poluostrova. *In* Izotopnaya geokhimiya protsessa rudoobrazovaniya, p. 150-166. Nauka, Leningrad.

**Rabinovich, Yu.I., 1978.** Petrokhimiya i nikelenost nekotorykh intruzivnykh kompleksov osnovnykh i ultraosnovnykh porod Pechengsko-Allarechenskogo raiona. *In* Dopolnitelnye kriterii poiskov mestorozhdenii poleznykh iskopaemykh v Karelii i na Kolskom Poluostrove, p. 3-25. Min. Geol. RSFSR, Moscow.

**Radchenko, A.T., 1984.** Tektonicheskie aspekty resheniya diskussionnykh voprosov stroeniya Pechengsko-Varzugskoi zony. *In* Geologiya i istoriya formirovaniya dokembriiskikh struktur Kolskogo Poluostrova, p. 3-8. Kolskii Filial Akad. Nauk SSSR, Apatity.

**Rajamani, V., Shivkumar, K., Hanson, G.N., Shirey, S.B., 1985.** Geochemistry and petrogenesis of amphibolites, Kolar Schist Belt, South India: Evidence for komatiitic magma derived by low percentages of melting of the mantle. J. Petrol., 26, 92-123.

**Rajamani, V., Shirey, S.B., Hanson, G.N., 1989.** Fe-rich Archean tholeiites derived from melt-enriched mantle sources: evidence from the Kolar Schist Belt, South India. J. Geol., 97, 487-501.

**Räsänen, J., Hanski. E., Lehtonen, M., 1989.** Komatiites, low-Ti tholeiites and andesites in the Möykkelmä area, Central Finnish Lapland. Geol. Survey Finland, Report of Investigation 88, 41 p.

**Ravizza, G., Turekian, K.K., 1989.** Application of the $^{187}$Re-$^{187}$Os system to black shale chronology. Geochim. Cosmochim. Acta, 53, 3257-3262.

**Ravizza, G., Turekian, K.K., 1992.** The osmium isotopic composition of organic-rich marine sediments. Earth Planet. Sci. Lett., 110, 1-6.

**Ravizza, G., Turekian, K.K., Hay, B.J., 1991.** The geochemistry of rhenium and osmium in recent sediments from the Black Sea. Geochim. Cosmochim. Acta., 55, 3741-3752.

**Reisberg, L.C., Allègre, C.J., Luck, J.-M., 1991.** The Re-Os systematics of the Ronda Ultramafic Complex of southern Spain. Earth Planet. Sci. Lett., 105, 196-213.

**Ringwood, A.E., 1979.** Origin of the Earth and Moon. Springer, New York, 295 p.

**Ringwood, A.E., 1989.** Constitution and evolution of the mantle. *In* J. Ross, A.L. Jaques et al. (Eds.), Kimberlites and Related Rocks, Vol. 1, Their Composition, Occurrence, Origin and Emplacement. Proc. 4th Internat. Kimberlite Conf., Geol. Soc. Austr. Spec. Publ., 14, 457-485.

**Robert, J.L., 1976.** Titanium solubility in synthetic phlogopite solid solutions. Chem. Geol., 17, 213-227.

**Roedder, E., 1979.** Silicate liquid immiscibility in magmas. *In* H.S. Yoder, Jr. (Ed.), The Evolution of Igneous Rocks, Fiftieth Anniversary Perspectives, p. 15-57. Princeton

Univ. Press, Princeton, N.J.

**Roedder, E., Weiblen, P.W., 1971.** Petrology of silicate melt inclusions, Apollo 11 and 12, and terrestrial equivalents. Proc. Lunar Sci. Conf., 2nd, Geochim. Cosmochim. Acta, Suppl. 2, 507-528.

**Roeder, P.L., Emslie, R.F., 1970.** Olivine-liquid equilibria. Contrib. Mineral. Petrol., 29, 275-289.

**Roeder, P.L., Campbell, I.H., 1985.** The effect of postcumulus reactions on composition of chrome-spinels from the Jimberlana intrusion. J. Petrol., 26, 763-786.

**Roeder, P.L., Reynolds, I., 1991.** Crystallization of chromite and chromium solubility in basaltic melts. J. Petrol., 32, 909-934.

**Romanko, A.E., Shipov, V.N., Efremova, L.B., Savichev, A.T., 1992.** Geokhimiya RZE i geodinamika Pechengskoi zony na Kolskom Poluostrove. Dokl. Akad. Nauk SSSR, 321, 1075-1079.

**Rosenberg, R.J., Kaistila, M., Zilliacus, R., 1982.** Instrumental epithermal neutron activation analysis of solid geochemical samples. J. Radioanal. Chem., 71, 419-428.

**Rusanov, M.S., 1981.** Toleit-komatiitovaya formatsiya Pechengskogo kompleksa. Sov. Geol., No. 2, 98-112.

**Russ, G.P., Bazan, J.M., Date, A.R., 1987.** Osmium isotope ratios measurements by inductively coupled plasma mass spectrometry. Anal. Chem., 59, 984-989.

**Ryder, G., Steele, A., 1987.** Apollo 15 olivine-normative mare basalts: new chemical analyses, chemical dispersion, and chemical relationships. Lunar Planet. Sci. Conf., XVIII, 862-863.

**Sack, R.O., Carmichael, I.S.E., Rivers, M., Ghiorso, M.S., 1980.** Ferric-ferrous equilibria in natural silicate liquids at 1 bar. Contrib. Mineral. Petrol., 75, 369-376.

**Sakai, H., Casadevall, T.J., Moore, J.G., 1982.** Chemistry and isotope ratios of sulfur in basalts and volcanic gases at Kilauea volcano, Hawaii. Geochim. Cosmochim. Acta., 46, 729-738.

**Scarfe, C.M., Mysen, B.O., Rai, C.S., 1979.** Invariant melting bahavior of mantle material: partial melting of two lherzolite nodules. Carn. Inst. Wash. Yearb., 78, 498-501.

**Schaefer, S.J., Morton, P., 1991.** Two komatiitic pyroclastic units, Superior Province, northwestern Ontario: their geology, petrography, and correlation. Can. J. Earth Sci., 28, 1455-1470.

**Schneider, M.E., Eggler, D.H., 1986.** Fluids in equilibrium with peridotite minerals: Implications for mantle metasomatism. Geochim. Cosmochim. Acta., 50, 711-724.

**Schreurs, J., van Kooperen, P., Westra, L., 1986.** Ultramafic metavolcanic rocks of early proterozoic age in West-Uusimaa, SW Finland. Neues Jahrbuch Miner. Abh., 155, 185-201.

**Sekine, T., Wyllie, P.J., 1973.** Effect of $H_2O$ on liquidus relationships in $MgO$-$Al_2O_3$-$SiO_2$ at 30 kilobars. J. Geol., 91, 195-210.

**Sen, G., 1982.** Composition of basaltic liquids generated from a partially depleted lherzolite at 9 kbar pressure. Nature, 299, 336-338.

**Sharkov, E.V., Smolkin, V.F., 1989.** Vysokotitanistye ferropikrity - spetsificheskie magmaticheskie obrazovaniya etapa perekhoda ot rannego k pozdnemy dokembriyu. Dokl. Akad. Nauk. SSSR, 309, 164-168.

**Sharkov, E.V., Smolkin, V.F., 1990.** Rannedokembriiskaya Pechengsko-Varzugskaya vulkanicheskaya zona Baltiiskogo Shchita. Izv. Akad. Nauk SSSR, Ser. Geol., No. 10, 37-49.

**Sharkov, E.V., Smolkin, V.F. (in press)** The early Proterozoic Pechenga-Varzuga belt: a case of Precambrian back-arc spreading. Precambrian Res.

**Shaw, D.M., 1970.** Trace element fractionation during anatexis. Geochim. Cosmochim. Acta., 34, 237-243.

**Shearer, C.K., Papike, J.J., Galbreath, K.C., Wentworth, S.J., Shimizu, N., 1990.** A SIMS study of lunar "komatiitic glasses": Trace element characteristics and possible origin. Geochim. Cosmochim. Acta., 54, 1851-1857.

**Shirey, S.B., 1991.** The Rb-Sr, Sm-Nd and Re-Os isotopic systems: A summary and comparison of their applications to the cosmochronology and geochronology of igneous rocks. *In* L. Heaman and J.N. Ludden (Eds.), Applications of Radiogenic Isotope Systems to Problems in Geology, Min. Assoc. Can. Short Course Handbook, 19, 103-166.

**Shirey, S.B., Carlson, R.W., 1991.** The Re-Os isotopic system: New applications in geochemistry at DTM. Carn. Inst. Wash. Yearb. 90, 58-71.

**Shirey, S.B., Carlson, R.W., Brown, L., Lambert, D.D., 1990.** A multi-ditector resonance ionization mass spectrometer for Re-Os isotopic studies of crust-mantle evolution. 7th Internat. Conf. Geochron. Cosmochron. Isot. Geol., Geol. Soc. Australia, Abstr. 27, p. 92.

**Sigurdsson, H., Schilling, J.-G., 1976.** Spinels in Mid-Atlantic ridge basalts: chemistry and occurrence. Earth Planet. Sci. Lett., 29, 7-20.

**Simkin, T., Smith, J.V., 1970.** Minor-element distribution in olivine. J. Geol., 78, 304-325.

**Sisson, P.R., Grove, T.L., Donelly-Nolan, J.M., 1991.** Origin of Glass Mountain rhyolite at Medicine Lake Volcano (MLV), N. California: experimental, field and geochemical constraints. Eos (Trans. Am. Geophys. Union), 72, p. 534.

**Skufin, P.K., 1980a.** Osobennosti vulkanizma proterozoiskoi Pechengskoi struktury. Byul. Mosk. O-va Ispyt. Prirody, otd. Geol., 55, 120-130.

**Skufin, P.K., 1980b.** Vulkanogennyi kompleks Pechengskoi zony (nizhnii proterozoi). *In* Vulkanity rannego dokembriya Kolskogo Poluostrova (Atlas tekstur i struktur), p. 49-56. "Nauka", Leningrad.

**Skufin, P.K., 1990.** O paleoignimbrites i kagusitakh v razreze vulkanitov Pechengskoi serii (Kolskii p-ov). Izvestiya Vysshikh Uchebnykh Zavedenii, Geologiya i Razvedka, No. 11, 26-33.

**Skufin, P., Fedotov, Zh.A., 1989.** Pikritovye sharovye lavy v razreze rannedokembriiskikh vulkanitov Pechengskoi struktury. Dokl. Akad. Nauk SSSR, 306, 956-962.

**Skufin, P.K., Pushkarev, Yu.D., Kravchenko, M.P., 1986.** Vulkanity mudzherit-trakhitovoi formatsii v pechengskoi vulkano-tektonicheskoi paleodepressii. Izv. Akad Nauk SSSR, Ser. Geol., No. 1, 18-29.

**Skufin, P.K., Gavrilenko, B.V., Fedotov, Zh.A., 1988.** Poroyarvinskaya vulkanokupolhaya struktura v Yuzhno-pechengskoi zone (Kolskii poluostrov). Byul. Mosk. O-va

Ispytatelei Prirody, Otd. Geol., 63, 98-107.

**Smith, A.D., Ludden, J.N., 1989.** Nd isotopic evolution of the Precambrian mantle. Earth Planet. Sci. Lett., 93, 14-22.

**Smolkin, V.F., 1974.** Sostav rassloennykh intruzivov Pechengi, rekonstruirovannyi po reliktovym mineralam. *In* Petrologiya, mineralogiya i geokhimiya, p. 48-54. Akad. Nauk SSSR, Apatity.

**Smolkin, V.F., 1977.** Petrologiya Pilguyarvinskogo rodonosnogo intrusiva (Pechenga). VINITI, No. 2114-77, 216 p.

**Smolkin, V.F., 1978.** Olivin i klinopiroksen Pilguyarvinskogo rudohosnogo intruziva (Pechenga). *In* Mineraly i paragenezicy mineralov, p. 55-71. Nauka, Leningrad.

**Smolkin, V.F., 1981.** Shpinelidy v porodakh Pechengskogo i Imandra-varzugskogo kompleksov i ikh petrogeneticheskoe znachenie. *In* Mineraly i mineralnye paragenezicy gornykh porod Kolskogo Poluostrova, s. 15-29. Kolskii Filial Akad. Nauk SSSR, Apatity.

**Smolkin, V.F., 1985.** Vulkano-plutonicheskie assotsiatsii nizhneproterozoiskikh poyasov i ikh rudonosnost. *In* Petrologiya i kriterii otsenki rudonosnosti dokembriiskikh bazit-giperbazitovykh formatsiii Karelo-Kolskogo regiona, p. 34-50. Kolskii Filial Akad. Nauk SSSR, Apatity.

**Smolkin, V.F., 1991.** Petrologiya i rudogenez komatiitovykh i pikritovykh assotsiatsii rannego dokembriya na primere severo-vostoka Baltiiskogo shchita. Dissertatsiya na soiskanie uchenoi stepeni doktora geologo-mineralocheskikh nauk, Tom I, Univ. of Saint-Petersburg, 439 p.

**Smolkin, V.F., Pakhomovskiy, Ya.A., 1985.** The petrogenetic significance of the olivine-chrome spinelide assemblage in Pechenga ultramafites. Int. Geol. Rev., 27, 709-725.

**Smolkin, V.F., Borisov, A.E., Marakushev, A.A., 1987.** Priznaki differentsiatsii i nesmeshivaniya rasplavov v pikritobazaltakh Pechengi. Dokl. Akad. Nauk SSSR, 294, 669-673.

**Sobolev, A.V., Slutskii, A.B., 1984.** Composition and crystallization conditions of the initial melt of the Siberian meimechites in relation to the general problem of ultrabasic magmas. Sov. Geol. Geophys., 25, 93-104.

**Sobolev, A.V., Kamenetsky, V.S., Kononkova, N.N., 1991.** Novye dannye po petrologii Sibirskikh meimechitov. Geokhimiya, No. 8, 1084-1095.

**Spadea, P., Espinosa, A., Orrego, A., 1989.** High-Mg extrusive rocks from the Romeral Zone ophiolites in the southwestern Colombian Andes. Chem. Geol., 77, 303-321.

**Spear, F.S., Kimball, K.L., 1984.** RECAMP - a FORTRAN IV program for estimating $Fe^{3+}$ contents in amphiboles. Computer Geosci., 10, 317-325.

**Spulber, S.D., Rutherford, M.J., 1983.** The origin of rhyolite and plagiogranite in oceanic crust: An experimental study. J. Petrol., 24, 1-25.

**Stacey, J.S., Kramers, G.D. 1975.** Approximation of terrestrial lead isotope evolution by a two-stage model. Earth Planet. Sci. Lett. 26, 207-221.

**Stone, W.E., Jensen, L.S., Church, W.R., 1987.** Petrography and geochemistry of an unusually Fe-rich basaltic komatiite from Boston Township, northeastern Ontario. Can. J. Earth Sci., 24, 2537-2550.

**Stormer, J.C., 1973.** Calcium zoning in olivine and its relationship to silica activity and pressure. Geochim. Cosmochim. Acta, 37, 1815-1821.

**Stromov, V.A., 1985.** O roli sulfidonosnykh gorizontov produktivnoi tolshchi Pechengi v razmeshchenii medno-nikelevykh mestorozhdenii. Sov. Geol., No. 2, 29-36.

**Sun, S.-S., McDonough, W.F., 1989.** Chemical and isotopic systematics of oceanic basalts: implications for mantle composition and processes. *In* A.D. Saunders and M.J. Norry (Eds.), Magmatism in the Ocean Basin, Geol. Soc. Spec. Publ., 42, 313-345.

**Sun, S.-S., Nesbitt, R.W., McCulloch, M.T., 1989.** Geochemistry and petrogenesis of Archaean and early Proterozoic siliceous high-magnesian basalts. *In* A.J. Crawford (Ed.), Boninites, p. 148-173. Unwin Hyman, London.

**Tait, S., Jaupart, C., Vergniolle, S., 1989.** Pressure, gas content and eruption periodicity of a shallow crystallizing magma chamber. Earth Planet Sci. Lett., 92, 107-123.

**Takahashi, E., 1986.** Melting of a dry peridotite KLB-1 up to 14 GPa: Implications on the origin of peridotitic upper mantle. J. Geophys. Res., 91, 9367-9382.

**Takahashi, E., Kushiro, I., 1983.** Melting of a dry peridotite at high pressures and basalt magma genesis. Am. Mineral., 68, 859-879.

**Takahashi, E., Scarfe, C.M., 1985.** Melting of peridotite to 14 GPa and the genesis of komatiite. Nature, 315, 566-568.

**Taylor, S.R., McLennan, S.M., 1985.** The Continental Crust: Its Composition and Evolution. Blackwell Sci. Publ., Oxford, 312 p.

**Thompson, R.N., 1984.** Dispatches from the basalt front. I. Experiments. Proc. Geol. Assoc., 95, 249-262.

**Thibault, Y., Edgar, A.D., Lloyd, F.E., 1992.** Experimental investigation of melts from a carbonated phlogopite lherzolite: Implications for metasomatism in the continental lithospheric mantle. Am. Mineral., 77, 784-794.

**Thompson, J.F.H., Naldrett, A.J., 1984.** Sulphide-silicate reactions as a guide to Ni-Cu-Co mineralization in central Maine, U.S.A. *In* D.L. Buchanan and M.J. Jones (Eds.), Sulfide Deposits in Mafic and Ultramafic Rocks, p. 103-113. Inst. Min. Metall. Spec. Publ., London.

**Thy, P., Lofgren, G.E., Imsland, P., 1991.** Melting relations and the evolution of the Jan Mayen magma system. J. Petrol., 32, 303-332.

**Touloukian, Y.S., Judd, W.R., Roy, R.F., 1981.** Physical Properties of Rocks and Minerals. Data Series on Material Properties, Vol. 1-2, McGraw-Hill, New York.

**Troll, G., Gilbert, M.C., 1974.** Stability of fluorine tremolite. Eos (Trans. Am. Geophys. Union), 55, p. 481.

**Ulmer, P., 1989.** The dependence of the $Fe^{2+}$-Mg cation-partitioning between olivine and basaltic liquid on pressure, temperature and composition. Contrib. Mineral. Petrol., 101, 261-273.

**Ulmer, P., 1988.** High-pressure phase equilibria of a calc-alkaline picro-basalt: Implications for the genesis of calc-alkaline magmas. Carn. Inst. Wash. Yearb., 1987-1988, p. 28-35.

**Ulmer, P., Trommsdorff, V., Dietrich, V.J., 1990.** Ex-

perimental constraints on the genesis of Cretaceous basanites from the Austrian Alps. International Volcanological Congress, 3.-8. Sept. 1990, Mainz (FGR), Abstracts.

**Usselman, T.M., Hodge, D.S., Naldrett, A.J., Campbell. I.H., 1979.** Physical constraints on the characteristics of nickel sulfide ore in ultramafic lavas. Can. Mineral., 17, 361-372.

**Vaasjoki, M., 1989.** Pb and S isotopic studies on the Rauhala Zn-Cu-Pb sulphide deposit and its environment. Geol. Surv. Finland, Spec. Paper 11, 59-65.

**Väyrynen, H., 1938.** Petrologie des Nickelerzfeldes Kaulatunturi-Kammikivitunturi in Petsamo. Bull. Comm. geol. Finlande 116, 1-198.

**Vinogradov, A.P., Tarasov, L.S., Zykov, S.I., 1959.** Isotopic composition of leads from the ores of the Baltic Shield. Geochemistry, 7, 689-749.

**Vuollo, J., Piirainen, T., 1992.** The 2.2 Ga old Koli layered sill: The low-Al tholeiitic (karjalitic) magma type and its differentiation in northern Karelia, eastern Finland. Geol. För. Stockh. Förhandl., 114, 131-142.

**Walker, D., Kirkpatrick, R.J., Longhi, J., Hays, J.F., 1976.** Crystallization history of lunar picritic basalt sample 12002: Phase-equilibria and cooling-rate studies. Bull. Geol. Soc. Am., 87, 646-656.

**Walker, R.J., 1988.** Low-blank chemical separation of rhenium and osmium from gram quantities of silicate rock for measurement by resonance ionization mass spectrometry. Anal. Chem., 60, 1231-1234.

**Walker, R.J., Fassett, J.D., 1986.** Isotopic measurement of subnanogram quantities of rhenium and osmium by resonance ionization mass spectrometry. Anal. Chem., 58, 2923-2927.

**Walker, R.J., Morgan, J.W., 1989.** Rhenium-osmium isotope systematics of carbonaceous chondrites. Science, 243, 519-522.

**Walker, R.J., Shirey, S.B., Stecher, O., 1988.** Comparative Re-Os, Sm-Nd, and Rb-Sr isotope and trace element systematics for Archean komatiite flows from Munro Township, Abitibi Belt, Ontario. Earth Planet. Sci. Lett., 87, 1-12.

**Walker, R.J., Carlson, R.W., Shirey, S.B., Boyd, F.R., 1989.** Os, Sr, Nd, and Pb isotope systematics of southern African peridotite xenoliths: Implications for the chemical evolution of subcontinental mantle. Geochim. Cosmochim. Acta, 53, 1583-1595.

**Walker, R.J., Morgan, J.W., Naldrett, A.J., Li, C., Fassett, J.D., 1991a.** Re-Os isotopic systematics of Ni-Cu sulfide ores, Sudbury Igneous Complex, Ontario: Evidence for a major crustal component. Earth Planet. Sci. Lett., 105, 416-429.

**Walker, R.J., Echeverria, L.M., Shirey, S.B., Horan, M.F., 1991b.** Re-Os isotopic constraints on the origin of volcanic rocks, Gorgona Island, Colombia: Os isotopic evidence for ancient heterogeneities in the mantle. Contrib. Mineral. Petrol., 107, 150-162.

**Walker, R.J., Hanski, E.J., Smolkin, V.F., 1991c.** Pechenga (U.S.S.R.) ferropicrites and associated nickel-ores: Re-Os isotope constraints on origin. Eos (Trans. Am. Geophys. Union), 72, p. 543.

**Watson, E., 1979.** Zircon saturation in felsic liquids: experimental data and applications to trace element geochemistry. Contrib. Mineral. Petrol., 70, 407-419.

**Whilshire, H.G., Meyer, C.E., Nakata, J.K., Calk, L.C., Shervais, J.W., Nielson, J.E., Schwarzman, E.C., 1988.** Mafic and ultramafic xenoliths from volcanic rocks of the Western United States. U.S. Geol. Survey Prof. Paper 1443, 179 p.

**Wilkinson, J.F.G., 1985.** Undepleted mantle composition beneath Hawaii. Earth Planet. Sci. Lett., 75, 129-138.

**Wilkinson, J.F.G., Binns, R.A., 1977.** Relatively iron-rich lherzolite xenoliths of the Cr-dioside suite: A guide to the primary nature of anorogenic tholeiitic andesite magmas. Contrib. Mineral. Petrol., 65, 199-212.

**Yakovlev, Yu.N., Astafeva, V.V., Astavev, Yu.A., 1968.** O raspredelenii selena v medno-nikelevykh rudakh Pechengskogo i Allarechenskogo raionov. Materialy po Mineralogii Kolskogo Poluostrova, 6, 50-66.

**Yakovleva, A.K., Osokin, A.N., Dokuchaeva, V.S., Neradovskii, Yu.N., Balabonin, N.L., Orsoev, D.A., Yakovlev, Yu.N., Kondratev, A.V., Spiridonov, G.V., 1983.** Analizy mineralov medno-nikelevykh mestorozhdenii Kolskogo poluostrova. Kolskii Filial Akad. Nauk SSSR, Apatity, 320 p.

**Zagorodnyi, V.G., 1980.** Osnovnye cherty geologii dokembriya Kolskogo Poluostrova. *In* Vulkanity rannego dokembriya Kolskogo Poluostrova (Atlas tekstur i struktur), p. 49-56. "Nauka", Leningrad.

**Zagorodnyi, V.G., Mirskaya, D.D., Suslova, S.N., 1964.** Geologicheskoe stroenie Pechengskoi osadochno-vulkanogennoi serii. Nauka, Moscow, 208 p.

**Zagorodny (Zagorodnyi), V.G., Melezhik, V.A., Lyubtsov, V.V., 1989.** Correlation of early Proterozoic complexes of Polmak-Pasvik-Pechenga. Guidebook to geological excursions in Pechenga region. Geol. Inst., Kola Sci. Center, USSR Acad. Sci., Apatity, 38 p.

**Zak, S.I., Makarov, V.N., Kochnev-Pervukhov, V.I., Proskuryakov, V.V., Zaskind, E.S., Batashev, E.V., Kolesnikov, G.P., 1982.** Geologiya, magmatizm i orudenenie Pechengskogo rudnogo polya. Nedra, Leningrad, 112 p.

**Zhangurov, A.A., Predovskii, A.A., 1974.** Khimizm porod i priroda pervichnoi magmy nikelenosnyk intruzii Pechengi. *In* Petrologiya, mineralogiya i geokhimiya, p. 72-83. Akad. Nauk SSSR, Apatity.

**Zindler, A., 1982.** Nd and Sr isotopic studies of komatiites and related rocks. *In* N.T. Arndt and E.G. Nisbet (Eds.), Komatiites, p. 399-420. Allen & Unwin, London.

**Zwicky, C.N., 1991.** Mineralogisch-petrographische Untersuchungen und K/Ar-Altersbestimmungen in der Opukasjärvi-Schieferzone (Nordfinnland). Lizentiatsarbeit, Philosophisch-Naturwissenschaftliche Fakultät der Universtät Bern, 104 p.

Appendix 1. Graphical presentation of the rationale for projecting $TiO_2$ and $Al_2O_3$ from the olivine composition by calculating $[TiO_2] = TiO_2/(2/3 - MgO - FeO)$ and $[Al_2O_3] = Al_2O_3/(2/3 - MgO - FeO)$ in mole proportions. A1-A3 and B1-B3 are rock suites whose compositions are controlled by olivine fractionation.

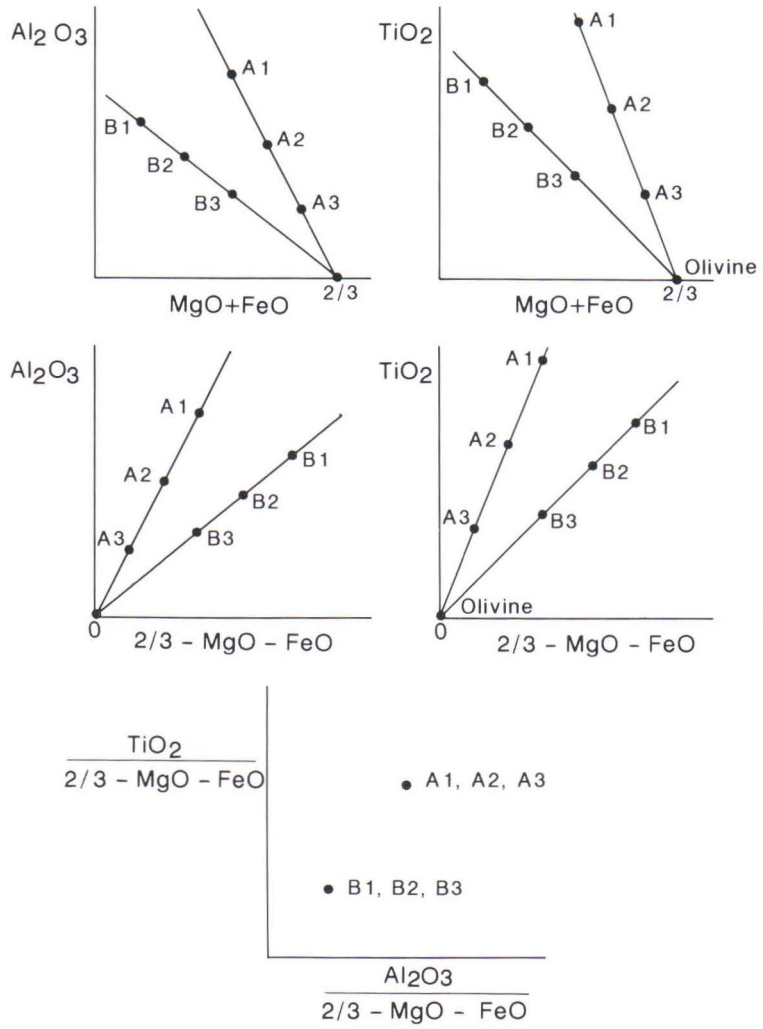

Appendix 2. Literature sources used in the construction of the diagrams in Figures 85-88. Full references available from the author upon request.

| Fig. 85 | Fig. 86 | Fig. 87 | Fig. 88 | References |
|---|---|---|---|---|
| | | X | X | Adam (1990) |
| | X | | | Agee (1988) |
| | X | | | Agee & Walker (1988) |
| X | | | | Agrawal et al. (1990) |
| | | | X | Allen & Boettcher (1978) |
| | | | X | Allen & Boettcher (1983) |
| | | | X | Apted & Boettcher (1981) |
| X | X | | | Arculus (1975) |
| | X | X | X | Arima & Edgar (1983a) |
| | | X | | Arima & Edgar (1983b) |
| | X | | | Arndt (1976) |
| X | | | | Baker & Eggler (1983) |
| | X | | | Baker & Eggler (1987) |
| | X | | | Bartels et al. (1988) |
| | | X | | Barton & Hamilton (1979) |
| | X | | | Bender et al. (1978) |
| X | X | | | Bertka & Holloway (1988) |
| | X | | | Bertka et al. (1990) |
| | X | | | Bickle (1978) |
| | X | | | Bickle et al. (1977) |
| | X | X | X | Brey & Green (1975,1976,1977) |
| | X | | | Brey et al. (1986) |
| X | X | | | Bultitude & Green (1967) |
| X | X | | | Bultitude & Green (1971) |
| | X | | | Cawthorn & Davies (1983) |
| | X | | | Chen & Lindsley (1983) |
| X | X | | | Chen et al. (1982) |
| X | X | | | Cohen et al. (1967) |
| | X | | | Cox & Jamieson (1974) |
| | X | | | Crawford et al. (1987) |
| X | X | | | Cundari & O'Hara (1976) |
| | X | | | Delano (1976) |
| X | X | | | Delano (1977) |
| | X | | | Delano (1980) |
| | X | | | Duncan & Green (1987) |
| | X | | | Dunn & Stringer (1990) |
| | X | X | | Edgar et al. (1976) |
| | X | X | X | Edgar et al. (1980) |
| | | X | | Edgar et al. (1988) |
| X | X | | | Eggins (1992) |
| X | X | | | Elthon & Scarfe (1984) |
| | | X | | Esperanca & Holloway (1987) |
| | X | | | Falloon & Green (1987) |
| X | X | | | Falloon & Green (1988) |
| | X | | | Falloon et al. (1989) |
| X | X | | | Fisk & Ford (1984) |
| | X | | | Fisk et al. (1988) |
| | | X | | Foden & Green (1992) |
| | | X | | Foley (1990) |
| | X | | | Fram & Longhi (1992) |
| | X | | | Fujii & Bougault (1983) |
| | X | | | Fujii & Scarfe (1985) |
| | X | | | Fujii et al. (1978) |
| | | | X | Genshaft et al. (1983) |
| | X | | | Girnis et al. (1987) |

Appendix 2. (*Continued*)

| Fig. 85 | Fig. 86 | Fig. 87 | Fig. 88 | References |
|---|---|---|---|---|
| | | X | X | Gorbachev (1989) |
| X | X | | | Green (1973) |
| | | | X | Green (1973b) |
| | X | | | Green (1981) |
| | X | X | | Green & Hibberson (1970) |
| X | X | | | Green & Ringwood (1967) |
| X | | | | Green & Ringwood (1968) |
| | X | | | Green & Ringwood (1973) |
| | X | | | Green et al. (1967) |
| | X | | | Green et al. (1972) |
| | X | X | | Green et al. (1975) |
| | X | | | Green et al. (1979) |
| | X | | | Green et al. (1971) |
| | X | | | Grove & Lindsley (1978) |
| | X | | | Grove et al. (1973) |
| | X | | | Grove et al. (1990) |
| | X | | | Grover et al. (1980) |
| | | | X | Gupta & Yagi (1979) |
| | X | | | Gust & Perfit (1987) |
| | X | | | Herzberg (1992) |
| | X | | | Hodges & Kushiro (1973) |
| X | X | | | Howells et al. (1975) |
| | | | X | Ishbulatov (1977) |
| X | X | | | Ito & Kennedy (1967) |
| X | X | | | Ito & Kennedy (1974) |
| | | X | | Jakobsson & Holloway (1986) |
| | X | | | Jaques & Green (1980) |
| | X | | | Jaques & Green (1983) |
| X | | | | Johnston (1986) |
| X | X | | | Kadik et al. (1989) |
| X | | | | Kato (1989) |
| | X | | | Kato et al. (1988) |
| | | X | | Kelemen et al. (1990) |
| | X | | | Kesson & Ringwood (1977) |
| | X | | | Kesson (1975) |
| | X | | | Kinzler & Grove (1992) |
| | X | | | Knutson & Green (1975) |
| X | X | | | Kornprobst (1970) |
| | X | | | Kuehner (1992) |
| | X | | | Kushiro (1972a) |
| | X | | | Kushiro (1973a) |
| | X | | | Kushiro (1973b) |
| | X | | | Kushiro (1987) |
| | | X | | Kushiro (1990) |
| | X | | | Kushiro & Thompson (1972) |
| | X | | | Kushiro et al. (1972a) |
| X | X | | | Kushiro et al. (1972b) |
| | X | | | Litvin & Ishchenko (1989) |
| | | X | | Lloyd et al. (1985) |
| | X | | | Longhi et al. (1978) |
| X | X | | | Maaløe & Jakobsson (1980) |
| X | X | | | Maaløe et al. (1986) |
| | X | | | Mahood & Baker (1986) |
| | | X | | McFarlane et al. (1989, 1990) |
| | | X | | Meen (1987) |
| | X | | | Meen (1990) |
| | | X | | Meen et al. (1989) |

Appendix 2. (*Continued*)

| Fig. 85 | Fig. 86 | Fig. 87 | Fig. 88 | References |
|---|---|---|---|---|
| | | X | X | Mengel & Green (1989) |
| | | X | X | Merrill & Wyllie (1975) |
| | X | X | | Mysen & Kushiro (1977) |
| X | | | X | Nicholls & Harris (1980) |
| | | X | | Nicholls & Lorenz (1973) |
| X | X | | X | Nicholls & Ringwood (1973) |
| | | X | X | Nicholls & Whitford (1983) |
| | X | | | Obata & Dickey (1976) |
| X | | | | O'Hara (1963) |
| | X | | | Ohtani (1987) |
| | X | | | Ohtani et al. (1986) |
| | X | | | Perchuk & Kushiro (1984) |
| | X | | | Perchuk (1983) |
| X | | | | Raheim & Green (1974) |
| X | | | X | Ren Guahao et al. (1991) |
| X | | | | Ringwood & Essene (1970) |
| | X | | | Ringwood (1976) |
| | X | | | Ringwood (1977) |
| | | X | | Ringwood et al. (1992) |
| | X | | | Scarfe & Takahashi (1986) |
| | X | | | Scarfe et al. (1979) |
| | X | | | Seitz & Kushiro (1974) |
| | X | | | Sen (1982) |
| X | | | | Shimizu (1980) |
| | X | | | Shimizu et al. (1982) |
| | | | X | Stern & Wyllie (1978) |
| X | | | X | Stern et al. (1975) |
| | X | | | Stolper (1980) |
| X | X | | | Takahashi (1980) |
| | X | | | Takahashi (1983) |
| X | X | | | Takahashi (1986) |
| | X | | | Takahashi & Kushiro (1983) |
| X | X | | | Takahashi & Scarfe (1985) |
| | | X | | Tatsumi (1981) |
| | X | X | | Tatsumi (1982) |
| | X | X | | Tatsumi & Koyaguchi (1989) |
| | X | X | | Tatsumi et al. (1983) |
| | | X | X | Thibault et al. (1992) |
| | X | | | Thompson (1974) |
| X | X | | | Thompson (1975) |
| | X | | | Thy (1991) |
| X | X | | | Tilley & Yoder (1964) |
| | X | | | Tracy & Stolper (1978) |
| X | X | | | Tronnes et al. (1992) |
| | X | | | Ulmer (1988) |
| | X | X | | Ulmer (1989) |
| | | X | X | Ulmer et al. (1990) |
| X | | | | Upton & Thomas (1980) |
| | X | | | Upton (1971) |
| | X | | | Walker & Agee (1988) |
| X | X | | | Walker et al. (1972) |
| | X | | | Walker et al. (1975) |
| | X | | | Walker et al. (1976) |
| | X | | | Walker et al. (1977) |
| X | X | | | Wei et al. (1990) |
| X | | | | Yoder & Tilley (1962) |
| | X | | | Zyryanov et al. (1984) |

Tätä julkaisua myy

GEOLOGIAN
TUTKIMUSKESKUS (GTK)
Julkaisumyynti
02150 Espoo
☎ 90-46931
Teleksi: 123 185 geolo sf
Telekopio: 90-462 205

GTK, Väli-Suomen
aluetoimisto
Kirjasto
PL 1237
70701 Kuopio
☎ 971-205 111
Telekopio: 971-205 215

GTK, Pohjois-Suomen
aluetoimisto
Kirjasto
PL 77
96101 Rovaniemi
☎ 960-297 219
Teleksi: 37 295 geolo sf
Telekopio: 960-297 289

Denna publikation säljes av

GEOLOGISKA
FORSKNINGSCENTRALEN (GFC)
Publikationsförsäljning
02150 Esbo
☎ 90-46931
Telex: 123 185 geolo sf
Telefax: 90-462 205

GFC, Mellersta Finlands
distriktsbyrå
Biblioteket
PB 1237
70701 Kuopio
☎ 971-205 111
Telefax: 971-205 215

GFC, Norra Finlands
distriktsbyrå
Biblioteket
PB 77
96101 Rovaniemi
☎ 960-297 219
Telex: 37 295 geolo sf
Telefax: 960-297 289

This publication can be obtained
from

GEOLOGICAL SURVEY
OF FINLAND (GSF)
Publication sales
SF-02150 Espoo, Finland
☎ 90-46931
Telex: 123 185 geolo sf
Telefax: 90-462 205

GSF, Regional office of
Mid-Finland
Library
P.O. Box 1237
SF-70701 Kuopio, Finland
☎ 971-205 111
Telefax: 971-205 215

GSF, Regional office of
Northern Finland
Library
P.O. Box 77
SF-96101 Rovaniemi, Finland
☎ 960-297 219
Telex: 37 295 geolo sf
Telefax: 960-297 289

ISBN 951-690-489-0
ISSN 0367-522-X